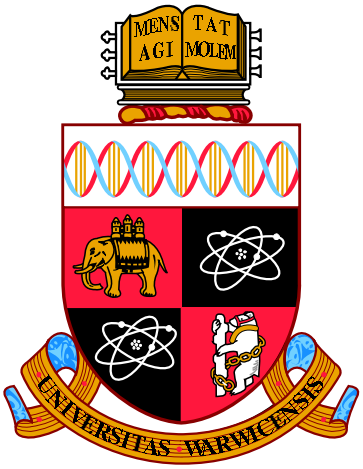

Performance Analysis of Energy Harvesting Relaying

by

Yulin Zhou

Thesis submitted to the University of Warwick

for the degree of

Doctor of Philosophy

School of Engineering

August 2019

Contents

List of Tables

List of Figures

Abbreviations

4G	fourth generation.
5G	fifth generation.
AC	alternating current.
ACEPS	ambient channel estimation power splitting.
ACPS	ambient combination power splitting.
ADTPS	ambient data transmission power splitting.
AF	amplify-and-forward.
AR	achievable rate.
AWGN	additive white Gaussian noise.
BER	bit-error-rate.
BFSK	binary frequency-shift keying.
BPSK	binary phase shift keying.
CCE	cascaded channel estimation.
CDMA	code division multiple access.
CEPS	channel estimation power splitting.
CPS	combination power splitting.
CR	cognitive radio.
CSI	channel signal information.
D2D	device-to-device.
DBPSK	differential binary phase-shift keying.
DC	direct current.
DCE	disintegrated channel estimation.
DF	decode-and-forward.
DPSK	differential phase shift keying.
DTPS	data transmission power splitting.
HD	half-duplex.
LMMSE	linear minimum mean squared error.
LS	least squares.

M-PAM	M-ary pulse amplitude modulation.
M2M4	second-order and fourth-order moments.
MB	moment-based.
MIMO	multiple-input-multiple-output.
ML	maximum-likelihood.
MMSE	minimum mean squared error.
MPPT	Maximum Power Point Tracking.
MSE	mean squared error.
NCBFSK	non-coherent binary frequency-shift keying.
NOMA	non-orthogonal multiple access.
OFDM	orthogonal-frequency-division-multiplexing.
PB	power beacon.
PDF	probability density function.
PS	power-splitting.
PSK	phase shift keying.
PV	photovoltaic.
QoS	Quality of Service.
QPSK	quadrature phase-shift keying.
RD	relay to destination.
RF	radio frequency.
RMSE	root mean squared error.
SNR	Signal-to-Noise Ratio.
SNV	Signal-to-Noise variance.
SR	source to relay.
SSME	split symbol moments estimator.
SVR	Signal-to-Variation ratio.
SWIPT	simultaneous wireless information and power transfer.
TDMA	time-division multiple access.
TS	time-switching.
WPC	wireless powered communications.

Acknowledgments

First and foremost, I would like to express my greatest gratitude to my supervisor, Dr. Yunfei Chen from the School of Engineering at University of Warwick for his careful supervision, constructive suggestions and valuable time. It would simply not have been possible to produce this work without his patient guidance, inspiration, encouragement and warm support. It is my very great privilege to have been his student. More importantly, I would like to thank my beloved parents for their unconditional sacrifices, constant encouragement, continuous support and endless love. They always have faith in me and are proud of me. I would like to dedicate this thesis to them. It is my fortune to meet my girl friend during my Ph.D. study in Warwick. I would like to thank her for the companionship during the happy and hard time. Last but not the least, I was very lucky to have met so many good friends in U.K., especially the members from Communications Systems Laboratory (ComSysLab) in University of Warwick. I would like to thank them all.

Declarations

This thesis is submitted in partial fulfillment for the degree of Doctor of Philosophy under the regulations set out by the Graduate School at the University of Warwick. This thesis is solely composed of research completed by Yulin Zhou, except where stated, under the supervision of Dr.Yunfei Chen between the dates of February 2016 and August 2019. This thesis has not previously been presented in identical or similar form to any other examination board.

Yulin Zhou

August, 2019

List of Publications

Published Journals

- **Y.Zhou**, Y.Chen "Novel Energy-Harvesting AF Relaying Schemes With Channel Estimation Errors", *IEEE Systems Journal*, 2019 (Early Access).
- **Y.Zhou**, Y.Chen " Performance analysis of end-to-end SNR estimators for AF relaying", *Telecommunication Systems*, vol. 67, no.2, pp269-280,2018.
- L. Li, **Y.Zhou**, N. Cao, J. Li "Analysis and optimization of energy harvesting AF relaying with channel estimation", *Physical Communication*,vol. 67, pp17-23,2018.
- F. Azmat, **Y.Zhou**, Y. Chen "New cooperative strategy for cognitive radios with wireless powered primary users", *International Journal of Communication Systems*, vol. 31, no.7, ppe3355,2018.
- Y. Gao, Y. Chen, **Y.Zhou**, N. Cao "BER and achievable rate analysis of wireless powered communications with correlated uplink and downlink", *IET Communications*, vol. 12, no.3, pp310-316,2017.
- M .Mao,N. Cao,Y. Chen, **Y.Zhou** "Multi-Hop Relaying Using Energy Harvesting", *IEEE Wireless Communications Letters*, vol. 4, no.5, pp565-568,2015.

Under Preparation Journal

- **Y.Zhou**, Y.Chen "Ambient Added Energy Harvesting AF Relaying Schemes With Channel Estimation Errors", 2019 (In preparation).

Abstract

Recently, energy harvesting has been exploited as a key technique in wireless communications. Because conventional wireless systems are powered by batteries and cables, they tend to have restricted lifetime and flexibility. In order to solve these problems, wireless power has been investigated as a replacement for conventional batteries.

This thesis focuses on energy harvesting in relaying. The data packet from the source to relay contains three parts: pilot for channel estimation, data symbols and pilots for harvesting. The data packet from the relay to the destination contains two parts: data symbols and pilots for estimation.

To study energy harvesting, the performance of wireless powered communications is evaluated in terms of achievable rate and bit error rate, for applications where the downlink and the uplink are correlated, in contrast to previous works that assume independent uplink and downlink. Semi-closed expressions for the achievable rate and series expressions for the bit error rate are derived in Nakagami m fading channels, based on which the effect of link correlation is examined. Numerical results show that the link correlation has a significant impact on the achievable rate. Consequently, the optimum system parameter for correlated links is very different from that for independent links, showing the usefulness of our results. Also, the link correlation has a noticeable effect on the bit error rate, depending on the system parameters considered.

Then, performance analysis has been performed for an AF relaying system with pilot-based channel estimation and time switching (TS) energy harvesting is conducted. Numerical results show the existence of the optimal values of the numbers of pilots for channel estimation and for energy harvesting, when the total size is fixed.

Next, three novel structures using simultaneous wireless information and power transfer in energy harvesting amplify-and-forward (AF) relaying are investigated. Different combinations of time-switching (TS) and power-splitting (PS) energy harvesting protocols are studied. Closed-form expressions for the cumulative distribution function (CDF) of the end-to-end signal-to-noise ratio (SNR) for the three structures are derived. Using these expressions, achievable rate (AR) and bit-error-rate (BER) are derived. Different parameters are examined. Numerical results show the optimal splitting ratio for channel estimation, energy harvesting and data transmission, when the packet size is fixed.

Finally, the energy from the source and the energy from the ambient are merged together. The three ambient structures are studied. The closed-form expressions for the cumulative distribution function (CDF) of the end-to-end signal-to-noise ratio (SNR) for the three ambient structures are derived. Curve fitting has been used to achieve the approximately achievable rate (AR) and bit-error-rate (BER). The results provide the optimal values for channel estimation pilots and power splitting ratio series for these ambient RF added structures.

Chapter 1

Introduction

Energy harvesting (EH) relaying communication network has recently become a crucial research area. It is a technique to power devices using energy harvested from the source or the ambient in the relaying. In conventional communications, devices depend on fixed wire connections or batteries, which present problems of such as mobility and limited lifetime of fixed capacity batteries. By substituting cables and batteries, EH can provide an attractive solution with flexible operations and an infinite energy support. Moreover, wireless devices such as mobile phones, wearable devices, and sensor nodes fully depend on batteries, the size of which affects the usage time for these devices. In many previous works [15], the authors have conducted researches to improve the energy efficiency of communications. EH in wireless communications contributes immensely to conventional wireless communications, as wireless devices can be powered by energy harvested from the ambient RF energy or the source. Thus, EH can provide a flexible operation and improved energy efficiency.

For wireless relaying communication systems, we expect to have applications powered by utilising environmental energy.

1.1 Background

In order to improve system performance, external sources energy can be used. For example, solar power, thermal energy, kinetic energy, and radio frequency (RF) en-

ergy can be converted to electrical power for wireless autonomous electronic devices. Compared with the traditional power sources (et. oil, coal), renewable energy harvester provides very little power for low-energy electronics. Consequently, it can be seen as technology to relieve energy consumption burdens. In this section, a brief description of some accessible renewable energy sources and RF energy will be presented. Renewable energy sources include solar, wind, and electromagnetic, which are commonly employed in our daily life. The RF is the source for EH in wireless communications. Those types of energy mentioned above are converted to electricity first before being used to power devices.

From Fig. 1.1 [3], we can see the different sources of energy used in the world over the long-term. As we can see, the traditional biofuels remain 60-70 per cent of the total source of energy. Traditional biomass fuel remains an excellent fuel source for cooking and heating across many low-income country households. From the report of the World Bank, only 7 per cent of the world's low-income people is able to use clean fuels and technologies for cooking, and the average rate in Sub-Saharan Africa was 13 per cent, with also approximately one-third in South Asia still use biomass fuel mainly. For different kinds of remaining renewable energy, hydropower is responsible for almost one-quarter of renewable consumption, while the other renewable energy occupied a small part of the amount. It is a challenge and also a chance for us to promote the renewable energy occupancy rate of the power consumption.

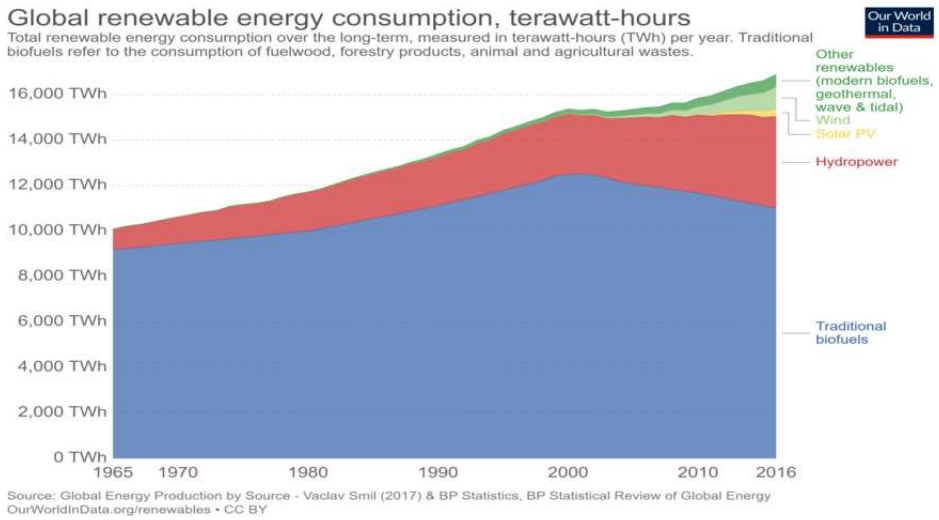

Figure 1.1: Global energy in long-term [3].

To sort renewable energy in greater detail, as shown in Fig. 1.2 [4], we can see different forms of energy are being used in our daily life. They are not limited to uses for application like food industry, personal devices, transportation sectors, and medical devices.

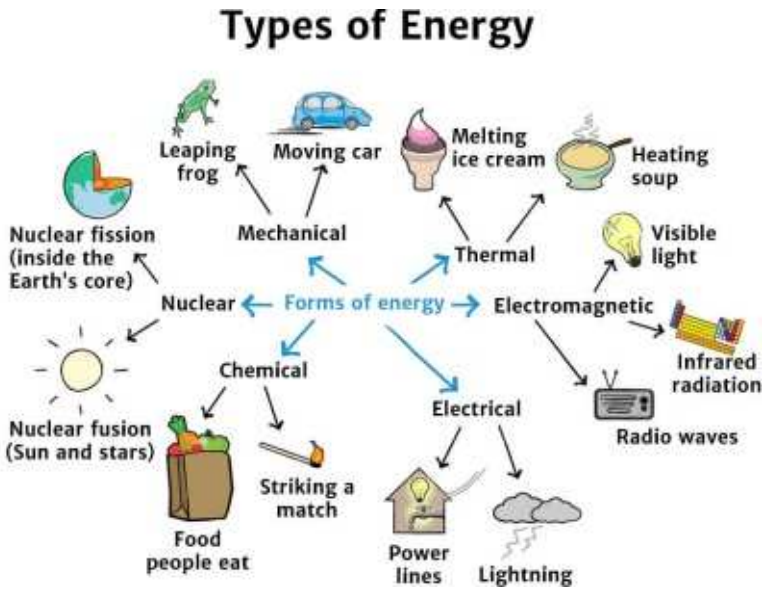

Figure 1.2: Energy resources in our life [4].

1.1.1 Energy sources

There are many different kinds of energy sources for wireless EH, and they will be discussed in the following in sequence.

Photovoltaic energy harvesting

In this part, we review the basics of photovoltaic energy and consider the optimal power user under different conditions.

The most commonly used renewable energy is the photovoltaic (PV) energy, which converts solar/light to electricity using semiconductor materials shown in Fig. 1.3 [5]. It can serve as the main power source to both outdoor and indoor uses. The indoor powering is through the windows with artificial light sources to any stand-alone electronic systems. For outdoor environment, the sun can provide around

Figure 1.3: Photovoltaic Energy [5].

100 mw/cm^2 power density of optimal situation, and the number can be reduced to 10 mw/cm^2 in a cloudy day, and around 0.5 mw/cm^2 in most well-lit indoor rooms. The efficiency of typical solar cells ranges of 5% to 20%, which means the energy loss is around 80% to 95% through the transmission. There are two main losses: intrinsic loss and extrinsic loss. The best PV device, concentrator' cells are designed to operate up to 40% efficient power. The efficiency is much less for indoor operations, where the indoor light energy can provide enough low power densities for applications like wireless sensor nodes [16–18].

It is also employed for isolated outdoor systems like weather stations, traffic boards, and outdoor lights. PV power generation has the advantages of zero pollution, reduced cost [19] (2019), increased reliability, and increased power efficiency [20, 21].

However, a major problem of PV systems is the power loss at 10-25% without direct sunlight, and there is no reliable tracking system to maintain the harvesting operation all the time [22]. Ambient environments like dust, clouds, and obstructions will also affect power output. Besides, the concentration of the production in the hours do not match the human peak activity, as compared to the primary insulation [23], which means electricity needs to be stored for later use with other power storage devices.

Kinetic energy harvesting

Kinetic EH involves converting mechanical energy into electrical power. Normally, kinetic energy is presented as vibrations, motion, stress, pressure, or forces, which converts into electrical energy by using electrostatic, piezoelectric, and electromagnetic mechanisms, as shown in Fig. 1.4 [6]. The vibration activities can be detected

in applications content household goods, moving structures, industrial plant equipment, and civil constructions like bridges and buildings. [24] The vibration energy can be achieved from different amplitudes and frequencies. For instance, human movement activities can provide low-frequency and high-amplitude energy. [25, 26] The various electrical energy which is generated by these cases also need to consider the quantity and number of kinetic energy available in our daily life. Both the efficiency of the generator and the power conversion electronics need improvements.

Kinetic energy is usually harvested from a range of applications such as human-based, industrial-based, transport-based, and structural-based. As such, a major challenge is that the kinetic energy harvested from different generators are not the same, hence makes the energy harder to store and use.

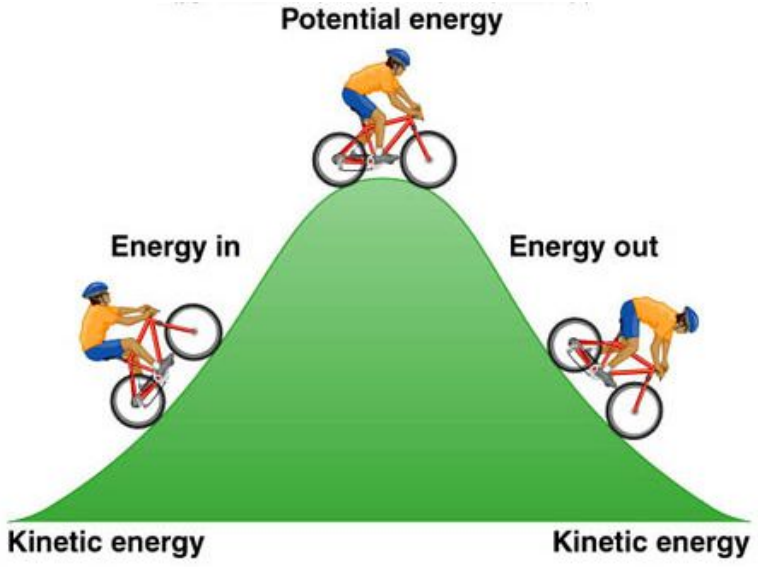

Figure 1.4: Kinetic Energy [6].

Thermoelectric energy harvesting

The thermoelectric energy is universal and can be found anywhere on the Earth. In the 1800s, Thomas Johann Seebeck discovered the phenomenon named 'Seebeck effect'. The Seebeck effect says that the temperature gradient between two conductors connected together can generate electricity [27], as shown in Fig. 1.5 [7].

For examples, there are lots of wasted heat from human body, radiators,

geothermal, and industrial processes. All the temperature differences can provide thermometric energy. By using thermoelectric generators to convert heat energy to electricity is known as the thermoelectric EH. This technology has been widely applied in the energy supply area. The thermoelectric generators can help harvest wasted energy, reduce CO2 emissions, and improve energy efficiency. The transformed electricity can be used to promote autonomous systems to elevate the battery lifetime and capability by harvesting wasted energy from the surrounding environment. On top of that, it can charge low-cost wireless devices such as sensors and mobile phones from human body heat energy [28].

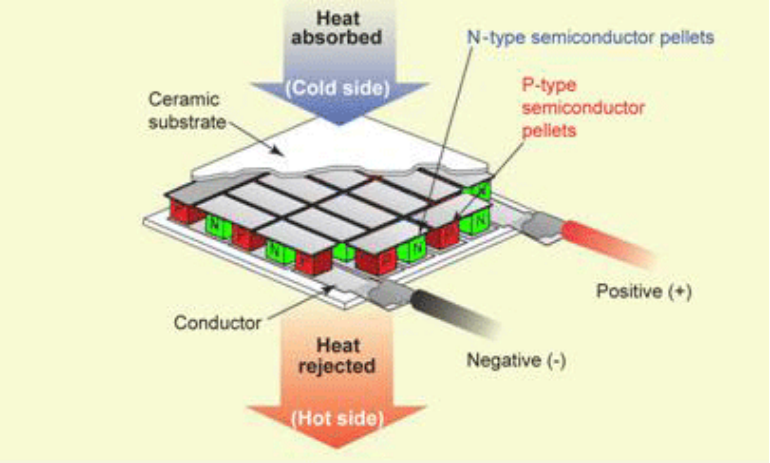

Figure 1.5: Thermoelectric energy [7].

Electromagnetic energy harvesting

The electromagnetic energy involves the use of electromagnetism to generate electricity, which has been done in the early 1930s as shown in Fig. 1.6 [8]. Since then, Faraday has made a breakthrough in fundamental electromagnetic induction. The fundamental part of the generators used today is based on rotation. Several applications have been developed from the large-scale generation of power in cars, and smaller scale in mobile phones to recharge the battery. Electromagnetic generators can also be used to harvest micro- to milliwatts levels of power using both rotational and linear devices, as long as a generator is correctly designed and not constrained in size. They can be extremely efficient converters of kinetic energy into electrical. Attempts to miniaturise the technique using micro-engineering technology to fabricate a generator, however, constantly reduce efficiency levels considerably. This part

introduces the fundamental principles of electromagnetic induction before exploring the scaling effects that work against successful miniaturisation. Conventional discrete magnets and coils are compared with their micro-machined equivalent, and the technical challenges of associated with micro-coils and deposited magnetic materials are highlighted. The part concludes with a comprehensive and up to date review and comparison of energy harvesters realised to date. The generators presented display many of the issues previously discussed.

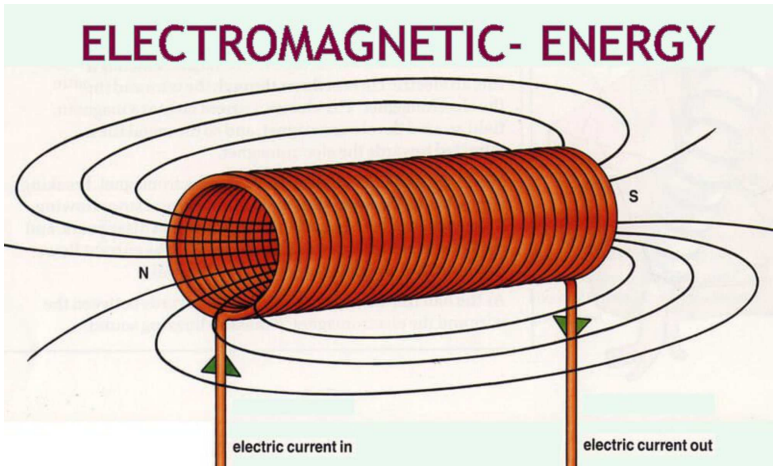

Figure 1.6: Electromagnetic energy [8].

Radio Frequency energy harvesting

Nowadays, RF has fully covered our daily life, such as cellular signals, Wifi signals, and radar signals. [29] RF represents an electromagnetic frequency that can be radiated into space shown in Fig. 1.7 [9]. The frequency range is from $300KHZ$ to $300GHZ$. RF is a kind of current, which is a grand sum for high-frequency AC to electromagnetic wave. The low-frequency current is the current changes for less than $1000times/per$ second. The high-frequency current is the current that changes for more than 10000 times/per second. Therefore, the RF is the higher frequency band of high frequency, and the microwave frequency band is the higher frequency band of RF. RF technology is widely used in wireless communications like telephones, radars, *etc.*.

The RF EH converts the energy from the source, ambient or dedicated RF transmitter into electricity, which is used to drive autonomous wireless devices. Be-

cause of the characteristics of coverage area and wirelessness of the radio waves, and also the prolonged lifetime of the low power devices for sustainable operations, RF EH is the most reliable energy source. It is also suitable to use the same signal for both power transfer and decoding information at the same time, which significantly promotes the efficiency of signal transmission as described in the following paragraphs.

It is observed that EH brings a new solution to the wireless communications problems, which allow the intermittency, infinity, and flexibly of the available energy. It also introduces the possibility of EH incorporated with the relaying nodes in wireless networks.

All wireless devices have power problems, resolved by either charging with cables or replacing batteries. Therefore, RF EH is a useful supplemental energy source to reduce the maintenance cost [30]. In various harsh environments or remote places, the devices such sensor nodes can use RF EH as energy provision [31]. It can even be used for embedded wireless devices in the human body, such as a cardiac pacemaker, which is difficult to replace or charge the battery. The replacement surgery will cost extra burden to the patient. In this case, RF EH is the best operation. RF EH can significantly improve wireless communication systems.

The average power density of ambient RF power is typically between 0.2 nw/cm^2 and 1 uw/cm^2. The quantity is smaller than other energy sources mentioned previously. Hence, it will be mainly used in low-power wireless sensor networks. In [32], measurements of the RF energy harvested from the GSM uplink from 880 to 915MHz in UK noticed that the input power was changing with both time and frequency. In order to fit the regression methods, a more advanced wavelet method was proposed to model the average RF ambient energy [33].

The power density of dedicated RF sources for close-field transfer can be around watts or tens of watts, with the power efficiency is more substantial than 80% [34], it is capable to power up most remote devices. Meanwhile, the power density for far-field transfer depends on the distance between the launcher and the user terminal, which regularly can be between 5% to 60%. In [35], the authors found the receiver can get milliwatts of energy when 1 Watt energy is sent from the transmitter $10m$ away. Besides that, the RF will also be influenced by the environment.

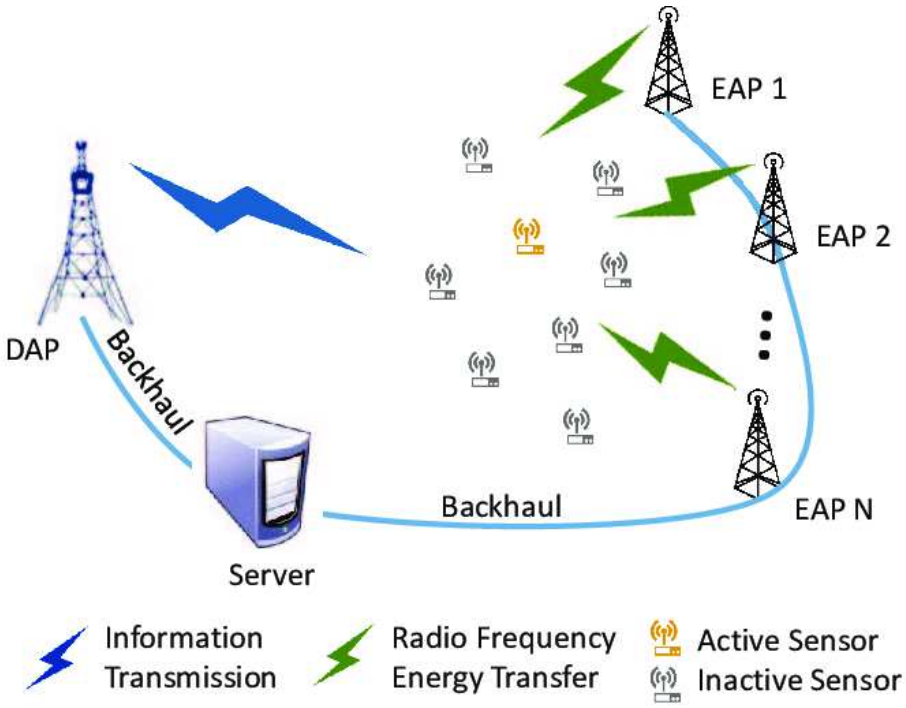

Figure 1.7: Radio frequency energy transfer network [9].

1.1.2 Energy harvesting devices

Photovoltaic energy harvesting devices

Photovoltaic solar cells provide the most common replace energy, and are probably the most regularly employed energy devices. Multiple types of researches and studies have been done on Maximum Power Point Tracking (MPPT) algorithms to collect as much energy from a solar source as possible. The PV can provide energy not only for outdoor wireless systems operating but also can support indoor system as long as there is light. Consider applications with PV energy, many devices like sensor nodes, roof panels, traffic boards, and satellite panels are powered by solar. From the past measurement, the sunlight energy gets to the surface of the Earth can expect with a density of $100mW/cm^2$. With the change of different environments, the solar energy density changes as well. For example, the power density is around $10mW/cm^2$ on cloudy days, and for an indoor room, it is roughly near $0.5mW/cm^2$.

A popular application is PV cell. It is an electrical device that converts the energy of light directly into electricity by the photovoltaic effect, as shown in Fig.

1.8. [10] The fundamental forms of single-junction silicon solar cell will produce a maximum voltage of approximately 0.5 to 0.6 volts. [36] The efficiency of the PV cell is commercial with a range from 5% to 35.9%. The world record one-sun efficiency reaches 35.9%, through dual-junction device mechanically stacked with a Si solar cell. [37]

This means that there are 65% to 95% solar energy wasted between transmission. Thus, for sunny days, around $5 - 35.9mW$ power will be available for wireless systems with a dimension of $1cm^2$. The power loss is usually caused, when the cells with a high fill factor have a low equivalent series resistance and a high equivalent shunt resistance, which makes less of the current given by the cell is dissipated in internal losses. Besides, situations like surface recombination, shading, incomplete absorption, and surface reflection will cause extrinsic loss [38].

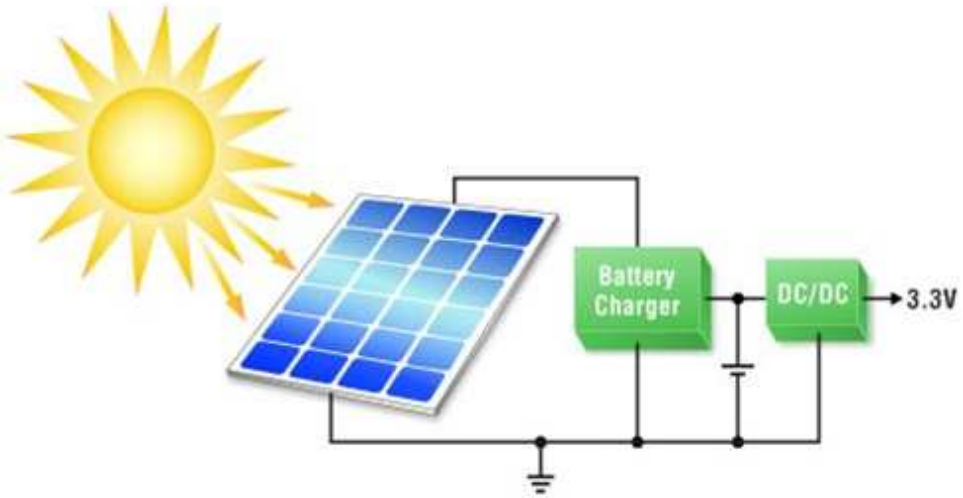

Figure 1.8: Photovoltaic energy transfer network [10].

Kinetic energy harvesting devices

The piezoelectric effect will convert mechanical strain energy into electrical energy, as shown in Fig. 1.9 [1]. The strain can be achieved from many sources: low-frequency seismic vibrations, human motion, and acoustic noise, for some examples. Most piezoelectric energy sources can produce power density in milliwatts, which are only suitable for low-power devices such as self-winding wristwatches. They are also suitable for micro-scale devices. The piezo energy harvester was first investigated

as an emerging energy since the 1990s in [39, 40].

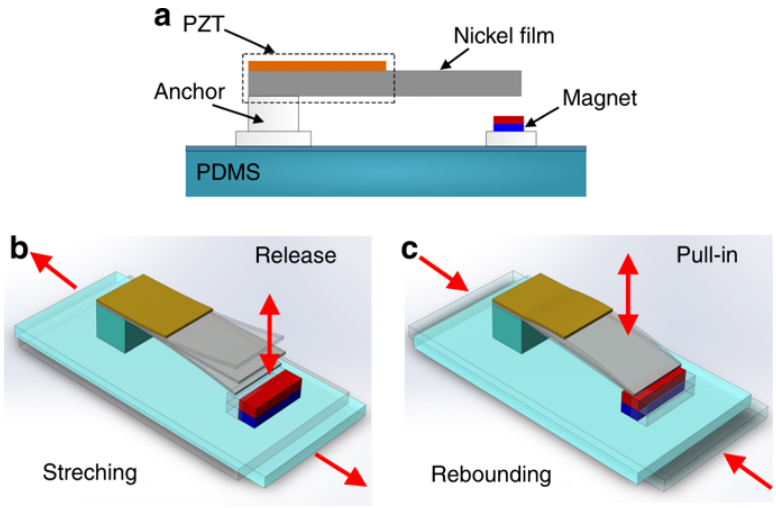

Figure 1.9: Kinetic energy harvester [1].

From Table. 1.1 [1], we can see for different types of piezoelectric harvesters with different power efficiency, has a range from 0.006% to 0.39%.

Thermoelectric energy harvesting devices

Thermoelectric is also very prevalent in our life. The thermoelectric generator also called a Seebeck generator shown, as shown in Fig. 1.10 [11]. It is a device that converts heat flux directly into electrical energy through a phenomenon called the Seebeck effect. Because of the unlimited power density of thermoelectric energy source, thermoelectric will have wider application areas.

The thermoelectric generator works like heat engines, but it is more expensive and less efficient. [47] The efficiency of the thermoelectric generator is ordinarily in a range of $5 - 8\%$. Moreover, compared to the traditional devices used bimetallic junctions, the more advanced materials were developed in the past years, such as bismuth telluride (Bi2Te3) proposed in [48], lead telluride (PbTe)developed in [49], and calcium manganese oxide (Ca2Mn3O8) introduced in [50].

Table 1.1: Energy conversion efficiency of various types of piezoelectric raindrop kinetic energy harvester [1].

Authors	Type of harvester structures	Water drop D or m v or h	Harvested energy /Kinetic energy, E/ Ek	Conversion Efficiency $\eta E = E/Ek$ 100%
R. Guigon [41]	Bridge (PVDF)	D=3 mm, v=4.5 ms-1	147nJ/0.143 mJ	0.1 %
		D=1.6 mm v=3.2 ms-1	16nJ/0.011mJ	0.146 %
V. K. Wong [42, 43]	Cantilever (bimorph PZT)	LSR	$*6.5J/1.96mJ$	0.33 %
		MSR	$*12.625J/3.92mJ$	0.32 %
		HT m=47.7 mg v=3.7 ms-1	$*23J/5.88mJ$	0.39 %
M. Al Ahmad [44]	Cantilever (5 layer PZT)	m=0.23 g v=3.43 ms-1	0.08J/1.353 mJ (75 drop /s)	0.006 %
			1.739J/1.353 mJ (at 200 drop/s)	0.128 %
S. Gart [45]	leaf cantilever (PVDF)	D=21.73 mm	23nJ/62J	0.037 %
Ilyas [46]	Cantilever (PVDF)	D=4 mm, v=2.13 ms-1 E=0.5(0.0335) v2 =27.4J76J	85 nJ/76J	0.11 %

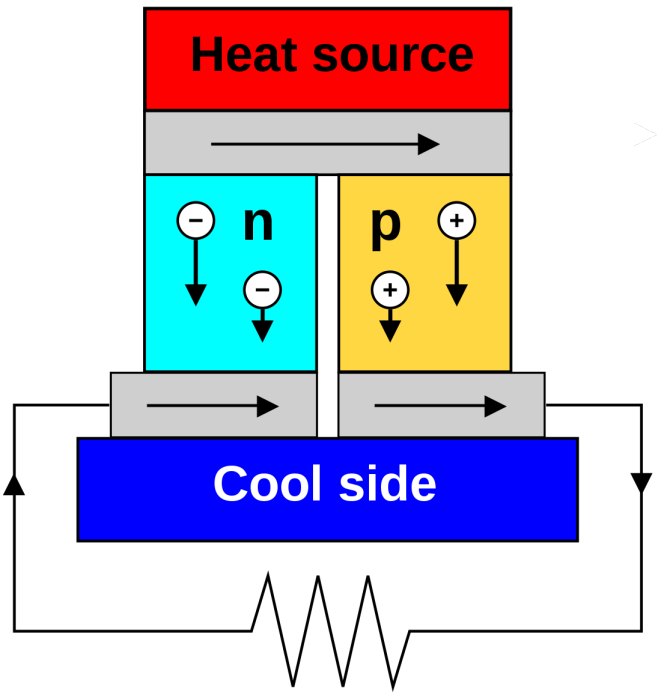

Figure 1.10: Thermoelectric energy harvester [11].

Electromagnetic energy harvesting devices

The electromagnetic harvester converts the electromagnetic radiation into electrical current or voltage, as shown in Fig. 1.11 [12]. There is a large amount of electromagnetic energy in the environment because of widely used radio and television broadcasting now. For electromagnetic induction wireless charging, there are various applications like a rechargeable torch, electric shaver, and lights. The efficiency has a range of 80% to 95%, which can charge devices effectively. Thus, there is wireless charging technology with electromagnetic induction for low power and resonance charging for high power, which is used to charge phone and vehicle, respectively. There are essentially five standards for wireless charge technology: Qi standard [51], Power Matters Alliance standard, A4WP standard, iNPOFi, and Wi-Po. However, because the long-distance high-power wireless magneto-electric conversion costs too much energy consumption, the electromagnetic harvester can barely be used for short-distance EH.

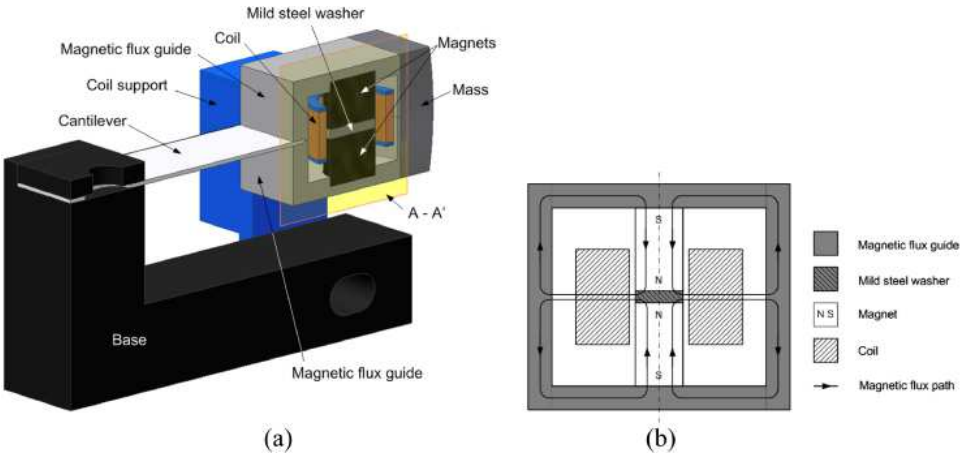

Figure 1.11: Electromagnetic energy harvester [12].

Radio Frequency energy harvesting devices

The RF energy harvester will convert the energy from the source, dedicated RF transmitter, and ambient RF into electrical energy, as shown in Fig. 1.12 [13]. From the other side, most of the wireless devices depends on radio waves for information transmission, this feature makes it beneficial to use the same radio signal for both information and EH at the same time, the details of which will be discussed in Chapter 3.

The total quantity of RF power density based on different types of energy sources have been discussed before. Most of the RF harvester includes an antenna, matching circuit, rectifier, charging circuit, and battery. It is called as "rectenna" in many works.

The antenna is an essential part of the harvester, which grabs the electromagnetic waves from the environment as the first step. It is an interface between the environment and the energy harvester. The different antenna types can be defined base on frequency band, antenna gain, polarisation, physical dimension, or application area. The design of single-band, multi-band, and broadband antennas can be used for RF EH systems. [52] Multiple antennas will be capable of increasing more potential power for harvesting [52–55], and this may enhance the RF-DC conversion more efficiency [54]. The multi-band RF energy harvester can achieve around 15% more than single-band in this scenario.

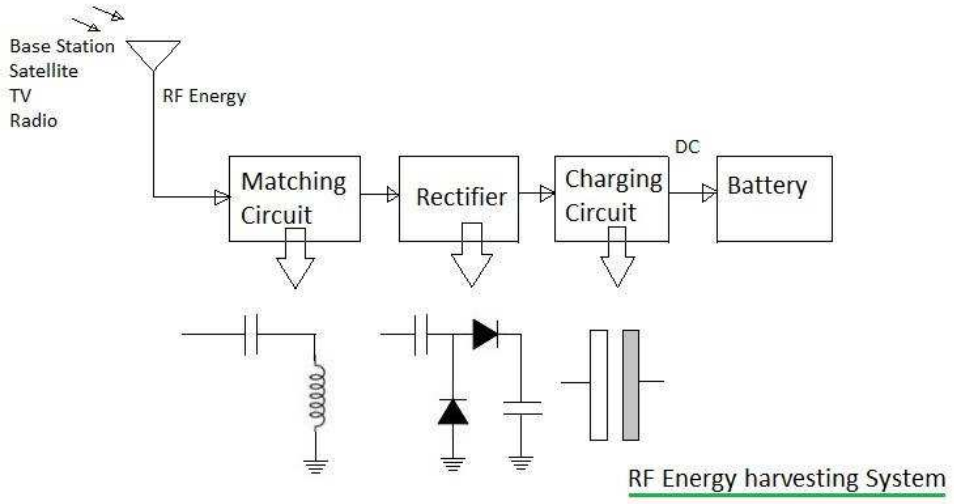

Figure 1.12: Radio frequency EH technology [13].

The marching circuit usually designed from a combination of resistance, inductor, or capacitor. It is used to match the impedance of the antenna and rectifier.

The rectifier is a circuit that converts RF or AC power to DC power. It is the central part of the RF energy harvester, which has a major impact on efficiency. Numerous studies have been done on rectifiers in [56, 57].

Then, the charging circuit must be used, because the output DC voltage level of the rectifier may not match the device. In order to avoid an accident, a DC-to-DC voltage convector circuits need to be applied, such as, voltage multiplier, and voltage booster, which are helpful to raise the output voltage level from the rectifier.

Eventually, batteries are commonly used as a energy storage alternative of super-capacitors, which utilised as a rechargeable power source in the energy harvester.

The comprehensive types of EH efficiency can be seen in Table. 1.2 [2].

EH wireless communication can be used in multiple exciting areas for different applications. The main application is to utilise EH technology into wireless sensor networks for energy support, which are studied in [71]. Since most of the sensors are designed with low-data-rate and low-power, EH can be beneficial for these

scenarios. These applications can principally use RF energy to power low power devices. For example, for those sensors embedded in buildings or human body with low-capacity battery. In [72], the authors using EH as a power supply for electrical devices. In other applications, a dedicated wireless power transmitter can be applied for wireless EH, such as in [73] where the application for cellular communications was studied. Furthermore, the development of fifth-generation (5G) mobile communications system brings us more opportunities to develop EH technology.

EH can be used for 5G to develop new communication networks. Recently, 5G network is expanding rapidly, a development that may provide critical support for cellular communications, vehicular communications, and the Internet of Things. In those cases, EH is an essential technology for wireless sensor networks. For example, in [74], an integrated energy and spectrum harvesting mechanism for 5G networks has been studied, where the spectrum harvesting was applied to cognitive radio (CR) using the RF ambient energy opportunities to support wireless communication. They considered a multi-tiered network with the efficiency of the spectrum and EH on device-to-device (D2D) communications. Numerical results show that spectrum and EH likely improve the efficiency of the network.

EH may also be used for 5G cellular network. The necessity of using EH to improve the energy efficiency of 5G systems has been investigated in [75], and various vital technologies and challenges were considered. In [76], the results show that in 5G service, which does not have rigorous requirements on reliability or QoS, the power can be harvested from RF ambient sources. For those 5G services require QoS, the authors gave a solution in [77], by proposing dedicated RF power transmitters to supply energy, so that the RF energy would always be available when requested.

For the EH used for non-orthogonal multiple access (NOMA), the NOMA users are powered by EH to send the data packet in 5G networks, as related works presented in [78].

EH could also be useful for millimetre waves, by combining EH and millimetre waves to improve the harvest efficiency, this particular ideal has been studied in [79].

Since relaying networks are widely used nowadays, it can also be used in various communication systems, because of functional reliability. There are many other interest applications of EH that can be expanded in the future.

1.1.3 Wireless relaying

Nowadays, the concept of relaying has been studied as an effective solution to provide extra coverage, enhance the reliability and improve the quality of service (QoS) in the conventional wireless signal transmission [80]. Relaying technology is a major area that forwards signal from the source to the destination across one or more idle nodes antennas. In contrast, the source in traditional systems sends a signal to the destination directly via one hop. That gives many applications in the electronic, environment, vehicle and communications fields.

Decades years later, the concept of wireless network was first prototyped under the brand ALOHAnet by the scientist Abramson Norman in 1969 at the University of Hawaii and became operational in June 1971 [81]. The relay channel was discussed comprehensively by E. C. van der Meulen in [82–84], where he considered the problem of transmitting information and followed with solutions for sending information. The concept of T-terminal was then proposed, which provided excellent guidance for time-switching (TS) channel protocol [85, 86].

For the second-generation (2G) digital cellular networks, the Global System for Mobile Communications (GSM) was first deployed in Finland in December 1991 [87]. It was a standard proposed by the European Telecommunications Standards Institute (ETSI) to depict the protocols for mobile devices.

Furthermore, CDMA (Code-Division Multiple Access) was proposed to any of the protocols used both in second-generation (2G) and third-generation (3G) wireless communications. CDMA is a form of multiplexing, which allows numerous signals to occupy a single transmission channel, thus optimizing the use of available bandwidths [88].

This case has been used in many applications, such as in LTE-Advanced as an imperative technique [89] for the fourth generation (4G) and fifth generation (5G) standards in wireless communications [90].

A typical cooperative wireless relaying system includes three nodes: the source, the relay, and the destination. The fundamental system is shown in Fig. 1.13 [14]. The source terminal generates information to be delivered to another node; the relay terminal helps to send information from source to the destination; the destination terminal is the node that aims to receive information from the source. The wireless relay system has two main benefits: extended coverage and improved

throughput. The relay node can not only communicate with the relay but also communicate directly with the destination node, which can provide the same extra signal at the destination. By merging these data together, the diversity gain can be achieved through shadowing or fading. For the signal coverage extension purpose, the direct link between the source and the destination does not exist because of the long-distance and obstacles. In this case, the relay can support to stretch the signal either in the transmission distance or obstacles. This can improve the reliability and capability of the wireless system.

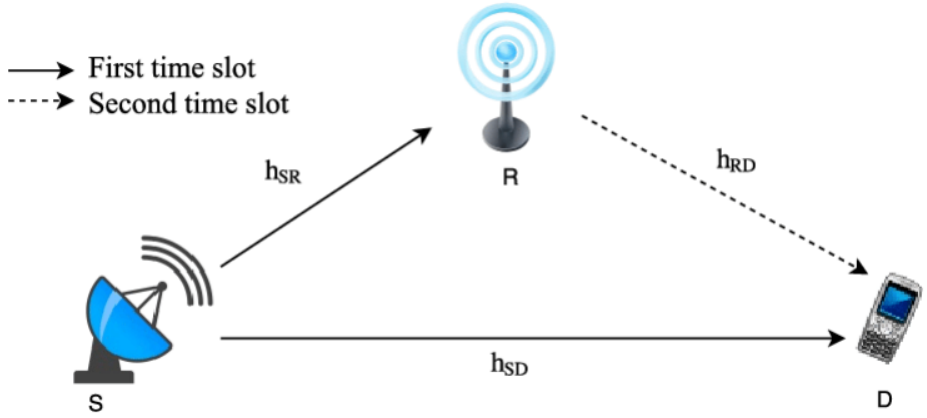

Figure 1.13: Cooperative wireless relaying system [14].

1.1.4 Relaying protocols

There are lots of relaying strategies proposed in the last few years. The signal relaying system contains two protocol ways: amplify-and-forward (AF) and decode-and-forward (DF). AF is a protocol that applies its received signal while maintaining a fixed average transmit power, which the relay amplifies the signal from the source and forward them to the destination in the second hop. DF is another forward protocol that decodes and re-encodes the received signal, before forwarding it to the destination. [91–94] Therefore, AF relaying can be seen as an analogue method, while DF relaying was as a digital method.

This signal processing at the relay is also known as making a challenge, as the information sent by the relay does not include any additional information about the reliability of the source-relay link.

Comparing the performance of these two kinds of relaying systems, DF has a complex calculation function, while AF relaying is more straightforward with identical performance. Therefore, this thesis focuses on applying AF protocol as the fundamental relaying to forward signal. ‘

1.1.5 Energy harvesting relaying

The current relay node uses its self-power to forward the information from source to the destination, which will not affect the infrastructure relaying with unlimited power support, but may interfere the signal efficiency in wireless relaying [95, 96]. Considering most wireless relaying is achieved between users, such as destination-to-destination (D2D) used for cellular network and vehicle-to-vehicle (V2V) technology for vehicle network. In these cases, they are all powered by batteries, and relaying will reduce the battery life by assassinating others [97, 98]. Thus, the limited capability of the battery is a big concern which leads to low signal transmission efficiency [99]. Hence, a solution is necessary for further improvement.

EH is an excellent solution to this kind of problem, which collects a certain value of energy from the source node at the relay and use the harvested energy to deliver information from the relay to the destination, instead of using its self-power at the relay. It can lessen the effect on the energy expenses incurred at the relay, and this technique can provide additional energy to maintain the system performance [30].

Moreover, EH does not only work on the system which the source transfers energy to the relay but also suitable for networks applying EH [79, 100–102]. For different types of communication network, there are various types of EH relaying systems, which harvest energy from the ambient, dedicated power transmitter, and the source.

The details of different EH systems will be discussed further in Chapter 2.

1.2 Open issues and challenges in energy harvesting

Those energy resources mentioned earlier, like solar and wind, are unpredictable and are easily affected by the environment. It is a problem as wireless devices

require stable power connections for data transmission and processing. Due to the RF coverage and limitation of battery capability, the efficiency and ability of wireless devices will be affected. In this thesis, we examine the situation in which RF energy is used as the power source to supply wireless devices. EH in relaying will harvest some energy from the source, and uses the harvested energy to forward the signal to the destination. Both the energy from the source and ambient will be considered in this thesis. In most scenarios, the relay uses its own power to spectrum resource to transfer the information to the destination. The fluctuation of wireless communication channel is always more substantial and dynamical than the EH rates, and channel fading is the main challenge through designing a satisfying and reliable wireless communication system.

In this section, the challenges of EH relaying are described in details as follows.

1.2.1 Challenges toward channel fading

For reliable wireless EH relaying communications, channel fading is one of the foremost challenges we need to handle. Conventionally, in the relaying system, the source sends the signal to relay in the first hop and then the relay forward signal to the destination at the second hop. The channels are assumed to be a Rayleigh fading channel, as the fading channel gain needs to be studied for the performance of the system model. Following the estimated fading channel gain, we will be able to derive the Signal-to-Noise Ratio (SNR) expressions with details.

Since the fading channel is the attenuation of a signal with various variables, therefore, fading is usually a random process. It is essential to analyse the fading channel gain for SR and RD links separately. In this thesis, we assume all fading channel coefficients are complex Gaussian random variables with zero mean and variance of $2\theta^2$.

In the former end-to-end SNR calculation, the first step is to observe the SNRs for the SR link and RD link, and then uses these two values to calculate the result for end-to-end SNR. The SNRs for the SR link and RD link are usually calculated independently, it is a challenge to present them in a combination expression. In my thesis, we derived the expressions to estimate the fading channel impact, which will be combined and considered into the end-to-end SNR expression. Eventually,

we can get a full expression which contains the estimated fading channel gain of SR link and RD link. However, one of the main challenges is fading channel coefficients estimating.

1.2.2 Challenges toward the power allocation

In order to fix the channel capacity, it is essential to use channel resources optimally. Therefore, because of the limitation of a fixed channel size, optimal power allocation is required to improve the efficiency of data transmission. Typically, the relaying system includes one source, one relay, and one destination. The data packet from the source to the relay and the data packet from the relay to the destination which contains two parts: channel estimation and information. However, to conduct EH, we have to distribute a part of the channel resource. It brings a challenge on channel resource allocation among channel estimation, information decoding, and EH. In most cases, when the communication system involves EH, it is necessary to rebuild the system model.

1.3 Motivation of this work

EH in communication system has been extensively studied in recent years. While most of these researches are detailed, there are still some concerns such as the optimum channel structures, the expansion functions of the system, and the optimal power allocations. Therefore, for studying RF EH, those problems need to be recognised and solved, which is the primary motivation of this research.

First of all, current EH studies mostly focus on simple EH from the ambient or dedicated RF power source [22]. In [103], the authors considered the problem without data transmission. For a full-featured EH system, we need to analyse data transmission and EH simultaneously. The data packet includes channel estimation, EH, and data transmission at the same time. Because the channel has a fixed capacity, optimization of the distribution of these resources is a fundamental problem. We will discuss it in details in this thesis.

Secondly, there are two EH protocols already proposed in [80]: TS protocol and PS protocols. Such as in [104], researcher have considered the TS and PS independently. However, these existing channel structures are not comprehensive enough

for all scenarios, which lead to an inspiration to merge two EH protocols into one channel. The system model plays a vital role in the EH efficiency and performance analysis, and an optimal structure model can adjust the system performance in EH communications. Numerous of EH structures were proposed in previous works, but the accuracy of these schemes were not perfect. More advanced EH structures are developed in this thesis.

Thirdly, regarding the broadcast channel in the relaying communication system, the current EH channel scheme in relaying system is not satisfactory [105–108]. There are many impairments like noise, fading, interference, and contributing errors in the wireless channels, which can affect the signal transmission. It is necessary to analyse the received signal through transmission from the source to the user terminal. A new design of the system channel is needed for the EH wireless communication systems.

1.4 Research objectives

The thesis focuses on designing the EH channels and estimating the relaying communication system performance, which is devoted to seek for the optimal EH channel scheme. Information decoding is considered in these novel schemes, so that they can not only harvest energy but also transmit data symbols at the same time. It is the first time that channel estimation, EH, and data transmission are considered concurrently.

Furthermore, to enhance the energy efficiency of the EH relaying system, the power allocation of different schemes are analysed with their performance. The aim is to seek the optimal EH scheme in AF relaying system.

The detailed description of the principal research objectives are shown below, which contains the following four parts: Correlated Uplink and Downlink analysis (which is similar to SR link and RD link): The performance of wireless powered communications (WPC) is evaluated in terms of achievable rate (AR) and bit-error-rate (BER), for applications where the downlink and the uplink are correlated, in contrast to previous works that only assume independent uplink and downlink. Semi-closed expressions for the achievable rate and series expressions for the BER are derived in Nakagami m fading channels, and the effect of link correlation is examined.

TS EH in AF relaying analysis: In EH relaying, channel estimation needs to be performed to acquire channel state information at the relay and destination. Thus, the data packet from the source to relay contains three parts: pilot for channel estimation, data symbols, and pilots for harvesting. The data packet from the relay to destination contains two parts: data symbols and pilots for estimation. In this part of work, for a fixed packet size, the outage and bit-error-rate performances are analysed and then optimised concerning power allocation between different parts in the data packet. The cumulative distribution function (CDF) of the end-to-end Signal-to-Noise Ratio is derived in closed-form, based on which the outage and error rate can be calculated.

Combination EH protocols analysis: Three novel structures using simultaneous wireless information and power transfer in EH AF relaying are investigated. Different combinations of TS and PS EH protocols are studied. Three dynamic schemes are proposed as channel estimation power splitting (CEPS), data transmission power splitting (DTPS), and Channel Estimation Power Splitting (CPS). From source to relay (SR) in these schemes, the data packet includes three parts: channel estimation, data transmission, and EH. From relay to destination (RD) in these schemes, the data packet includes two parts: data transmission and channel estimation. Closed-form expressions for the CDF of the end-to-end Signal-to-Noise Ratio of these three structures are derived. By using these expressions, achievable rate and bit-error-rate are derived. Different parameters are examined afterwards.

Additional ambient EH analysis: Based on the EH structures proposed in Chapter 5, the ambient RF energy has been taken into account, which improves these three new schemes as ambient channel estimation power splitting (ACEPS), ambient data transmission power splitting (ADTPS), and ambient combination power splitting (ACPS). The closed-form expressions for the CDF of the end-to-end Signal-to-Noise Ratio for these three schemes are derived. By using these expressions, the achievable rate and bit-error-rate formulations are derived, and various parameters are examined to obtain the optimal resource allocations.

1.5 Thesis outline and contributions

This thesis have been organised as follows.

Chapter 2: Literature review and state of the art. In this chapter, the

architecture of the EH relay system is presented; the components which are used for channel estimation are discussed, and the previous works on uplink and downlink are studied; the RF energy types are presented in details; and the previous works on EH structure design are also investigated.

Chapter 3: The WPC with correlated uplink and downlink. In this chapter, the performance of wireless communications is assessed in the ways of bit-error-rate and achievable rate, where the uplink and downlink are correlated. The contributions of this chapter are given as follows:

It is the first time that WPC is presented with the correlated downlink and the uplink due to fast fading Nakagami m channels. The Jakes' model is used to describe the correlation between different links.

Based on the system model, the semi-closed expressions for the achievable rate and series expressions for the BER are derived. By using these expressions, the effect of link correlation on the system performance is examined by comparing it with that of a system assuming independent links.

Chapter 4: The TS EH in AF relaying system. An AF relaying system with pilot-based channel estimation and TS EH is presented in this chapter. The performance is analysed in terms of outage probability (OP) and bit-error-rate. The contributions of this chapter are as follows.

The AF relaying system with pilot-based channel estimation and TS EH is designed in this chapter. The CDF of the end-to-end Signal-to-Noise Ratio is derived. Using this, the outage probability and the bit-error-rate are calculated. Moreover, the performance is compared under different parameters. The system with an unequal ratio between the number of pilots for channel estimation and EH is also investigated.

Finally, the optimal allocation between the three parts of the data packet in the first hop and the two parts of the data packet in the second hop is analysed under different scenarios.

Chapter 5: Three novel schemes with two EH resources. In this chapter, three novel structures using simultaneous wireless information and power transfer in EH AF relaying are investigated. The system performance is investigated in regard to the achievable rate and bit-error-rate. The contributions of this chapter

are given as follows:

It is the first time three dynamic schemes are proposed as channel estimation power splitting (CEPS), data transmission power splitting (DTPS), and combination power splitting (CPS) in AF relaying. Both information decoding and EH are considered at the same time. The CDF of the end-to-end SNR for the three novel EH structures are derived in this chapter. The performance in terms of achievable rate and bit-error-rate is analysed and compared with the power allocation.

Finally, by using the achievable rates and BER results obtained from simulation analysis, the comparisons between the pilots of channel estimation and EH are discussed. The simulation results can provide us the optimal power allocation.

Chapter 6: Three novel ambient added EH schemes. In order to examine the efficiency of ambient RF energy, based on the EH structures designed in Chpater 5, the ambient RF added EH structures are designed. At the relay node, both the energy from the source and RF are harvested. The performance is based on the achievable and bit-error-rate, which will be analysed for ambient energy efficiency and power allocation optimisation. The contribution of this chapter is as follows.

Based on the EH relaying models designed in Chapter 5, three ambient added EH structures in AF relaying are proposed as ambient channel estimation power splitting (ACEPS), ambient data transmission power splitting (ADTPS), and ambient combination power splitting (ACPS). Both information decoding and EH are considered at the same time.

Using the same procedures as presented Chapter 5, the CDF of the end-to-end SNR of the three ambient added EH structures are derived in this chapter. The performance in terms of achievable rate and bit-error-rate is analysed and compared to obtain the most suitable power allocation.

Lastly, by using achievable rate and BER results from the simulation analysis, the effect of ambient RF energy can be racognised as well as the best power allocation.

Chapter 7: Conclusions and further work In this chapter, full summary of the thesis is presented. The thesis research objectives are restated and discussed in details. Finally, future research directions are included in this chapter.

All the research presented in this thesis is simulated using MATLAB.

Table 1.2: Types of EH efficiency [2].

Ref.	Frequency(GHz)	Band	Conversion Efficiency(%)	Input Power(dBm)	Output Voltage(V)	Antenna Type	Antenna Gain(dBi)	Antenna Dim.(mm)	Topology	Load()	Diode Type
[58]	2.45	Single	83	0	1	Microstrip	8.6	80*87	Shunt diode	1400	HSMS-2852
[59]	2.45	Single	78	295.3		Patch	7.45(H)	70*70	Shunt diode	550	HSMS-2860
[60]	2.45	Single	73.9	10.4		Patch	7.63(V)	70*100	Diff. driven	1400	HSMS-2860
[61]	2.45	Single	70	3	1.6	Patch	5.47		Dickson multiplier	13000	HSMS-2852
[62]	2.45 5.8	Dual	66.8 51.5	10	2.6	no antenna	4		Series diode	1050	HSMS-2860
[63]	0.915 2.45	Dual	65 55	0 0	2.3	no antenna			Series diode	1000	SMS-7630
[64]	0.85 1.85	Dual	15 15	-20		Patch			Series diode	2200	SMS-7630
[65]	0.5-1.0 1.5-2.0 2.3-3.6	Triple	55	27		no antenna			Series diode	50	HSMS-282
[52]	0.9 1.8 2.45	Triple	45 46 25	-15		Patch	3.26 3.02 6.88	170*48	Dickson multiplier	50000	HSMS-2852
[55]	0.876-0.959 1.71-1.88 1.92-2.17 2.41-2.48	Quad	84	5.8	0.9	no antenna	6	100*100	Voltage doubler	11000	MSS20-141
[66]	0.6-1.15	Broad	80.1	39.03		no antenna			Class-F	34	
[67]	0.9-1.1 1.8-2.5	Broad	75	20		Dipole	1.8 3.5 3.3		Shunt diode	250-3000	HSMS-2820
[68]	0.9-2.45	Broad	50 68 78	-3 14 23	2.1 1.45 4.2	Patch	6	50*50	Series diode Shunt diode Bridge rectifier	2400 750 200	HSMS-2850 HSMS-2860 HSMS-2820
[69]	0.47-0.86	Broad	60	10		no antenna			Dickson multiplier	12200	SMS-7630
[70]	1.8-2.5	Broad	55	-10		Dipole	2.5-4.12	70*70	Bridge rectifier	14700	SMS-7630

Chapter 2

Background and literature review

2.1 Introduction

EH has became an essential topic in wireless communications recently, with increasing researches on both the practical and theoretical side. In this chapter, the overview of five main areas is described and organised as follows. In Section 2.2, the architecture of the EH relay system is presented. In Section 2.3, the components which are used for channel estimation are discussed. In Section 2.4, the previous works on uplink and downlink are studied. In Section 2.5, the previous works on EH structure design are investigated. In Section 2.6, the RF energy types are listed in details.

2.2 Architecture of the EH relay system

2.2.1 Conventional AF relaying

This section assumes a single antenna has been used and the system operates in half-duplex (HD) mode. The half-duplex mode has been studied in [109]. Different kinds of measurements are then examined to analyse the reliability and capacity performance of the relaying system in the next subsection. The signal from source

to destination will travel through two hops. The first hop is the channel from the source to the relay (SR), and the second hop is the channel from the relay to the destination. Assuming a total of D symbols is used for both the first hop and the second hop, each symbol occupies a time duration of T seconds. Then there is no direct link between the source and the destination.

In the first phase ($\frac{T}{2}$ seconds), the source transmits the data packet to the relay. The received signal for the first part of the packet can be expressed as [22]

$$y_r = \sqrt{P_s} h x + n_1 \tag{2.1}$$

where D is the total number of symbols in the packet, P_s is the transmitted power of the source, h is the complex fading gain in the channel between the source and the relay which is a complex Gaussian with mean zero and variance $2\theta^2$, x is the transmitted pilot symbol with unit power $E\{x[i]^2\} = 1$, $E\{.\}$ represents the expectation operator, and n_1 is the complex additive white Gaussian noise (AWGN) with mean zero and noise power N_1.

In the second phase ($\frac{T}{2}$ seconds), the signal from (2.1) will be amplified and forwarded to the destination. The AF relay was assumed to forward the data symbols from the source to the destination.

The received signal at the destination can be expressed as [22]

$$y_d = \sqrt{P_r} g a y_r + n_2 \tag{2.2}$$

where n_2 is the AWGN at the destination during this transmission, and it is a complex Gaussian random variable with mean zero and variance $2\theta^2$. a is the amplification factor which will be discussed later. P_r is the relay transmission power, g is the fading channel coefficient in the RD link which is a complex Gaussian random variable with mean zero and variance $2\theta^2$.

Following the study presented in [110], the amplification factor is determined at the relay, which affects signal transmission performance. The amplification factor can be expressed as [22]

$$\hat{a}^2_{var} = \frac{1}{E|y_r|^2} = \frac{1}{P_s h^2 + N_1} \tag{2.3}$$

which will normalise the received signal at the relay. The channel-assisted AF has

been studied in [111]. Since the value of a can be affected by the values of h as a random variable, so it is necessary to adjust the value of a before analysing, so-called variable gain AF relaying. This is the most commonly used amplification factor, which will be discussed in the following chapters.

Using the received signal in (2.2), the energy harvested by the relay can be expressed as [22]

$$E_r = \eta P_s |h|^2 D \tag{2.4}$$

where η is the conversion efficiency of the energy harvester. We assume that each symbol has an interval of $T = 1$ second for simplicity, so $P_s|h|^2$ is the amount of energy picks up by the harvester at the relay. This energy will be used to transmit symbols to the destination in the second hop from the relay to destination.

2.2.2 Conventional EH

Because the data and energy carried by the same signal can't be processed at the same time slot, the simplest way is to separate the signal into two parts: information decoding and energy transfer. Two main protocols have been proposed in [80]: time-switching (TS) and power-splitting (PS). Details of the two protocols are defined below.

Time-switching protocol

Firstly, the TS splits the signal into several time domains in [112]. During the signal transmission, by using a switch, one part of the transmission time in the received signal is used for power transfer, and another part is switched for information decoding. The most important parameter in this protocol is the TS coefficient, which has a range of $0 < \alpha < 1$. In one packet, the data transmission and power transfer have been included together with the switch. Assuming there is no loss during transmission, then the total transmission time can be fixed as T seconds. Therefore, αT seconds will be used for power transfer, and the rest $(1 - \alpha)T$ seconds will be used for information decoding. Hence, the received signal can be written as [22]

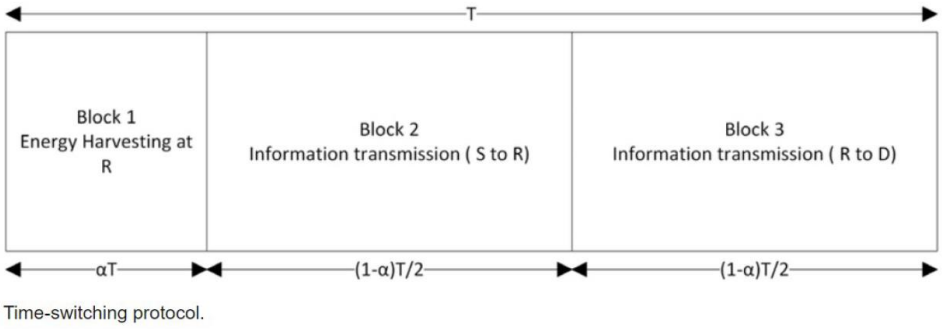

Figure 2.1: Time-switching protocol

$$y(t) = h\sqrt{P_s}(t) + n(t) \begin{cases} 0 \leq t \leq \alpha T & \text{power transfer} \\ \alpha T \leq t \leq T & \text{information decoding} \end{cases} \tag{2.5}$$

where P_s is the transmission power from the transmitter, $s(t)$ is the transmitted data symbol, h is the channel gain, and $n(t)$ is a complex AWGN with mean zero and variance $2\sigma^2$ in [113]. The harvested energy from the transmitter can be given as [22]

$$E = \eta\alpha P_s|h|^2 T \tag{2.6}$$

where η is the EH conversion efficiency from the transmitter, and $E|s(t)|^2 = 1$ assumes that all the transmitted symbols have unit power. According to the signal received for information decoding, the achievable rate can be expressed as [22]

$$C = (1-\alpha)log_2(1 + \frac{P_s|h|^2}{2\sigma^2}). \tag{2.7}$$

Afterward, the scheme can be constructed as in Fig. 2.1 [80].

Power-splitting protocol

The PS protocol makes the signal splitting in the power domain in [114]. The received signal will separate into two parts by using power splitter: one for power

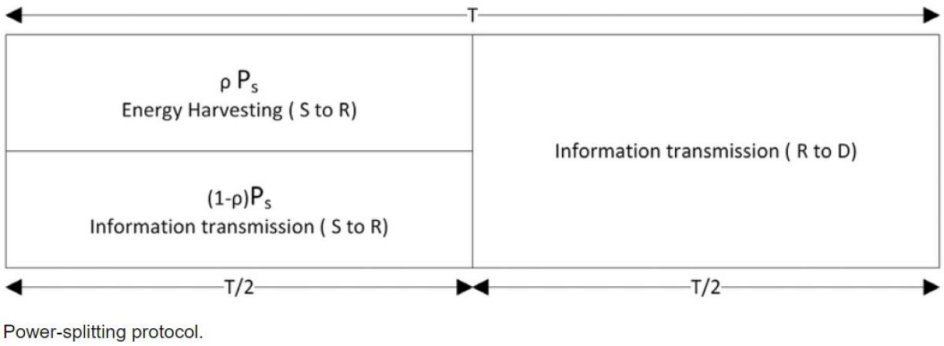

Figure 2.2: Power-splitting protocol

transfer and one for information decoding. However, EH and information decoding are processed at the same time, which is different from the TS protocol. The PS factor has a range of $0 < \rho < 1$. Therefore, the received signal for EH can be written as [22]

$$y_1(t) = \sqrt{\rho P_s} h_s(t) + \sqrt{\rho} n_a(t) + n_d(t) \tag{2.8}$$

and the received signal for information decoding can be expressed as [22]

$$y_1(t) = \sqrt{(1-\rho)P_s} h s(t) + \sqrt{1-\rho} n_a(t) + n_d(t) \tag{2.9}$$

where ρ is the power splitting factor, $n_a(t)$ and $n_d(t)$ are both additive White Gaussian noises with mean zero and variance $2\sigma_a^2$, $2\sigma_d^2$. According to the expressions above, the harvested energy can be given by [22]

$$E = \eta\rho|h|^2 T \tag{2.10}$$

and the corresponding achievable rate can be expressed as [22]

$$C = log_2[1 + \frac{(1-\rho)P_s|h|^2}{(1-\rho)2\sigma_a^2 + 2\sigma_d^2}]. \tag{2.11}$$

Then, the scheme can be constructed as in Fig. 2.2. [80]

2.3 Components in channel estimation

2.3.1 Channel models

The channel model is a fundamental part of the physical layer communication simulation [115]. It is a mathematical representation to show the influence of a wireless communication channel when signals are being processed. The channel model reflects the important characteristics of the channel medium according to the impulse response. Normally the impulse response is randomly changed over time in the wireless communication system. A brief discussion of the mathematical models is provided as follows.

Channel estimation is an essential part of the performance analysis in wireless relaying system [116]. Using known pilots have been studied for relaying systems, such as the variable gain for AF relaying, both the channel statement at the relay and destination are needed for channel estimation. Therefore, the estimators are required to estimate the channel state information (CSI), individual channel coefficients, as well as the individual channel power. For instance, in [117], linear minimum mean squared error (LMMSE) estimation was studied in details, where the instantaneous CSI was estimated at both the destination for coherent demodulation and at the relay to calculate the amplification factor. There were a lot of other works in regard to relaying channel estimation. For instance, in [117], [118] and [119], the authors designed several different types of minimum mean squared error (MMSE) estimators. Least squares (LS) estimator was proposed in [120]. Estimators for individual channel coefficients were studied in [121]. Besides, the individual channel power has been estimated by using moment-based (MB) estimators, which was created in [122]. All these estimators were designed for conventional AF relaying by sending the pilots from relay to destination using the relay's energy.

The root mean squared error (RMSE) is frequently used to measure the differences between values predicted by a model or an estimator and the values defined. In this thesis, BER and outage probability are the parameters used to compare the performance of different channel modules. [123, 124]

In [125], the authors analysed the performance in regard to BER and outage probability in the AF relaying system. They proposed two unconventional pilot-aided ML channel estimation methods in slowly fading Rayleigh channels: disintegrated channel estimation (DCE) and cascaded channel estimation (CCE). The

optimal values of pilot power at the source and at the relay were obtained. Meanwhile, the optimal power allocation for different parts of roles was obtained when the wireless power was fixed. These two methods have better performance than conventional systems in [117–119, 126].

Another investigation in [104], the authors studied various MB channel estimators for AF relaying, at the same time, harvesting energy from the source and applying the harvested energy to transmit information to the destination for channel estimation. The TS protocol and PS protocol were analysed separately. Two schemes that perform channel estimation only at the destination are worse than the two schemes that perform channel estimation at both the relay and the destination. Thus, in this thesis, we examine the channel estimation at both the relay and the destination.

As mentioned above, this problem was either considered without data transmission or without EH, hence the two parts. In Chapter 4, the data packet carries channel estimation, EH, and data transmission will be discussed in details.

In the last section, the time-switching and PS EH protocols were described comprehensively. In most of the previous studies [80,127], the harvest-use structures were used for either TS or PS, without considering different combinations of TS and PS simultaneously. In Chapter 5, the different combinations of TS and PS EH protocols will be studied.

Additive white Gaussian noise

In the existing communication models, AWGN is one of the most common model in the information theory. [128] The transmitted signal is considered for the additive random noise which can be interfered or amplified. AWGN is often a linear addition of the white noise with a constant spectral density and a Gaussian distribution of amplitudes. This model is not explained for fading, frequency selectivity, or interference. However, it provides a simple and approachable mathematical model. The AWGN channel is a useful model for many commonly used communication links. However, it is not suitable for most terrestrial links because of the multi-path and interference.

The AWGN mathematical model is

$$r(t) = s(t) + n(t) \tag{2.12}$$

where t is the time symbol, $r(t)$ is the complete received signal in communication systems, and $n(t)$ is the additive white Gaussian noise in AWGN channel of a specific channel.

However, the probability density function of the model can be presented with the mean m and variance $2\sigma^2$ as

$$f_d(x) = \frac{1}{\sqrt{2\pi\sigma^2}} e^{-\frac{(x-m)^2}{2\sigma^2}} \tag{2.13}$$

where d represents the Gaussian distribution as $t \sim N(m, \sigma^2)$.

According to the PDF expression, the CDF can be derived as

$$F_d(x) = 1 - Q(\frac{x-m}{\sigma}) \tag{2.14}$$

where the $Q(.)$ function can be defined as [129]

$$Q(x) = \frac{1}{\sqrt{2\pi}} \int_x^{\inf} e^{-\frac{t^2}{2}} dt. \tag{2.15}$$

Rayleigh Fading Channel

The Rayleigh fading is a statistical model, which can be used to measure the effect of a propagation environment with RF signal. [130] The signal usually goes through fading in channels during the signal transmission process. Its phase and envelope of the channel response will be a Rayleigh distribution.

Several different models can represent the behaviour of the fading channel. However, Rayleigh fading channel is the most fundamental and widely used one as proposed in [130]. It is a reasonable model when there are various objects in the environment due to the heavily built-up urban environments or the ionosphere and troposphere on radio signals [131]. The central limit theorem will remain when there is enough scatter, and the channel impulse responsible will be well-modelled as a Gaussian process with mean zero, furthermore, the phase evenly distributed between 0 and 2π radiant. [132]

If we assume X_1 and X_2 are two independent distributed Gaussian random variables, one has

$$C = \sqrt{{X_1}^2 + {X_2}^2} \tag{2.16}$$

where $X_1, X_2 \sim (0, \sigma^2)$ are assumed to be two identically distributed Gaussian random variables.

Moreover, the PDF of Rayleigh random variable can be expressed as

$$f_c(x) = \frac{d}{\sigma^2} e^{-\frac{x^2}{2\sigma^2}}, x \geq 0 \tag{2.17}$$

where c can be seen as the channel fading amplitude. The CDF of Rayleigh random variable is defined as

$$F_c(x) = 1 - e^{-\frac{x^2}{2\sigma^2}} x \geq 0 \tag{2.18}$$

where the instantaneous SNR per symbol can be given as $\gamma = \frac{c^2 E_s}{N_0}$, and E_s is the energy per symbol, $E(.)$ is the expectation operator, c^2 is the power for the received instantaneous signal, and have $E(c^2) = 2\sigma^2$ with the power of Gaussian noise N_0. Thus, the PDF of the instantaneous SNR can be presented as an exponential distribution, and the expression is [130]

$$f_\gamma(\gamma) = \frac{1}{\bar{\gamma}} e^{-\frac{\gamma}{\bar{\gamma}}}, \gamma > 0. \tag{2.19}$$

This will be used in future chapters.

2.3.2 Digital modulation scheme

Binary phase shift keying

The binary phase shift keying (BPSK) is the digital modulation scheme with two phases. It is the simplest form of phase shift keying (PSK) and has attracted great interests. There are two different phase states, and the carrier signal can be represented as: $= 0$ for binary 1 and $= 180$ for binary 0. Therefore, this scheme has the highest noise level before demodulation. The easiest way to represent BPSK is by using a constellation diagram, as shown in Fig. 2.3 [133]. [134] The general

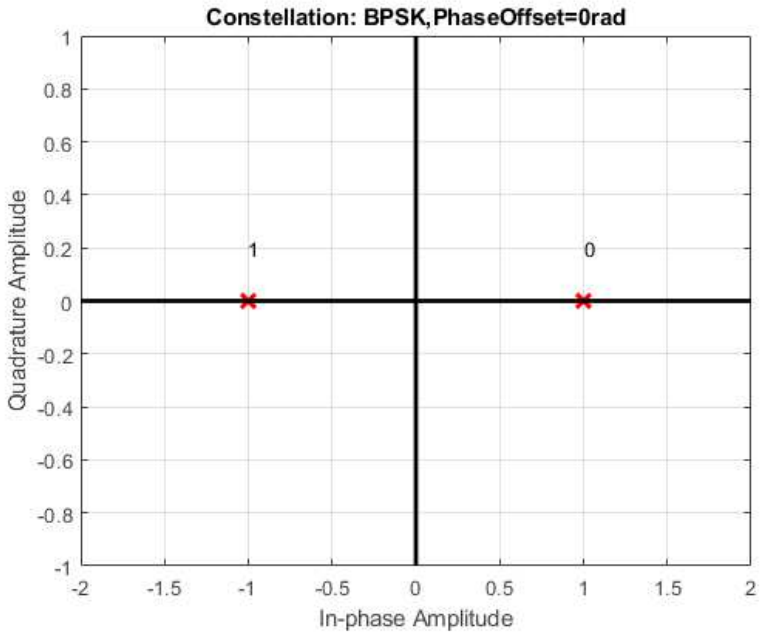

Figure 2.3: Plot BPSK modulator reference constellation

form of BPSK follows as [134]

$$s_n(t) = \sqrt{\frac{2E_b}{T_b}} cos(2\pi ft + \pi(1-n))n = 0 \; or \; 1. \tag{2.20}$$

Considering the signal transmitted in AWGN, the received signal can be written as [134]

$$y(t) = \sqrt{E_d} + n(t) \tag{2.21}$$

when 1 is transmitted, and E_d is the transmitted signal energy per symbol. However, when -1 is transmitted, the received signal is defined as [134]

$$y(t) = -\sqrt{E_d} + n(t). \tag{2.22}$$

The basic functions shown above, the BER of BPSK under the model of white Gaussian noise can be expressed as [134]

$$P_b = Q(\sqrt{\frac{2E_b}{N_0}}) \tag{2.23}$$

or

$$P_b = \frac{1}{2} erfc(\sqrt{\frac{E_b}{N_0}}) \tag{2.24}$$

where $Q(.)$ is the Gaussian Q-function and N_0 is the white Gaussian noise power. Details of the modulation will be analyzed in Chapter 3, Chapter 4, Chapter 5, and Chapter 6.

2.3.3 System performance measurement

In the wireless communication systems, there are various measurements that can be used to evaluate the performance and give a guideline into the wireless system design. In the following section, four main ones will be discussed.

Signal-to-Noise Ratio

The Signal-to-Noise Ratio (SNR) estimation is a necessary guidance in the communication system. The information can be applied in system module algorithms to achieve the optimal performance by SNR estimation when the SNR is fixed over a certain time period. The knowledge of the SNR can also be used for comparing the performance of different communication systems. There are groups of technologies and applications that required the SNR estimation to reach the most suitable operation performance.

There are numerous SNR estimators previously proposed in the early review for one-hop systems. They are designed to operate with AWGN. Split symbol moments estimator (SSME) is normally used to estimate an estimation of SNR for BPSK, which has been discussed in [135]. From samples of a complex received signal, the maximum-likelihood (ML) estimator has been derived by using probability density functions in [136]. The authors also offered an estimator called Signal-to-Noise variance (SNV) estimator in [137], which uses data decisions based on the BPSK modulation in real AWGN and then expand into higher orders of modulation in multiple channels. The second-order and fourth-order moments (M2M4) estimator performs badly at low SNR and best at medium SNR, as discussed in [138]. For M-ary PSK-modulated signals, the Signal-to-Variation ratio (SVR) estimator h_s was designed in [139]. Since the relaying system is a two-hop system which includes one source, one relay, and one destination, for the first hop from source to the

relay and the second hop from the relay to the destination, we can use these known estimators to estimate the SNR under different expressions. In order to improve the performance of SNR in the fading channel estimation, we assume both the hop from source to the relay and the hop from the relay to the destination are Rayleigh fading channels, and the fading gains have been estimated. [140]

The SNR is an important performance measured in the wireless communication system, which compares the levels of desired signal to the noise levels. SNR is defined as the ratio of signal to noise power as

$$SNR = \frac{P_{signal}}{P_{noise}}. \tag{2.25}$$

Therefore, the average SNR can be given as

$$\overline{\gamma_{SNR}} = \int_0^\infty \gamma_{SNR} f(\gamma_{SNR}) d\gamma_{SNR} \tag{2.26}$$

where $f(\gamma_{SNR})$ is the PDF of the instantaneous SNR.

The overall SNR after AF can be written as

$$\gamma_{end} = \frac{\gamma_r \gamma_d}{\gamma_r + \gamma_d + 1}. \tag{2.27}$$

where $\gamma_r = \frac{P_s |h|^2}{2\sigma^2}$ is the SNR of the first hop and $\gamma_d = \frac{P_r |g|^2}{2\sigma^2}$ is the SNR of the second hop. These two SNRs can affect each other, when one of them is much smaller than the other one, and its end-to-end SNR is almost equal to the bigger one. In some scenarios, to reduce the mathematical loads, the approximation can be written as

$$\gamma_{end} = \frac{\gamma_r \gamma_d}{\gamma_r + \gamma_d}. \tag{2.28}$$

In this function, when the SNR is very large, it can predict $\gamma_r + \gamma_d + 1 \approx \gamma_r + \gamma_d$. This mode is called harmonic mean, and was proposed by authors in [141].

There is also another SNR mode called minimum mode, which compares the values to obtain the minimum value.

Outage probability

The outage probability is an important measurement to evaluate the performance of wireless communication systems, and it has been widely used in the wireless channels. The outage probability can be defined as the probability when the information rate is less than the required threshold information rate. It is the probability that an outage will occur within a specified time period. [130] The outage probability threshold of the SNR can be written as [130]

$$F_{\gamma_{end}}(x) = P_r\{\gamma_{end} < \gamma_{th}\} = \int_0^{\gamma_{th}} p_\gamma(\gamma) d\gamma \tag{2.29}$$

where γ_{th} is the receiver sensitivity, and γ_{end} is the end-to-end SNR. R is the transmission rate, and the expression above is the CDF of the end-to-end SNR.

Bit-error-rate

The BER is the number of bit errors divided by the total number of entire bits during a certain time interval. Bit error rate performance is often expressed in percentage.

There are multiple schemes for BER that have been discussed in [125], including BPSK, quadrature phase-shift keying (QPSK) and M-ary pulse amplitude modulation (M-PAM). Results show that BPSK gives the best BER performance while M-PAM gives the worst BER performance. Therefore we use BPSK scheme in this section.

The BER is defined as the error probability of discovery channel structure, and it is a nonlinear function of SNR, which is a significant performance measure. For a general form of coherent binary modulation, it can be derived as [142]

$$BER = aQ(\sqrt{bx}) \tag{2.30}$$

where x is the instantaneous SNR. There is $(a, b) = (1, 1)$ for binary frequency-shift keying (BFSK), $(a, b) = (2\frac{M-1}{M}, \frac{6}{M^2-1})$ for M-PAM, and $(a, b) = (1, 2)$ for BPSK.

In the case of BPSK modulation in AWGN channels, the BER expression

can be written as [142]

$$BER = \frac{1}{2} erfc(\sqrt{\frac{E_b}{N_0}}) \tag{2.31}$$

where the E_b is the energy and the N_0 is the noise, and $erfc(x)$ is the complementary error function evaluated for each element of x. The equation $\frac{E_b}{N_0}$ is the energy per bit to noise power spectral density ratio. The BER result will be used to describe the performance of digital communication system. It helps us to choose the appropriate forward error correction codes.

Also, for non-coherent modulation, the BER expression is written as

$$BER = ae^{-bx} \tag{2.32}$$

where $(a, b) = (0.5, 0.5)$ for non-coherent binary frequency-shift keying (NCBFSK) [143], and $(a, b) = (0.5, 1)$ for differential binary phase-shift keying (DBPSK) [144]. In order to get the average BER values, we need a further integral of the instantaneous BER function with respect to the instantaneous SNR, together with the PDF expression of SNR.

Achievable rate

The achievable rate can be used to measure the capacity of the system if the harvested energy is used immediately after the relay node harvested from variable-power transmission. By using the same SNR in (2.13), the achievable rate can be derived as

$$AR = log_2(1 + \gamma_r P_r) \tag{2.33}$$

where P_r is the transmission power at the relay node.

2.4 RF energy harvesting

2.4.1 Previous work on WPC

Earlier works on wireless power communication commonly considered a standard system structure, where the wireless power is broadcasted in the downlink follows by a wireless information transmission in the uplink using the harvested wireless

power. They are conducted mainly based on the assumption that the downlink and uplink are independent.

In [145], the authors proposed a novel type of wireless RF powered communication network with the harvest-then-transmit protocol. Firstly, the hybrid access point broadcasts the power to distribute users into the downlink. The users then transmit their information to the hybrid access point in the uplink by time-division multiple access (TDMA). The new phenomenon they found is called doubly near-far problem, which is caused by the folded attenuation in both downlink wireless energy transfer and uplink wireless information transmission. It can occur when the conventional metric of network sum-throughput is maximised and a problem on the wrong time and throughput allocation. To solve this problem, the authors have given a new common-throughput maximisation approach, in order to allocate equal rates without consider their distances from the hybrid access point to users. The transmission time to users and the distances are inversely proportional.

The above investigation is conducted mainly based on the assumption that the downlink and the uplink are independent. However, in practice, it is crucial to analyse the performance when the downlink and the uplink are correlated. The details of the correlated study will be presented in Chapter 3.

2.4.2 Energy harvesting model

The present literature work [146] for SWIPT networks and the related resource allocation algorithms [147–149] are in line with a linear EH model where independent power conversion efficiency from RF-to-direct current (DC) is compared with the input power level of the EH circuit.

In practice, however, most of the EH circuits studied in [150–152] are frequently appeared as a non-linear end-to-end wireless power transfer. Therefore, a conventional linear EH model cannot correctly model the power which is dependent to the EH efficiency causing a mistake for resource allocation.

Fig. 1. shows a transmitter with $N_T > 1$ antennas for K information receivers (IRs) and J EH receivers (ERs). All IRs are low complexity single-antenna devices, and each ER is fitted with N_R receive antennas to improve EH. In every slot, the transmitter transmits a vector of data symbols to the K IRs.

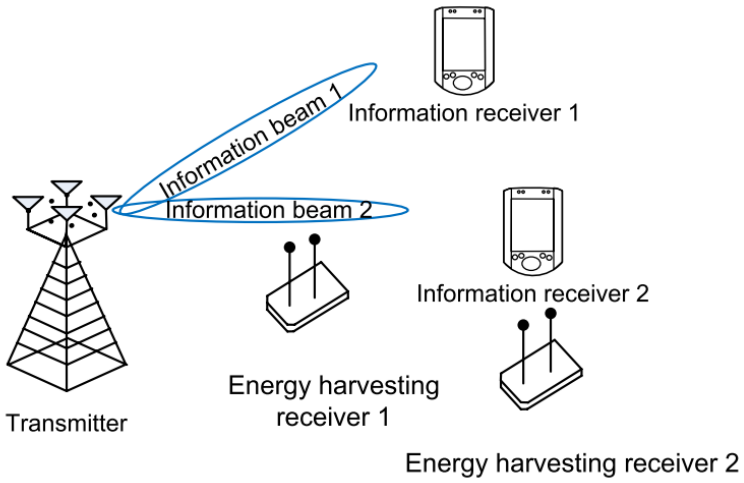

Figure 2.4: A downlink SWIPT system.

The received signal at the information receiver k is given by

$$y_k = h_k^H \sum_{k=1}^{K} w_k s_k + n_k, k = 1.....K \tag{2.34}$$

The received signal at the EH receiver j is given by

$$y_j = g_j^H \sum_{k=1}^{K} w_k s_k + n_j, j = 1.....J \tag{2.35}$$

where s_k is the data symbol and $w_k \in C^{N_T \times 1}$ is the beamforming vector for IR k, h_k is the channel vector between the transmitter and IR k, and G_j is the channel matrix between the transmitter and ER j, $n_k \sim CN(0, \sigma_s^2)$ and $n_j \sim CN(0, \sigma_s^2 I_{N_R})$ are the additive white Gaussian noises (AWGN) at the IRs and the ERs, respectively. σ_s^2 represents the noise power. For the linear EH, the harvested energy at ER j is typically modelled as

$$E_j^{linear}(N) = \eta_j P_j \tag{2.36}$$

and the received RF power at ER j can be written as

$$P_j = \sum_{k=1}^{K} Tr(w_k w_k^H G_j G_j^H) \tag{2.37}$$

where $0 < \eta_j < 1$ is the fixed energy conversion efficiency of ER j. In this linear EH model, the independent energy conversion efficiency is compared to the input power level at the ER, which means that the total harvested energy at the ER is linearly and directly proportional to the received RF power. Normally, the conventional linear EH model is only used for the specific case when the received power at all ERs is constant. Therefore, a practical non-linear EH model is needed, which considers the dynamics of the RF energy conversion efficiency under different input power levels. So as to separate the system model from the specific implementation details of the EH circuit, the non-linear EH model from logistic (sigmoidal) function can be presented as [153]

$$E_j^{non-linear} = \frac{\psi_j^{non-linear} - M_j\omega_j}{1-\omega_j} \tag{2.38}$$

$$\omega_j = \frac{1}{1+expa_jb_j} \tag{2.39}$$

and the traditional logistic function related to the received RF power P_j can be written as

$$\psi_j^{non-linear} = \frac{M_j}{1+exp{-}a_j(P_j-b_j)} \tag{2.40}$$

where ω_j is a constant to guarantee zero-input/zero-output answer for EH, M_j is a constant representing the maximum harvested power at ER j. Parameters a_j and b_j are two constants affected by the diode turn-on voltage, capacitance, and resistance. The parameters a_j, b_j, and M_j in (4) can be easily found according to the standard curve fitting tool [153]. This proposed non-linear EH model can achieve the joint effect of the non-linear phenomena by current leakage and circuit sensitivity limitations [151, 152].

2.4.3 RF energy types

There are numerous forms of RF-based wireless power, such as energy from the source, energy from ambient, and energy from the dedicated transmitter. Two staple types of power both from the source and from the ambient will be investigated in this thesis.

For the energy from the source, in [154] and [147], simultaneous wireless power information and power transfer were proposed, where both wireless power and the information were sent together via the electromagnetic wave. In [154],

the authors discussed the fundamental trade-offs between power transfer and information decoding over a single noise line. They are seeking to characterise the communication system with immense received energy and substantial information per unit time. Numerical results show that consideration of transmitted power is desired.

In [147], the authors considered the electromagnetic or radio signal with wireless power transfer, in particular, when radio carries both energy and information at the same time. Meanwhile, a multiple-input-multiple-output (MIMO) wireless system includes three nodes, with one receiver harvests energy and another receiver transmits information separately. Two scenarios were discussed, when the energy receiver and information receiver were divided into different MIMO channels, or used the same MIMO channels. The RF-based energy from the source will be used in Chapter 3,4,5,6.

For energy harvested from the ambient environment, it was already studied extensively in Chapter 1, with different kinds of harvesters and various electromagnetic environments, which will be used in Chapter 6, where the EH structures promoted by combining two types of energy resources simultaneously.

Chapter 3

The WPC with correlated uplink and downlink

3.1 Introduction and related works

The main study in this chapter is to analyse the performance of WPC in regards of achievable rate and BER, and for most scenarios, the uplink is related to the downlink. This chapter of work considered the link correlation in the design of WPC systems. The WPC and relaying system have similarities, as the downlink is corresponded to the SR link and the uplink corresponded to the RD link. The only difference is the WPC user sends the signal back to the base station instead of the another user. The correlation between uplink and downlink provides a foundation system model for future analysis of correlation between the SR link and RD link, which is not studied in the rest of the chapters, but will be investigatived as further work.

Previous works assumed constant of independent channels between the time-multiplexed uplink and downlink in the two-hop relaying system. It is known that practical channels can be described by the Jake's model, which induces time correlation. In the work of [145], the authors proposed the WPC time-division structure, which the optimization of throughput based on different timing parameters. The application of WPC in relaying has been studied in [155], the throughput performance for different kinds of relaying protocols. For multiple-output-multiple-output (MIMO) systems, the multiple antennas provide extra coverage for energy beam-

forming have been discussed in [156–158]. In [159], the full-duplex radios have been considered which allow the WPC system to hold more energy and information.

In this chapter, we analyzed the performance of WPC in [145] for the case when the downlink and the uplink are correlated due to fast fading Nakagami m channels. Semi-closed expressions for the achievable rate (AR) and series expressions for the BER are derived. Using these expressions, the effect of link correlation on the system performance is examined by comparing it with that of a system assuming independent links. Numerical results show that the link correlation has a significant impact on the achievable rate performance of WPC. Because of this, the optimum system parameter for correlated links is considerably different from that for independent links. The effect of link correlation on the BER performance of WPC is also noticeable. These results give useful guidance on WPC system design.

In this chapter, the Nakagami m fading channel has been studied, which can be applied to describe scenarios for land radio and indoor roadie. The results also included the previous works even at the link correlation does not considered.

The remaining of this chapter is organized as follows. The system module of the uplink and downlink is given in Section 3.2. In Section 3.3, the SCI of system model will be estimated with details. In Section 3.4, the expressions of achievable rate and bit-error-ratio will be derived, the channel capacity is analyzed. In Section 3.5, the performance of the wireless powered communication with correlated uplink and downlink will be discussed regards to achievable rate and bit-error-ratio. The conclusion of this chapter will be presented in Section 3.6.

3.2 The WPC system model

In this section, the system model will be studied, where the WPC system is similar to the relaying in [145]. The communications session starts by broadcasting wireless power in the downlink from the access point to all the users for $\tau_0 T$ seconds, where T is the total time of power and information transmission and $0 < \tau_0 < 1$ is the portion of the time for wireless power transfer. There are I users in the system. The first user sends its information to the access point for $\tau_1 T$ seconds in the uplink, followed by the second user for $\tau_2 T$ seconds and the i-th user for $\tau_i T$ seconds. Thus, time-division-multiple-access (TDMA) is adopted for different users. One has $\sum_{i=0}^{I} \tau_i = 1$. Without loss of generality, $T = 1$ second. A detailed diagram of the

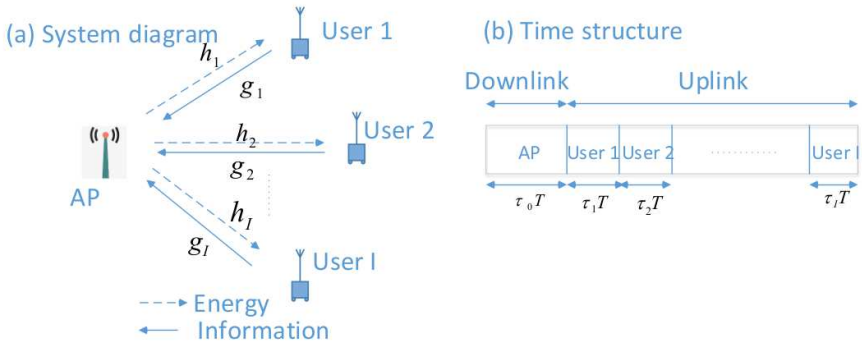

Figure 3.1: Diagram and time structure of WPC system.

considered WPC system and its time structure can be found in Fig. 3.1.

Using the above model, the received signal at the i-th user can be expressed as

$$y_i = h_i \sqrt{P_A} x_A + z_i \tag{3.1}$$

where $i = 1, 2, \cdots, I$, h_i is the fading coefficient of the downlink from the access point to the i-th user, P_A is the transmission power of the access point, x_A is the transmitted symbol and can be set to $x_A = 1$ for power transfer, and z_i is the additive white Gaussian noise (AWGN) in the channel with mean zero and variance σ^2.

The i-th user transmits information in the uplink to the access point for $\tau_i T$ seconds so that the received signal at the access point is given by

$$r_i = g_i \sqrt{P_i} x_i + n_i \tag{3.2}$$

where g_i is the fading coefficient of the uplink from the i-th user to the access point, P_i is the transmission power of the i-th user, x_i is the transmitted symbol of the i-th user assumed to be binary phase shift keying (BPSK) modulated with $x_i = \pm 1$, and n_i is the AWGN with mean zero and variance σ^2. In the next section, the harvested energy in relay and the channel estimation will be introduced.

3.3 Time-division estimation

3.3.1 Harvested energy estimation

In the WPC system, the received signal gives the harvested energy at the i-th user as

$$G_i = \eta |h_i|^2 P_A \tau_0 \tag{3.3}$$

where η is the energy conversion efficiency of the energy harvester. It could be a nonlinear function of the input power, such as [160] and [153], but in most literature, it is assumed to be a constant. We make the same assumption here for simplicity. It can be shown that, if a nonlinear function is considered, the final results will be in the form of one-dimensional integrals.

The harvested power is $\frac{\chi_i G_i}{\tau_i}$, where χ_i denotes the fixed portion of power used. Similar to [145], we assume a harvest-then-use protocol where all the harvested energy is used for data transmission at the i-th user such that one has

$$P_i = \frac{G_i}{\tau_i} = \frac{\tau_0}{\tau_i} \eta P_A |h_i|^2 \tag{3.4}$$

where we set $\chi_i = 1$ for all users. This is the case, for example, when the users have a battery with limited capacity such that energy storage is not viable. From (3.2) and using (3.4), the Signal-to-Noise Ratio (SNR) of the received signal at the access point can be calculated as

$$\gamma_i = \frac{\eta P_A \tau_0}{\sigma^2 \tau_i} |g_i|^2 |h_i|^2. \tag{3.5}$$

3.3.2 Cascaded channel estimation

Thus,in WPC, the achievable rate of the i-th user is

$$R_i = \tau_i \log_2(1 + \gamma_i) = \tau_i \log_2 \left(1 + \frac{\eta P_A \tau_0}{\sigma^2 \tau_i} |g_i|^2 |h_i|^2 \right). \tag{3.6}$$

Similarly, the BER of the information transmission is

$$E_i = \frac{1}{2} erfc(\sqrt{\gamma_i}) = \frac{1}{2} erfc \left(\sqrt{\frac{\eta P_A \tau_0}{\tau_i \sigma^2}} |g_i||h_i| \right) \tag{3.7}$$

where $erfc(\cdot)$ is the complementary error function of the Gaussian distribution. In this work, BPSK is assumed. For higher-level modulation schemes, it has been reported in [130] and [125] that the BER can be written as $E_i = \frac{c}{2} erfc(\sqrt{\frac{d}{2}\gamma_i})$, where $c = 2\frac{M-1}{M}$ and $d = 1$ for M-ary amplitude shift keying, and $c = 2$ and $d = 2\sin^2(\pi/M)$ for M-ary phase shift keying as a good approximation. Also, wireless power is mainly used for low-power applications, such as sensor networks and RF identification, where reliability is more important than data rate. Thus, BPSK is advantageous over higher-level modulation in these applications.

In [145] and other works in the literature, g_i and h_i are often assumed independent. However, in practical fast fading channels, they can be correlated. Assume Nakagami m fading channels. The joint probability density function (PDF) of $|g_i|$ and $|h_i|$ is given by [130]

$$f_{|g_i|,|h_i|}(y_1, y_2) = \frac{4m^{m+1}(y_1 y_2)^m}{\Gamma(m)\Omega_1\Omega_2(1-\rho_i)(\Omega_1\Omega_2\rho_i)^{\frac{m-1}{2}}} e^{-\frac{m}{1-\rho_i}(\frac{y_1^2}{\Omega_1}+\frac{y_2^2}{\Omega_2})} I_{m-1}\left(\frac{2m\sqrt{\rho_i}y_1y_2}{\sqrt{\Omega_1\Omega_2}(1-\rho_i)}\right) \tag{3.8}$$

where $I_{m-1}(\cdot)$ is the $(m-1)$-th order modified Bessel function of the first kind [161, eq. (8.406)], $\Gamma(\cdot)$ is the Gamma function [161, eq. (8.310)], m is the Nakagami m parameter, Ω_1 is the average fading power in the uplink, Ω_2 is the average fading power in the downlink, and ρ_i is the correlation coefficient between $|g_i|$ and $|h_i|$. The model in (3.8) is restricted to integer values of m [130]. Thus, our results are also limited to integer values of m. They may be used as bounds for non-integer values of m. If the Jakes' model applies, using [130], the correlation coefficient is determined by

$$\rho_i = J_0^2\left(2\pi f_m T \sum_{k=0}^{i-1} \tau_k\right) \tag{3.9}$$

where $J_0(\cdot)$ is the zero-th order Bessel function of the first kind [161, eq. (8.402)] and f_m is the maximum Doppler shift. In addition, the Doppler effect induced by the WPC system users mobility is assumed to be perfectly compensated at the receivers. The time difference between g_i and h_i in the fading process is given by $\sum_{k=0}^{i-1}\tau_k$, as the uplink data transmission from the users to the access point takes place sequentially. For example, the first user transmits data right after the power transfer. Hence, the time difference between g_1 and h_1 is τ_0. The second user transmits data after the first user finishes its transmission so that the time difference between g_2 and h_2 is $\tau_0 + \tau_1$, and so on. These time difference actually accounts for the time-variance of the instantaneous channel state information in the system

design, in contrast to previous works that assumed the channel state information to be either constant or independent.

When g_i and h_i are independent, which is the case assumed in the literature and is an approximation to (3.8) when $f_m T$ or τ_i are large such that $\rho_i \to 0$, one has

$$f_{|g_i|,|h_i|}(y_1, y_2) = \frac{4m^{m+1}(y_1 y_2)^{2m-1}}{\Gamma^2(m)(\Omega_1\Omega_2)^m} e^{-\frac{m}{\Omega_1}y_1^2 - \frac{m}{\Omega_2}y_2^2}. \tag{3.10}$$

In the following, we are going to use (3.8) and (3.10) to derive the average achievable rate and the average BER of the i-th user and use them to examine the effect of correlation.

3.4 Achievable rate and BER in WPC

This section first derives the achievable rate and the BER expressions for WPC. In the first subsection, the details of achievable derivation were presented. In the second subsection, the details of BER derivation were presented. From these expressions, more comprehensive results will be discussed in Section 3.4.

3.4.1 Achievable rate for WPC analysis

In this section, by using (3.6), the average achievable rate can be calculated as

$$\begin{aligned} \bar{R}_i &= \int_0^\infty \int_0^\infty \tau_i \log_2(1 + \frac{\eta P_A \tau_0}{\sigma^2 \tau_i} y_1^2 y_2^2) \\ &\quad f_{|g_i|,|h_i|}(y_1, y_2) dy_1 dy_2 \end{aligned} \tag{3.11}$$

which requires the solution via a two-dimensional integral. After performing a two-dimensional variable transformation as $x = y_1$ and $z = y_1 y_2$ and solving the integration over x using [161, eq. (3.478.4)], one has

$$\begin{aligned} \bar{R}_i = & \frac{4m^{m+1}\tau_i}{\Gamma(m)\Omega_1\Omega_2(1-\rho_i)(\Omega_1\Omega_2\rho_i)^{\frac{m-1}{2}}} \\ & \int_0^\infty \log_2(1 + \frac{\eta P_A \tau_0}{\sigma^2 \tau_i} z^2) z^m \\ & I_{m-1}(\frac{2m\sqrt{\rho_i} z}{\sqrt{\Omega_1\Omega_2}(1-\rho_i)}) K_0(\frac{2mz}{(1-\rho_i)\sqrt{\Omega_1\Omega_2}}) dz \end{aligned} \tag{3.12}$$

where $K_0(\cdot)$ is the zero-th order modified Bessel function of the second kind [161, eq. (8.407)]. This integral cannot be simplified further unless approximations are applied. However, such a one-dimensional integral is very easy to calculate using standard mathematical software, such as MATLAB and MATHEMATICA. On the other hand, if one does need an approximation, from (3.12), one has

$$\begin{aligned}\bar{R}_i &= \frac{4m^{m+1}\tau_i}{\Gamma(m)\Omega_1\Omega_2(1-\rho_i)(\Omega_1\Omega_2\rho_i)^{\frac{m-1}{2}}} \\ &\quad \sum_{k=0}^{\infty}\frac{(m\sqrt{\rho_i}/(\sqrt{\Omega_1\Omega_2}(1-\rho_i)))^{m+2k-1}}{k!\Gamma(m+k)} \\ &\quad \int_0^{\infty}\log_2(1+\frac{\eta P_A\tau_0}{\sigma^2\tau_i}z^2)z^{2m+2k-1} \\ &\quad K_0(\frac{2mz}{(1-\rho_i)\sqrt{\Omega_1\Omega_2}})dz \end{aligned} \tag{3.13}$$

where the series expansion of $I_{m-1}(\cdot)$ in [161, eq. (8.445)] has been used. The function of $K_0(x)$ decays very fast with x. It can be shown that the integrand in (3.13) is very small when $x > 10$. Thus, we can perform a least-squares curve-fitting on $K_0(x)$for $0 < x < 10$, which gives us $K_0(x) \approx 2.7e^{-1.9x}$. Using this approximation in (3.13), one has

$$\begin{aligned}\bar{R}_i &\approx \frac{10.8m^{m+1}\tau_i}{\Gamma(m)\Omega_1\Omega_2(1-\rho_i)(\Omega_1\Omega_2\rho_i)^{\frac{m-1}{2}}} \\ &\quad \sum_{k=0}^{\infty}\frac{(m\sqrt{\rho_i}/(\sqrt{\Omega_1\Omega_2}(1-\rho_i)))^{m+2k-1}}{k!\Gamma(m+k)\ln 2} \\ &\quad (\frac{(1-\rho_i)\sqrt{\Omega_1\Omega_2}}{3.8m})^{2m+2k} \\ &\quad F(\frac{\eta P_A\tau_0}{\sigma^2\tau_i}\frac{(1-\rho_i)^2\Omega_1\Omega_2}{3.8m^2}, 2m+2k-1) \end{aligned} \tag{3.14}$$

where

$$\begin{aligned}F(a,n) &= \int_0^{\infty}\ln(1+at^2)t^n e^{-t}dt \\ &= nF(a,n-1)+G(a,n) \end{aligned} \tag{3.15}$$

$F(a,0) = \ln a + 2[\ln\frac{1}{\sqrt{a}} - ci(\frac{1}{\sqrt{a}})\cos(\frac{1}{\sqrt{a}}) - si(\frac{1}{\sqrt{a}})\sin(\frac{1}{\sqrt{a}})]$ by using [161, eq. (4.338.1)] and $G(a,n) = (-1)^{\frac{n+1}{2}}(\frac{1}{\sqrt{a}})^n[ci(\frac{1}{\sqrt{a}})\sin(\frac{1}{\sqrt{a}}) - si(\frac{1}{\sqrt{a}})\cos(\frac{1}{\sqrt{a}})] + \sum_{j=1}^{\frac{n+1}{2}}(n+1-2j)!(-\frac{1}{a})^{j-1}$ for odd values of n, $G(a,n) = (-1)^{\frac{n}{2}-1}(\frac{1}{\sqrt{a}})^n[ci(\frac{1}{\sqrt{a}})\cos(\frac{1}{\sqrt{a}}) + si(\frac{1}{\sqrt{a}})\sin(\frac{1}{\sqrt{a}})] + \sum_{j=1}^{\frac{n}{2}}(n+1-2j)!(-\frac{1}{a})^{j-1}$ for even values of n, using [161, eq.

(3.356.1)] and [161, eq. (3.356.2)], $ci(\cdot)$ and $si(\cdot)$ are the cosine integral and the sine integral, respectively [161, eq. (8.230)].

Similarly, if the links are independent, one has

$$\begin{aligned}\bar{R}_i &= \frac{4m^{2m}\tau_i}{\Gamma^2(m)(\Omega_1\Omega_2)^m}\int_0^\infty \log_2(1+\frac{\eta P_A\tau_0}{\sigma^2\tau_i}z^2) \\ &\quad z^{2m-1}K_0(\frac{2mz}{\sqrt{\Omega_1\Omega_2}})dz. \end{aligned} \tag{3.16}$$

Equation (3.16) can also be obtained from (3.13) by using the series expansion of the Bessel function $I_{m-1}(\cdot)$ [161, eq. (8.445)] and letting $\rho_i \to 0$ in the expanded result, assuming that the integration and the limiting operations can exchange orders. Using $K_0(x) \approx 2.7e^{-1.9x}$, a simpler approximation can also be derived as

$$\begin{aligned}\bar{R}_i &\approx \frac{10.8m^{2m}\tau_i}{\Gamma^2(m)(\Omega_1\Omega_2)^m \ln 2}(\frac{\sqrt{\Omega_1\Omega_2}}{3.8m})^{2m} \\ &\quad F(\frac{\eta P_A\tau_0}{\sigma^2\tau_i}\frac{\Omega_1\Omega_2}{3.8^2m^2}, 2m-1) \end{aligned} \tag{3.17}$$

where $F(a,n)$ is given by (3.15).

3.4.2 BER for WPC analysis

In this section, by using (3.7) and integration by parts, the average BER can be obtained as

$$\bar{E}_i = \sqrt{\frac{\eta P_A\tau_0}{\pi\sigma^2\tau_i}}\int_0^\infty e^{-\frac{\eta P_A\tau_0}{\tau_i\sigma^2}z^2}F_{|g_i||h_i|}(z)dz \tag{3.18}$$

where $F_{|g_i||h_i|}(z)$ is the cumulative distribution function (CDF) of $|g_i||h_i|$. Using (3.8) and [161, eq. (8.445)], the CDF of $|g_i||h_i|$ is

$$\begin{aligned}&F_{|g_i||h_i|}(z) = \frac{4m^{m+1}}{\Gamma(m)\Omega_1\Omega_2(1-\rho_i)(\Omega_1\Omega_2\rho_i)^{\frac{m-1}{2}}} \\ &\sum_{k=0}^\infty \frac{1}{k!\Gamma(m+k)}\left[\frac{m\sqrt{\rho_i}}{\sqrt{\Omega_1\Omega_2}(1-\rho_i)}\right]^{m-1+2k} \\ &\int_0^\infty y_2^{2m-1+2k}e^{-\frac{m}{1-\rho_i}\frac{y_2^2}{\Omega_2}}\int_0^{z/y_2} \\ &y_1^{2m+2k-1}e^{-\frac{m}{1-\rho_i}\frac{y_1^2}{\Omega_1}}dy_1dy_2. \end{aligned} \tag{3.19}$$

The inner integral can be solved by letting $t = y_1^2$ and using [161, eq. (3.351.1)] as

$$\begin{aligned}
&\int_0^{z/y_2} y_1^{2m+2k-1} e^{-\frac{m}{1-\rho_i}\frac{y_1^2}{\Omega_1}} dy_1 \\
= \;& \frac{(m+k-1)!}{2(\frac{m}{(1-\rho_i)\Omega_1})^{m+k}}[1 - e^{-\frac{m}{1-\rho_i}\frac{z^2}{\Omega_1 y_2^2}} \\
& \sum_{j=0}^{m+k-1} \frac{(z^2/y_2^2)^j}{j!}[\frac{(1-\rho_i)\Omega_1}{m}]^j].
\end{aligned} \tag{3.20}$$

Then, using [161, eq. (3.461.3)] and [161, eq. (3.478.4)], the CDF becomes

$$\begin{aligned}
& F_{|g_i||h_i|}(z) = \sum_{k=0}^{\infty} \frac{2\rho_i^k m^{2m+2k}}{k!\Gamma(m)(\Omega_1\Omega_2)^{m+k}(1-\rho_i)^{m+2k}} \\
& [\frac{(m+k-1)!(\Omega_1\Omega_2)^{m+k}(1-\rho_i)^{2m+2k}}{2m^{2m+2k}} \\
& - \sum_{j=0}^{m+k-1} \frac{1}{j!}(\frac{z(1-\rho_i)\sqrt{\Omega_1\Omega_2}}{m})^{m+k-i} \\
& K_{m+k-i}(\frac{2mz}{(1-\rho_i)\sqrt{\Omega_1\Omega_2}})].
\end{aligned} \tag{3.21}$$

Thus, the average BER can be derived by using (3.21), [161, eq. (3.461.3)] and [161, eq. (6.631.3)] as

$$\begin{aligned}
\bar{E}_i \;=\; & \sqrt{\frac{\eta P_A \tau_0}{\pi\sigma^2\tau_i}} \sum_{k=0}^{\infty} \frac{2\rho_i^k m^{2m+2k}}{k!\Gamma(m)(\Omega_1\Omega_2)^{m+k}(1-\rho_i)^{m+2k}} \\
& [\frac{(m+k-1)!(\Omega_1\Omega_2)^{m+k}(1-\rho_i)^{2m+2k}}{4m^{2m+2k}\sqrt{\eta P_A\tau_0/(\pi\tau_i\sigma^2)}} \\
& - \sum_{j=0}^{m+k-1} \frac{1}{j!}(\frac{(1-\rho_i)\sqrt{\Omega_1\Omega_2}}{m})^{m+k-i+1} \\
& \frac{\Gamma(m+k+0.5)\Gamma(i+0.5)}{4(\sqrt{\frac{\eta P_A\tau_0}{\tau_i\sigma^2}})^{m+k+i}} e^{\frac{m^2\tau_i\sigma^2}{2(1-\rho_i)^2\Omega_1\Omega_2\eta P_A\tau_0}} \\
& W_{-\frac{m+k+i}{2},\frac{m+k-i}{2}}(\frac{m^2\tau_i\sigma^2}{(1-\rho_i)^2\Omega_1\Omega_2\eta P_A\tau_0})]
\end{aligned} \tag{3.22}$$

where $W(\cdot)$ is the Whittaker function [161, eq. (9.220.4)].

When the links are independent, using a similar method, the CDF of $|g_i||h_i|$

can be obtained as

$$F_{|g_i||h_i|}(z) = 1 - \frac{2m^m}{\Gamma(m)\Omega_2^m} \sum_{k=0}^{m-1} \frac{(m/\Omega_1)^k}{k!} (\frac{\Omega_2}{\Omega_1})^{\frac{m-k}{2}} z^{m+k} K_{m-k}(\frac{2mz}{\sqrt{\Omega_1\Omega_2}}). \quad (3.23)$$

Using (3.23), the average BER in this case is given by

$$\bar{E}_i = \frac{1}{2} - \frac{1}{2} \frac{m^{m-1}}{\Gamma(m)\sqrt{\pi}(\Omega_1\Omega_2)^{\frac{m-1}{2}}} (\sqrt{\frac{\eta P_A \tau_0}{\tau_i \sigma^2}})^{1-m} \sum_{k=0}^{m-1} \frac{\Gamma(m+0.5)\Gamma(k+0.5)}{k!} (m\sqrt{\frac{\tau_i\sigma^2}{\Omega_1\Omega_2\eta P_A\tau_0}})^k e^{\frac{m^2\tau_i\sigma^2}{2\eta P_A\tau_0\Omega_1\Omega_2}} W_{-\frac{m+k}{2},\frac{m-k}{2}}(\frac{m^2\tau_i\sigma^2}{\eta P_A\tau_0\Omega_1\Omega_2}). \quad (3.24)$$

Both (3.22) and (3.24) are derived in series expressions. One can also let $m = 1$ in (3.22) and (3.24) to obtain the results for Rayleigh fading channels. This will simplify the results further. Next, we will show some numerical examples using the expressions derived.

3.5 Numerical results and discussion

In this section, the performance of WPC in correlated links will be examined through numerical examples and compared with the performance of WPC in independent links as assumed in the literature. In the examination, we fix $\eta = 0.5$, $\Omega_1 = \Omega_2 = 1$, while we vary the values of τ_0, $f_m T$, m, $\bar{\gamma} = \frac{P_A}{\sigma^2}$. From (3.14), (3.17), (3.22) and (3.24), the performance is determined by $\frac{P_A\Omega_1\Omega_2}{\sigma^2}$. Thus, we can either fix $\frac{P_A}{\sigma^2}$ or fix Ω_1 and Ω_2, as they are equivalent. The presented results are mainly for the case of one user when $\tau_0 + \tau_1 = 1$, unless it is explicitly stated that other numbers of users are used. The analytical results are calculated by using the equations derived in the previous two sections, and they are verified by simulation denoted as the star marker in the figures.

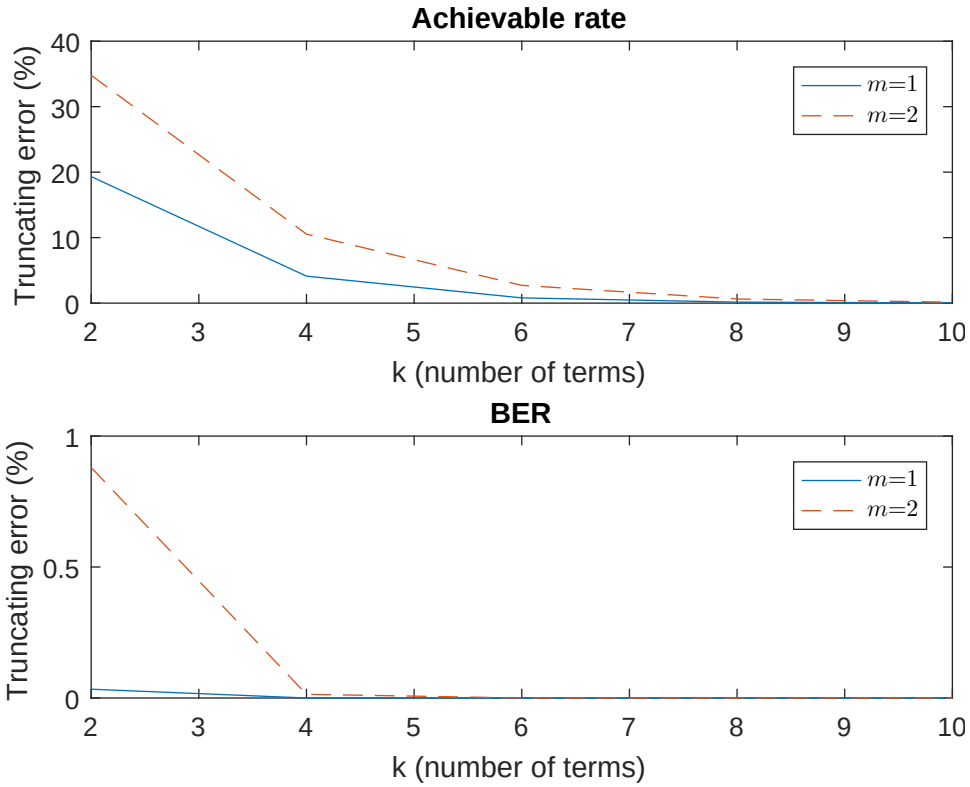

Figure 3.2: Truncation error vs. the number of truncated terms k.

3.5.1 Truncation error evaluation

Fig. 3.2 shows how the error changes with the number of terms used to calculate the infinite series in (3.14) and (3.22) for the analytical results, when $\tau_0 = 0.4$, $\bar{\gamma} = 10dB$, $f_m T = 0.5$. The error is calculated as the absolute value of the difference between the true value and the truncated value normalized by the true value. We can see that the error approaches zero quickly when the number of terms used increases. In particular, the error for the BER is much smaller than that for the achievable rate, and the error for $m = 1$ is smaller than that for $m = 2$. In the following figures, we use $k = 10$ terms. This means that the error is less than 0.14% in the cases considered.

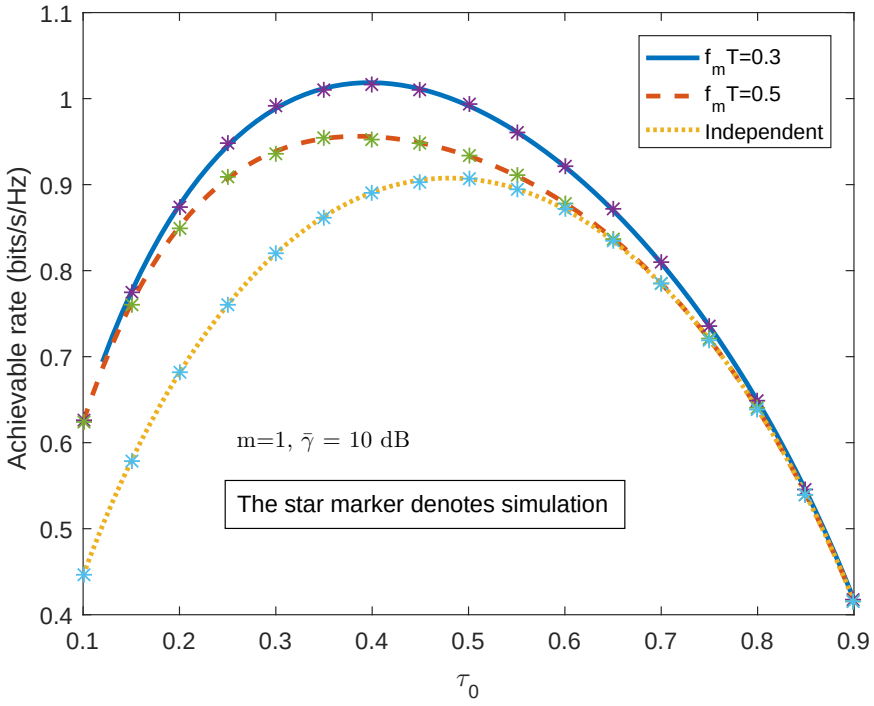

Figure 3.3: Achievable rate vs. τ_0 for different values of $f_m T$ in the Jakes' model.

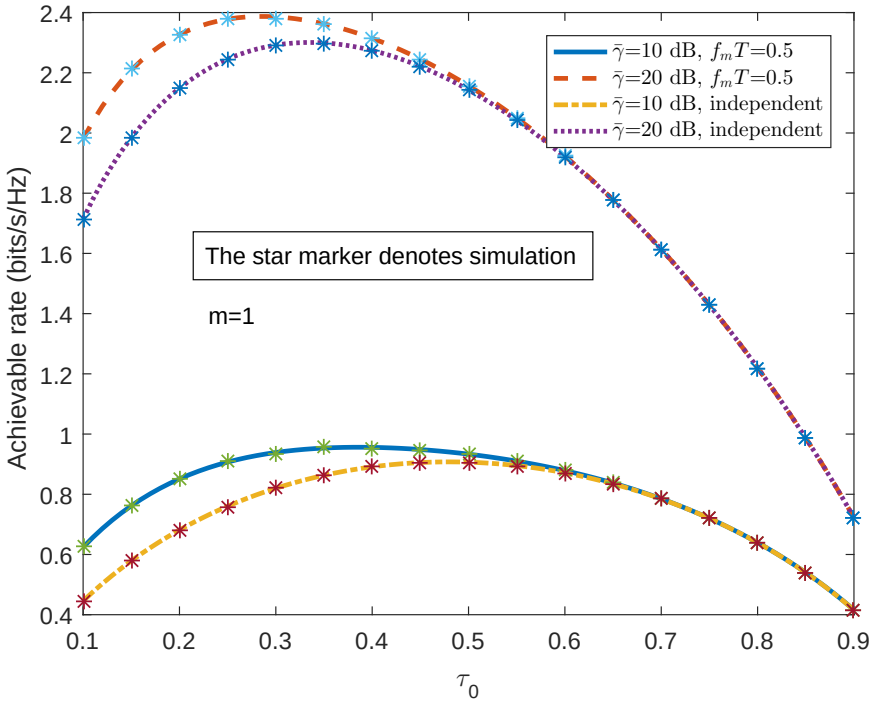

Figure 3.4: Achievable rate vs. τ_0 for different values of $\bar{\gamma}$ in the channel.

3.5.2 Achievable rate performance evaluation

Figs. 3.3 - 3.7 examine the achievable rate performance of the WPC system under different conditions. In particular, Fig. 3.3 shows the achievable rate versus τ_0 for different values of f_mT. The value of f_mT determines the correlation of the links. The smaller the value of f_mT is, the more correlated the links will be. Several observations can be made from Fig. 3.3. First, there exists an optimum τ_0 in all the cases considered, as expected, as a larger τ_0 generates more harvested power and higher SNR in the received signal at the access point, but it also reduces the effective time for data transmission. Second, different values of f_mT give different achievable rates. For example, the optimum τ_0 for $f_mT = 0.5$ is around 0.4, while the optimum τ_0 for independent links is around 0.5. Their maximum achievable rates are different too. Thus, the link correlation affects the WPC performance significantly. On the other hand, when $\tau_0 > 0.6$, their performance is very similar. From (3.9), $\rho_1 = J_0^2(2\pi f_mT\tau_0)$. Thus, the correlation coefficient in general decreases when τ_0 increases. When $\tau_0 = 0.6$ and $f_mT = 0.5$, one can find that $\rho_1 \approx 0.08$, which is very close to 0. Thus, although the correlation affects the WPC performance, this effect may be ignored when the correlation coefficient is small. Finally, if one considers the independent links as the case when $f_mT \to \infty$, one sees that the achievable rate increases and the optimum τ_0 decrease when f_mT decreases, as the link correlation, benefits the WPC performance and for smaller correlation a larger value of τ_0 is needed to harvest more power.

Figs. 3.4 and 3.5 show the achievable rate versus τ_0 for different values of $\bar{\gamma}$ and m, respectively. One sees that the achievable rate performance of the WPC system can also be significantly affected by the values of $\bar{\gamma}$ and m. Specifically, the achievable rate increases when $\bar{\gamma}$ and m increase, as expected, as the channel conditions become better for larger values of $\bar{\gamma}$ and m. In Fig. 3.4, the optimum τ_0 decreases when $\bar{\gamma}$ increases, while in Fig. 3.5, the optimum τ_0 increases when m increases. Similar to Fig. 3.3, comparing the WPC performance for correlated links with that for independent links, one sees that their performance is similar when τ_0 is large due to low correlation but are significantly different when τ_0 is small with large correlation. Comparing Figs. 3.4 and 3.5 with Fig. 3.3, one sees that $\bar{\gamma}$ has the largest impact on the rate performance, followed by m and then f_mT. Thus, increasing the transmission power P_A is still the most effective way of improving the system performance. Also, in all these figures, the rate of increase at small values of τ_0 is higher than the rate of decrease at large values of τ_0. This implies that

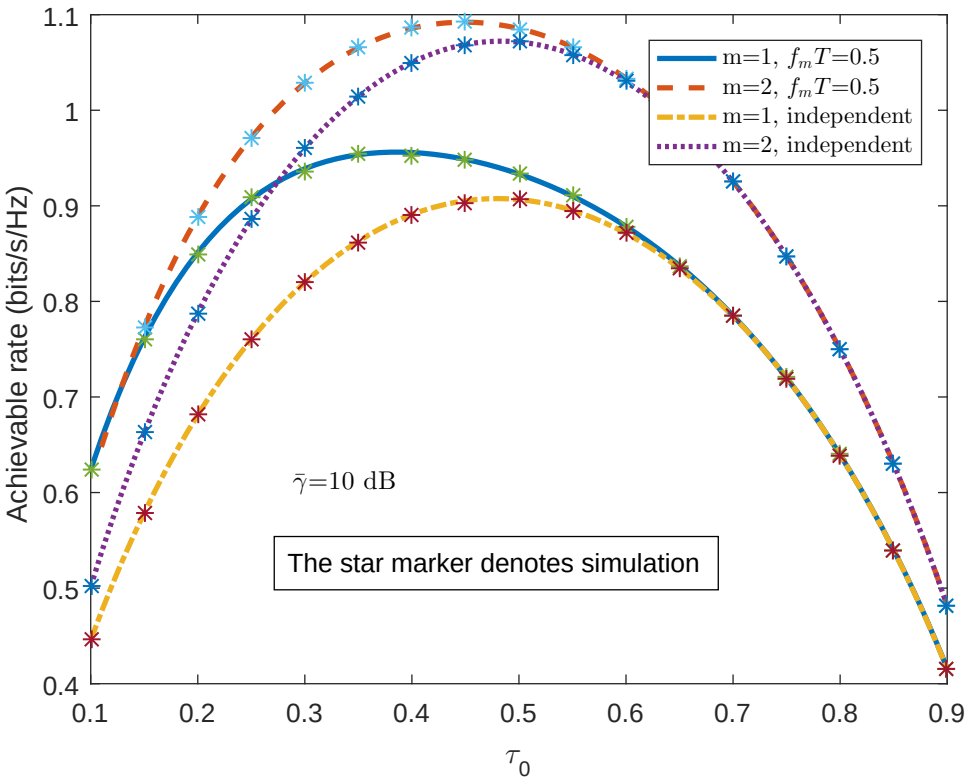

Figure 3.5: Achievable rate vs. τ_0 for different values of the Nakagami m parameter in the channel.

the achievable rate is more sensitive to the harvesting time at small values of τ_0. Mathematically, from (3.6), when τ_0 is very small, $\log_2(1+x) \approx x$ such that R_i approximately linearly increases with τ_0, as τ_i is cancelled out. When τ_0 is large, τ_i cannot be cancelled. In this case, due to τ_i, R_i decreases at a slower rate.

Fig. 3.6 shows the maximum achievable rate versus f_mT for different values of $\bar{\gamma}$. One sees from Fig. 3.6 that the maximum rate increases slowly when f_mT decreases. However, when $\bar{\gamma}$ increases, the maximum rate increases significantly, indicating that $\bar{\gamma}$ has a larger impact on the rate performance than f_mT. Fig. 3.7 shows the optimum τ_0 versus $\bar{\gamma}$ for different values of f_mT. From this figure, the optimum values of τ_0 are significantly different between correlated links and independent links. For example, when $\bar{\gamma} = 10\ dB$, the optimum τ_0 for independent links is 0.48, while the optimum τ_0 for correlated links is around 0.38. Since the maximum value of τ_0 is 1, this represents 12% difference. This difference increases when $\bar{\gamma}$ decreases. This implies that, for low-power applications, the link correlation has a huge impact on system performance. In general, the difference between different

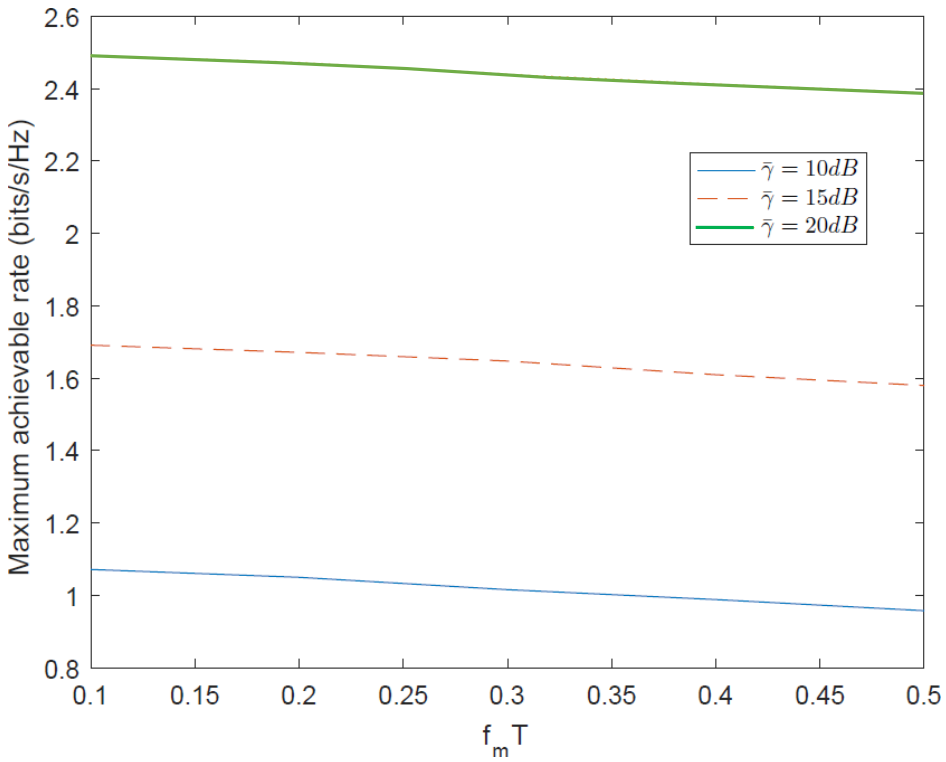

Figure 3.6: Maximum achievable rate vs. $f_m T$ for different values of $\bar{\gamma}$ in the Jakes' model.

correlations is much smaller than the difference between correlated and independent links. This allows a more robust choice of the harvesting time for correlated links. This shows that our results are useful for practical WPC system designs when the link may be correlated due to a short power transfer time.

3.5.3 BER performance evaluation

Fig. 3.8 shows the BER performance of the WPC system for different parameters. One sees from this figure that the BER decreases when $\bar{\gamma}$ increases. The BER does change considerably when $f_m T$ changes in the cases considered, implying that the link correlation also has a noticeable effect on the BER performance of the WPC system. Also, the BER always decreases when τ_0 increases, as a larger τ_0 will produce more harvested power and hence higher SNR in the received signal. In this case, BER is not determined by τ_i and thus, unlike the achievable rate, there is no optimum τ_0 for BER. Again, $\bar{\gamma}$ has a larger impact than $f_m T$. The decrease of BER

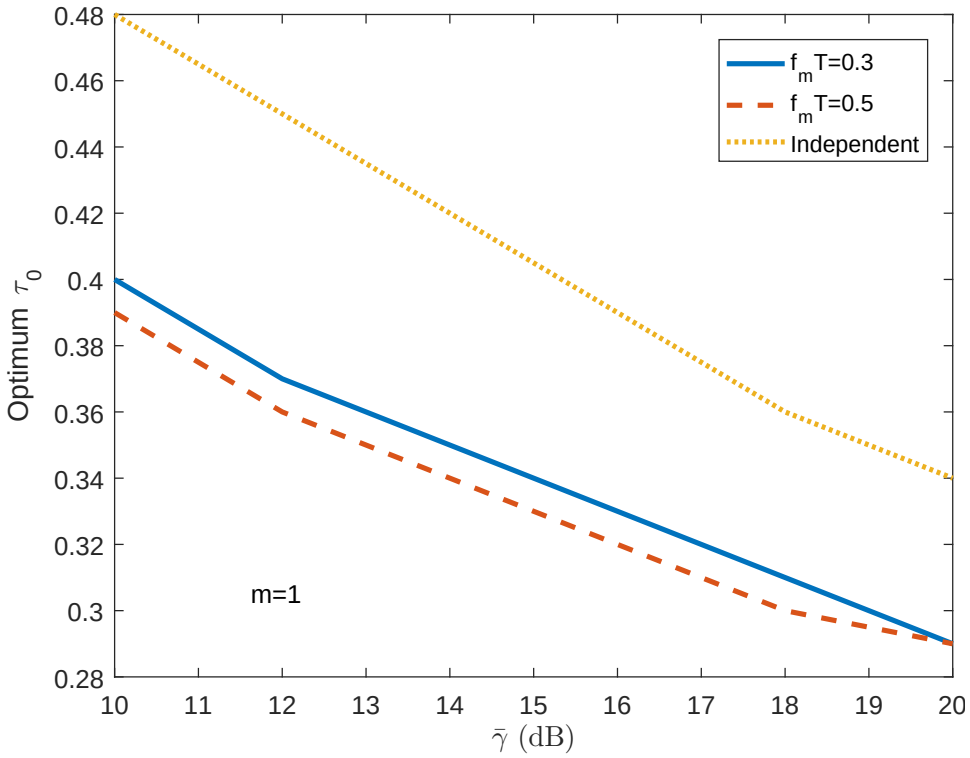

Figure 3.7: Optimum τ_0 vs. $\bar{\gamma}$ for different values of $f_m T$ in the Jakes' model.

with τ_0 is noticeable but not as dramatic as that of achievable rate. Also, the BER is relatively high even for $\bar{\gamma} = 20dB$, because the signal suffers from one power loss from the downlink and another power loss from the uplink when it is received at the access point. Besides, only part of the transmitted power is harvested.

Fig. 3.9 shows the BER vs. $\bar{\gamma}$ for different channel conditions and m. One sees from this figure that the BER decreases with $\bar{\gamma}$, as expected. It is noted that the BER decreases with the value of m. Both $\bar{\gamma}$ and m have a significant impact on the BER performance. For example, at 10^{-3}, $m = 2$ has a gain of about 15 dB over $m = 1$. Again, the correlated links have higher BER than the independent links. The gap increases when m increases. Fig. 3.10 shows the sum rate of two users vs. τ_0, when $\bar{\gamma} = 10dB$, $f_m T = 0.5$ and $m = 1$ for different values of τ_1. In this case, $\tau_0 + \tau_1 + \tau_2 = 1$. One sees that there exists an optimum τ_0 that maximizes the sum rate for a fixed value of τ_1, when the value of τ_1 increases from 0.05 to 0.30 with a step size of 0.05, the maximum rate increases and the corresponding optimum τ_0 decreases. When τ_1 is larger than 0.30 and keeps increasing, the maximum rate decreases again, implying that there is a global maximum sum rate.

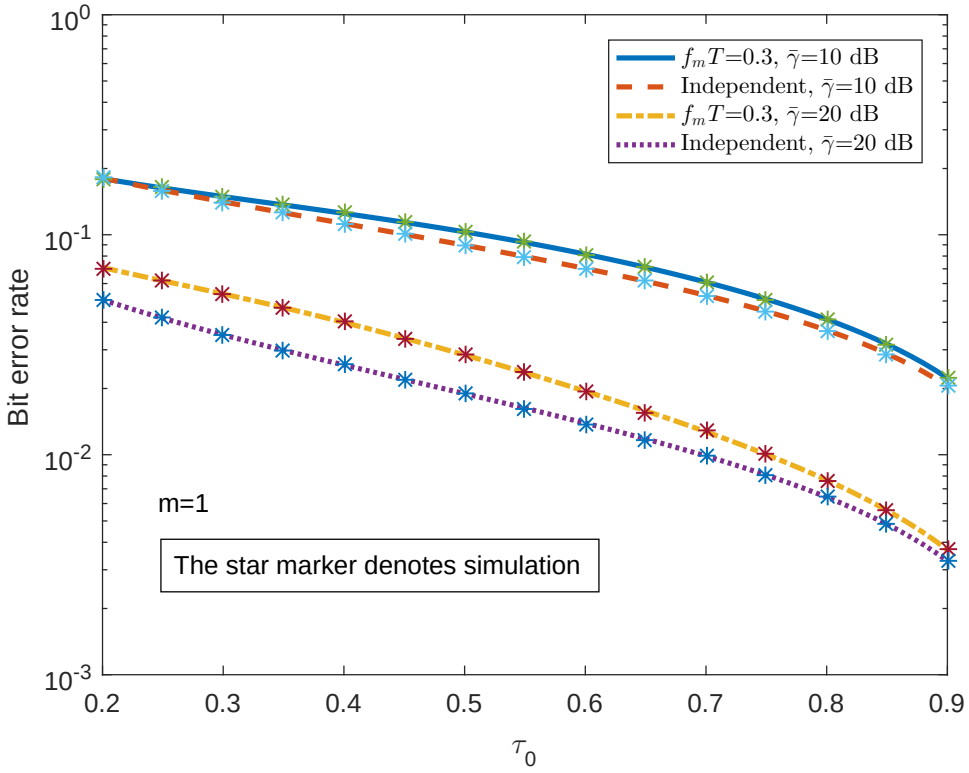

Figure 3.8: BER vs. τ_0 for different values of f_mT and $\bar{\gamma}$ in the Jakes' model.

3.6 Conclusions

The performance of the WPC system has been analyzed when the downlink and the uplink are correlated in Nakagami m fading channels. Semi-closed expressions for the achievable rate and series expressions for the BER have been derived. The effect of the link correlation on the achievable rate and the BER has been examined for different system settings. Numerical results have quantified the performance degradation due to link correlation. From these results, the rate degradation is significant when $\tau_0 < 0.6$ or less than 60% of the transmission time is used for EH. They have also shown that the transmission power has the largest impact, followed by the Nakagami m parameter and then the Doppler shift, on the achievable rate in the correlated case. This leads to a considerably different choice of the optimum harvesting time, compared with the independent case. On the other hand, the BER change is noticeable but not as significant as the rate change. The transmission power and the Nakagami m parameter still have the largest impact. Finally, for the sum rate of two users, there exists a global maximum at certain values of τ_0 and τ_1.

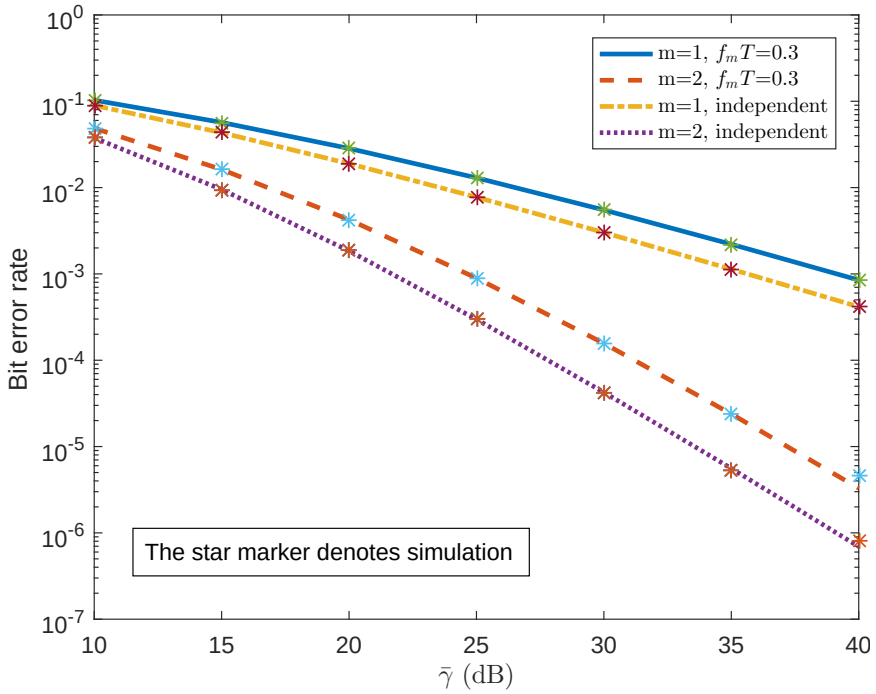

Figure 3.9: BER vs. $\bar{\gamma}$ for different values of m.

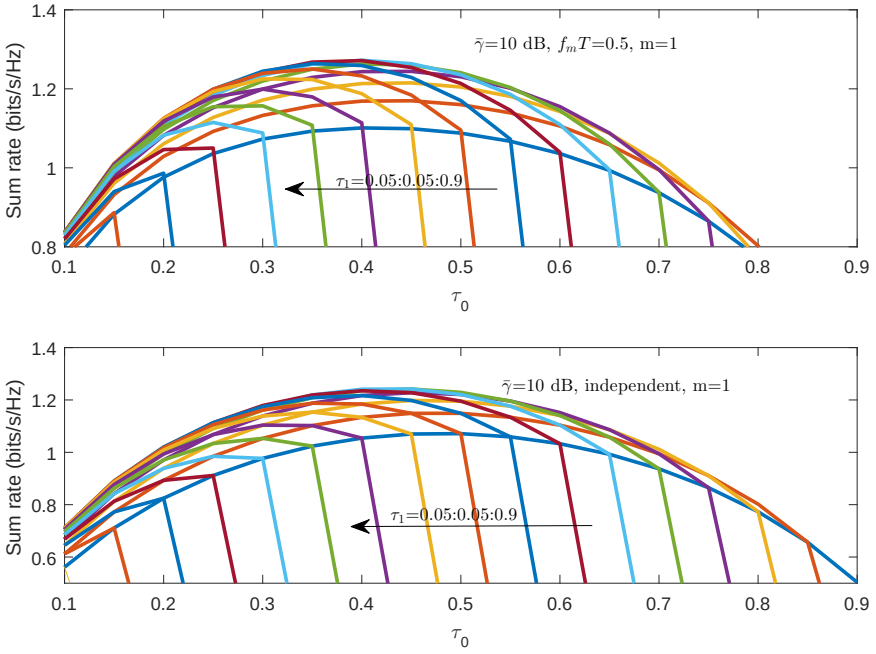

Figure 3.10: Sum rate vs. τ_0 for different values of τ_1 for two users.

Chapter 4

Allocation between harvesting, estimation and detection for TS relaying

4.1 Introduction and related works

As mentioned in Chapter 3, the relation between uplink and downlink is a significant consideration of wireless powered communication systems. In the conventional wireless powered communication system, which assumed one antenna point and several users. In this chapter, it is an AF relaying system with one source, one relay and one destination, the main focus will analysis the AF relaying system with pilot-based channel estimation through time-switching (TS) EH protocol. We aim to find the optimum resource allocation for both the three parts of the data packet in the first hop and the two parts of the data packet in the second hop. Also, the model designed in this chapter will be used for further analysis in Chapter 5.

For AF relaying, the relay node also consumes extra energy for the amplification and forwarding actions. With a limited battery life when relays operate on batteries, the extra energy consumed for amplification, forwarding, and channel estimation will stop them from taking part in relaying. To solve this problem, EH information relaying has been proposed, where the relay harvests energy from the source and uses the harvested energy to forward the information signal [80], [162], [163].

There is only a small amount of literature in this area of relaying applied to channel state information and EH together. In the previous works, this problem was either considered without data transmission [104] or without EH [125] and hence for two parts only. In [164], the authors studied a harvest-use structure, where the relay only has a supercapacitor such that harvested energy must be used immediately. In [165], the power allocation problem for EH relaying has been studied. In general, EH can exploit any forms of energy in the network, including interference and jamming signals [166], [167], [168].

In this work, to perform channel estimation, the data packets from the source to the relay need to contain pilots as overheads for pilot-based channel estimation, to allow EH at the relay simultaneously. If time-switching is used, the data packets from the source to the relay need to contain pilots as overheads for EH too. Thus, the data packet from the source to the relay contains three parts: pilots for channel estimation, data symbols for information, and pilots for EH. The data packet from the relay to the destination contains two parts: pilots for channel estimation and data symbols from the source. If the total size of the data packet is fixed, as is the case in most practical systems with a fixed data rate, there is an optimal allocation between channel estimation, data information and EH.

In this chapter, the EH relaying with channel state information have been proposed, the data packet from the source to the relay contains three parts. The data packet from the relay to the destination contains two parts. For a fixed packet size, the outage and bit-error-rate performances are analysed and then optimised with respect to power allocation between different parts in the data packet. The cumulative distribution function (CDF) of the end-to-end SNR is derived. Using the derived expression, the outage probability and the bit-error-rate are calculated. Numerical results show the existence of the optimal values of the numbers of pilots for channel estimation and for EH, when the total size is fixed.

The remaining of this chapter will be organised is as follows. The system module of the time-switching EH is given in Section 4.2. In Section 4.3, the CSI of the system model will be estimated. In Section 4.4, the expressions for outage probability and bit-error-rate will be derived. In Section 4.5, the performance of the time-switching used in AF relaying will be discussed regards to outage probability and bit-error-ratio. The conclusion of this chapter will be presented in Section 4.6.

4.2 The time-switching EH system model

The AF relaying system with EH and channel estimation considered in the chapter is illustrated in Figure 4.1, α are the pilots for channel estimation at SR link,α_1 are the pilots for channel estimation at RD link, and β is the data symbols at SR link. The AF system comprises one source, one relay and one destination. There are two hops: the first hop is source to relay, and the second hop is relay to destination. We also assumed there is no direct link between source and destination due to obstacles. Further modelling improvements will be studied in the last Chapters.

The transmission in the first hop involves three parts: channel estimation, EH,

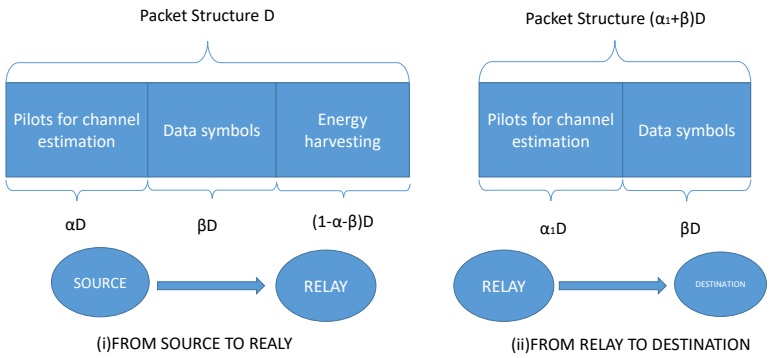

Figure 4.1: EH AF relaying (i) from source to relay (ii) from relay to destination

and data symbols. However, in the second hop merely contains two parts: channel estimation and data symbols.

Assume all the nodes operate in the half-duplex mode and has a single antenna for simplicity. In [169], the half-duplex and full-duplex performance have been compared. Time division is used in all the schemes, which has been studied in Chapter 3. The communication process is as follows: the source first sends information to the relay, and then the relay sends information to the destination. From Fig. 4.1, a total of D symbols are used for both the first hop and the second hop. Each symbol occupies a time duration of T seconds. Moreover, all fading channel coefficients are complex Gaussian random variables. The block fading channels are assumed,

which have been studied in [170]. For all noises in this scheme, the noise is additive white Gaussian noise (AWGN). The variable-gain AF relaying is used in this work, which uses different relaying gain values and achieves more accurate performance. However, the amplification factor also changes with the estimated channel gain in the SR link. For the parameters in this work, all the items α, α_1, β and $\alpha + \beta$ are smaller than 1. In addition, the items $\alpha D, \beta D, (\alpha + \beta)D$ are always integer.

In the first phase (broadcast phase), the source transmits the data packet to the relay. The received signal for the first part of the packet that contains pilot symbols for channel estimation can be expressed as

$$y_r[i] = \sqrt{P_s} h x[i] + n_1[i] \tag{4.1}$$

where $i = 1, 2, \ldots, \alpha D$, D is the total number of symbols in the packet, αD is the total number of pilots used for channel estimation, $0 < \alpha < 1$ is the fraction, P_s is the transmitted power of the source, h is the complex fading gain in the channel between the source and the relay and is complex Gaussian with zero mean and variance $2\theta^2$, $x[i]$ is the transmitted pilot symbol with unit power $E\{x[i]^2\} = 1$, $E\{.\}$ represents the expectation operator, and $n_1[i]$ is the complex AWGN with mean zero and noise power N_1. Also, the received signal of the data symbols at the relay in the second part of the data packet can be expressed as

$$y_r[j] = \sqrt{P_s} h x[j] + n_1[j] \tag{4.2}$$

where $j = \alpha D + 1, \ldots, (\alpha + \beta)D$, βD is the total number of data symbols, $x[j]$ is the transmitted data symbol with unit power that $E\{\mid x[j] \mid^2\} = 1$, $n_1[j]$ is the complex AWGN during data reception at the relay with mean zero and noise power N_1.

Finally, the received signal for EH in the third part of the data packet can be expressed as

$$y_r(k) = \sqrt{P_s} h x[k] + n_1(k) \tag{4.3}$$

where $k = (\alpha+\beta)D+1, \ldots, D$, $(1-\alpha-\beta)D$ is the total number of pilot symbols used for EH, $x[k]$ is the transmitted pilot symbol with unit power $E\{\mid x[k] \mid^2\} = 1$, and $n_1(k)$ is the AWGN complex with mean noise power and variance N_1. In (4.1)-(4.3), the channel gain h remains the same.

4.3 Time-switching EH maximum-likelihood estimation

Using the received signal in (4.3), the energy harvested by the relay can be expressed as

$$E_r = \eta P_s |h|^2 (1 - \alpha - \beta) D \tag{4.4}$$

where η is the conversion efficiency of the energy harvester and we have assumed that each symbol has an interval of $T = 1$ second for simplicity , $P_s|h|^2$ is the amount of energy picked up by the harvester at the relay. This energy will be used to transmit $\alpha_1 D$ pilot symbols to the destination for the channel estimation of the second hop from relay to destination as well as βD data symbols from the source. Thus, the transmission power of the relay is

$$P_r = \frac{\eta P_s |h|^2 (1 - \alpha - \beta) D}{\alpha_1 D + \beta D}. \tag{4.5}$$

Also, using the received signal in (4.1), the channel gain of the first hop from SR can be estimated as

$$\hat{h} = \frac{\Sigma_{i=1}^{\alpha D} y_r(i)}{\alpha D \sqrt{P_s}} = h + \frac{\Sigma_{i=1}^{\alpha D} n_1[i]}{\alpha D \sqrt{P_s}} = h + \varepsilon_1 \tag{4.6}$$

where $\varepsilon_1 = \frac{\Sigma_{i=1}^{\alpha D} n_1[i]}{\alpha D \sqrt{P_s}}$ is the estimation error. Thus, one has $h = \hat{h} - \varepsilon_1$.

The received signal in (4.2) will be amplified and forwarded to the destination by using the energy from (4.3) and the channel estimate of h from (4.1). The amplification factor can be expressed as [10]

$$\hat{a}_{var}^2 = \frac{1}{P_s \left|\hat{h}_1\right|^2 + N_1} \tag{4.7}$$

where $\hat{h}_1$ is the estimated channel gain for the hop between source and relay, and N_1 is the noise power of the relay.

In the second phase (relaying phase), in addition to sending $\alpha_1 D$ pilots to the destination for channel estimation, the relay also forwards the βD data symbols from the source to the destination.

The received signal of the pilots for channel estimation at the destination

can be expressed as

$$y_d[i_2] = \sqrt{P_r} g \hat{a}_{var} x[i_2] + n_2[i_2] \tag{4.8}$$

where $i_2 = 1, 2, \ldots, \alpha_1 D$, and $x[i_2] = 1$ is assumed for the pilot value, $n_2[i_2]$ is the AWGN at the destination during this transmission, and it is a complex Gaussian random variable with mean zero and variance N_2, $\hat{a}_{var}$ is the amplification factor given in (4.7), P_r is the relay transmission power given in (4.5), g is the fading channel coefficient in the RD link and is a complex Gaussian random variable with zero mean and variance $2\theta^2$.

Also, the received signals of the data symbols at the destination can be expressed as

$$y_d[j_1] = \sqrt{P_r} g \hat{a}_{var} \left(\sqrt{P_s} h x[j] + n_1[j] \right) + n_2[j_1] \tag{4.9}$$

where $n_2[j_1]$ is AWGN at the destination during this transmission and is a complex Gaussian with zero mean and variance N_2, and all the other symbols are defined as before.

Using the received signals in (4.8), the channel gain of the second hop can be estimated as

$$\begin{aligned} \hat{g} &= \frac{\Sigma_{m=1}^{\alpha_1 D} y_d(m)}{\alpha_1 D \hat{a}_{var} \sqrt{\hat{P}_r}} \\ &= \frac{\sqrt{P_r}}{\sqrt{\hat{P}_r}} g + \frac{\Sigma_{i=1}^{\alpha_1 D} n_2[i]}{\alpha_1 D \hat{a}_{var} \sqrt{\hat{P}_r}} \\ &= \frac{\sqrt{P_r}}{\sqrt{\hat{P}_r}} g + \varepsilon_2 \end{aligned} \tag{4.10}$$

where $\varepsilon_2 = \frac{\Sigma_{i=1}^{\alpha_1 D} n_2[i]}{\alpha_1 D \hat{a}_{var} \sqrt{\hat{P}_r}}$ is the estimation error and $\hat{P}_r = \frac{\eta P_s |\hat{h}|^2 (1-\alpha-\beta) D}{\alpha_1 D + \beta D}$ from (4.5). Thus, one also has

$$g = \frac{\sqrt{\hat{P}_r}}{\sqrt{P_r}} (\hat{g} - \varepsilon_2). \tag{4.11}$$

4.4 BER and optimal allocation in channel estimation

This section first derives the received signal at the destination, and the end-to-end SNR description, then the outage probability and BER of AF relaying using a variable gain in TS EH and the optimal resource allocation in the total signal transmission was analysed.

4.4.1 Estimation of CSI at both relay and destination

End-to-end SNR

By using (4.10) and (4.6) in (4.9), The received signal at the destination has

$$\begin{aligned} y_d[m] &= \sqrt{P_r} g \hat{a}_{var} \left(\sqrt{P_s} h x[j] + n_1[j] \right) + n_2[m] \\ &= \sqrt{\hat{P}_r} \hat{g} \hat{a}_{var} \sqrt{P_s} \hat{h} x[j] - \sqrt{\hat{P}_r} \hat{g} \hat{a}_{var} \sqrt{P_s} \varepsilon_1 x[j] + \sqrt{\hat{P}_r} \hat{g} \hat{a}_{var} n_1[j] - \\ &\sqrt{\hat{P}_r} \sqrt{P_s} \hat{h} \hat{a}_{var} \varepsilon_2 x[j] + \sqrt{\hat{P}_r} \sqrt{P_s} \hat{a}_{var} \varepsilon_1 \varepsilon_2 x[j] - \sqrt{\hat{P}_r} \varepsilon_2 \hat{a}_{var} n_1[j] + n_2[m] \end{aligned} \tag{4.12}$$

where g and h have been replaced by $\hat{g}$ and $\hat{h}$, respectively. Thus, the end-to-end Signal-to-Noise Ratio (SNR) can be derived from (4.12) as

$$\gamma_{end} = \frac{E[|\sqrt{\hat{P}_r} \hat{g} \hat{a}_{var} \sqrt{P_s} \hat{h} x[j]|^2]}{e} \tag{4.13}$$

where $e = E[|\sqrt{\hat{P}_r} \hat{g} \hat{a}_{var} \sqrt{P_s} \varepsilon_1 x[j]|^2] + E[|\sqrt{\hat{P}_r} \hat{g} \hat{a}_{var} n_1[j]|^2] + E[|\sqrt{\hat{P}_r} \sqrt{P_s} \hat{h} \hat{a}_{var} \varepsilon_2 x[j]|^2] + E[|\sqrt{\hat{P}_r} \sqrt{P_s} \hat{a}_{var} \varepsilon_1 \varepsilon_2 x[j]|^2] + E[|\sqrt{\hat{P}_r} \varepsilon_2 \hat{a}_{var} n_1[i]|^2] + E[|n_2[j]|^2]$ is the equivalent noise power.

One has $E[|x[j]|^2] = 1$, $E[|n_1[j]|^2] = N_1$ and $E[|n_2[j]|^2] = N_2$. Also denote $E[|\varepsilon|_1^2] = \varepsilon_{1var}$, $E[|\varepsilon|_2^2] = \varepsilon_{2var}$. Equation (4.13) can be rewritten as

$$\gamma_{end} = \frac{P_s |\hat{g}|^2 |\hat{h}|^2}{P_s |\hat{g}|^2 \varepsilon_{1var} + |\hat{g}|^2 N_1 + P_s \varepsilon_{2var} |\hat{h}|^2 + P_s \varepsilon_{1var} \varepsilon_{2var} + N_1 \varepsilon_{2var} + \frac{N_2}{\hat{P}_r \hat{a}_{var}^2}}. \tag{4.14}$$

Outage probability analysis

In this section, we first derive the cumulative distribution function (CDF) of the end-to-end SNR in (4.14). To do this, we calculate ε_{1var} and ε_{2var} first. From (4.6), one has

$$\varepsilon_1 = \frac{\Sigma_{i=1}^{\alpha D} n_1[i]}{\alpha D \sqrt{P_s}}. \tag{4.15}$$

Thus,

$$\begin{aligned}|\varepsilon_1|^2 &= \frac{\left|\Sigma_{i=1}^{\alpha D} n_1[i]\right|^2}{\alpha^2 D^2 P_s} \\ &= \Sigma_{i=1}^{\alpha D}(\frac{|n_1[i]|^2}{\alpha^2 D^2 P_s}) + \Sigma_{k=1}^{\alpha D}\Sigma_{j=1 k\neq j}^{\alpha D}(\frac{n_1[j]\times n_1[k]}{\alpha^2 D^2 P_s}).\end{aligned} \tag{4.16}$$

From (4.15), the variance of ε_1 can be derived as

$$\begin{aligned}\varepsilon_{1var} &= E\left[\Sigma_{i=1}^{\alpha D}(\frac{|n_1[i]|^2}{\alpha^2 D^2 P_s})\right] + E\left[\Sigma_{k=1}^{\alpha D}\Sigma_{j=1 k\neq j}^{\alpha D}(\frac{n_1[j]\times n_1[k]}{\alpha^2 D^2 P_s})\right] - \left[E(\frac{\Sigma_{i=1}^{\alpha D} n_1[i]}{\alpha D P_s})\right]^2 \\ &= \frac{N_1}{\alpha D P_s}.\end{aligned} \tag{4.17}$$

Similarly, one has from (4.10)

$$\begin{aligned}|\varepsilon_2|^2 &= \frac{\left|\Sigma_{i=1}^{\alpha_1 D} n_2[i]\right|^2}{{\alpha_1}^2 D^2 \hat{a}_{var}^2 \hat{P}_r} = \Sigma_{i=1}^{\alpha_1 D}(\frac{{n_2[i]}^2(\alpha_1+\beta)\left(P_s|\hat{h}|^2+N_1\right)}{[\eta P_s|\hat{h}|^2(1-\alpha-\beta)]{\alpha_1}^2 D^2}) \\ &+ \Sigma_{k=1}^{\alpha_1 D}\Sigma_{j=1 k\neq j}^{\alpha_1 D}(\frac{n_2[j]\times n_2[k](\alpha_1+\beta)\left(P_s|\hat{h}|^2+N_1\right)}{[\eta P_s|\hat{h}|^2(1-\alpha-\beta)]{\alpha_1}^2 D^2}).\end{aligned} \tag{4.18}$$

Thus, the variance of ε_2 can be expressed as

$$\begin{aligned}\varepsilon_{2var} &= Var(\varepsilon_2) = E\left(\Sigma_{i=1}^{\alpha_1 D}\frac{|n_2[i]|^2(\alpha_1+\beta)\left(P_s|\hat{h}|^2+N_1\right)}{[\eta P_s|\hat{h}|^2(1-\alpha-\beta)]{\alpha_1}^2 D^2]}\right) \\ &+ E\left(\Sigma_{k=1}^{\alpha_1 D}\Sigma_{j=1 k\neq j}^{\alpha_1 D}\frac{n_2[j]\times n_2[k](\alpha_1+\beta)\left(P_s|\hat{h}|^2+N_1\right)}{[P_s\eta|\hat{h}|^2(1-\alpha-\beta)]{\alpha_1}^2 D^2}\right) \\ &- \left[E\left(\frac{\Sigma_{i=1}^{\alpha_1 D} n_2[i]\sqrt{P_s|\hat{h}|^2+N_1}\sqrt{\alpha_1+\beta}}{\alpha_1 D\sqrt{\eta P_s|\hat{h}|^2(1-\alpha-\beta)}}\right)\right]^2 \\ &= \frac{N_2(\alpha_1+\beta)\left(P_s|\hat{h}|^2+N_1\right)}{[\eta P_s|\hat{h}|^2(1-\alpha-\beta)]\alpha_1 D}.\end{aligned} \tag{4.19}$$

Using (4.17) and (4.20) in (4.14), the end-to-end SNR can be derived as

$$\gamma_{end} = \frac{|\hat{g}|^2|\hat{h}|^2 P_s}{u+v} \tag{4.20}$$

where $u = \frac{N_1|\hat{g}|^2}{\alpha D} + |\hat{g}|^2 N_1 + \frac{N_2 N_1(\alpha_1+\beta)\left(P_s|\hat{h}|^2+N_1\right)}{[\eta P_s|\hat{h}|^2(1-\alpha-\beta)]\alpha\alpha_1 D^2} + \frac{P_s|\hat{h}|^2 N_2(\alpha_1+\beta)\left(P_s|\hat{h}|^2+N_1\right)}{[\eta P_s|\hat{h}|^2(1-\alpha-\beta)]\alpha_1 D}$ and $v = \frac{N_2 N_1(\alpha_1+\beta)\left(P_s|\hat{h}|^2+N_1\right)}{[\eta P_s|\hat{h}|^2(1-\alpha-\beta)]\alpha_1 D} + \frac{N_2(\alpha_1+\beta)\left(P_s|\hat{h}|^2+N_1\right)}{[\eta P_s|\hat{h}|^2(1-\alpha-\beta)]}$. Next, we obtain the distributions of $\hat{h}$ and $\hat{g}$. Using the expression of $\hat{h}$ in (4.6), its second-order moment can be derived as [125]

$$E(|\hat{h}|^2) = E|h+\varepsilon_1|^2 = 2\theta^2 + |\frac{N_1}{\alpha D P_s}|. \tag{4.21}$$

Since h and ε_1 are complex Gaussian, $\hat{h}$ as a sum is also complex Gaussian. Thus, $|\hat{h}|^2$ is an exponential random variable with parameter

$$\lambda_1 = \frac{1}{2\theta^2 + |\frac{N_1}{\alpha D P_s}|}. \tag{4.22}$$

Then, the probability density function (PDF) of $|\hat{h}|^2$ in the SR link can be expressed as [125]

$$f_{|\hat{h}|^2}(x) = \lambda_1 e^{-\lambda_1 x}. \tag{4.23}$$

The CDF of $|\hat{h}|^2$ is then

$$F_{|\hat{h}|^2}(x) = 1 - e^{-\lambda_1 x}. \tag{4.24}$$

Also, from (4.10), one has

$$|\hat{g}|^2 = \frac{|h|^2}{|\hat{h}|^2}|g|^2 + |\frac{\Sigma_{i=1}^{\alpha_1 D} n_2[i]}{\alpha_1 D \hat{a}_{var}\sqrt{\hat{P}_r}}|^2 + 2Re\{\frac{|h|}{|\hat{h}|}g \times \frac{\Sigma_{i=1}^{\alpha_1 D} n_2[i]^*}{\alpha_1 D \hat{a}_{var}\sqrt{\hat{P}_r}}\}. \tag{4.25}$$

Thus, the expectation of $|\hat{g}|^2$ can be derived as

$$E(|\hat{g}|^2) = 2\theta^2 E\{\frac{|h|^2}{|\hat{h}|^2}\} + E\{\frac{|N_2||\alpha_1+\beta||P_s|\hat{h}|^2 + N_1|}{|\alpha_1 D|\eta P_s|\hat{h}|^2|1-\alpha-\beta|}\} \tag{4.26}$$

where $E(|g|^2) = 2\theta^2$, $E(\Sigma_{i=1}^{\alpha_1 D} n_2[i]) = 0$ and $E\left(\frac{2\Sigma_{k=1}^{\alpha_1 D}\Sigma_{j=1}^{\alpha_1 D} Re\{n_2[j]n_2[k]^*\}}{|\alpha_1|^2|D|^2|\hat{a}_{var}|^2|\hat{P}_r|}\right) = 0$ have been used. Assume that $E\left\{\frac{|h|^2}{|\hat{h}|^2}\right\} \approx \frac{E\{|h|^2\}}{E\{|\hat{h}|^2\}}$. One has

$$E\left\{\frac{|h|^2}{|\hat{h}|^2}\right\} \approx \frac{E\left\{|h|^2\right\}}{E\left\{|\hat{h}|^2\right\}} = \frac{E\left\{|h|^2\right\}}{E\left\{|h|^2\right\} + \frac{|N_1|}{\alpha D P_s}} = \frac{2\theta^2}{2\theta^2 + \frac{|N_1|}{\alpha D P_s}}. \tag{4.27}$$

Also,

$$E\left\{\frac{|N_2||\alpha_1+\beta||P_s|\hat{h}|^2+N_1|}{|\alpha_1|D\eta P_s|\hat{h}|^2|1-\alpha-\beta|}\right\}=\left(1+\int_0^\infty \frac{N_1}{P_s x} f_{|\hat{h}|^2}(x)dx\right)\frac{|N_2||\alpha_1+\beta|}{|\alpha_1 D|\eta|1-\alpha-\beta|}$$
$$=\frac{|N_2||\alpha_1+\beta|}{|\alpha_1 D|\eta|1-\alpha-\beta|}-\frac{|N_2||\alpha_1+\beta|}{P_s|\alpha_1 D|\eta|1-\alpha-\beta|}\frac{N_1 Ei(0)}{2\theta^2+\frac{|N_1|}{|\alpha D P_s|}} \tag{4.28}$$

where one has

$$E\left\{\frac{N_1}{|\hat{h}|^2}\right\}=\int_0^\infty \frac{N_1}{x} f_{|\hat{h}|^2}(x)dx=-\frac{N_1}{2\theta^2+\frac{|N_1|}{|\alpha D P_s|}}Ei(0) \tag{4.29}$$

and $Ei(0)$ is the exponential integral function [161, eq,(8.211.1)]. Thus, one finally has

$$E\left(|\hat{g}|^2\right)$$
$$=\frac{4\theta^4}{2\theta^2+\frac{|N_1|}{\alpha D P_s}}+\frac{|N_2||\alpha_1+\beta|}{|\alpha_1 D|\eta|1-\alpha-\beta|}-\frac{|N_2||\alpha_1+\beta|}{P_s|\alpha_1 D|\eta|1-\alpha-\beta|}\frac{N_1 Ei(0)}{2\theta^2+\frac{|N_1|}{|\alpha D P_s|}}=\frac{1}{\lambda_2}. \tag{4.30}$$

Similarly, $|\hat{g}|^2$ can be approximated as an exponential random variable when ε_1 is small. Thus, its PDF is [125]

$$f_{|\hat{g}|^2}(x)=\lambda_2 e^{-\lambda_2 x} \tag{4.31}$$

and its CDF is

$$F_{|\hat{g}|^2}(x)=1-e^{-\lambda_2 x}. \tag{4.32}$$

Using these results, we can derive the CDF of γ_{end}. One has from (4.21)

$$F_{\gamma_{end}}(x)=P_r\{\gamma_{end}<x\}=I_1+I_2 \tag{4.33}$$

where

$$I_1=P_r\{P_s|\hat{h}|^2-\frac{xN_1}{\alpha D}-xN_1<0\} \tag{4.34}$$

$$I_2=P_r\{|\hat{g}|^2<\frac{m}{\left[\eta\alpha_1\alpha D^2\left(1-\alpha-\beta\right)P_s|\hat{h}|^2\right]\left(P_s|\hat{h}|^2-\frac{xN_1}{\alpha D}-xN_1\right)}$$
$$|\left(P_s|\hat{h}|^2-\frac{xN_1}{\alpha D}-xN_1\right)>0\}. \tag{4.35}$$

Equation (4.34) is on the condition that $P_s|\hat{h}|^2-\frac{xN_1}{\alpha D}-xN_1<0$, and

equation (4.35) is on the condition that $P_s|\hat{h}|^2 - \frac{xN_1}{\alpha D} - xN_1 > 0$. Also, in (4.35) $m = \gamma_0 N_2 N_1 (\alpha_1 + \beta)\left(P_s|\hat{h}|^2 + N_1\right) + \alpha D \gamma_0 N_2 N_1 (\alpha_1 + \beta)\left(P_s|\hat{h}|^2 + N_1\right) + x\alpha_1 \alpha D^2 N_2 (\alpha_1 + \beta)\left(P_s|\hat{h}|^2 + N_1\right) + \alpha D x P_s |\hat{h}|^2 N_2 (\alpha_1 + \beta)\left(P_s|\hat{h}|^2 + N_1\right)$. It is quite easy to use the CDF of $|\hat{h}|^2$ in (4.34) to have

$$I_1 = 1 - e^{-\frac{\frac{xN_1}{\alpha D P_s} + \frac{xN_1}{P_s}}{2\theta^2 + |\frac{N_1}{\alpha D P_s}|}}. \tag{4.36}$$

Thus (4.35) can be solved by using the CDF of $|\hat{g}|^2$ as

$$I_2 = \int_{\frac{xN_1}{\alpha D P_s} + \frac{xN_1}{P_s}}^{\infty} F_{(|\hat{g}|^2)}\left[\frac{m}{\eta \alpha_1 \alpha D^2 (1 - \alpha - \beta) P_s y (P_s y - \frac{xN_1}{\alpha D} - xN_1)}\right] \times f_{\left(|\hat{h}|^2\right)}(y)\, dy. \tag{4.37}$$

Let $P_s y - \frac{xN_1}{\alpha D} - xN_1 = t; P_s y = \frac{1}{P_s}(t + \frac{xN_1}{\alpha D} + xN_1)$. Using this variable transformation to replace y with t in (4.37), one has

$$\begin{aligned} I_2 = & \int_0^{\infty} \frac{1}{\left(2\theta^2 + |\frac{N_1}{\alpha D P_s}|\right)} e^{-\frac{\frac{t}{P_s} + \frac{xN_1}{\alpha D P_s} + \frac{xN_1}{P_s}}{2\theta^2 + |\frac{N_1}{\alpha D P_s}|}} dt \frac{1}{P_s} - \frac{1}{\left(2\theta^2 + |\frac{N_1}{\alpha D P_s}|\right)} e^{-\frac{\lambda_2 b}{d} - \frac{xN_1 + xN_1 \alpha D}{2\theta^2 \alpha D P_s + |N_1|}} \\ & \times \int_0^{\infty} e^{-\frac{\frac{\lambda_2 (c + ba)}{d}}{t} - \frac{\alpha D}{2\theta^2 \alpha D P_s + |N_1|} t} dt \frac{1}{P_s} \end{aligned} \tag{4.38}$$

where $a = \frac{xN_1}{\alpha D} + xN_1; c = xN_2 N_1 (\alpha_1 + \beta) + \alpha D x N_2 N_1 (\alpha_1 + \beta) + x\alpha_1 \alpha D^2 N_2 (\alpha_1 + \beta)$;
$b = \alpha D x N_2 (\alpha_1 + \beta); d = \eta \alpha_1 \alpha D^2 (1 - \alpha - \beta)$.

By solving the two integrals in (4.38), one has

$$\begin{aligned} I_2 = & \frac{1}{\left(2\theta^2 + |\frac{N_1}{\alpha D P_s}|\right)} e^{-\frac{xN_1 + xN_1 \alpha D}{2\theta^2 \alpha D P_s + |N_1|}} \frac{2\theta^2 \alpha D P_s + |N_1|}{\alpha D} \\ & - \frac{1}{\left(2\theta^2 + |\frac{N_1}{\alpha D P_s}|\right)} e^{-\frac{\alpha D x N_2 (\alpha_1 + \beta)}{q} - \frac{xN_1 + xN_1 \alpha D}{2\theta^2 \alpha D P_s + |N_1|}} \\ & \times \frac{2}{P_s}\left(\frac{p(2\theta^2 \alpha D P_s + |N_1|)}{q \alpha D}\right)^{\frac{1}{2}} \times K_1\left(2\sqrt{\frac{p \alpha D}{q(2\theta^2 \alpha D P_s + |N_1|)}}\right) \end{aligned} \tag{4.39}$$

where $p = \left(\left[xN_2 N_1 (\alpha_1 + \beta) + \alpha D x N_2 N_1 (\alpha_1 + \beta) + x\alpha_1 \alpha D^2 N_2 (\alpha_1 + \beta)\right]\right.$
$+ \left.\left[\alpha D x N_2 (\alpha_1 + \beta)\right]\left[\frac{xN_1}{\alpha D} + xN_1\right]\right), q = \left(\frac{4\theta^4}{2\theta^2 + \frac{|N_1|}{\alpha D P_s}} + \frac{|N_2||\alpha_1 + \beta|}{|\alpha_1 D|\eta|1 - \alpha - \beta|} -\right.$

$\frac{|N_2||\alpha_1+\beta|}{P_s|\alpha_1 D|\eta|1-\alpha-\beta|}\frac{Ei(0)}{2\theta^2+\frac{|N_1|}{|\alpha D P_s|}}\big)\left[\eta\alpha_1\alpha D^2\left(1-\alpha-\beta\right)\right]$. Thus, we have a closed-form expression for the CDF of γ_{end}.

Using the CDF of γ_{end}, the outage probability can be calculated as

$$\begin{aligned} P_0(\gamma_0) &= 1 - \frac{1}{\left(2\theta^2 + |\frac{N_1}{\alpha D P_s}|\right)} e^{-\frac{\alpha D\gamma_0 N_2(\alpha_1+\beta)}{q} - \frac{\gamma_0 N_1 + \gamma_0 N_1 \alpha D}{2\theta^2 \alpha D P_s + |N_1|}} \\ &\times \frac{2}{P_s}\left(\frac{p(2\theta^2\alpha D P_s + |N_1|)}{q\alpha D}\right)^{\frac{1}{2}} \times K_1\left(2\sqrt{\frac{p\alpha D}{q(2\theta^2\alpha D P_s + |N_1|)}}\right). \end{aligned} \tag{4.40}$$

Bit-error-rate analysis

In addition, the BER can be calculated as [125]

$$BER = \int_0^\infty \frac{1}{2} erfc(\sqrt{x}) * dF_\gamma(x) = \frac{1}{2}\int_0^\infty \frac{exp(-x)}{\sqrt{x*\pi}} F_{\gamma_{end}}(x)dx, \tag{4.41}$$

where $erfc(x)$ is the complementary error function evaluated for each element of x and $exp(x)$ is the exponential function.

It is difficult to find the optimal values of α, β, α_1 that maximise the outage probability and the BER analytically, as they contain highly nonlinear functions, such as the modified Bessel function and the exponential function.

4.5 Numerical results and destination

In this section, the outage probability and the BER for AF relaying derived the previous section will be examined. In the examination, numerical methods are used to find possible optimal values of α, β and α_1 that gives the best allocation of the data packet. Intuitively, they exist when the value of D is fixed. Denote γ_1 as the instantaneous SNR of the SR link, and γ_2 as the instantaneous SNR of the RD link.

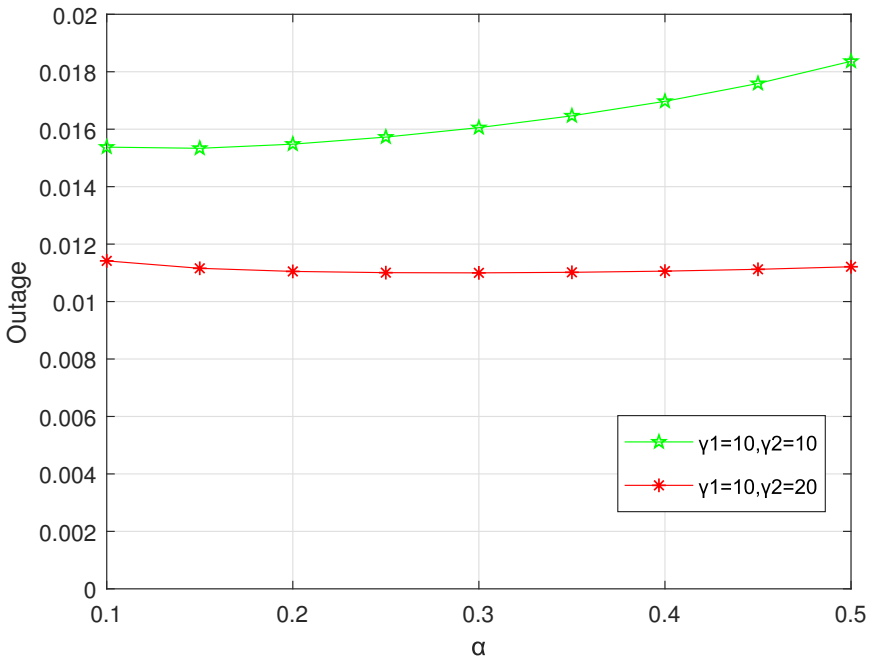

Figure 4.2: outage probability versus α.

4.5.1 Outage probability analysis

Outage Probability Versus α

In Fig. 4.2, we fix $P_s = 1$, $\eta = 0.3, D = 100, N_1 = N_2 = 1, \alpha_1 = 0.1, \beta = 0.1, \gamma_0 = -10$ to show the relationship between the outage probability and α.

One sees that the outage probability decreases when γ_1 or γ_2 increases, as expected. When $\gamma_1 = 10\ dB$, $\gamma_2 = 10\ dB$ or when $\gamma_1 = 10\ dB$, $\gamma_2 = 20\ dB$, the outage probability first decreases very slowly and then increases quickly, when the value of α increases. The optimal α is around 0.15 and 0.4, respectively. A smaller α means a less accurate estimate of $\hat{h}$, but more energy for harvesting. The slow rate at small α and the quick rate at large α imply that the outage performance is more sensitive to the harvested energy then to the channel estimation error, as the increase of α with better estimation accuracy does not improve the outage much.

Fig. 4.3 shows the outage probability vs. α when β is fixed at 0.1 or 0.4. In this case, $\gamma_1 = 10\ dB$ and $\gamma_2 = 10\ dB$ and other parameters are the same as

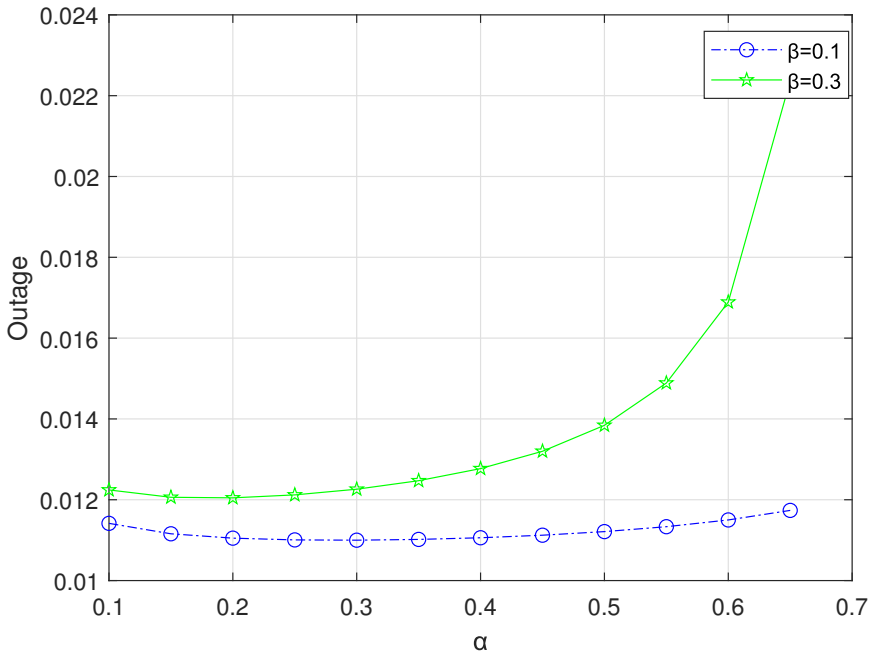

Figure 4.3: The outage probability versus α when β is fixed at 0.1 or 0.4.

before. By comparing the results for $\beta = 0.1$ with that for $\beta = 0.3$, one can see that both of them decrease first and then increase when α increases, similar to before. When $\beta = 0.1$, the outage probability only rises up to around 0.012. When $\beta = 0.3$, the outage probability decreases first and then increases to around 0.022. Moreover, they have different optimal values. For $\beta = 0.1$, the optimal value is around $\alpha = 0.3$. For $\beta = 0.3$, the optimal value is around $\alpha = 0.2$.

Outage probability versus α_1

In Fig. 4.4, we fix $P_s = 1, \eta = 0.3, D = 100, N_1 = N_2 = 1, \alpha_1 = 0.1, \beta = 0.1, \gamma_0 = -2$ to show the relationship between the outage probability and α_1.

One sees that the outage probability decreases when γ_1 or γ_2 increase, as expected. When $\gamma_1 = 20\ dB$, $\gamma_2 = 0\ dB$ or when $\gamma_1 = 30\ dB$, $\gamma_2 = 0\ dB$, the outage probability first decreases very slowly and then increases quickly, when the value of α_1 increases. The optimal α_1 is around 0.2. Again, the slow rate at small α_1 and the quick rate at large α_1 implies that the outage performance is more sensitive to

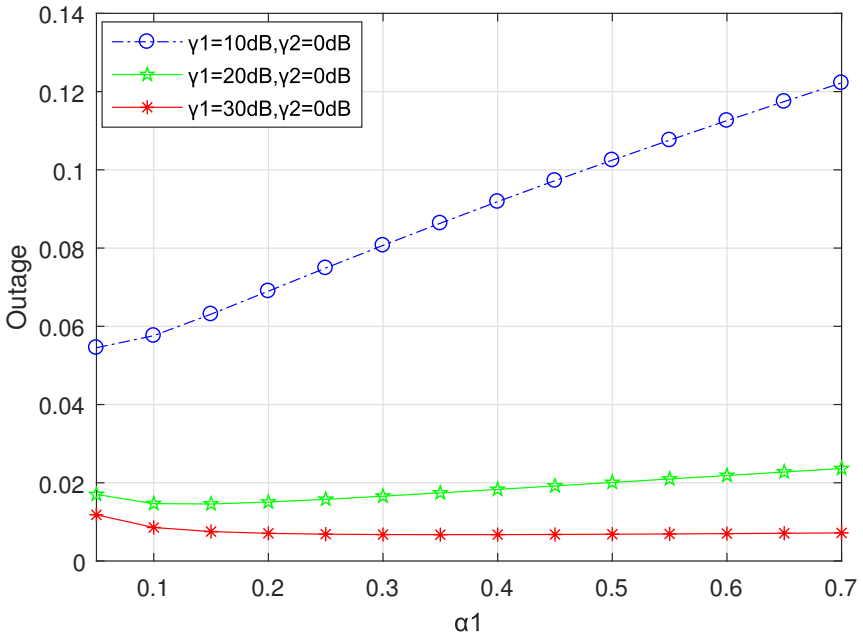

Figure 4.4: Outage probability versus α_1.

the harvested energy than to the channel estimation error. In general, the outage does not change much when α_1 changes in this case.

Fig. 4.5 shows the Outage probability vs. α_1 when β is fixed at 0.1 or 0.3. In this case, $\gamma_1 = 10\ dB$ or $\gamma_2 = 0\ dB$ and other parameters are the same as before. By comparing the results for $\beta = 0.1$ with that for $\beta = 0.3$, again both of them decrease first and then increase when α_1 increases, similar to before. In this case, when $\beta = 0.1$, the outage probability only rises up to around 0.013 while when $\beta = 0.3$, the outage probability increases to around 0.011. Moreover, they have different optimal values. For $\beta = 0.1$ the optimal value is around $\alpha_1 = 0.35$. For $\beta = 0.3$, the optimal value is around $\alpha_1 = 0.65$.

4.5.2 Bit-error-rate analysis

BER versus α

In Fig. 4.6, we fix $P_s = 1$, $\eta = 0.3, D = 100, N_1 = N_2 = 1, \alpha_1 = 0.1, \beta = 0.1$ to show the relationship between the BER and α. [104]

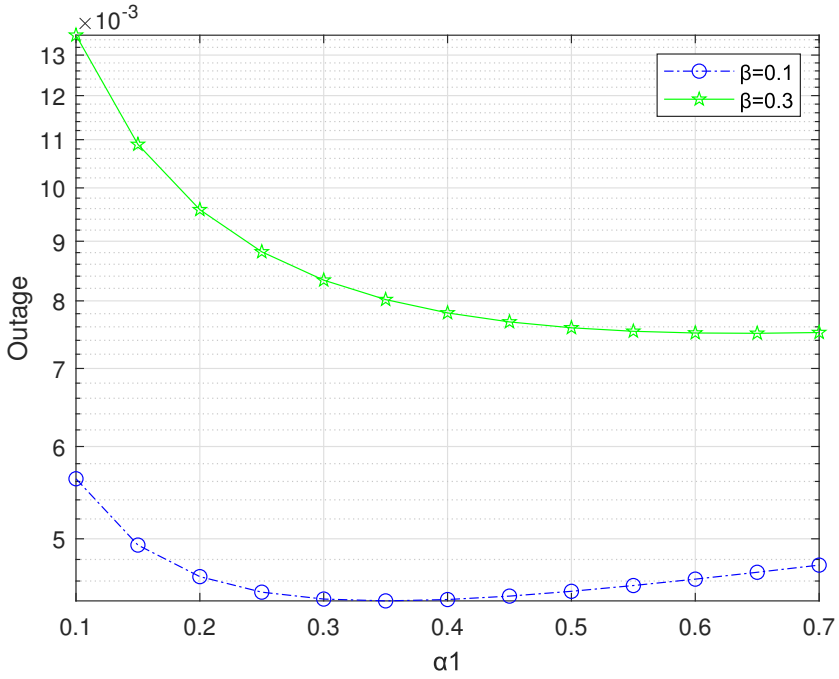

Figure 4.5: The outage probability versus α_1 when beta is fixed at 0.1 or 0.3.

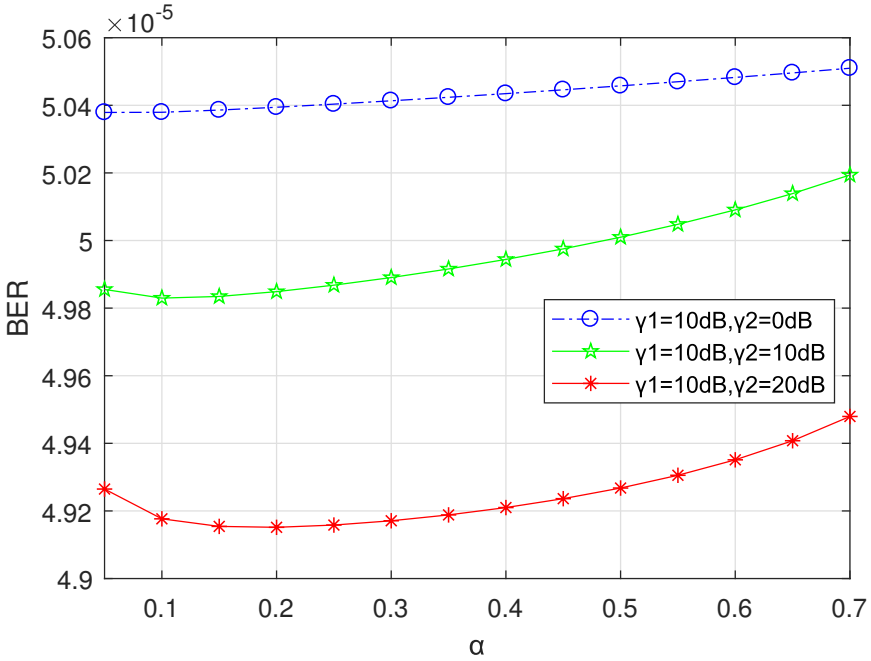

Figure 4.6: BER versus α.

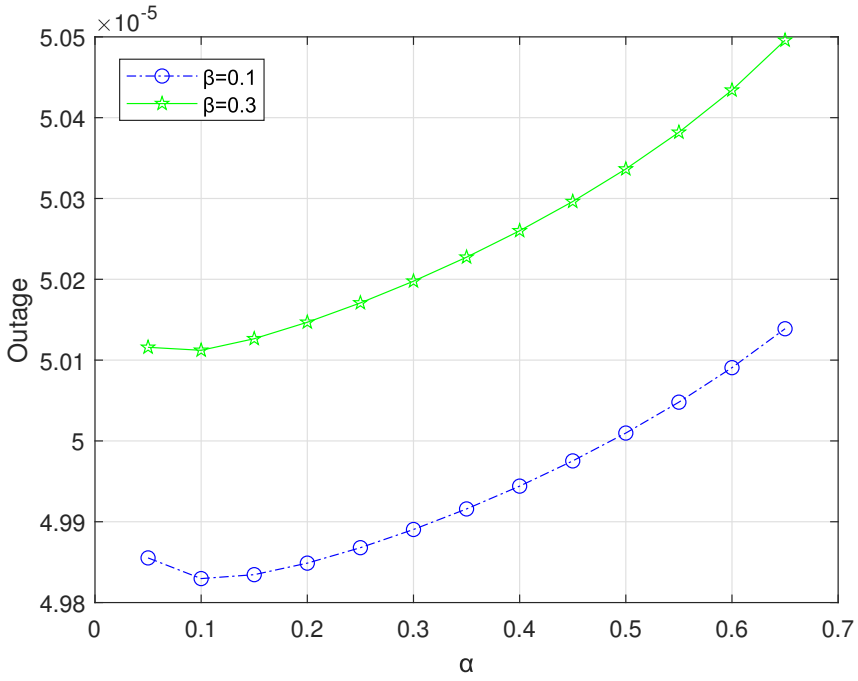

Figure 4.7: BER versus α when β is fixed at 0.1 or 0.3.

One sees that the BER decreases when γ_1 or γ_2 increase. Better channel conditions often give better performance. In all the three curves, the BER first decreases very slowly and then increases quickly, when the value of α increases. The optimal α is around 0.08 for $\gamma_1 = 10\ dB$ and $\gamma_2 = 0\ dB$, is around 0.1 for $\gamma_1 = 10\ dB$ and $\gamma_2 = 10\ dB$ and is around 0.2 for $\gamma_1 = 10\ dB$ and $\gamma_2 = 20\ dB$.

Fig. 4.7 shows the BER vs. α when β is fixed at 0.1 or 0.4. In this case, $\gamma_1 = 10\ dB$ or $\gamma_2 = 10\ dB$ and other parameters are the same as before. By comparing $\beta = 0.1$ and $\beta = 0.3$, one can see the BER decreases when β decreases. For $\beta = 0.1$, the optimal α is around $\alpha = 0.1$. For $\beta = 0.3$, the optimal α is around $\alpha = 0.1$.

BER versus α_1

In Fig. 4.8, we fix $P_s = 1$, $\eta = 0.3, D = 100, N_1 = N_2 = 1, \alpha_1 = 0.1, \beta = 0.1$, to show the relationship between the BER and α_1. Similar to α, the BER also decrease then increase with α_1. The optimal α_1 in this case is around 0.15.

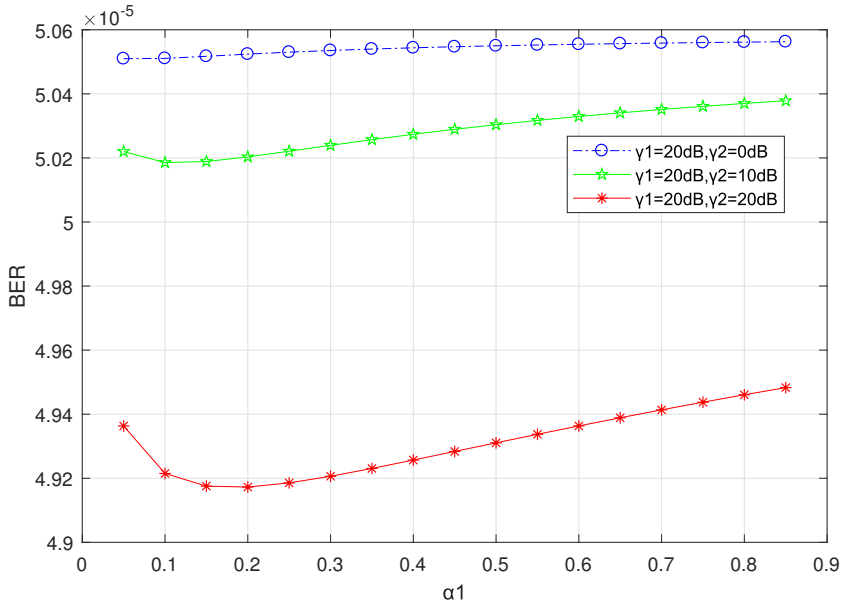

Figure 4.8: BER versus α_1.

In Fig 4.9, we fix $P_s = 1$, $\eta = 0.3, D = 100, N_1 = N_2 = 1, \beta = 0.5$, (a) shows the outage probability when the value α increases. (b) shows the outage probability decreases first and then increases to around 0.048, and the optimal α_1 in this case is around 0.275. (c) show the BER for α increases when the value α increases.

4.6 Conclusions

In this chapter, an AF relaying system with EH and channel estimation have been considered. The optimal power allocation between channel estimation data transmission and EH has been examined in term of outage and BER. Numerical results have confirmed the existence of the optimal values of the numbers of pilots for channel estimation and for EH, when the total size is fixed. Further, theses results specify actual values of these optimal parameters that can be used to achieve best outage and BER performance, under different system settings. They further confirm that the performance is more sensitive to EH than estimation.

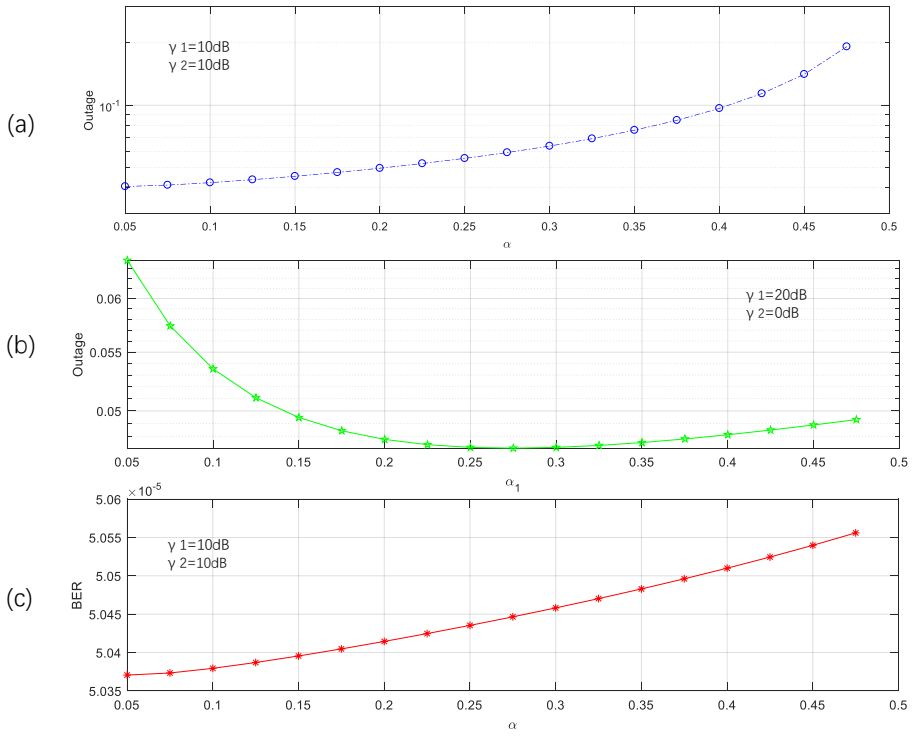

Figure 4.9: (a) The outage probability versus α when β is fixed at 0.5 (b) The outage probability versus α_1 when β is fixed at 0.5 (c) BER versus α when β is fixed at 0.5.

Chapter 5

Allocation between harvesting, estimation and detection for hybrid TS/PS relaying

5.1 Introduction and related works

As mentioned in Chapter 4, an AF relaying system with pilot-based channel estimation equipped time-switching (TS) EH was proposed to analyse the performance of the communications system. From the previous researches, there are two EH protocols: power-splitting (PS) and Time-Switching (TS). The conventional way is used time-switching (TS) and power-splitting (PS) protocols independently, either design the relaying EH model only depended on TS protocol or PS protocol. They have been put forward in [171], where the authors discussed the performance of TS and PS protocols under the relaying system.

To make the structure more comprehensive, we have designed three novel EH structures by using wireless simulation information and power transfer in AF relaying. For different combinations of TS and PS EH protocols have been studied in this chapter. We have proposed three dynamic schemes: channel estimation power splitting (CEPS), data transmission power splitting (DTPS), and combination power splitting (CPS). These models will also be used for further studies in Chapter 6.

In previous works [104], the authors considered TS and PS separately. More-

over, the signal channels are only considered channel estimation before this work. Additionally, the previous researches either used the EH in information decoding or used the EH in channel estimation [127], but they haven't been considered at the same time.

In this part of work, three novel EH structures in AF relaying are proposed. Different combinations of TS and PS EH protocols in the first hop have been considered for improving the efficiency of EH. Also, the optimal power allocation includes different parts of the data packet are explored, where the data packet in the second hop we have only comprised channel estimation and information transmission. The distance between the source, the relay, and the destination have been considered in this work as well. There is also a direct link between the source and the destination, which can improve the information decoding efficiency.

In this chapter, the data packet from SR is split into three parts: channel estimation, data transmission and EH. The data packet from relay to destination (RD) is divided into two parts: data transmission and channel estimation. Closed-form expressions for the cumulative distribution function (CDF) of the end-to-end Signal-to-Noise Ratio (SNR) for three novel structures are derived. Using these expressions, achievable rate (AR) and bit-error-rate (BER) are calculated. The impact of different parameters is examined. Numerical results are presented to show the existence of the optimal splitting for channel estimation and EH, when the total packet size is fixed.

In this work, it is the first one on AF relaying that considered data packets including channel estimation, EH, and information decoding altogether. Secondly, for three different EH structures, the cumulative distribution function (CDF) of the end-to-end Signal-to-Noise (SNR) expressions are derived base on probability density function (PDF). Based on the achievable rate and BER, the optimal power allocation is founded in this work.

The rest of this chapter is organised as follows. The system of three novel EH structures will be given in Section 5.2. In Section 5.3, the end-to-end SNR for different structures will be presented. The expressions of achievable rate and BER will be derived in Section 5.4. In Section 5.5, the performance of the EH structures will be discussed according to the achievable rate and bit-error-ratio. Finally, the conclusion of this chapter will be presented in Section 5.5.

5.2 Three novel EH AF relaying system models

Fig. 5.1 shows the AF relaying network including a source S, a relay R and a destination D. Let d_{sr}, d_{rd}, d_{sd} denote the distances between S and R, R and D and S and D, respectively. Denote h_1, h_2 and h_3 as the fading gains for CEPS, DTPS, CPS, respectively, in the channel between the source and the relay and are complex Gaussian with mean zero and variance $2\theta^2$. Denote g_1, g_2 and g_3 as the fading channel coefficients of the RD links and are complex Gaussian random variables with mean zero and variance $2\theta^2$. For simplification, the pilots used for channel estimation in the SR link and RD link are assumed to have equal values. Fig. 5.2(a) shows the channel estimation power splitting (CEPS) structure. Using power splitting, the source sends m_{11} pilots using its own power, each of which is split in power with power ratio ρ_p for EH and $(1-\rho_p)$ for channel estimation, while the data is added using time-switching. Note that these pilots are not sent by using the harvested power in this case. Fig. 5.2(b) shows the data transmission power splitting (DTPS) structure. In this structure, the source sends m_{21} pilots for channel estimation, and the data symbols are split in power with power ratio ρ_d for EH and $(1-\rho_d)$ for data transmission. Fig. 5.2(c) shows the combined power splitting (CPS) structure. In this structure, the source sends m_{31} pilots for channel estimation and $(D-m_{31})$ data symbols for information delivery. The energy is harvested by splitting all symbols for both channel estimation and data transmission with power splitting ratio ρ_c.

Assumed time division is used in all the structures to achieve orthogonal channels. Therefore, the source first sends the data packet to the relay, and then the relay sends the data packet to the destination. A total of D symbols are used in each structure for channel estimation, data transmission and EH. Each symbol occupies a time duration of T seconds. Moreover, all fading channel coefficients are complex Gaussian random variables with mean zero, which are fixed for each data packet but vary from packet to packet. All noises are symmetrical complex additive white Gaussian noise (AWGN). Each transmits symbol in the block is assumed to be a Gaussian distribution with noise and power 1. The variable-gain relaying is assumed so that the amplification factor changes with the estimated channel gain in the SR link [172], [173]. However, all the values of m_{11}, m_{21} and m_{31} in Fig. 5.2 are integers and smaller than D. Also, $0 \leqslant \rho_p, \rho_d, \rho_c \leqslant 1$.

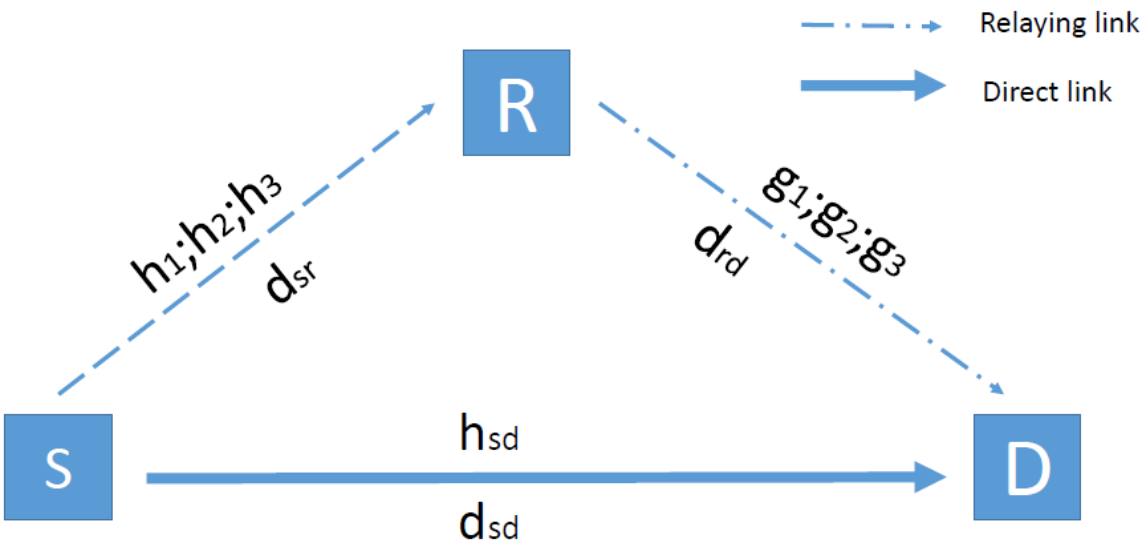

Figure 5.1: AF relaying network.

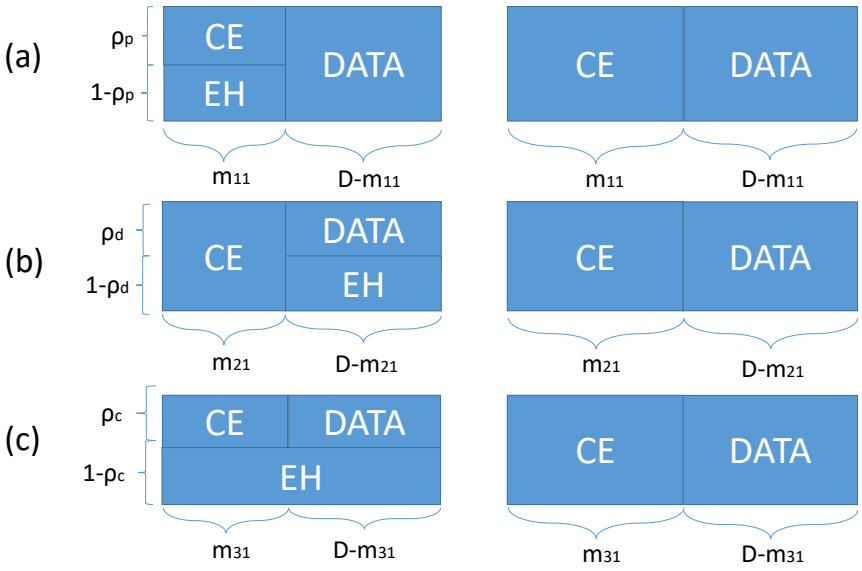

Figure 5.2: (a) Channel estimation power splitting (CEPS) structure; (b) Data transmission power splitting (DTPS) structure; (c) Combination power splitting (CPS) structure.

5.2.1 Channel estimation power splitting scheme

In the CEPS structure, there are three parts in the first hop: pilots for channel estimation and EH, and data symbols for data transmission. At the relay, the received signals of the m_{11} pilots are split into two parts with a power splitting factor $0 < \rho_p < 1$. First, the received pilot at relay for channel estimation is given by

$$y_r[i_{11}] = \sqrt{\frac{\rho_p P_{s1}}{{d_{sr}}^e}} h_1 x[i_{11}] + n_{11}[i_{11}] \tag{5.1}$$

where $i_{11} = 1, 2, \ldots, m_{11}$ is the total number of pilots in the data packet, $0 < m_{11} < D$ is an integer, P_{s1} is the transmitted power of the source, d_{sr} is the distance between source and relay, e is the path loss exponent, $x[i_{11}]$ is the transmitted pilot with unit power $E\{\mid x[i_{11}] \mid^2\} = 1$, $E\{.\}$ represents the expectation operator, and $n_{11}[i_{11}]$ is the complex AWGN with mean zero and noise power N_{11}.

The received signal of the data symbols at relay can be expressed as

$$y_r[j_{11}] = \sqrt{\frac{P_{s1}}{{d_{sr}}^e}} h_1 x[j_{11}] + n_{11}[j_{11}] \tag{5.2}$$

where $j_{11} = m_{11} + 1, \ldots, D$, $x[j_{11}]$ is the transmitted data symbol with unit power $E\{\mid x[j_{11}] \mid^2\} = 1$, $n_{11}[j_{11}]$ is the complex AWGN with mean zero and noise power N_{11}. This power is supplied by source, not the harvester.

Next, the received signal of pilots for EH in the second part of the data packet can be expressed as

$$y_r(k_1) = \sqrt{\frac{(1-\rho_p)P_{s1}}{{d_{sr}}^e}} h_1 x[k_1] + n_{11}(k_1) \tag{5.3}$$

where $k_1 = 1, 2, 3, 4, 5, \ldots, m_{11}$, and $m_{11}(1-\rho_p)$ is the total number of pilot symbols used for EH, $x[k_1]$ is the transmitted pilot symbol with unit power $E\{\mid x[k_1] \mid^2\} = 1$, and $n_{11}(k_1)$ is the AWGN complex with mean noise power and variance N_{11}. In (5.1)-(5.2), the channel gain h_1 remains the same.

Hence, the harvested energy at the relay is

$$E_{r1} = \frac{\eta P_{s1} |h_1|^2 (1-\rho_p) m_{11}}{{d_{sr}}^e} \tag{5.4}$$

where η stands for the conversion efficiency of the energy harvester and we have

assumed $T = 1$ for simplicity. The harvested energy will be used to transmit m_{11} pilots to the destination for the channel estimation and $D - m_{11}$ data symbols from the source in the second hop to keep the same data rate. Thus the transmission power of the relay is

$$P_{r1} = \frac{\eta P_{s1} |h_1|^2 (1 - \rho_p) m_{11}}{D {d_{sr}}^e}. \tag{5.5}$$

Using (5.1), we can get an estimate of h_1 as

$$\begin{aligned} \hat{h_1} &= \frac{\Sigma_{i_{11}=1}^{m_{11}} [\sqrt{\rho_p P_{s1}} h_1 + n_{11}[i_{11}]]}{m_{11} \sqrt{\frac{\rho_p P_{s1}}{{d_{sr}}^e}}} \\ &= h_1 + \frac{\Sigma_{i_{11}=1}^{m_{11}} n_{11}[i_{11}]}{m_{11} \sqrt{\frac{\rho_p P_{s1}}{{d_{sr}}^{pl1}}}} = h_1 + \varepsilon_{11} \end{aligned} \tag{5.6}$$

where $\varepsilon_{11} = \frac{\Sigma_{i_{11}=1}^{m_{11}} n_{11}[i_{11}]}{m_{11} \sqrt{\frac{\rho_p P_{s1}}{{d_{sr}}^e}}}$ is the estimation error. Thus, one has $h_1 = \hat{h_1} - \varepsilon_{11}$.

The received signal in (5.2) is amplified-and-forwarded to the destination by using the harvested energy in (5.4) and the channel estimate in (5.6). Thus, the amplification factor can be written as

$$\hat{a}_{1var}^2 = \frac{1}{\frac{P_{s1} |\hat{h_1}|^2}{{d_{sr}}^e} + N_{11}} \tag{5.7}$$

where $\hat{h_1}$ is the estimated channel gain for the first hop between source node and relay node in (5.6).

During the second hop, the received pilots for channel estimation at the destination node can be written as

$$y_d[i_{12}] = \sqrt{\frac{P_{r1}}{{d_{rd}}^e}} g_1 \hat{a}_{1var} x[i_{12}] + n_{12}[i_{12}] \tag{5.8}$$

where $i_{12} = 1, 2, \ldots, m_{11}$, $x[i_{12}]$ is the pilot value, $n_{12}[i_{12}]$ is the AWGN with zero-mean and noise power N_{12}, $\hat{a}_{1var}$ is the amplification factor given in (5.7), P_{r1} is the relay transmission power given in (5.5), d_{rd} is the distance between relay and destination.

Also, the received data symbols at the destination can be expressed as

$$y_d[j_{12}] = \sqrt{\frac{P_{r1}}{{d_{rd}}^e}} g_1 \hat{a}_{1var} \left(y_r[j_{11}]\right) + n_{12}[j_{12}] \tag{5.9}$$

where $n_{12}[j_{12}]$ is additive white Gaussian noise (AWGN) at the destination node with zero mean and noise power N_{12}, and all the other symbols are defined as before.

By using the received signals in (5.8), the channel gain of the RD link can be estimated as

$$\hat{g_1} = \frac{\Sigma_{i_1=1}^{m_{11}} \left(\sqrt{\frac{P_{r1}}{{d_{rd}}^e}} g_1 \hat{a}_{1var} + n_{12}[i_1]\right)}{m_{11} \hat{a}_{1var} \sqrt{\frac{\hat{P_{r1}}}{{d_{rd}}^e}}} = \frac{\sqrt{\frac{P_{r1}}{{d_{rd}}^e}}}{\sqrt{\frac{\hat{P_{r1}}}{{d_{rd}}^e}}} g_1 + \varepsilon_{12} \tag{5.10}$$

where $\varepsilon_{12} = \frac{\Sigma_{i_{12}=1}^{m_{11}} n_{12}[i_{12}]}{m_{11} \hat{a}_{1var} \sqrt{\frac{P_{r1}}{{d_{rd}}^e}}}$ and $\hat{P_{r1}} = \frac{\eta P_{s1} |\hat{h_1}|^2 (1-\rho_p) m_{11}}{D {d_{sr}}^e}$.

The received data symbols at the destination in the direct link can be expressed as

$$y_d[j_{11}] = \sqrt{\frac{P_{s1}}{{d_{sd}}^e}} h_{sd} x[j_{11}] + n_{sd}[j_{11}] \tag{5.11}$$

where d_{sd} is the distance between source and destination, and $n_{sd}[j_{11}]$ is the complex AWGN with mean zero and noise power N_{sd}.

5.2.2 Data transmission power splitting scheme

The DTPS structure is similar to CEPS, except that energy is harvested from the data symbols.

First, the pilots received at the relay for channel estimation in the first hop is

$$y_r[i_{21}] = \sqrt{\frac{P_{s2}}{{d_{sr}}^e}} h_2 x[i_{21}] + n_{21}[i_{21}] \tag{5.12}$$

where $i_{21} = 1, 2, \ldots, m_{21}$, m_{21} is the number of pilots used for channel estimation, P_{s2} is the transmitted power of the source, $x[i_{21}]$ is the transmitted pilot with unit power $E\{|\, x[i_{21}]\, |^2\} = 1$, and $n_{21}[i_{21}]$ is the complex AWGN with mean zero and noise power N_{21}.

Also, the received signals of the data symbols in the second part of the data packet in the first hop can be expressed as

$$y_r[j_{21}] = \sqrt{\frac{\rho_d P_{s2}}{{d_{sr}}^e}} h_2 x[j_{21}] + n_{21}[j_{21}] \tag{5.13}$$

where $j_{21} = m_{21}+1, \ldots, D$, $x[j_{21}]$ is the data symbol with $E\{\mid x[j_{21}] \mid^2\} = 1$, $n_{21}[j_{21}]$ is the complex AWGN during data reception at the relay with zero-mean and noise power N_{21}.

Next, the received signal of pilots for EH in the third part of the data packet can be expressed as

$$y_r(k_2) = \sqrt{\frac{(1-\rho_d) P_{s2}}{{d_{sr}}^e}} h_2 x[k_2] + n_{21}(k_2) \tag{5.14}$$

where $k_2 = 1, 2, 3, 4, 5, \ldots, m_{21}$, and $(D - m_{21})(1 - \rho_d)$ is the total number of pilot symbols used for EH, $x[k_2]$ is the transmitted pilot symbol with unit power $E\{\mid x[k_2] \mid^2\} = 1$, and $n_{21}(k_2)$ is the AWGN complex with zero-mean and noise power N_{21}. In (10)-(12), the channel gain h_2 remains the same.

Use the function (5.14), we can get the harvested energy at relay is

$$E_{r2} = \frac{P_{s2} \eta |h_2|^2 (1-\rho_d)(D - m_{21})}{{d_{sr}}^e} \tag{5.15}$$

where a remaining $P_{s2}|\hat{h_2}|^2$ is the amount of energy collected by the harvester at the relay node through EH protocol. The harvested energy will be used to transmit m_{22} pilot symbols to the destination node for the channel estimation of the second hop, which from the relay node to destination node $\rho_d(D - m_{21})$ data symbols are from the source.

The transmission power of the relay is

$$P_{r2} = \frac{\eta P_{s2} |\hat{h_2}|^2 (1-\rho_d)(D - m_{21})}{D {d_{sr}}^e}. \tag{5.16}$$

Using (5.12), we estimate h_2 as

$$\begin{aligned}\hat{h_2} &= \frac{\Sigma_{i_{21}=1}^{m_{21}}\sqrt{\frac{P_{s2}}{d_{sr}{}^{e}}}h_2 + n_{21}[i_{21}]}{m_{21}\sqrt{\frac{P_{s2}}{d_{sr}{}^{e}}}} \\ &= h_2 + \frac{\Sigma_{i_{21}=1}^{m_{21}} n_{21}[i_{21}]}{m_{21}\sqrt{\frac{P_{s2}}{d_{sr}{}^{e}}}} = h_2 + \varepsilon_{21}\end{aligned} \tag{5.17}$$

where $\varepsilon_{21} = \frac{\Sigma_{i_{21}=1}^{m_{21}} n_{21}[i_{21}]}{m_{21}\sqrt{\frac{P_{s2}}{d_{sr}{}^{e}}}}$ is the estimation error. Thus, one has $h_2 = \hat{h_2} - \varepsilon_{21}$.

The received data in (5.13) is sent to the destination by using the transmission power of the relay in (5.16) and the estimate of h_2 in (5.17). Thus, the amplification factor can be written as

$$\hat{a}_{2var}^2 = \frac{1}{\frac{P_{s2}}{d_{sr}{}^{e}}|\hat{h_2}|^2 + N_{21}}. \tag{5.18}$$

During the second hop, the received pilots for channel estimation at the destination can be written as

$$y_d[i_{22}] = \sqrt{\frac{P_{r2}}{d_{rd}{}^{e}}} g_2 \hat{a}_{2var} x[i_{22}] + n_{22}[i_{22}] \tag{5.19}$$

where $i_{22} = 1, 2, \ldots, m_{21}$ and $x[i_{22}] = 1$ is the pilot value, $n_{22}[i_{22}]$ is the additive white Gaussian noise (AWGN), $\hat{a}_{2var}$ is the amplification factor given in (5.18), and P_{r2} is the relay transmission power given in (5.16).

Using the received signals in (5.19), one has

$$\hat{g_2} = \frac{\sqrt{\frac{P_{r2}}{d_{rd}{}^{e}}}}{\sqrt{\frac{\hat{P_{r2}}}{d_{rd}{}^{e}}}} g_2 + \varepsilon_{22} \tag{5.20}$$

where $\varepsilon_{22} = \frac{\Sigma_{i_{22}=1}^{m_{21}} n_{22}[i_{22}]}{m_{21}\hat{a}_{2var}\sqrt{\frac{\hat{P_{r2}}}{d_{rd}{}^{e}}}}$ and $\hat{P_{r2}} = \frac{\eta P_{s2}|\hat{h_2}|^2(1-\rho_d)(D-m_{21})}{D d_{sr}{}^{e}}$ from (5.16).

Also, the received data symbols at the destination are

$$y_d[j_{22}] = \sqrt{\frac{P_{r2}}{d_{rd}{}^{e}}} g_2 \hat{a}_{2var} \left(y_r[j_{21}]\right) + n_{22}[j_{22}]. \tag{5.21}$$

The equivalent expression for direct link is still given by (5.11).

5.2.3 Combination power splitting scheme

In the CPS structure, energy is harvested by splitting power from both pilot symbols and data symbols.

The pilot received at the relay for channel estimation is

$$y_r[i_{31}] = \sqrt{\frac{\rho_c P_{s3}}{{d_{sr}}^e}} h_3 x[i_{31}] + n_{31}[i_{31}] \tag{5.22}$$

where $i_{31} = 1, 2, \ldots, m_{31}$, $0 < m_{13} < D$ is the number of pilots used for channel estimation, P_{s3} is the transmitted power of the source, $x[i_{31}]$ is the transmitted pilot symbol with $E\{x[i_{31}]^2\} = 1$, and $n_{31}[i_{31}]$ is the complex AWGN with mean zero and noise power N_{31}.

The received data symbols can be expressed as

$$y_r[j_{31}] = \sqrt{\frac{\rho_c P_{s3}}{{d_{sr}}^e}} h_3 x[j_{31}] + n_{31}[j_{31}] \tag{5.23}$$

where $j_{31} = m_{31}+1, \ldots, D$, $x[j_{31}]$ satisfies $E\{\mid x[j_{31}] \mid^2\} = 1$, $n_{31}[j_{31}]$ is the complex AWGN during data reception at the relay with mean zero and noise power N_{31}.

Following, the received signal of pilots for EH in the third part of the data packet can be expressed as

$$y_r[k_3] = \sqrt{\frac{(1-\rho_c) P_{s3}}{{d_{sr}}^e}} h_3 x[k_3] + n_{31}[k_3] \tag{5.24}$$

where $k_3 = 1, 2, 3, 4, 5, \ldots, D$, and $(1-\rho_c)D$ is the total amount used for EH, $x[k_3]$ is the transmitted pilot symbol with unit power $E\{\mid x[k_3] \mid^2\} = 1$, and $n_{31}[k_3]$ is the AWGN complex with mean noise power and variance N_{31}. In (18)-(20), the channel gain h_3 remains the same.

Use the function(20), we can get the harvested energy at relay is

$$E_{r3} = \frac{\eta |h_3|^2 (1-\rho_c) D P_{s3}}{{d_{sr}}^e}. \tag{5.25}$$

The remaining $P_{s3}|\hat{h_3}|^2$ is the amount of energy collected by the harvester at the relay node through EH protocol. The harvested energy will be used to transmit m_{32} pilot symbols to the destination node for the channel estimation of the second hop from the relay node to destination node as well as $\rho_c(D - m_{31})$ data symbols from the source. The transmission power of the relay as

$$P_{r3} = \frac{\eta P_{s3}|h_3|^2(1-\rho_c)}{{d_{sr}}^e}. \tag{5.26}$$

Using (5.22), h_3 can be estimated as

$$\hat{h_3} = \frac{\Sigma_{i_{31}=1}^{m_{31}} \sqrt{\frac{\rho_c P_{s3}}{{d_{sr}}^e}} h + n_{31}[i_{31}]}{m\sqrt{\frac{\rho_c P_{s3}}{{d_{sr}}^e}}} = h_3 + \varepsilon_{31} \tag{5.27}$$

with $\varepsilon_{31} = \frac{\Sigma_{i_{31}=1}^{m_{31}} n_{31}[i_{31}]}{m_{31}\sqrt{\rho_c \frac{P_{s3}}{{d_{sr}}^e}}}$ and $h_3 = \hat{h_3} - \varepsilon_{31}$.

In this case, the amplification factor can be written as

$$\hat{a}_{3var}^2 = \frac{1}{\frac{P_{s3}}{{d_{sr}}^e}|\hat{h_3}|^2 + N_{31}}. \tag{5.28}$$

The received pilots for channel estimation at the destination are

$$y_d[i_{32}] = \sqrt{\frac{P_{r3}}{{d_{rd}}^e}} g_3 \hat{a}_{3var} x[i_{32}] + n_{32}[i_{32}] \tag{5.29}$$

where $i_{32} = 1, 2, \ldots, m_{31}$ denotes the pilots for channel estimation, and $x[i_{32}] = 1$ is the pilot value, $n_{12}[i_{32}]$ is the additive white Gaussian noise (AWGN).

Using the received signal in (5.29), the channel gain of the RD link can be estimated as

$$\hat{g_3} = \frac{\sqrt{\frac{P_{r3}}{{d_{rd}}^e}}}{\sqrt{\frac{\hat{P_{r2}}}{{d_{rd}}^e}}} g_3 + \varepsilon_{32} \tag{5.30}$$

where $\varepsilon_{32} = \frac{\Sigma_{i_{32}=1}^{m_{31}} n_{32}[i_{32}]}{m_{31}\hat{a}_{3var}}$ is the estimation error and $\hat{P_{r3}} = \frac{\eta P_{s3}|h_3|^2(1-\rho_c)}{{d_{sr}}^e}$ from (5.26).

Also, the received data symbols at the destination can be expressed as

$$y_d[j_{32}] = \sqrt{\frac{P_{r3}}{{d_{rd}}^e}} g_3 \hat{a}_{3var} \left(y_r[j_{31}] \right) + n_{32}[j_{32}], \tag{5.31}$$

where $n_{32}[j_{32}]$ is additive white Gaussian noise (AWGN) at the destination node. The equivalent expression for direct link is also given by (5.11).

5.3 End-to-end SNR

In this part, the end-to-end SNR expressions will be derived for three different EH structures, which can be used to analyse the performance and the optimal power allocations with several combinations.

5.3.1 End-to-end SNR for CEPS

By using (5.10) and (5.6) in (5.9), the received signal at destination for data transmission can be written as

$$\begin{aligned}
y_d[j_{12}] &= \sqrt{\frac{P_{r1}}{{d_{rd}}^e}} g_1 \hat{a}_{1var} \left(\sqrt{\frac{P_{s1}}{{d_{sr}}^e}} h_1 x[j_{11}] + n_{11}[j_{11}] \right) + n_{12}[j_{12}] \\
&= \frac{\sqrt{\frac{\hat{P_{r1}}}{{d_{rd}}^e}}}{\sqrt{\frac{P_{r1}}{{d_{rd}}^e}}} \sqrt{\frac{P_{r1}}{{d_{rd}}^e}} (\hat{g_1} - \varepsilon_{12}) \hat{a}_{1var} \left(\sqrt{\frac{P_{s1}}{{d_{sr}}^e}} (\hat{h_1} - \varepsilon_{11}) x[j_{11}] + n_{11}[j_{11}] \right) + n_{12}[j_{12}] \\
&= \sqrt{\frac{\hat{P_{r1}}}{{d_{rd}}^e}} \hat{g_1} \hat{a}_{1var} \sqrt{\frac{P_{s1}}{{d_{sr}}^e}} \hat{h_1} x[j_{11}] - \sqrt{\frac{\hat{P_{r1}}}{{d_{rd}}^e}} \hat{g_1} \hat{a}_{1var} \sqrt{\frac{P_{s1}}{{d_{sr}}^e}} \varepsilon_{11} x[j_{11}] \\
&+ \sqrt{\frac{\hat{P_{r1}}}{{d_{rd}}^e}} \hat{g_1} \hat{a}_{1var} n_{11}[j_{11}] - \sqrt{\frac{\hat{P_{r1}}}{{d_{rd}}^e}} \sqrt{\frac{P_{s1}}{{d_{sr}}^e}} \hat{h_1} \hat{a}_{1var} \varepsilon_2 x[j_{11}] \\
&+ \sqrt{\frac{\hat{P_{r1}}}{{d_{rd}}^e}} \sqrt{P_{s1}} \hat{a}_{1var} \varepsilon_{11} \varepsilon_{12} x[j_{11}] - \sqrt{\frac{\hat{P_{r1}}}{{d_{rd}}^e}} \varepsilon_{12} \hat{a}_{1var} n_{11}[j_{11}] + n_{12}[j_{12}]
\end{aligned} \tag{5.32}$$

where g_1 and h_1 have been replaced by $\hat{g_1}$ and $\hat{h_1}$, respectively.

The received signal at the destination can be expanded to give the end-to-end

SNR expression as

$$\gamma_{1end} = \frac{E[|\sqrt{\frac{\hat{P_{r1}}}{{d_{rd}}^e}}\hat{g_1}\hat{a}_{1var}\sqrt{\frac{P_{s1}}{{d_{sr}}^e}}\hat{h_1}x[j_{11}]|^2]}{u} \tag{5.33}$$

where $u = E[|\sqrt{\frac{\hat{P_{r1}}}{{d_{rd}}^e}}\hat{g_1}\hat{a}_{1var}\sqrt{\frac{P_{s1}}{{d_{sr}}^e}}\varepsilon_{11}x[j_{11}]|^2]$
$+ E[|\sqrt{\frac{\hat{P_{r1}}}{{d_{rd}}^e}}\hat{g_1}\hat{a}_{1var}n_{11}[j_{11}]|^2]$
$+ E[|n_{12}[j_{12}]|^2] + E[|\sqrt{\frac{\hat{P_{r1}}}{{d_{rd}}^e}}\sqrt{\frac{P_{s1}}{{d_{sr}}^e}}\hat{h_1}\hat{a}_{1var}\varepsilon_2 x[j_{11}]|^2]$
$+ E[|\sqrt{\frac{\hat{P_{r1}}}{{d_{rd}}^e}}\sqrt{\frac{P_{s1}}{{d_{sr}}^e}}\hat{a}_{1var}\varepsilon_{11}\varepsilon_{12}x[j_{11}]|^2]$
$+ E[|\sqrt{\frac{\hat{P_{r1}}}{{d_{rd}}^e}}\varepsilon_{12}\hat{a}_{1var}n_{11}[i]|^2]$.

One has $E[|x[j_{11}]|^2] = 1$, $E[|n_{11}[j_{11}]|^2] = N_{11}$ and $E[|n_{12}[j_{12}]|^2] = N_{12}$. Also, denote $E[|\varepsilon|_1^2] = \varepsilon_{11var}$,$E[|\varepsilon|_2^2] = \varepsilon_{12var}$. Equation (5.33) becomes

$$\gamma_{1end} = \frac{\frac{P_{s1}}{{d_{sr}}^e}|\hat{g_1}|^2|\hat{h_1}|^2}{v_1} \tag{5.34}$$

where $v_1 = \frac{P_{s1}}{{d_{sr}}^e}|\hat{g_1}|^2\varepsilon_{11var} + |\hat{g_1}|^2 N_{11} + \frac{P_{s1}}{{d_{sr}}^e}\varepsilon_{12var}|\hat{h_1}|^2 + \frac{P_{s1}}{{d_{sr}}^e}\varepsilon_{11var}\varepsilon_{12var} + N_{11}\varepsilon_{12var} + \frac{N_{12}}{\frac{\hat{P_{r1}}}{{d_{rd}}^e}\hat{a}_{1var}^2}$.

5.3.2 End-to-end SNR for DTPS

Substituting (5.20) and (5.17) in (5.21), one has

$$\begin{aligned} y_d[j_{22}] &= \sqrt{\frac{\hat{P_{r2}}}{{d_{rd}}^e}}\hat{g_2}\hat{a}_{2var}\sqrt{\frac{\rho_d P_{s2}}{{d_{sr}}^e}}\hat{h_2}x[j_{21}] - \sqrt{\frac{\hat{P_{r2}}}{{d_{rd}}^e}}\hat{g_2}\hat{a}_{2var}\sqrt{\frac{\rho_d P_{s2}}{{d_{sr}}^e}}\varepsilon_{21}x[j_{21}] + \\ &\sqrt{\frac{\hat{P_{r2}}}{{d_{rd}}^e}}\hat{g_2}\hat{a}_{2var}n_{21}[j_{22}] - \sqrt{\frac{\hat{P_{r2}}}{{d_{rd}}^e}}\sqrt{\frac{\rho_d P_{s2}}{{d_{sr}}^e}}\hat{h_2}\hat{a}_{2var}\varepsilon_2 x[j_{21}] \\ &+ \sqrt{\frac{\hat{P_{r2}}}{{d_{rd}}^e}}\sqrt{\frac{\rho_d P_{s2}}{{d_{sr}}^e}}\hat{a}_{2var}\varepsilon_{21}\varepsilon_{22}x[j_{21}] - \sqrt{\frac{\hat{P_{r2}}}{{d_{rd}}^e}}\varepsilon_{22}\hat{a}_{2var}n_{21}[j_{21}] + n_{22}[j_{22}] \end{aligned} \tag{5.35}$$

where g_2 and h_2 have been replaced by $\hat{g_2}$ and $\hat{h_2}$, respectively.

Therefore, the end-to-end SNR can be derived as

$$\gamma_{2end} = \frac{\rho_d \frac{P_{s2}}{d_{sr}{}^e} |\hat{g_2}|^2 |\hat{h_2}|^2}{v_2} \tag{5.36}$$

where $v_2 = \rho_d \frac{P_{s2}}{d_{sr}{}^e} |\hat{g_2}|^2 \varepsilon_{21var} + |\hat{g_2}|^2 N_{21} + \rho_d \frac{P_{s2}}{d_{sr}{}^e} \varepsilon_{22var} |\hat{h_2}|^2 + \rho_d \frac{P_{s2}}{d_{sr}{}^e} \varepsilon_{21var} \varepsilon_{22var} + N_{21} \varepsilon_{22var} + \frac{N_{22}}{\frac{\hat{P_{r2}}}{d_{rd}{}^e} \hat{a}^2_{2var}}$.

5.3.3 End-to-end SNR for CPS

Substituting (5.30) and (5.27) in (5.31), one has

$$\begin{aligned}
y_d[j_{32}] &= \sqrt{\frac{P_{r3}}{d_{rd}{}^e}} g_3 \hat{a}_{3var} \left(\sqrt{\frac{\rho_c P_{s3}}{d_{sr}{}^e}} h_3 x[j_{31}] + n_{31}[j_{31}] \right) + n_{32}[j_{31}] \\
&= \sqrt{\frac{\hat{P_{r3}}}{d_{rd}{}^e}} \hat{g_3} \hat{a}_{3var} \sqrt{\frac{\rho_c P_{s3}}{d_s r^e}} \hat{h_3} x[j_{31}] - \sqrt{\frac{\hat{P_{r3}}}{d_{rd}{}^e}} \hat{g_3} \hat{a}_{3var} \sqrt{\frac{\rho_c P_{s3}}{d_s r^e}} \varepsilon_{31} x[j_{31}] \\
&+ \sqrt{\frac{\hat{P_{r3}}}{d_{rd}{}^e}} \hat{g_3} \hat{a}_{3var} n_{31}[j_{31}] - \sqrt{\frac{\hat{P_{r3}}}{d_{rd}{}^e}} \sqrt{\frac{\rho_c P_{s3}}{d_s r^e}} \hat{h_3} \hat{a}_{3var} \varepsilon_2 x[j_{31}] \\
&+ \sqrt{\frac{\hat{P_{r3}}}{d_{rd}{}^e}} \sqrt{\frac{\rho_c P_{s3}}{d_s r^e}} \hat{a}_{3var} \varepsilon_{31} \varepsilon_{32} x[j_{31}] - \sqrt{\frac{\hat{P_{r3}}}{d_{rd}{}^e}} \varepsilon_{32} \hat{a}_{3var} n_{31}[j_{31}] + n_{32}[j_{32}]
\end{aligned} \tag{5.37}$$

where g_3 and h_3 have been replaced by $\hat{g_3}$ and $\hat{h_3}$, respectively.

The end-to-end SNR can be derived from (5.31) as

$$\gamma_{3end} = \frac{|\hat{h_3}|^2 |\hat{g_3}|^2 \frac{P_{s3}}{d_{sr}{}^e}}{v_3} \tag{5.38}$$

where $v_3 = \frac{P_{s3}}{d_{sr}{}^e} |\hat{g_3}|^2 \varepsilon_{31var} + \frac{P_{s3}}{d_{sr}{}^e} \varepsilon_{32var} |\hat{h_3}|^2 + |\hat{g_3}|^2 N_{31} + \frac{P_{s3}}{d_{sr}{}^e} \varepsilon_{31var} \varepsilon_{32var} + \varepsilon_{32var} N_{31} + \frac{N_{32}}{\frac{\hat{P_{r2}}}{d_{rd}{}^e} \hat{a}^2_{3var}}$, $\varepsilon_{31var} = E\{|\varepsilon_1|^2\}$ and $\varepsilon_{32var} = E\{|\varepsilon_2|^2\}$.

5.4 Achievable rate and BER in channel estimation

The achievable rate and bit-error-rate (BER) will be used as parameters, which are important to compare structures performance. Firstly, we will derive the CDF of the end-to-end SNR for the three novel structures in (5.33),(5.20),(5.30). Then, we

will calculate the achievable rate and BER.

5.4.1 Achievable rate and BER for CEPS

To derive the CDF, we first calculate $Var(\varepsilon_{11})$ and $Var(\varepsilon_{12})$. From (5.6), one has

$$\varepsilon_{11} = \frac{\Sigma_{i_{11}=1}^{m_{11}} n_{11}[i_{11}]}{m_{11}\sqrt{\rho_p \frac{P_{s1}}{{d_{sr}}^e}}}. \tag{5.39}$$

It has a mean of zero. Also, since $|\varepsilon_{11}|^2 = \Sigma_{i_{11}=1}^{m_{11}}(\frac{|n_{11}[i_{11}]|^2}{{m_{11}}^2 \rho_p \frac{P_{s1}}{{d_{sr}}^e}}) + \Sigma_{k_1=1}^{m_{11}}\Sigma_{j_{11}=1 k_1 \neq j_{11}}^{m_{11}}(\frac{n_{11}[j_{11}]\times n_{11}[k_1]}{{m_{11}}^2 \rho_p \frac{P_{s1}}{{d_{sr}}^e}})$, the variance of ε_{11} can be calculated as

$$Var(\varepsilon_{11}) = E\{|\varepsilon_{11}|^2\} = \frac{N_{11}}{m_{11}\rho_p \frac{P_{s1}}{{d_{sr}}^e}}. \tag{5.40}$$

Similarly, the variance of ε_{12} can be calculated as

$$Var(\varepsilon_{12}) = \frac{N_{12}D\left(\frac{P_{s1}}{{d_{sr}}^e}\left|\hat{h_1}\right|^2 + N_{11}\right)}{[\eta \frac{P_{s1}}{{d_{sr}}^e}\left|\hat{h_1}\right|^2 (1-\rho_p)\, m_{11}]m_{11}}. \tag{5.41}$$

The variance of ε_{sd} can be written as

$$Var(\varepsilon_{sd}) = \frac{N_{sd}}{D\frac{P_{s1}}{{d_{sd}}^e}}. \tag{5.42}$$

Using (5.40) and (5.41) in (5.34), the end-to-end SNR expression can be derived as

$$\gamma_{1end} = \frac{|\hat{g_1}|^2 \left|\hat{h_1}\right|^2 \frac{P_{s1}}{{d_{sr}}^e}}{w_1} \tag{5.43}$$

where $w_1 = \frac{N_{11}|\hat{g_1}|^2}{m_{11}\rho_p} + |\hat{g_1}|^2 N_{11} + \frac{N_{12}N_{11}D\left(\frac{P_{s1}}{{d_{sr}}^e}\left|\hat{h_1}\right|^2 + N_{11}\right)}{[\eta \frac{P_{s1}}{{d_{sr}}^e}\left|\hat{h_1}\right|^2 (1-\rho_p)]{m_{11}}^2 m_{11}\rho_p} + \frac{\frac{P_{s1}}{{d_{sr}}^e}\left|\hat{h_1}\right|^2 N_{12}D\left(\frac{P_{s1}}{{d_{sr}}^e}\left|\hat{h_1}\right|^2 + N_{11}\right)}{[\eta \frac{P_{s1}}{{d_{sr}}^e}\left|\hat{h_1}\right|^2 (1-\rho_p)m_{11}]m_{11}} + \frac{N_{12}D\left(\frac{P_{s1}}{{d_{sr}}^e}\left|\hat{h_1}\right|^2 + N_{11}\right)[\frac{N_{11}}{m_{11}}+1]}{[\eta \frac{P_{s1}}{{d_{sr}}^e}\left|\hat{h_1}\right|^2 (1-\rho_p)m_{11}]}$.

The instantaneous link signal to noise ratios (SNRs) in the i_{SD} signalling

interval at D are written as:

$$\gamma_{sd} = \frac{\frac{P_{s1}}{{d_{sd}}^{e}}|\hat{h_{sd}}|^2}{\frac{P_{s1}}{{d_{sd}}^{e}}Var(\varepsilon_{sd}) + N_{sd}} = \frac{\frac{P_{s1}}{{d_{sd}}^{e}}|\hat{h_{sd}}|^2}{\frac{N_{sd}}{D} + N_{sd}}. \tag{5.44}$$

To move forward, we need the distributions of $\hat{h_1}$ and $\hat{g_1}$. By using the expression of $\hat{h_1}$ in (5.6), its second-order moment can be derived as

$$\begin{aligned}
E(|\hat{h_1}|^2) &= E|h_1 + \frac{\Sigma_{i_{11}=1}^{m_{11}} n_{11}[i_{11}]}{m_{11}\sqrt{\rho_p \frac{P_{s1}}{{d_{sd}}^{e}}}}|^2 \\
&= E(|h_1|^2 + |\frac{\Sigma_{i_{11}=1}^{m_{11}} n_{11}[i_{11}]}{m_{11}\sqrt{\rho_p \frac{P_{s1}}{{d_{sd}}^{e}}}}|^2 + 2Re\{h_1 \times \frac{\Sigma_{i_{11}=1}^{m_{11}} n_{11}[i_{11}]^*}{m_{11}\sqrt{\rho_p \frac{P_{s1}}{{d_{sd}}^{e}}}}\}) \\
&= E(|h_1|^2) + E\left(|\frac{\Sigma_{i_{11}=1}^{m_{11}} n_{11}[i_{11}]}{m_{11}\sqrt{\rho_p \frac{P_{s1}}{{d_{sd}}^{e}}}}|^2\right) \\
&= E(|h_1|^2) + |\frac{N_{11}}{{m_{11}}^2 \rho_p \frac{P_{s1}}{{d_{sd}}^{e}}}| \times m_{11} = 2\theta^2 + \frac{N_{11}}{m_{11}\rho_p \frac{P_{s1}}{{d_{sr}}^{e}}}.
\end{aligned} \tag{5.45}$$

Also, $E\{Re\{h_1 \times \frac{\Sigma_{i_{11}=1}^{m_{11}} n_{11}[i_{11}]}{{m_{11}}^2\sqrt{\rho_p \frac{P_{s1}}{{d_{sr}}^{e}}}}\}\} = 0$. Since h_1 and ε_{11} are complex Gaussian, $\hat{h_1}$ is also complex Gaussian. Thus, $|\hat{h_1}|^2$ is an exponential random variable with scale parameter

$$\lambda_{11} = \frac{1}{2\theta^2 + \frac{N_{11}}{m_{11}\rho_p \frac{P_{s1}}{{d_{sr}}^{e}}}}. \tag{5.46}$$

The probability density function (PDF) of $|\hat{h_1}|^2$ can be written as

$$f_{|\hat{h_1}|^2}(x) = \lambda_{11} e^{-\lambda_{11} x}. \tag{5.47}$$

Its CDF is

$$F_{|\hat{h_1}|^2}(x) = 1 - e^{-\lambda_{11} x}. \tag{5.48}$$

Similarly, one has

$$E(|\hat{g_1}|^2) = 2\theta^2 E\{\frac{|\hat{h_1}|^2}{|\hat{h_1}|^2}\} + E\{\frac{N_{12} D(\rho_p \frac{P_{s1}}{{d_{sr}}^{e}}|\hat{h_1}|^2 + N_{11})}{\eta \frac{P_{s1}}{{d_{sr}}^{e}}|\hat{h_1}|^2 (1-\rho_p) m_{11}^2}\}. \tag{5.49}$$

Assuming that $E\left\{\frac{|h_1|^2}{|\hat{h_1}|^2}\right\} \approx \frac{E\left\{|h_1|^2\right\}}{E\left\{|\hat{h_1}|^2\right\}}$, we can get

$$\begin{aligned} E\left(|\hat{g_1}|^2\right) \approx & \frac{4\theta^4}{2\theta^2 + \frac{|N_{11}|}{m_{11}\rho_p \frac{P_{s1}}{d_{sr}{}^e}}} + \frac{N_{12}D}{(m_{11})\eta(1-\rho_p)m_{11}} \\ & - \frac{N_{12}D}{\frac{P_{s1}}{d_{sr}{}^e} m_{11}\eta(1-\rho_p)m_{11}} \frac{N_{11}Ei(0)}{2\theta^2 + \frac{N_{11}}{(m_{11}\rho_p \frac{P_{s1}}{d_{sr}{}^e})}} \end{aligned} \tag{5.50}$$

where $E[\frac{N_{11}}{|\hat{h_1}|^2}] = N_{11} \times \int_0^\infty \frac{1}{x}\lambda_{11}e^{-\lambda_{11}x}dx = -\frac{N_{11}}{m_{11}\rho_p \frac{P_{s1}}{d_{sr}{}^e}}Ei(0)$ has been used. When ε_{11} is small, $|\hat{g_1}|^2$ can be approximated as an exponential random variable. Therefore, let $\lambda_{12} = \frac{1}{\frac{4\theta^4}{2\theta^2 + \frac{|N_{11}|}{m_{11}\rho_p \frac{P_{s1}}{d_{sr}{}^e}}} + \frac{|N_{12}||D|\rho_p}{|m_{11}|\eta|1-\rho_p|m_{11}}}$. Its PDF can be approximated as

$$f_{|\hat{g_1}|^2}(x) = \lambda_{12}e^{-\lambda_{12}x} \tag{5.51}$$

and its CDF can be approximated as

$$F_{|\hat{g_1}|^2}(x) = 1 - e^{-\lambda_{12}x}. \tag{5.52}$$

Similarly, let $\lambda_{sd} = \frac{1}{2\theta^2 + \frac{N_{sd}}{D\frac{P_{s1}}{d_{sd}{}^e}}}$. Its PDF can be calculated as

$$f_{|\hat{h_{sd}}|^2}(x) = \lambda_{sd}e^{-\lambda_{sd}x} \tag{5.53}$$

and its CDF can be calculated as

$$F_{|\hat{h_{sd}}|^2}(x) = 1 - e^{-\lambda_{sd}x}. \tag{5.54}$$

By using these expressions, we can derive the CDF of γ_{1end}. One has from (5.43)

$$F_{\gamma_{1end}}(\gamma_{01}) = P_{1r}\{\gamma_{1end} < \gamma_{01}\} = I_{11} + I_{12} \tag{5.55}$$

with

$$I_{11} = P_{r1}\{\frac{P_{s1}}{d_{sr}{}^e}|\hat{h_1}|^2 - \frac{xN_{11}}{m_{11}\rho_p} - xN_{11} < 0\} \tag{5.56}$$

$$I_{12} = P_{r1}\{|\hat{g_1}|^2 < \frac{z}{w_2}|\left(\frac{P_{s1}}{d_{sr}{}^e}|\hat{h_1}|^2 - \frac{xN_{11}}{m_{11}\rho_p} - xN_{11}\right) > 0\} \tag{5.57}$$

where $w_2 = [\eta\rho_p m_{11}\left(1-\rho_p\right)m_{11}{}^2\frac{P_{s1}}{d_{sr}{}^e}|\hat{h_1}|^2](\frac{P_{s1}}{d_{sr}{}^e}|\hat{h_1}|^2 - \frac{xN_{11}}{m_{11}\rho_p} - xN_{11})$ and $z = xN_{12}N_{11}D\left(\frac{P_{s1}}{d_{sr}{}^e}|\hat{h_1}|^2 + N_{11}\right) + m_{11}x\rho_p N_{12}N_{11}D\left(\frac{P_{s1}}{d_{sr}{}^e}|\hat{h_1}|^2 + N_{11}\right) + xm_{11}m_{11}\rho_p N_{12}D\left(\frac{P_{s1}}{d_{sr}{}^e}|\hat{h_1}|^2 + N_{11}\right) + m_{11}\rho_p x\frac{P_{s1}}{d_{sr}{}^e}|\hat{h_1}|^2 N_{12}D\left(\frac{P_{s1}}{d_{sr}{}^e}|\hat{h_1}|^2 + N_{11}\right)$. Using the CDF of $|\hat{h_1}|^2$ in (5.43), one has

$$I_{11} = 1 - e^{-\frac{\frac{xN_{11}}{m_{11}\rho_p\frac{P_{s1}}{d_{sr}{}^e}} + \frac{xN_{11}}{\frac{P_{s1}}{d_{sr}{}^e}}}{2\theta^2 + |\frac{N_{11}}{m_{11}\rho_p\frac{P_{s1}}{d_{sr}{}^e}}|}}. \tag{5.58}$$

Also, (5.57) can be solved by using the CDF of $|\hat{g_1}|^2$ as

$$I_{12} = \int_{\frac{xN_{11}}{m_{11}\rho_p\frac{P_{s1}}{d_{sr}{}^e}} + \frac{xN_{11}}{\frac{P_{s1}}{d_{sr}{}^e}}}^{\infty} F_{|\hat{g_1}|^2}(\frac{z}{w_3}) f_{|\hat{h_1}|^2}(y)dy \tag{5.59}$$

where $w_3 = [\eta\rho_p m_{11}(1-\rho_p)m_{11}{}^2\frac{P_{s1}}{d_{sr}{}^e}y](\frac{P_{s1}}{d_{sr}{}^e}y - \frac{xN_{11}}{m_{11}\rho_p} - xN_{11})$. Let $\frac{P_{s1}}{d_{sr}{}^e}y - \frac{xN_{11}}{m_{11}\rho_p} - xN_{11} = t$. By using this variable transformation, one has

$$\begin{aligned} I_{12} = {} & \frac{1}{\frac{P_{s1}}{d_{sr}{}^e}\left(2\theta^2 + |\frac{N_{11}}{m_{11}\rho_p\frac{P_{s1}}{d_{sr}{}^e}}|\right)} e^{-\frac{xN_{11}+xN_{11}m_{11}\rho_p}{2\theta^2 m_{11}\rho_p\frac{P_{s1}}{d_{sr}{}^e}+|N_{11}|}} \\ & \frac{2\theta^2 m_{11}\rho_p\frac{P_{s1}}{d_{sr}{}^e} + |N_{11}|}{m_{11}\rho_p} - \frac{1}{\left(2\theta^2 + |\frac{N_{11}}{m_{11}\rho_p\frac{P_{s1}}{d_{sr}{}^e}}|\right)} \\ & e^{-\frac{\lambda_{12}m_{11}xN_{12}\rho_p D}{\eta\rho_p m_{11}(1-\rho_p)m_{11}{}^2\frac{P_{s1}}{d_{sr}{}^e}y} - \frac{xN_{11}+xN_{11}m_{21}}{2\theta^2 m_{11}\rho_p\frac{P_{s1}}{d_{sr}{}^e}+|N_{11}|}} \\ & \frac{2}{\frac{P_{s1}}{d_{sr}{}^e}}(\frac{z_1(x)}{(\eta m_{11}\left(1-\rho_p\right)m_{11}{}^2)m_{11}\rho_p})^{\frac{1}{2}} K_1(2\sqrt{\frac{z_2(x)}{w_4}}) \end{aligned} \tag{5.60}$$

where $w_4 = (\eta m_{11}\left(1-\rho_p\right)m_{11}{}^2)(2\theta^2 m_{11}\rho_p\frac{P_{s1}}{d_{sr}{}^e} + |N_1|)$, $z_1(x) = (\frac{1}{\frac{4\theta^4}{2\theta^2+\frac{|N_1|}{m_{11}\rho_p\frac{P_{s1}}{d_{sr}{}^e}}} + \frac{|N_{12}||D|\rho_p}{|m_{11}|\eta|1-\rho_p|m_{11}}})\ (xN_{12}N_1D + m_{11}\rho_p xN_{12}N_1D + xm_{11}m_{11}\rho_p N_{12}D + m_{11}xN_{12}D * \frac{xN_1\rho_p}{m_{11}\rho_p} + xN_1\rho_p)$ $(2\theta^2 m_{11}\rho_p\frac{P_{s1}}{d_{sr}{}^e} + |N_1|)$ and $z_2(x) = (\frac{1}{\frac{4\theta^4}{2\theta^2+\frac{|N_1|}{m_{11}\rho_p\frac{P_{s1}}{d_{sr}{}^e}}} + \frac{|N_{12}||D|\rho_p}{|m_{11}|\eta|1-\rho_p|m_{11}}})\ (xN_{12}N_1D + m_{11}\rho_p xN_{12}N_1D + xm_{11}m_{11}\rho_p N_{12}D + m_{11}xN_{12}D * \frac{xN_1\rho_p}{m_{11}\rho_p} + xN_1\rho_p)m_{11}\rho_p$.

The outage probability can then be derived as

$$P_0(\gamma_{01}) = 1 - \frac{1}{\frac{P_{s1}}{{d_{sr}}^e}\left(2\theta^2 + |\frac{N_1}{m_{11}\rho_p\frac{P_{s1}}{{d_{sr}}^e}}|\right)} e^{-\frac{\gamma_{01}N_1+\gamma_{01}N_1m_{11}\rho_p}{2\theta^2 m_{11}\rho_p\frac{P_{s1}}{{d_{sr}}^e}+|N_1|}} \frac{2\theta^2 m_{11}\rho_p\frac{P_{s1}}{{d_{sr}}^e} + |N_1|}{m_{11}\rho_p} -$$
$$\frac{1}{\left(2\theta^2 + |\frac{N_1}{m_{11}\rho_p\frac{P_{s1}}{{d_{sr}}^e}}|\right)} e^{-\frac{\lambda_{12}m_{11}\gamma_{01}N_{12}\rho_p D}{\eta\rho_p m_{11}(1-\rho_p){m_{11}}^2\frac{P_{s1}}{{d_{sr}}^e}y} - \frac{\gamma_{01}N_1+\gamma_{01}N_1m_{11}}{2\theta^2 m_{11}\rho_p\frac{P_{s1}}{{d_{sr}}^e}+|N_1|}}$$
$$\frac{2}{\frac{P_{s1}}{{d_{sr}}^e}}\left(\frac{z_1(\gamma_{01})}{(\eta m_{11}(1-\rho_p){m_{11}}^2)m_{11}\rho_p}\right)^{\frac{1}{2}} K_1\left(2\sqrt{\frac{z_2(\gamma_{01})}{w_4}}\right). \tag{5.61}$$

The CDF for direct link can be calculated as

$$F_{\gamma_{sd}}(\gamma_{01}) = P_{sdr}\{\gamma_{sd} < \gamma_{01}\} \tag{5.62}$$

and the outage probability for direct link can be calculated as

$$\begin{aligned} P_{sd}(\gamma_{01}) &= P_{sdr}\{|\hat{h_{sd}}|^2 < \frac{N_{sd}\gamma_{th}{d_{sd}}^e}{DP_{s1}} + \frac{\gamma_{th}N_{sd}{d_{sd}}^e}{P_{s1}}\} \\ &= P_{sdr}\{|\hat{h_{sd}}|^2 - \frac{N_{sd}\gamma_{th}{d_{sd}}^e}{DP_{s1}} - \frac{\gamma_{th}N_{sd}{d_{sd}}^e}{P_{s1}} < 0\} \\ &+ P_{sdr}\{|\hat{h_{sd}}|^2 - \frac{N_{sd}\gamma_{th}{d_{sd}}^e}{DP_{s1}} - \frac{\gamma_{th}N_{sd}{d_{sd}}^e}{P_{s1}} > 0\} \\ &= 1 + (\lambda_{sd} - 1)e^{-\lambda_{sd}(\frac{N_{sd}\gamma_{th}{d_{sd}}^e}{DP_{s1}} + \frac{\gamma_{th}N_{sd}{d_{sd}}^e}{P_{s1}})}. \end{aligned} \tag{5.63}$$

Thus, the achievable rate without direct link can be derived as

$$AR_1 = [1 - P_0(\gamma_{01})] \times \frac{D - m_{11}}{D} \tag{5.64}$$

and the achievable rate with direct link can be derived as

$$AR_{1d} = [1 - P_{sd}(\gamma_{01})P_0(\gamma_{01})] \times \frac{D - m_{11}}{D}. \tag{5.65}$$

Moreover, the BER without direct link can be calculated as

$$\begin{aligned} BER_1 &= \int_0^\infty \frac{1}{2} erfc(\sqrt{x}) * dF_{\gamma_{1end}}(x) \\ &= \frac{1}{2}\int_0^\infty \frac{e^{-x}}{\sqrt{x * \pi}} F_{\gamma_{1end}}(x)dx. \end{aligned} \tag{5.66}$$

Table 5.1: Channel estimation power splitting (CEPS)

Scheme 1 Procedure Achievable rate and BER
Input: m_{11}, m_{12}, ρ_p, P_s, η, D, N_{11}, N_{12},γ_{01}, γ_h, γ_g, ${\sigma_d}^2$ and ${\sigma_r}^2$
Output: Achievable rate and BER Values
1.Solve the expressions for (5.64) and (5.66) by applying Scheme 1.
2.**if** $m_{11} + m_{12} < D$ **then**
3. Calculate achievable rate and BER, respectively.
4.**else**
5. Stop and make it zero.
6.**end if**.

and the BER with direct link can be calculated as

$$\begin{aligned} BER_{1d} &= \int_0^\infty \frac{1}{2} erfc(\sqrt{x}) * d(F_{\gamma_{1end}}(x) F_{\gamma_{sd}}(x)) \\ &= \frac{1}{2} \int_0^\infty \frac{e^{-x}}{\sqrt{x * \pi}} F_{\gamma_{1end}}(x) F_{\gamma_{sd}}(x) dx. \end{aligned} \tag{5.67}$$

where $erfc(x)$ is the complementary error function. The algorithm was presented in Table 5.4.1.

5.4.2 Achievable rate and BER for DTPS

To derive the CDF, we first calculate $Var(\varepsilon_{21})$ and $Var(\varepsilon_{22})$. From (5.17), one has

$$\varepsilon_{21} = \frac{\Sigma_{i_{21}=1}^{m_{21}} n_{21}[i_{21}]}{m_{21} \sqrt{\frac{P_{s2}}{{d_{sr}}^e}}} \tag{5.68}$$

thus, the variance of ε_{21} can be derived as

$$Var(\varepsilon_{21}) = \frac{N_{21}}{m_{21} \frac{P_{s2}}{{d_{sr}}^e}}. \tag{5.69}$$

Similarly, the variance of ε_{22} can be derived as

$$Var(\varepsilon_{22}) = \frac{N_{22} \left(\frac{P_{s2}}{{d_{sr}}^e} |\hat{h_2}|^2 + N_{21} \right) D}{[\eta \frac{P_{s2}}{{d_{sr}}^e} |\hat{h_2}|^2 (1 - \rho_d)(D - m_{21})] m_{21}}. \tag{5.70}$$

Using (5.62) and (5.65) in (5.36), the end-to-end SNR expression can be derived as

$$\gamma_{2end} = \frac{\rho_d \frac{P_{s2}}{d_{sr}{}^{e}} |\hat{g_2}|^2 |\hat{h_2}|^2}{u_1} \tag{5.71}$$

where $u_1 = \rho_d |\hat{g_2}|^2 \frac{N_{21}}{m_{21}} + |\hat{g_2}|^2 N_{21} + \frac{((\rho_d \frac{P_{s2}}{d_{sr}{}^{e}} |\hat{h_2}|^2 + N_{21}) m_{21} + \rho_d N_{21} + {m_{21}}^2) N_{22} D \left(\frac{P_{s2}}{d_{sr}{}^{e}} |\hat{h_2}|^2 + N_{21} \right)}{{m_{21}}^2 [\eta \frac{P_{s2}}{d_{sr}{}^{e}} |\hat{h_2}|^2 (1-\rho_d)(D-m_{21})]}$.

The probability density function (PDF) of $|\hat{h_2}|^2$ can be derived as

$$f_{|\hat{h_1}|^2}(x) = \lambda_{21} e^{-\lambda_{21} x} \tag{5.72}$$

and the CDF of $|\hat{h_2}|^2$ is

$$F_{|\hat{h_2}|^2}(x) = 1 - e^{-\lambda_{21} x} \tag{5.73}$$

where $\lambda_{21} = \frac{1}{2\theta^2 + |\frac{N_{21}}{m_{21} \frac{P_{s2}}{d_{sr}{}^{e}}}|}$, by using a similar method to that of (5.47) and (5.48)

Also,the PDF of $|\hat{g_2}|^2$ can be derived as

$$f_{|\hat{g_2}|^2}(x) = \lambda_{22} e^{-\lambda_{22} x} \tag{5.74}$$

and its CDF can be written as

$$F_{|\hat{g_2}|^2}(x) = 1 - e^{-\lambda_{22} x} \tag{5.75}$$

where $\lambda_{22} = \frac{1}{\frac{4\theta^4}{2\theta^2 + \frac{|N_{21}|}{m_{21} \frac{P_{s2}}{d_{sr}{}^{e}}}} + \frac{N_{22} D}{[\eta(1-\rho_d)(D-m_{21})] m_{21}}}$.

By using these expressions, we can derive the CDF of γ_{2end} as

$$F_{\gamma_{2end}}(x) = P_{1r}\{\gamma_{2end} < x\} = I_{21} + I_{22} \tag{5.76}$$

where

$$I_{21} = 1 - e^{-\frac{\frac{xN_{21}}{m_{21} \frac{P_{s2}}{d_{sr}{}^{e}}} + \frac{xN_{21}}{\rho_d \frac{P_{s2}}{d_{sr}{}^{e}}}}{2\theta^2 + |\frac{N_{21}}{m_{21} \frac{P_{s2}}{d_{sr}{}^{e}}}|}} \tag{5.77}$$

and

$$I_{22} = \frac{1}{\frac{P_{s2}}{{d_{sr}}^e}\left(2\theta^2 + |\frac{N_{21}}{m_{21}\frac{P_{s2}}{{d_{sr}}^e}}|\right)} e^{-\frac{xN_{21}\rho_d + xN_{21}m_{21}}{2\theta^2 m_{21}\frac{P_{s2}}{{d_{sr}}^e}\rho_d + \rho_d N_{21}}} \frac{2\theta^2 m_{21}\frac{P_{s2}}{{d_{sr}}^e}\rho_d + |N_{21}\rho_d|}{m_{21}}$$
$$- \frac{1}{\left(2\theta^2 + |\frac{N_{21}}{m_{21}\frac{P_{s2}}{{d_{sr}}^e}}|\right)} e^{-\frac{\frac{xN_{22}m_{21}D}{N_{22}D}}{(\frac{4\theta^4}{2\theta^2 + \frac{|N_{21}|}{m_{21}\frac{P_{s2}}{{d_{sr}}^e}}} + \frac{}{[\eta(1-\rho_d)(D-m_{21})]m_{21}})\eta(1-\rho_d)(D-m_{21}){m_{21}}^2}}$$
$$e^{-\frac{xN_{21}\rho_d + xN_{21}m}{2\theta^2\rho_d m_{21}\frac{P_{s2}}{{d_{sr}}^e} + |N_{21}\rho_d|}} \frac{2}{\frac{P_{s2}}{{d_{sr}}^e}} (\frac{z_3(x)}{\eta(1-\rho_d)(D-m_{21})m_{21}^3})^{\frac{1}{2}} K_1(2\sqrt{\frac{z_4(x)}{w_5}}) \tag{5.78}$$

with $w_5 = \eta(1-\rho_d)(D-m_{21})m_{21}^2$ $(2\theta^2 m_{21}\frac{P_{s2}}{{d_{sr}}^e}\rho_d + |N_{21}\rho_d|), z_3(x) = \frac{1}{\frac{4\theta^4}{2\theta^2 + \frac{|N_{21}|}{m_{21}\frac{P_{s2}}{{d_{sr}}^e}}} + \frac{N_{22}D}{[\eta(1-\rho_d)(D-m_{21})]m_{21}}}$ $[xN_{21}N_{22}\rho_d D + xm_{21}N_{22}N_{21}D + xN_{22}m_{21}^2 D + xN_{22}m_{21}D * \frac{x\rho_d N_{21}}{m_{21}} + xN_{21}](2\theta^2 m_{21}\rho_d\frac{P_{s2}}{{d_{sr}}^e} + |N_{21}\rho_d|)$ and $z_4(x) = \frac{1}{\frac{4\theta^4}{2\theta^2 + \frac{|N_{21}|}{m_{21}\frac{P_{s2}}{{d_{sr}}^e}}} + \frac{N_{22}D}{[\eta(1-\rho_d)(D-m_{21})]m_{21}}}$ $(xN_{21}N_{22}\rho_d D + xm_{21}N_{22}N_{21}D + xN_{22}m_{21}^2 D + xN_{22}m_{21}D * \frac{x\rho_d N_{21}}{m_{21}} + xN_{21})m_{21}$.

By using the CDF of γ_{2end}, the outage probability can be derived as

$$P_0(\gamma_{02}) = 1 + (\rho_d - 1)e^{\frac{\gamma_{02}N_{21}\rho_d + \gamma_{02}N_{21}m_{21}}{2\theta^2\rho_d m_{21}P_{s2} + \rho_d N_{21}}}$$
$$- e^{-\frac{\gamma_{02}N_{22}m_{21}D}{(\frac{4\theta^4}{2\theta^2 + \frac{|N_{21}|}{m_{21}\frac{P_{s2}}{{d_{sr}}^e}}} + \frac{N_{22}D}{[\eta(1-\rho_d)(D-m_{21})]m_{21}})\eta(1-\rho_d)(D-m_{21}){m_{21}}^2}}$$
$$e^{-\frac{\gamma_{02}N_{21}\rho_d + \gamma_{02}N_{21}m_{21}}{2\theta^2\rho_d m_{21}\frac{P_{s2}}{{d_{sr}}^e} + |N_{21}\rho_d|}} \frac{1}{\left(2\theta^2 + |\frac{N_{21}}{m_{21}\frac{P_{s2}}{{d_{sr}}^e}}|\right)}$$
$$\frac{2}{\frac{P_{s2}}{{d_{sr}}^e}} (\frac{z_3(\gamma_{02})}{\eta(1-\rho_d)(D-m_{21})m_{21}^3})^{\frac{1}{2}} K_1(2\sqrt{\frac{z_4(\gamma_{02})}{w_5}}). \tag{5.79}$$

Thus, the achievable rate without direct link can be derived as

$$AR_2 = [1 - P_0(\gamma_{02})] \times (\frac{D - m_{21}}{D}) \tag{5.80}$$

Table 5.2: Data transmission power splitting (DTPS)

Scheme 2 Procedure Achievable rate and BER
Input: m_{21}, m_{22}, ρ_d, P_s, η, D,N_{21}, N_{22},γ_{02}, γ_h, γ_g, ${\sigma_d}^2$ and ${\sigma_r}^2$
Output: Achievable rate and BER Values
1.Solve the expressions for (5.80) and (5.82) by applying Scheme 2.
2.**if** $m_{21} + m_{22}$<D **then**
3. Calculate achievable rate and BER, respectively.
4.**else**
5. Stop and make it zero.
6.**end if**.

and the achievable rate with direct link can be derived as

$$AR_{2d} = [1 - P_0(\gamma_{02})P_{sd}(\gamma_{02})] \times (\frac{D - m_{21}}{D}). \tag{5.81}$$

The BER without direct link can be calculated as [125]

$$BER_2 = \frac{1}{2}\int_0^\infty \frac{e^{-x}}{\sqrt{x * \pi}} F_{\gamma_{2end}}(x)dx \tag{5.82}$$

and the BER with direct link can be calculated as

$$BER_2 = \frac{1}{2}\int_0^\infty \frac{e^{-x}}{\sqrt{x * \pi}} F_{\gamma_{2end}}(x)F_{\gamma_{sd}}(x)dx. \tag{5.83}$$

The algorithm has been presented in Table 5.2.

5.4.3 Achievable rate and BER for CPS

To derive the CDF, we first calculate $Var(\varepsilon_{31})$ and $Var(\varepsilon_{32})$. Using similar methods, the variances of ε_{31} and ε_{32} can be calculated as

$$Var(\varepsilon_{31}) = \frac{N_{31}}{m_{31}\rho_c \frac{P_{s3}}{{d_{sr}}^e}} \tag{5.84}$$

$$Var(\varepsilon_{32}) = \frac{N_{32}\left(\frac{P_{s3}}{{d_{sr}}^e}{\left|\hat{h_3}\right|}^2 + N_{31}\right)}{[\eta\frac{P_{s3}}{{d_{sr}}^e}{\left|\hat{h_3}\right|}^2(1-\rho_c)]m_{31}}. \tag{5.85}$$

Using (5.84) and (5.85) into (5.38), the end-to-end SNR expression can be derived as

$$\gamma_{3end} = \frac{|\hat{g_3}|^2 |\hat{h_3}|^2 \frac{P_{s3}}{d_{sr}{}^e}}{v_4} \tag{5.86}$$

where $v_4 = \frac{N_{31}|\hat{g_3}|^2}{m_{31}\rho_c} + |\hat{g_3}|^2 N_{31} + \frac{(N_{31}+\frac{P_{s3}}{d_{sr}{}^e}|\hat{h_3}|^2\rho_c m_{31}+N_{31}m_{31}+m_{31}^2)N_{32}\left(\frac{P_{s3}}{d_{sr}{}^e}|\hat{h_3}|^2+N_{31}\right)}{[\eta\frac{P_{s3}}{d_{sr}{}^e}|\hat{h_3}|^2(1-\rho_c)]\rho_c m_{31}^2}$.

Then, the PDF of $|\hat{h_3}|^2$ can be derived as

$$f_{|\hat{h_3}|^2}(x) = \lambda_{31} e^{-\lambda_{31} x} \tag{5.87}$$

and the CDF of $|\hat{h_3}|^2$ is

$$F_{|\hat{h_3}|^2}(x) = 1 - e^{-\lambda_{31} x} \tag{5.88}$$

where $\lambda_{31} = \frac{1}{2\theta^2 + |\frac{N_{31}}{m_{31}\rho_c \frac{P_{s3}}{d_{sr}{}^e}}|}$.

Similarly, the PDF of $|\hat{g_3}|^2$ can be written as

$$f_{|\hat{g_3}|^2}(x) = \lambda_{32} e^{-\lambda_{32} x} \tag{5.89}$$

and its CDF can be written as

$$F_{|\hat{g_3}|^2}(x) = 1 - e^{-\lambda_{32} x}. \tag{5.90}$$

where $\lambda_{32} = \frac{1}{\frac{4\theta^4}{2\theta^2 + \frac{|N_{31}|}{m_{31}\rho_c \frac{P_{s3}}{d_{sr}{}^e}}} + \frac{\rho_c |N_{32}|}{|m_{31}|\eta|1-\rho_c|}}$.

By using these expressions, we can derive the CDF of γ_{3end}. One has from (5.86)

$$F_{\gamma_{3end}}(x) = P_{1r}\{\gamma_{3end} < x\} = I_{31} + I_{32} \tag{5.91}$$

where

$$I_{31} = 1 - e^{-\frac{\frac{xN_{31}}{\rho_c{}^2 m_{31}\frac{P_{s3}}{d_{sr}{}^e}} + \frac{xN_{31}}{\frac{P_{s3}}{d_{sr}{}^e}\rho_c}}{2\theta^2 + |\frac{N_{31}}{m_{31}\rho_c \frac{P_{s3}}{d_{sr}{}^e}}|}} \tag{5.92}$$

and

$$I_{32} = \frac{1}{\frac{P_{s3}}{d_{sr}{}^{e}}\left(2\theta^2 + |\frac{N_{31}}{m_{31}\rho_c\frac{P_{s3}}{d_{sr}{}^{e}}}|\right)} e^{-\frac{\frac{xN_{31}}{\rho_c}+xN_{31}m_{31}}{2\theta^2\rho_c m_{31}\frac{P_{s3}}{d_{sr}{}^{e}}+|N_{31}|}} \frac{2\theta^2 m_{31}\rho_c\frac{P_{s3}}{d_{sr}{}^{e}} + |N_{31}|}{m_{31}}$$
$$- \frac{1}{\left(2\theta^2 + |\frac{N_{31}}{m_{31}\rho_c\frac{P_{s3}}{d_{sr}{}^{e}}}|\right)} e^{-\frac{\lambda_{32}{}^{b}}{d}-\frac{\frac{xN_{31}}{\rho_c}+xN_{31}m_{31}}{2\theta^2\rho_c m_{31}\frac{P_{s3}}{d_{sr}{}^{e}}+|N_{31}|}} \tag{5.93}$$
$$\frac{2}{\frac{P_{s3}}{d_{sr}{}^{e}}}(\frac{z_5(x)}{[\eta(1-\rho_c)(D-m_{31})]m_{31}^3})^{\frac{1}{2}} K_1(2\sqrt{\frac{z_6(x)}{w_6}})$$

with $w_6 = [\eta(1-\rho_c)(D-m_{31})m_{31}^2](2\theta^2\rho_c m_{31}\frac{P_{s3}}{d_{sr}{}^{e}} + |N_{31}|), z_5(x) = \frac{1}{\frac{4\theta^4}{2\theta^2+\frac{|N_{31}|}{m_{31}\rho_c\frac{P_{s3}}{d_{sr}{}^{e}}}}+\frac{\rho_c|N_{32}||D|}{|m_{31}|\eta|1-\rho_c|D}}[xN_{31}N_{32}D + xm_{31}N_{32}N_{31}D + xN_{32}m_{31}^2D + xN_{32}m_{31}D * \frac{xN_{31}}{\rho_c{}^2m_{31}} + \frac{xN_{31}}{\rho_c}](2\theta^2 m_{31}\rho_c\frac{P_{s3}}{d_{sr}{}^{e}} + |N_{31}|)$ and $z_6(x) = \frac{1}{\frac{4\theta^4}{2\theta^2+\frac{|N_{31}|}{m_{31}\rho_c\frac{P_{s3}}{d_{sr}{}^{e}}}}+\frac{\rho_c|N_{32}|||}{|m_{31}|\eta|1-\rho_c|}}(xN_{31}N_{32}D + xmN_{32}N_{31}D + xN_{32}m_{31}^2D + xN_{32}m_{31}D * \frac{xN_{31}}{\rho_c{}^2m_{31}} + \frac{xN_{31}}{\rho_c})m_{31}$.

By using the CDF of γ_{3end}, the outage probability can be derived as

$$P_0(\gamma_{03}) = 1 + (\rho_c - 1)e^{\frac{\frac{\gamma_{03}N_{31}}{\rho_c}+\gamma_{03}N_{31}m_{31}}{2\theta^2\rho_c m_{31}P_{s3}+N_{31}}} - \frac{1}{\left(2\theta^2 + |\frac{N_{31}}{m_{31}\rho_c\frac{P_{s3}}{d_{sr}{}^{e}}}|\right)}$$
$$e^{-\frac{\lambda_{32}{}^{b}}{d}-\frac{\frac{\gamma_{03}N_{31}}{\rho_c}+\gamma_{03}N_{31}m}{2\theta^2\rho_c m_{31}\frac{P_{s3}}{d_{sr}{}^{e}}+|N_{31}|}} \frac{2}{\frac{P_{s3}}{d_{sr}{}^{e}}}(\frac{z_5(\gamma_{03})}{[\eta(1-\rho_c)(D-m_{31})]m_{31}^3})^{\frac{1}{2}} K_1(2\sqrt{\frac{z_6(\gamma_{03})}{w_6}}). \tag{5.94}$$

Thus, the achievable rate without direct link can be derived as

$$AR_3 = (1 - P_0(\gamma_{03})) \times (\frac{D-m_{31}}{D}) \tag{5.95}$$

and the achievable rate with direct link can be derived as

$$AR_{3d} = (1 - P_0(\gamma_{03})P_{sd}(\gamma_{03})) \times (\frac{D-m_{31}}{D}). \tag{5.96}$$

The BER without direct link can be calculated as

$$BER_3 = \frac{1}{2}\int_0^{\infty} \frac{e^{-x}}{\sqrt{x*\pi}} F_{\gamma_{3end}}(x)dx \tag{5.97}$$

and the BER with direct link can be calculated as

$$BER_{3d} = \frac{1}{2}\int_0^{\infty} \frac{e^{-x}}{\sqrt{x*\pi}} F_{\gamma_{3end}}(x)F_{\gamma_{sd}}(x)dx. \tag{5.98}$$

The above expressions can be used to calculate the achievable rate and BER for the three structures. All the BER results are one-dimensional integrals, which can be easily calculated using simple mathematical software, i.e., MATLAB. All the AR results are in closed-form. Next, we will provide some numerical examples.

The algrithm has been presented in Table 5.3.

Table 5.3: Combination power splitting (CPS)

Scheme 3 Procedure Achievable rate and BER
Input: m_{31}, m_{32}, ρ_c, P_s, η, D, N_{31}, N_{32}, γ_{03}, γ_h, γ_g, ${\sigma_d}^2$ and ${\sigma_r}^2$
Output: Achievable rate and BER Values
1.Solve the expressions for (5.95) and (5.97) by applying Scheme 3.
2.**if** $m_{31} + m_{32} < D$ **then**
3. Calculate achievable rate and BER, respectively.
4.**else**
5. Stop and make it zero.
6.**end if**.

5.5 Numerical results and discussion

In this section, we study the performances of three novel structures in terms of achievable rate and bit-error-rate. In the study, we fix $P_{s1} = P_{s2} = P_{s3} = 1$, $\eta = 0.5, D = 100, N_{11} = N_{12} = N_{21} = N_{22} = N_{31} = N_{32} = 1$. Define $\gamma_1 = \frac{|h|^2}{2\sigma^2}$ as the instantaneous SNR of the SR link, and $\gamma_2 = \frac{|g|^2}{2\sigma^2}$ as the instantaneous SNR of the RD link, where $g_1 = g_2 = g_3 = g$, $h_1 = h_2 = h_3 = h$. The values of g and h will change with γ_1 and γ_2, and their real and imaginary parts are the same.

Fig. 5.3 shows the outage probability of different structures by using simula-

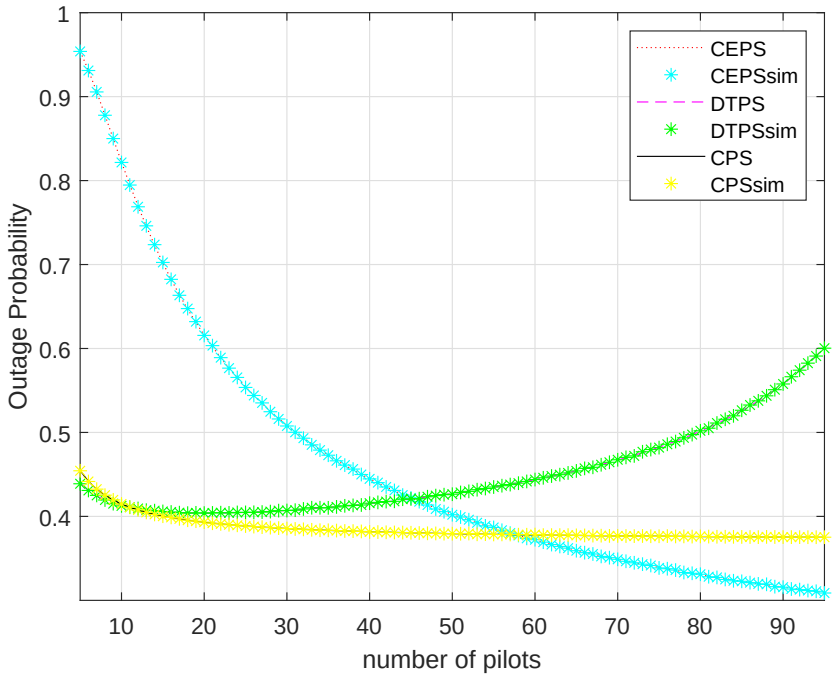

Figure 5.3: Comparison of simulation and analysis, when γ_1 and γ_2 are fixed at 10 dB and 10 dB.

tion and analysis for comparison. One sees that there is an excellent match between simulation and analysis. This applies to all the following figures but to maintain the readability of the figures, simulation results are not shown, as they are not visible in 3D plots.

5.5.1 Outage probability evaluation

In Fig.5.4, the normalized outage probability of $g_{1,\hat{2},3}$ and $h_{1,\hat{2},3}$ in three structures versus the values of $m_{11,21,31}$, when γ_1 and γ_2 with fixed channel realization. They were fixed at $\gamma_1 = 10, \gamma_2 = 10$, $\gamma_1 = 10, \gamma_2 = 20$ and $\gamma_1 = 10, \gamma_2 = 30$,respectively. Also, $m_{12,22,32}$ is fixed at 10 and $\rho_{p,d,c}$ is fixed at 0.5. By comparing the results for three groups of γ_1 and γ_2, one can see that both of them decrease first and then increase when $m_{11,21,31}$ increases. A bigger $m_{11,21,31}$ means more accurate estimate of $h_{1,\hat{2},3}$, and more energy for harvesting. For CEPS, the optimal value of m_{11} is around 73, 80 and 60, respectively. For DTPS, the value of m_{21} is around 20, 30 and 40, respectively. And for CPS, the value of m_{31} is around 20, 30 and 30, respectively.

In Fig.5.5, the normalized outage probability of $g_{1,\hat{2},3}$ and $h_{1,\hat{2},3}$ in three structures versus the values of $\rho_{p,d,c}$, when γ_1 and γ_2 with fixed channel realization. They were fixed at $\gamma_1 = -10, \gamma_2 = 10$, $\gamma_1 = -10, \gamma_2 = 20$ and $\gamma_1 = -20, \gamma_2 = 10$,respectively. Also, $m_{11,21,31}$ is fixed at 20. By comparing the results for three groups of γ_1 and γ_2, one can see that the outage probability first decreases very quickly and then increases slowly, when the value of $\rho_{p,d,c}$ increases. A bigger $\rho_{p,d,c}$ means more accurate estimate of $g_{1,\hat{2},3}$, and less energy for harvesting. The optimal value of ρ_p is around 0.15, 0.75 and 0.85, respectively. The optimal value of ρ_d is around 0.7, 0.85 and 0.93, respectively. The optimal value of ρ_c is around 0.7, 0.75 and 0.83, respectively.

5.5.2 Achievable rate evaluation

Fig. 5.6 illustrates the achievable rate of the CEPS structure versus the power splitting ratio ρ_p, when γ_1 and γ_2 are fixed at 10 dB and 10 dB, respectively. The value of ρ_p is changing between 0 to 1, with an interval of 0.05. The value of m_{11} is changing between 0 to 100 with an interval 1. First of all, we can see that the achievable rate increases first and then decreases when m_{11} or ρ_p increase. The peak point represents the optimal value. In this case, it can be observed that the optimal

value is achieved at $m_{11} = 88$ and $\rho_p = 0.24$, and the maximum achievable rate is around 0.1734. A bigger m_{11} means more accurate estimate of $\hat{h_1}$, and more energy for harvesting but less time for data transmission. A bigger ρ_p means more accurate estimate of $\hat{h_1}$, but less energy for harvesting. Thus, one must choose ρ_p carefully using our results to achieve the best performance.

Fig. 5.7 is similar to Fig. 5.6, expect that γ_1 , γ_2 are fixed at 10 dB and 20 dB, respectively. In this case, the rate increases in most cases. The optimal values are $m_{11} = 94$ and $\rho_p = 0.2$, and the maximum rate is around 0.2342. Thus, the performance of the CEPS structure can be improved by increasing γ_2, but the optimal values change too. The optimal m_{11} increases and the optimal ρ_p decreases.

Fig. 5.8 illustrates the achievable rate of the DTPS structure versus the number of pilots for channel estimation m_{11} and the power splitting ratio ρ_d, when γ_1 , γ_2 are fixed at 10 dB and 10 dB, respectively. Again, we can see that the achievable rate increases first and then decreases when m_{21} or ρ_d increase, implying that the optimal value exists. For this structure, the optimal values are $m_{21} = 69$ and $\rho_d = 0.22$, and the maximum achievable rate is around 0.01981. Fig. 5.8 is similar to Fig. 5.7, expect that γ_1 , γ_2 are fixed at 10 dB and 20 dB, respectively. Again, the optimal values change with γ_2. In particular, the optimal values are $m_{21} = 85$ and $\rho_d = 0.2$ and the maximum rate is around 0.1092.

For DTPS, by comparing Fig. 5.8 and Fig. 5.9, we can see when γ_2 increases, the optimal m_{21} increases and the optimal ρ_d decreases. Also, comparing the DTPS structure with the CEPS structure, it can be seen that the rate performance is more sensitive in DTPS that in CEPS to the power splitting ratio and the number of pilots.

Fig. 5.10 and Fig. 5.11 show the rate of the CPS structure versus the number of pilots for channel estimation m_{31} and the power splitting ratio ρ_c, when γ_1 , γ_2 are fixed at 10 dB and 10 dB and when γ_1 , γ_2 are fixed at 10 dB and 20 dB, respectively. Similar observations can be made. The optimal values in Fig. 5.10 are $m_{31} = 71$ and $\rho_c = 0.25$ with a maximum rate of around 0.01463, in Fig. 5.11 are $m_{31} = 86$ and $\rho_c = 0.21$ with a maximum rate of around 0.1036. Again, when γ_2 increases, the optimal m_{31} increases and the optimal ρ_c decreases.

By comparing the achievable rates of the three different structures, one can see that CEPS has a lower maximum achievable rate than DTPS and CPS. Also, DTPS and CPS have similar optimal achievable rates from our calculations, and

CPS has a slightly bigger maximum achievable rate than DTPS. Therefore, CPS has the best performance among these three structures, and CEPS has the worst.

5.5.3 BER evaluation

In Fig.5.12 shows the normalized BER of $g_{1,\hat{2},3}$ and $h_{1,\hat{2},3}$ in structure 1 versus the values of $m_{11,21,31}$, when γ_1 and γ_2 with fixed channel realization. They were fixed at $\gamma_1 = 20, \gamma_2 = 10$, $\gamma_1 = 20, \gamma_2 = 15$ and $\gamma_1 = 20, \gamma_2 = 20$,respectively. Also, $\rho_{p,d,c}$ is fixed at 0.5. By comparing the results for three groups of γ_1 and γ_2, one can see that both of them decrease first and then increase when $m_{11,21,31}$ increases. For CEPS, the optimal value of m_{11} is around 10 pilots. For DTPS, the m_{21} value is around 20. And for CPS, the m_{31} value is around 10.

In Fig.5.13 shows the normalized BER of $g_{1,\hat{2},3}$ and $h_{1,\hat{2},3}$ in three structures versus the values of $\rho_{p,d,c}$, when γ_1 and γ_2 with fixed channel realization. They were fixed at $\gamma_1 = 10, \gamma_2 = 0$, $\gamma_1 = 10, \gamma_2 = 10$ and $\gamma_1 = 20, \gamma_2 = 20$,respectively. Also, m_{11} is fixed at 90. By comparing the results for three groups of γ_1 and γ_2, one can see that the outage probability first decreases very quickly and then increases slowly, when the value of $\rho_{p,d,c}$ increasing. A bigger ρ_p means more accurate estimate of $g_{1,\hat{2},3}$, and less energy for harvesting. The optimal value of ρ_p is around 0.65, 0.82 and 0.85, the optimal value of ρ_d is around 0.85, 0.65 and 0.79, and the optimal value of ρ_c is around 0.65, 0.65 and 0.8, respectively.

Fig. 5.14 illustrates the relationship between the BER of the CEPS structure versus the power splitting ratio ρ_p, when γ_1 and γ_2 are fixed at 10 dB and 10 dB, respectively. In this case, we can see that the BER decreases first and then rises up when m_{11} or ρ_p increase. In this case, it can be observed that the optimal values are $m_{11} = 84$ and $\rho_p = 0.29$, and the minimum BER is around $4.646e^{-5}$.

Fig. 5.15 shows the relationship between BER of the DTPS structure versus the power splitting ratio ρ_d, when γ_1 and γ_2 are fixed at 10 dB and 10 dB, respectively. Again, we can see that the BER decreases first and then raises up when m_{21} or ρ_d increase. In this case, it can observed that the optimal values are $m_{21} = 72$ and $\rho_d = 0.16$, and the minimum BER is around $4.94e^{-5}$.

Fig. 5.16 illustrates the relationship between BER of the CPS structure versus the power splitting ratio ρ_c, when γ_1 and γ_2 were fixed at 10 dB and 10 dB, respectively. In this case, it can be observed that the optimal values are $m_{31} = 74$

and $\rho_c = 0.18$, and the minimize BER is around $4.948e^{-5}$.

From Figs. 5.14-5.16, it can be observed that DTPS and CPS have similar optimal BER from our calculations. One can also see that CEPS has smaller BER than another the other two. One can conclude that CEPS has the best performance among these three structures.

5.5.4 Effect of direct link

In this part, we provide a sample of CEPS with direct link compared with the one without. The DTPS and CPS show same performance as CEPS, when they have a direct link. Fig. 5.17 shows the curves of CEPS and CEPS with a direct link in different power splitting ratio of 0.4 and 0.8, respectively. The achievable rate is higher with a direct link in the structure, but its challenging to find the optimal value.

5.5.5 Effect of conversion efficiency

Fig. 5.18 shows the relationship between achievable rate of three structures versus RF-to-DC conversion efficiency, respectively. It can observed that the DTPS and CPS has similar achievable rate with conversion efficiency. Also for CPES, the rate increases faster with the increases of conversion efficiency. Compared with another two, the performance of CEPS is worse than DTPS and CPS before 0.5, and better than them over 0.5.

5.5.6 Previous work compare

Fig. 5.19 shows the outage probability of novel strcture and basic TS/PS structures. We can see outage probability values of all three structures are smaller than TS/PS, which means they have better performance than basic TS/PS structures discussed before. The CEPS has higher outage probability than DTPS and CPS in the first half and lower in the second half, and DTPS has better performance than CPS.

Fig. 5.20 presents the BERs of novel structures and basic TS/PS structures, resprctively, where the BER values of all three structures are smaller than TS/PS. Therefore, our novel structures have better performance than the normal TS/PS

structures mentioned in previous work. Also, the CPES has higher BER than DTPS and CPS, and DTPS and CPS have similar performance. From above two figues, for PS structure, the outage probability and BER are slightly increased with limited change.

5.6 Conclusions

To conclude, three novel combination structures for EH AF relaying have been investigated in this chapter. Both distance and direct link have been considered, and the improvement of TS and PS EH protocols with different combinations has been discussed. Meanwhile, we maximised the achievable rate and minimise the BER to optimise the power allocation among channel estimation, data transmission, EH and power splitting ratio. The power allocation and power splitting are important in term of rate and BER. Numerical results have verified the existence of an optimal number of pilots and an optimal value of power splitting ratio for channel estimation, data transmission and EH, when the packet size is fixed. We also show the direct link in relaying can improve the performance of relaying system. Compared with normal TS relaying, we have certified the novel structures is better than previous work. We found that CPS has the best performance compare to DTPS and CEPS.

(a)

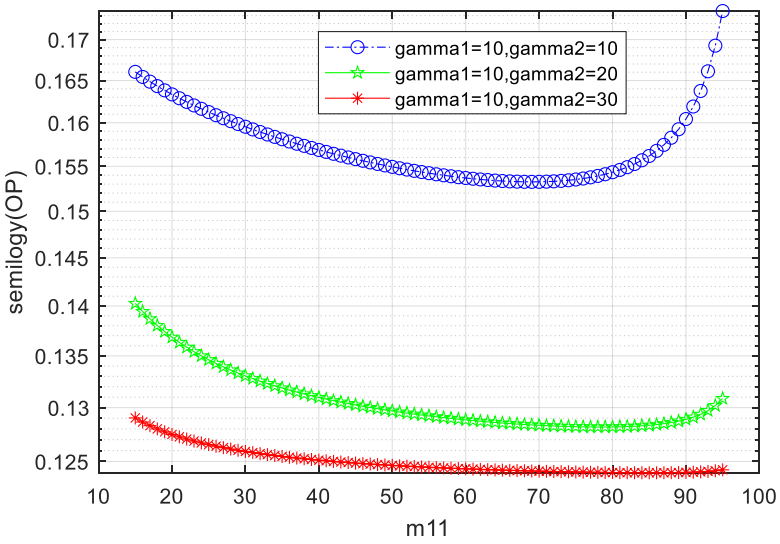

(b)

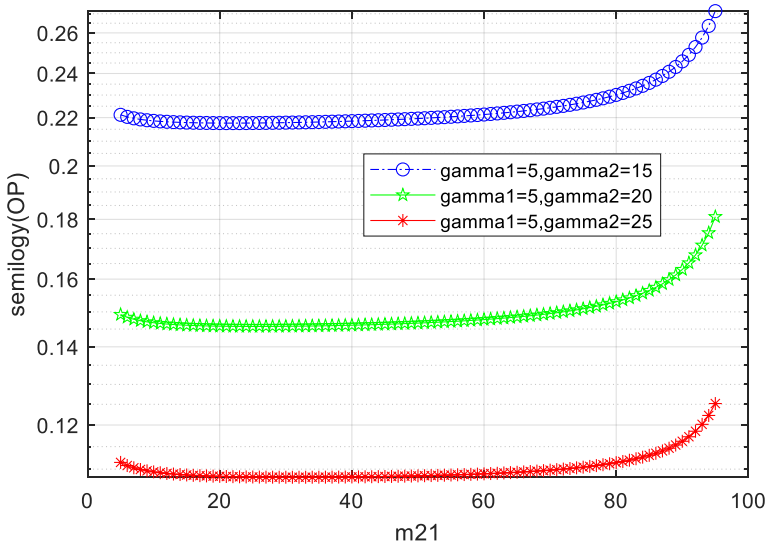

(c)

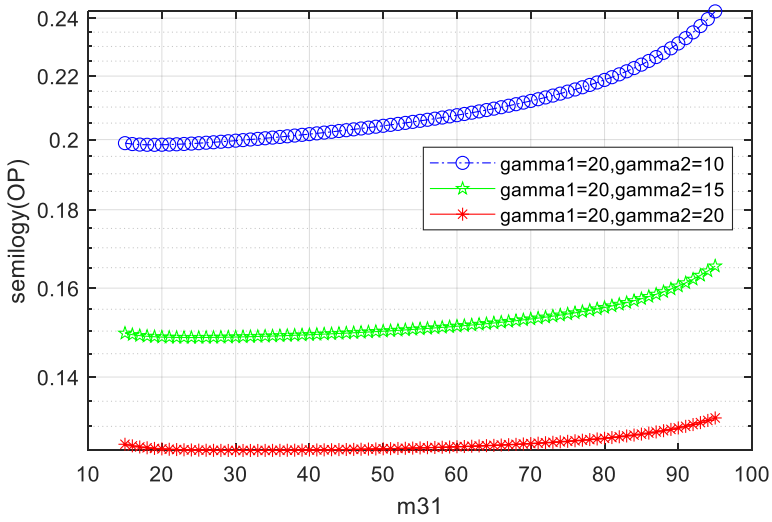

Figure 5.4: The outage probability versus (a) pilots for channel estimation and EH m_{11} in the first hop of CEPS (b) pilots for channel estimation m_{21} in the first hop of DTPS (c) pilots for channel and part of EH m_{31} in the first hop of CPS.

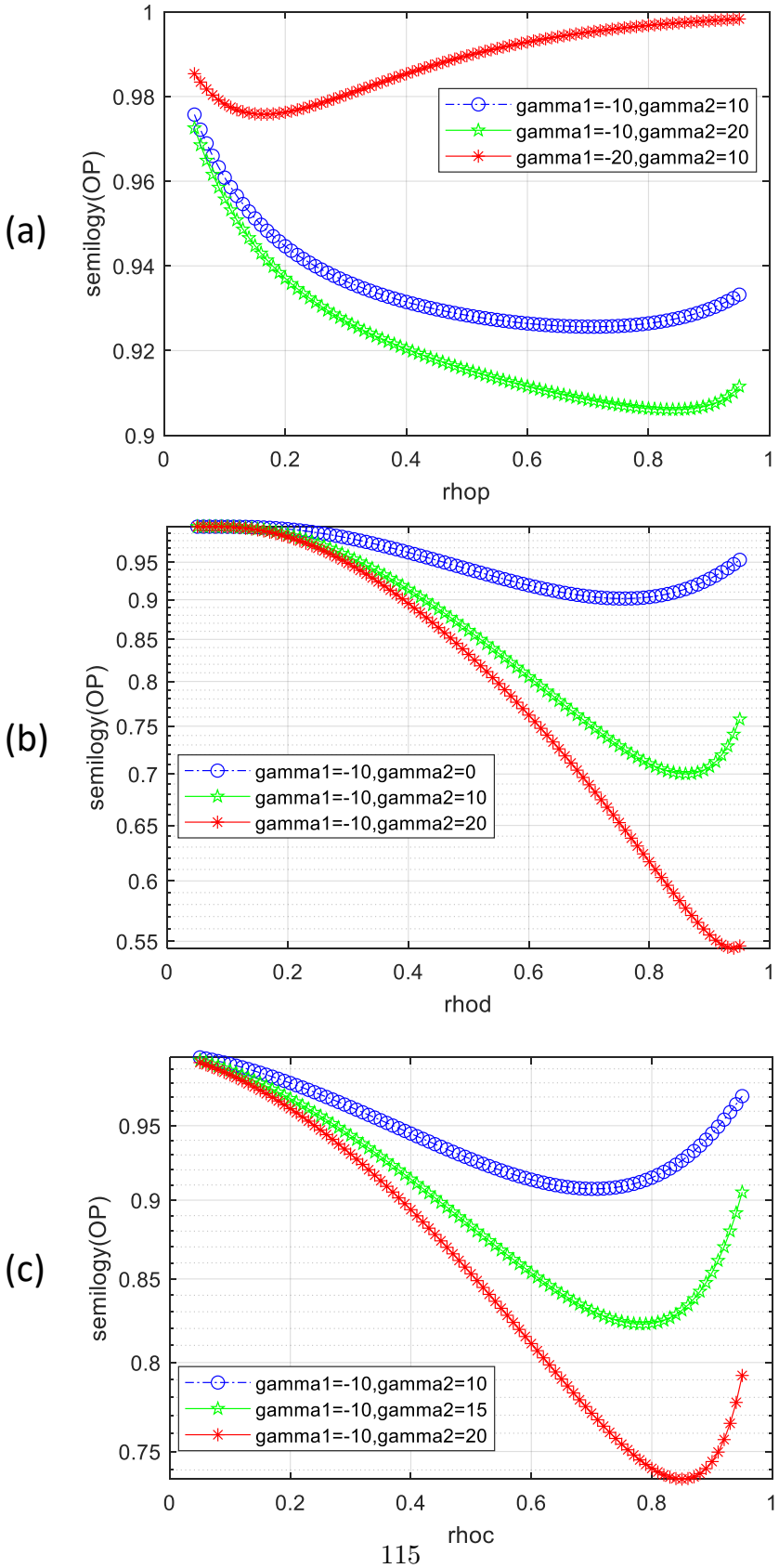

Figure 5.5: The outage probability versus power ratio (a) Power ratio ρ_p for CEPS (b) Power ratio ρ_d for DTPS (c) Power ratio ρ_c for CPS.

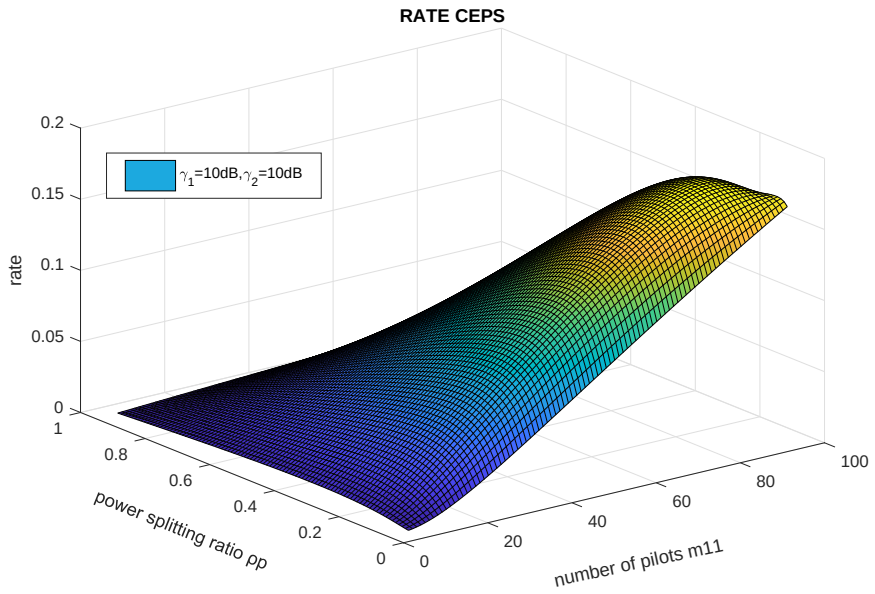

Figure 5.6: Achievable rate of the CEPS structure versus the power splitting ratio ρ_p, when γ_1 and γ_2 are fixed at 10 dB and 10 dB.

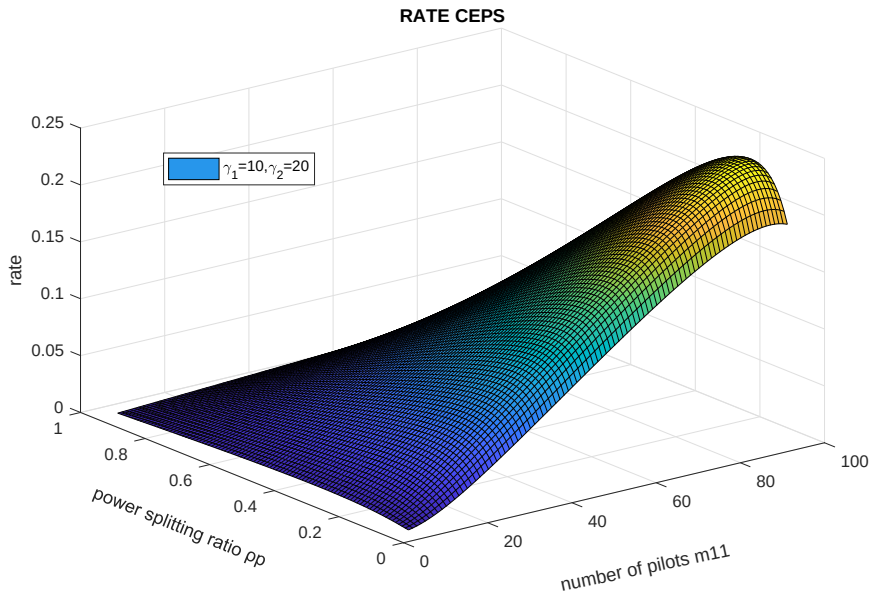

Figure 5.7: Achievable rate of the CEPS structure versus the power splitting ratio ρ_p, when γ_1 and γ_2 are fixed at 10 dB and 20 dB.

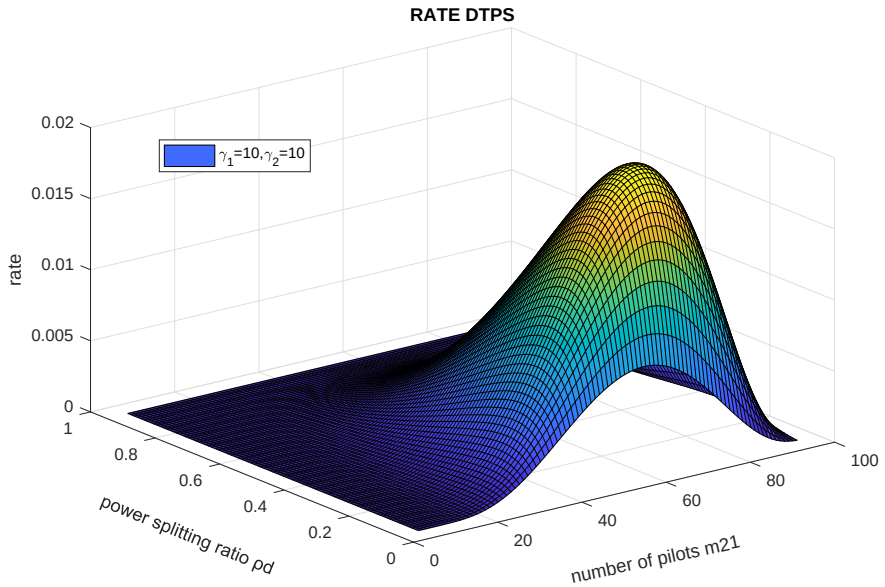

Figure 5.8: Achievable rate of the DTPS structure versus the power splitting ratio ρ_d, when γ_1 and γ_2 are fixed at 10 dB and 10 dB.

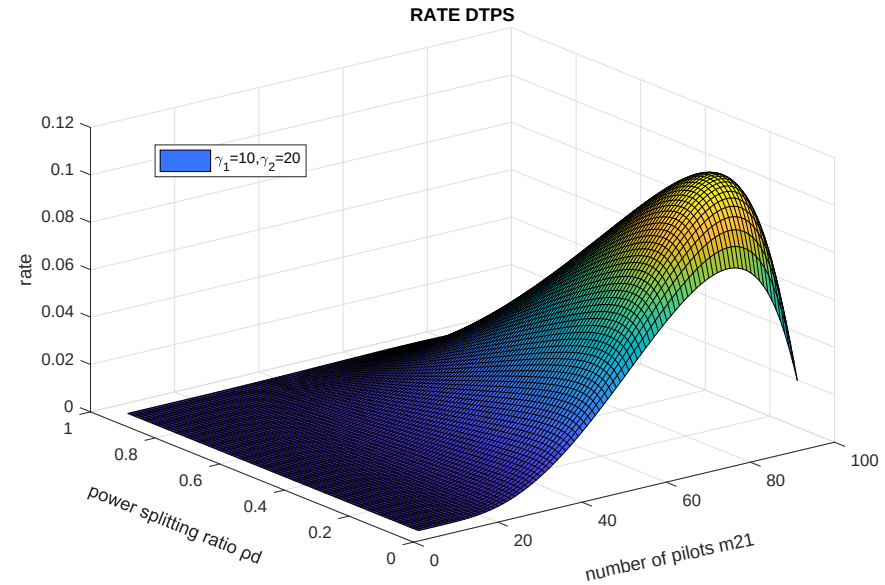

Figure 5.9: Achievable rate of the DTPS structure versus the power splitting ratio ρ_d, when γ_1 and γ_2 are fixed at 10 dB and 20 dB.

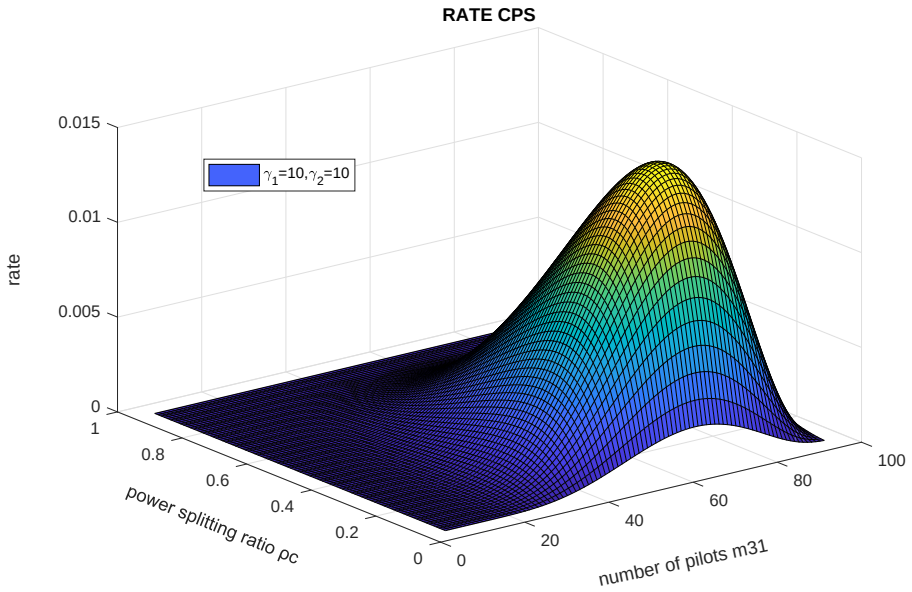

Figure 5.10: Achievable rate of the CPS structure versus the power splitting ratio ρ_c, when γ_1 and γ_2 are fixed at 10 dB and 10 dB.

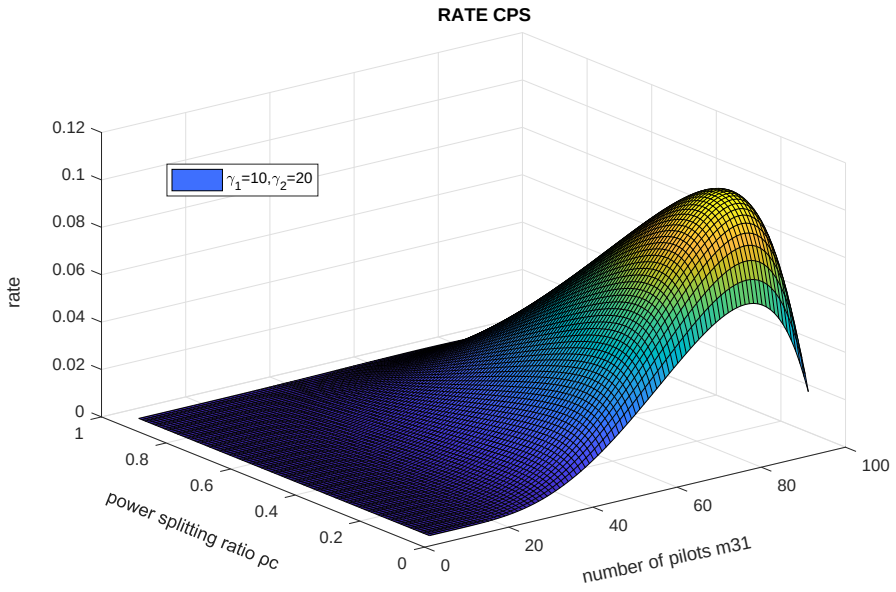

Figure 5.11: Achievable rate of the CPS structure versus the power splitting ratio ρ_c, when γ_1 and γ_2 are fixed at 10 dB and 20 dB.

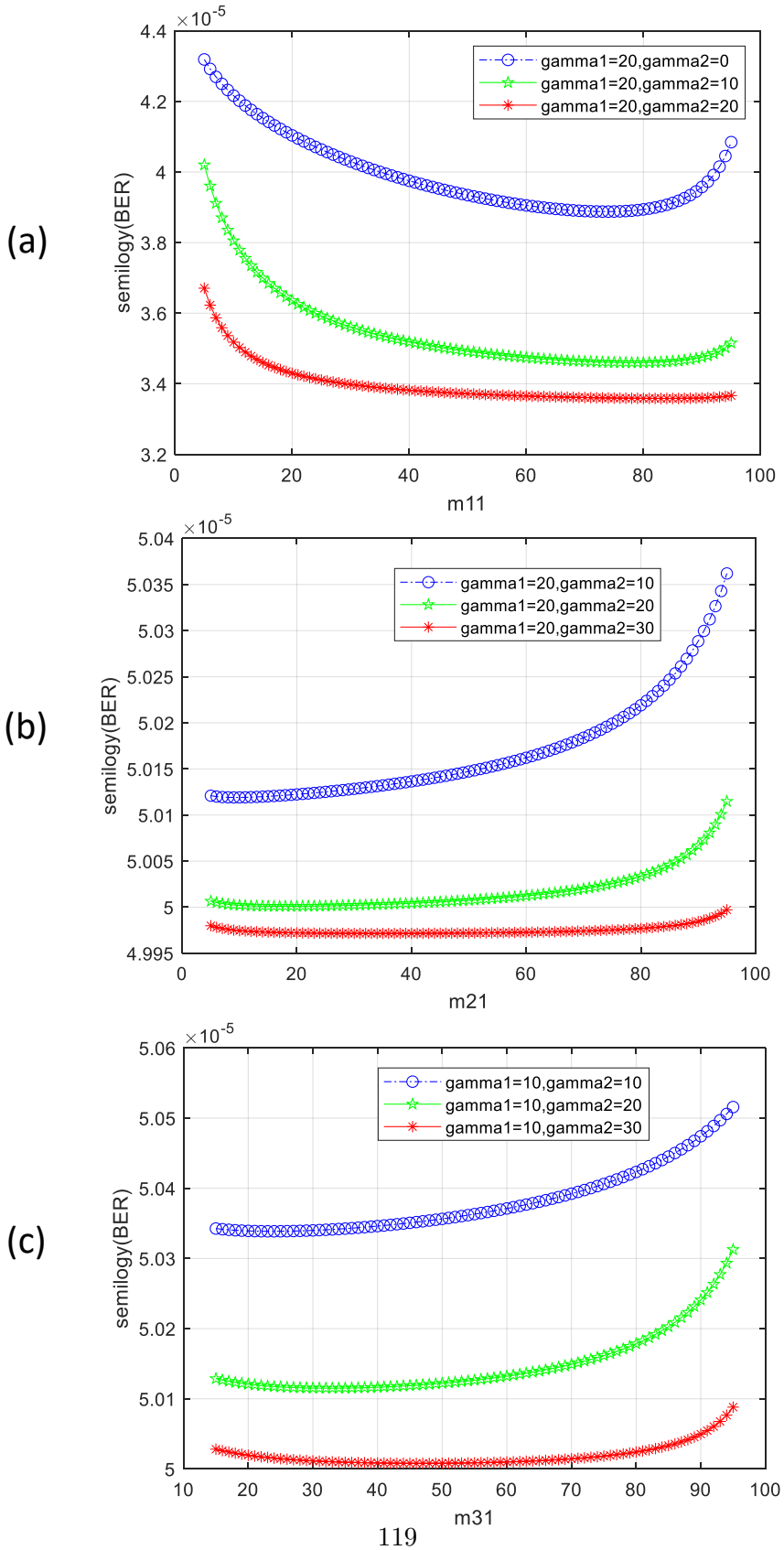

Figure 5.12: The BER versus (a) pilots for channel estimation and EH m_{11} in the first hop for CEPS (b) pilots for channel estimation m_{21} in the first hop for DTPS (c) pilots for channel and part of EH m_{31} in the first hop for CPS.

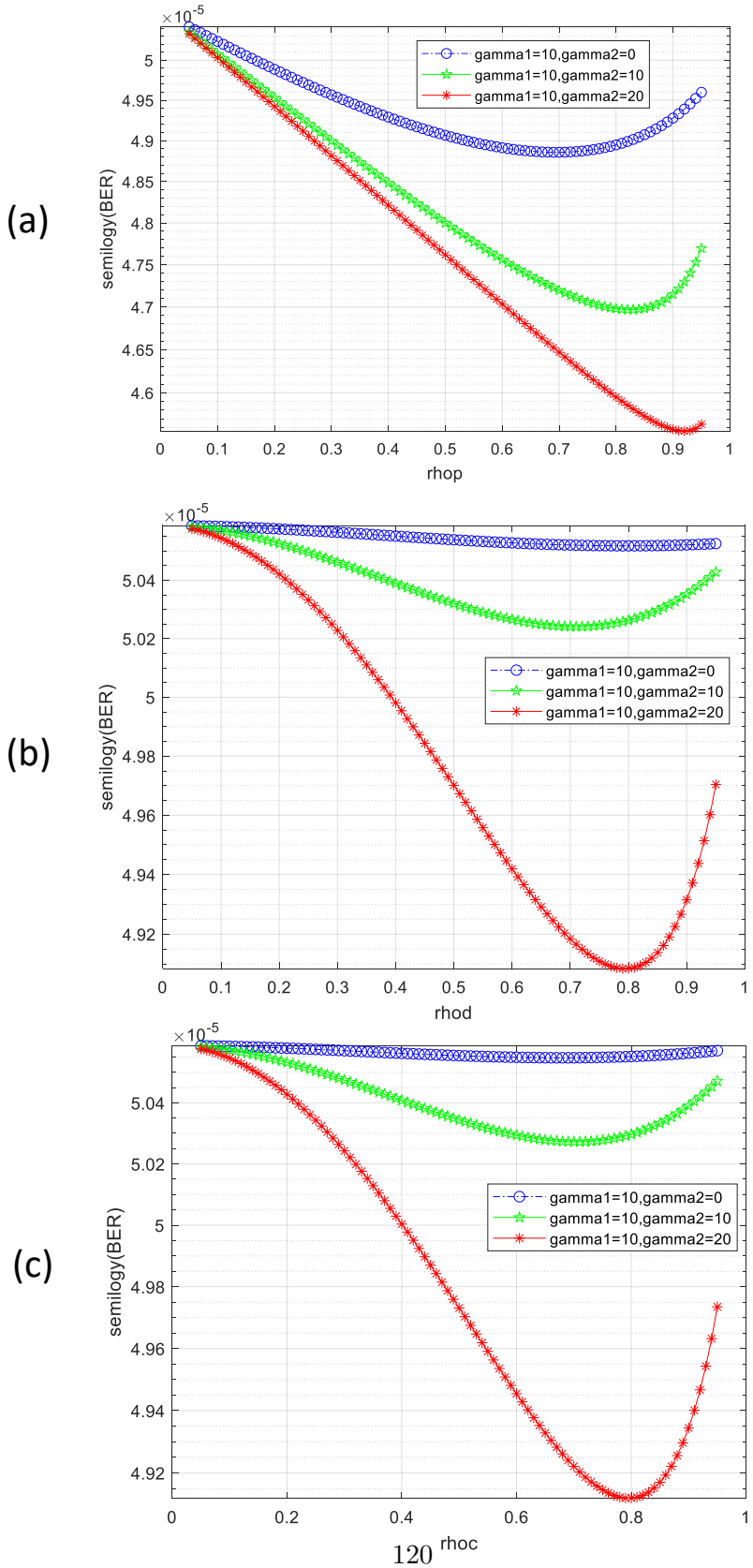

Figure 5.13: The BER versus pilots for channel estimation in the second hop (a) Pilots for channel estimation in the second hop m_{12} for CEPS (b) Pilots for channel estimation in the second hop m_{22} for DTPS (c) Pilots for channel estimation in the second hop m_{32} for CPS.

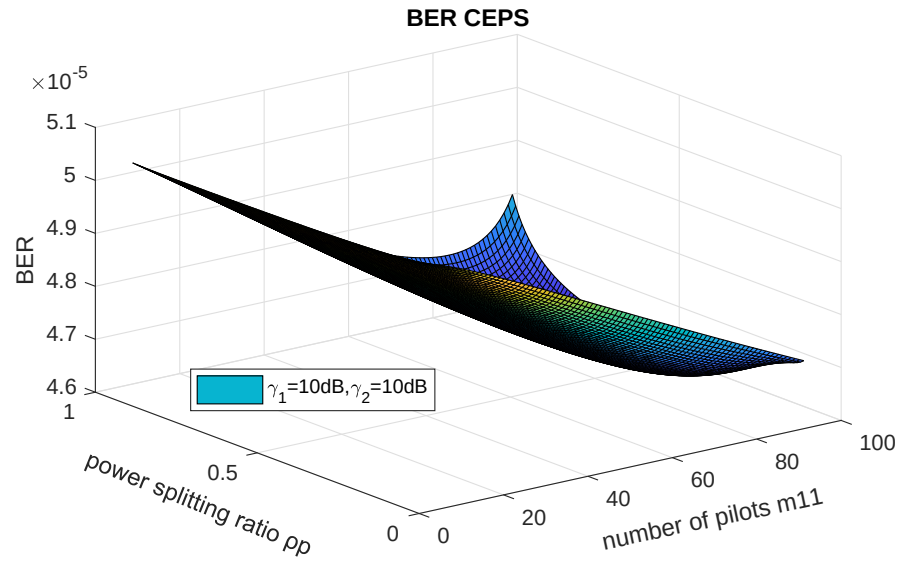

Figure 5.14: BER of the CEPS structure versus the power splitting ratio ρ_p, when γ_1 and γ_2 are fixed at 10 dB and 10 dB.

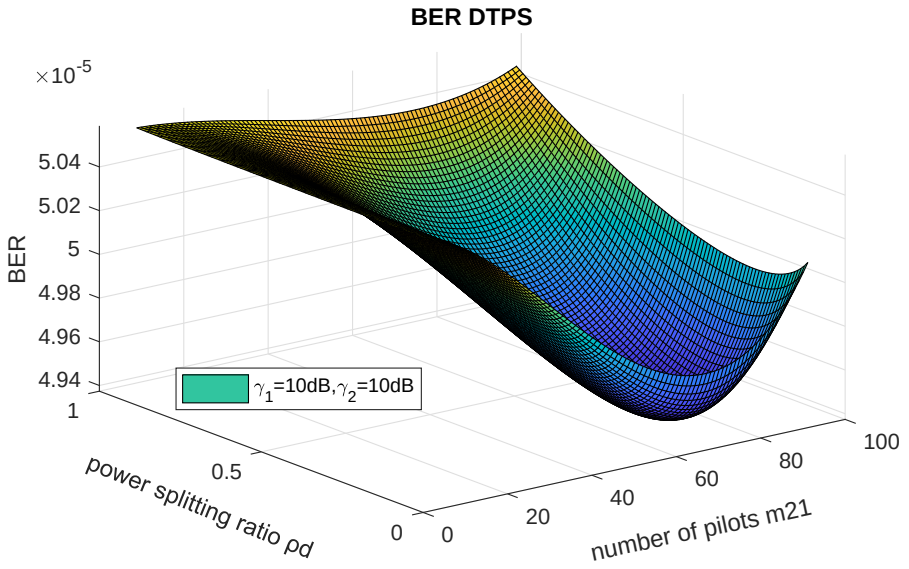

Figure 5.15: BER of the DTPS structure versus the power splitting ratio ρ_d, when γ_1 and γ_2 are fixed at 10 dB and 10 dB.

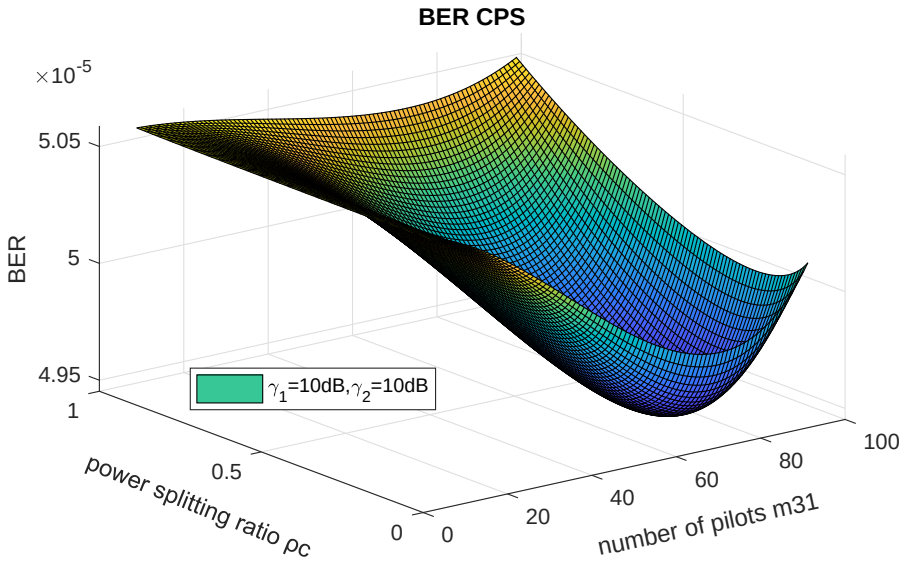

Figure 5.16: BER of the CPS structure versus the power splitting ratio ρ_c, when γ_1 and γ_2 are fixed at 10 dB and 10 dB.

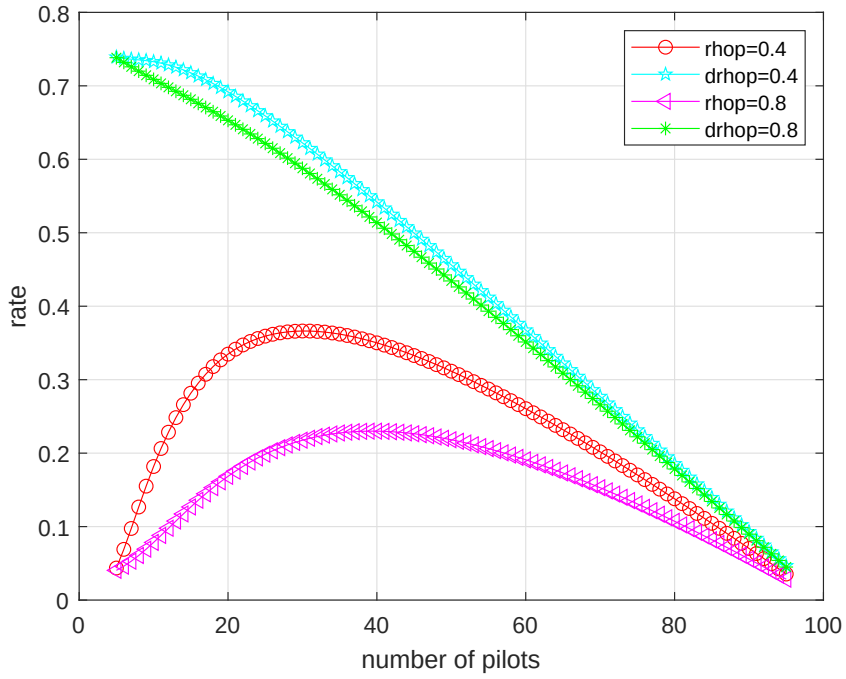

Figure 5.17: Achievable rate of CEPS with direct link versus the channel estimation pilots, when γ_1 and γ_2 are fixed at 10dB and 10dB.

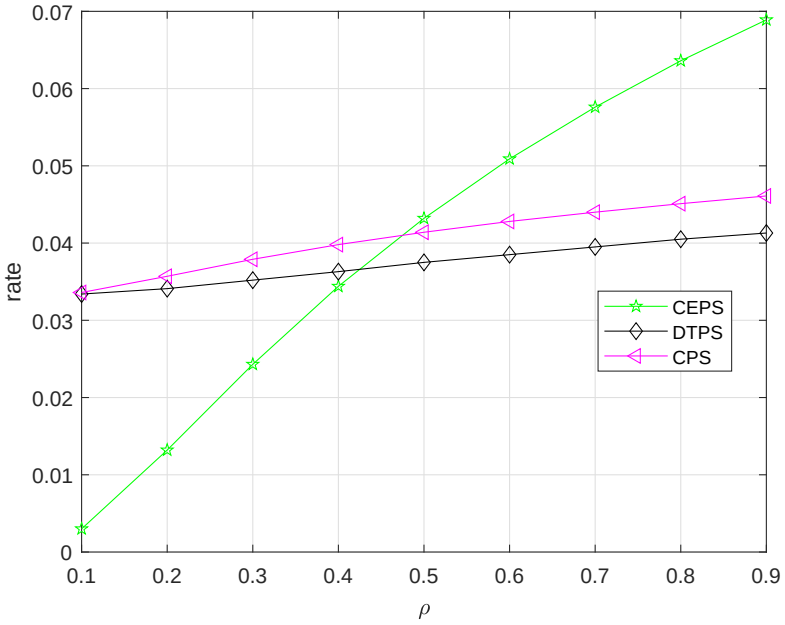

Figure 5.18: Achievable rate of CEPS,DTPS,CPS versus the power conversion efficiency.

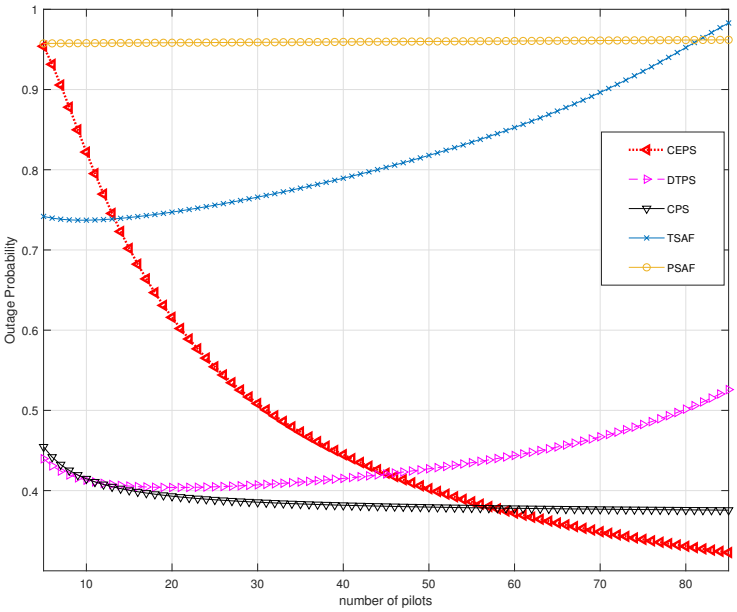

Figure 5.19: Outage probability comparison between Novel structures and basic TS/PS structures

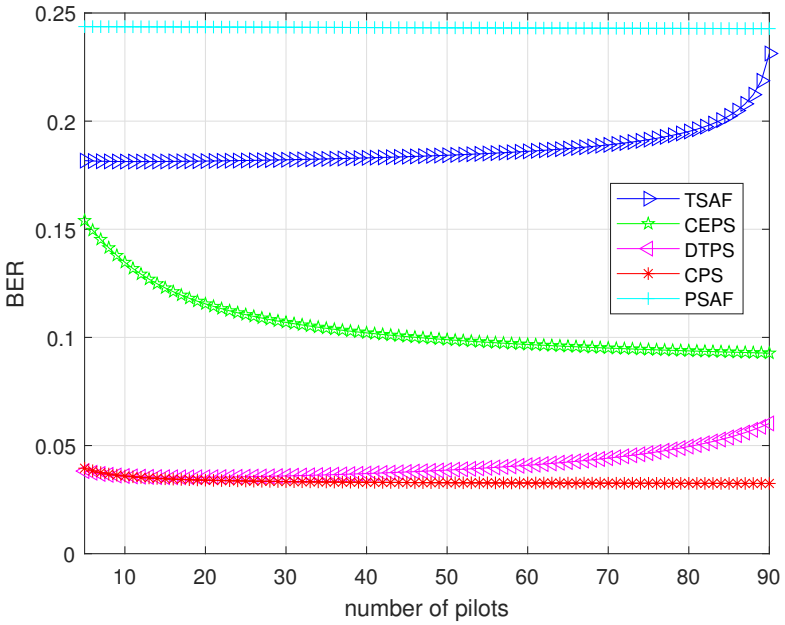

Figure 5.20: BER comparison between Novel structures and basic TS/PS structures

Chapter 6

Allocation between estimation, detection and harvesting with ambient Energy

6.1 Introduction and related works

In the last chapter, three novel EH structures were proposed. Those schemes harvested energy from the source exclusively. Given the wide usage of RF devices, the RF energy can be detected everywhere, making it an excellent power source for low-power devices. The ambient RF EH is considered in numerous works [34, 174, 175]. The concept of ambient RF EH has been first noticed in 1900. Unfortunately, this idea was not accepted by the multitude at the time. In [176], this theory was raised again by Mi, Minhong. The ambient RF energy has a comparably low energy density of 0.2 nW/cm2 $\sim$ 1 W/cm^2 as compared to the other energy sources [177], [34]. The free or living ambient energy density of the ambient RF and wireless sources are increasing due to the explosion of wireless communication and broadcasting infrastructures, such as analogue/digital TV, AM/FM radio, WiFi networks, and cellular networks. The ambient RF power density is normally more powerful in downtown urban areas and in the proximity of the power sources (e.g., TV towers) [34]. Since then, more applications in various areas have been developed, such as on personal devices, military applications, IoT and medical appliances.

Previous works either considered the system with RF ambient EH and chan-

nel estimation without data transmission [68] or merely harvested energy from the source without examining the ambient energy [104]. Therefore, in this chapter, the EH and information decoding are considered concurrently, with two neutralised harvest energy sources. We intend to fill the gap of the EH model in AF relaying system with multiple energy sources.

In this chapter, more realistic schemes with added ambient RF energy are presented. Based on the schemes designed in Chapter 5, three ambient added structures are designed, 'ACEPS', 'ADTPS' and 'DTPS', which are based on 'CEPS', 'DTPS', and 'CPS', respectively. The cumulative density functions (CDF) are derived from the probability density functions (PDF). Then, the expressions of the achievable rate (AR) and bit-error-rate (BER) for these models are generated. The system performance is investigated in terms of AR and BER, with variable channel estimation rates and power splitting ratios. Consequently, the characteristics can be achieved through simulation results analysis. It is a straightforward way to obtain the optimal power allocations for different schemes.

Because of the high similarities between the new models and the system models given in Chapter 5, in Section 6.1, the description of the system models with same expressions will not be repeated. This chapter takes additional RF ambient energy into account, which increases the amount of energy harvested at the relay node. Same system models in Chapter 5 are applied here as the fundamental framework, with ambient RF EH appended. Beyond that, the EH capacity is developed, and the signal efficiency is enhanced as well.

The remainder of this chapter will be organised as follows. The system model of ambient added EH structures: ACEPS, ADTPS and ACPS are proposed in Section 6.2. Then, the end-to-end SNR and variables for different structures will be derived in Section 6.3. In Section 6.4, the EH system performance is examined according to the outage probability and achievable rate for different schemes. The numerical results are analysed in Section 6.5, and finally, the conclusion is presented in Section 6.6.

6.2 Three ambient added EH AF relaying schemes

In this section, the ambient RF added system models: ACEPS, ADTPS, and ACPS are displayed in details. Following, we will present the system models for different

structures.

The system structures examined in this chapter are the same as Chapter 5, which shown in Fig.5.1. Under the AF relaying frame, it has one source, one relay and one destination. Each system with a single antenna and works in half-duplex mode. Entirely two hops are included into transmission: SR and RD link.

6.2.1 Channel estimation power splitting scheme with ambient energy (ACEPS)

The received signals at the relay and the received signals at the destination have the same expressions, which are described in Chapter 5 Section 5.2.1. In the first hop, the received signal for channel estimation, the received signal of the data symbols and the received signal of pilots for EH are the equivalent as (5.1),(5.2) and (5.3), respectively.

However, because the additional ambient RF energy is considered, the harvested energy at the relay node is improved, based on the initial energy harvested from the source (5.4), and additional RF energy from the environment, the harvested energy at the relay can be written as

$$E_{r1} = \eta \frac{P_{s1}}{d_{sr}^{e}} |h_1|^2 (1 - \rho_p) m_{11} + P_e \tag{6.1}$$

where P_e is the ambient RF energy harvested at the relay node, and followed with Poisson distribution with probability density $pr = 1$, η stands for the conversion efficiency of the energy harvester and $T = 1$ is assumed for simplicity. The harvested energy will be used to transmit m_{11} pilots to the destination for the channel estimation and $D - m_{11}$ data symbols from the source in the second hop to keep the same data rate. Thus the transmission power of the relay is

$$P_{r1} = \frac{\eta \frac{P_{s1}}{d_{sr}^{e}} |h_1|^2 (1 - \rho_p) m_{11} + P_e}{D}. \tag{6.2}$$

Furthermore, the estimate h_1 is expressed as (5.6). The amplification factor can be written as (5.7). For the second hop, the received pilots for channel estimation at the destination, the received data symbols at the destination are written as (5.8) and (5.9), respectively. The received data symbols at the destination in the direct link can be expressed as (5.11).

6.2.2 Data transmission power splitting scheme with ambient energy (ADTPS)

The received signals at the relay and the destination for ADTPS structure are similar to the DTPS, which were described in Chapter 5 Section 5.2.2.

In the first hop, the pilots received at the relay for channel estimation, the received signal of the data symbols and the received signal of pilots for EH are presented as (5.12),(5.13) and (5.14), respectively. However, compared with the DTPS harvested energy in (5.15), there is additional ambient RF energy involved. The harvested energy at the relay node then can be expressed as

$$E_{r2} = \frac{P_{s2}\eta|h_2|^2(1-\rho_d)(D-m_{21})}{{d_{sr}}^e} + P_{e2} \tag{6.3}$$

where the remaining $P_{s2}|\hat{h_2}|^2$ is the amount of energy selected by the harvester at the relay node through EH protocol. The harvested energy then will be used to send m_{22} pilot symbols to the destination node for the channel estimation of the second hop, which from relay node to destination node, there are total $\rho_d(D-m_{21})$ data symbols from the source.

The transmission power at the relay node is

$$P_{r2} = \frac{\eta\frac{P_{s2}}{{d_{sr}}^e}|\hat{h_2}|^2(1-\rho_d)(D-m_{21})}{D} \tag{6.4}$$

where the estimate h_2 is the same as (5.17), and similarly, the amplification factor for this scheme can be written as (5.18).

For the second hop, the received pilots for channel estimation and the received data symbols at the destination can be expressed as (5.19) and (5.21), respectively.

The direct link expression is also given by (5.11).

6.2.3 Combination power splitting scheme with ambient energy (ACPS)

Identically as above two models, the received signals are the same as the CPS structure in Chapter 5 Section 5.2.3. At the relay node, the pilot received at the

relay for channel estimation, the collected data symbols and the pilots for EH are presented in (5.22), (5.23), and (5.24), respectively.

The harvested energy from the source can be expressed as

$$E_{r3} = \eta |h_3|^2 (1 - \rho_c) D \frac{P_{s3}}{d_{sr}{}^e} + P_{e3}. \tag{6.5}$$

The remaining $P_{s3}|\hat{h_3}|^2$ is the amount of energy collected by the harvester at the relay node through EH protocol. The harvested energy will be used to transmit m_{32} pilot symbols to the destination node for the channel estimation of the second hop from the relay node to destination node, as well as $\rho_c(D - m_{31})$ data symbols from the source. The transmission power at the relay, which used to send signal from the relay to the destination is

$$P_{r3} = \frac{\eta |h_3|^2 (1 - \rho_c) D \frac{P_{s3}}{d_{sr}{}^e} + P_{e3}}{D} \tag{6.6}$$

with the estimated h_3 is the same as (5.27), the amplification factor can be written as (5.28).

For the second hop, the received pilots for channel estimation and the received data symbols at the destination can be stated as (5.29) and (5.31), respectively.

6.3 Maximum-likelihood channel estimation

In this section, the end-to-end SNR and measurement parameters for different structures are derived. The performance analysis will be discussed for seeking the optimal power allocation.

6.3.1 ACEPS channel estimation

Following the received signals in (5.8), with the same derivation procedures, the end-to-end SNR expression of ACEPS structure can be written as

$$\begin{aligned}\hat{g_1} &= \frac{\Sigma_{i_{12}=1}^{m_1}\left(\sqrt{\frac{P_{r1}}{{d_{rd}}^e}}g_1\hat{a}_{1var}+n_{12}[i_{12}]\right)}{m_1\hat{a}_{1var}\sqrt{\frac{\hat{P_{r1}}}{{d_{rd}}^e}}} = \frac{\sqrt{\frac{P_{r1}}{{d_{rd}}^e}}}{\sqrt{\frac{\hat{P_{r1}}}{{d_{rd}}^e}}}g_1 + \frac{\Sigma_{i_{12}=1}^{m_1}n_{12}[i_{12}]}{m_1\hat{a}_{1var}\sqrt{\frac{\hat{P_{r1}}}{{d_{rd}}^e}}} \\ &= \frac{\sqrt{\frac{P_{r1}}{{d_{rd}}^e}}}{\sqrt{\frac{\hat{P_{r1}}}{{d_{rd}}^e}}}g_1 + \varepsilon_{12}\end{aligned} \tag{6.7}$$

where has $\varepsilon_{12} = \frac{\Sigma_{i_{12}=1}^{m_{11}}n_{12}[i_{12}]}{m_{11}\hat{a}_{1var}\sqrt{\frac{P_{r1}}{{d_{rd}}^e}}}$ and $\hat{P_{r1}} = \frac{\eta\frac{P_{s1}}{{d_{sr}}^e}|\hat{h_1}|^2(1-\rho_p)m_1T+P_{e1}}{DT}$.

To integrate the expressions (6.7) and (5.6) in (5.9), the received signal for data transmission in at the destination can be expressed as (5.32).

The end-to-end SNR function for the received signal at the destination can be expanded as

$$\gamma_{1end} = \frac{|\hat{h_1}|^2|\hat{g_1}|^2\frac{P_{s1}}{{d_{sr}}^e}}{A_a} \tag{6.8}$$

where the $A_a = \frac{P_{s1}}{{d_{sr}}^e}|\hat{g_1}|^2\varepsilon_{11var} + \frac{P_{s1}}{{d_{sr}}^e}\varepsilon_{12var}|\hat{h_1}|^2 + |\hat{g_1}|^2N_{11} + \frac{P_{s1}}{{d_{sr}}^e}\varepsilon_{11var}\varepsilon_{12var} + \varepsilon_{12var}N_{11} + \frac{N_{12}}{\frac{\hat{P_{r1}}}{{d_{rd}}^e}\hat{a}_{1var}^2}$, with assumptions $E[|x[j_{11}]|^2] = 1$, $E[|n_{11}[j_{11}]|^2] = N_{11}$ and $E[|n_{12}[j_{12}]|^2] = N_{12}$. Also, denote $E[|\varepsilon|_1^2] = \varepsilon_{11var}$,$E[|\varepsilon|_2^2] = \varepsilon_{12var}$.

6.3.2 ADTPS channel estimation

Similarly, with the received signal in (5.19), the fading channel gain between relay node and destination node can be estimated as

$$\hat{g_2} = \frac{\sqrt{\frac{P_{r2}}{{d_{rd}}^e}}}{\sqrt{\frac{\hat{P_{r2}}}{{d_{rd}}^e}}}g_2 + \varepsilon_{22} \tag{6.9}$$

where we have $\varepsilon_{22} = \frac{\Sigma_{i_{22}=1}^{m_{21}}n_{22}[i_{22}]}{m_{21}\hat{a}_{2var}\sqrt{\frac{\hat{P_{r2}}}{{d_{rd}}^e}}}$ and $\hat{P_{r2}} = \frac{\eta\frac{P_{s2}}{{d_{sr}}^e}|\hat{h_2}|^2(1-\rho_d)(D-m_2)T+P_{e2}}{DT}$.

The data transmission at the destination in (5.35) can be obtained by substituting (6.9) and (5.17) in (5.21). Thus, the end-to-end SNR expression of ADTPS structure can be written as

$$\gamma_{2end} = \frac{|\hat{h_2}|^2 |g_2|^2 \frac{P_{s2}}{{d_{sr}}^e} \rho_d}{A_b} \tag{6.10}$$

where $A_b = \frac{\rho_d |g_2|^2 N_{21}}{m_2} + |g_2|^2 N_{21} + \frac{N_{22}\rho_d \frac{P_{s2}}{{d_{sr}}^e} |\hat{h_2}|^2 \left(\frac{P_{s2}}{{d_{sr}}^e} |\hat{h_2}|^2 + N_{21}\right) DT {d_{rd}}^e}{[\eta |\hat{h_2}|^2 (1-\rho_d)(D-m_2)T + P_{e2}] m_2} + \frac{N_{21}N_{22}\rho_d \left(\frac{P_{s2}}{{d_{sr}}^e} |\hat{h_2}|^2 + N_{21}\right) DT {d_{rd}}^e}{{m_2}^2 [\eta \frac{P_{s2}}{{d_{sr}}^e} |\hat{h_2}|^2 (1-\rho_d)(D-m_2)T + P_{e2}]} + \frac{N_{22}N_{21}\left(\frac{P_{s2}}{{d_{sr}}^e} |\hat{h_2}|^2 + N_{21}\right) DT {d_{rd}}^e}{[\eta \frac{P_{s2}}{{d_{sr}}^e} |\hat{h_2}|^2 (1-\rho_d)(D-m_2)T + P_{e2}] m_2} + \frac{N_{22}\left(\frac{P_{s2}}{{d_{sr}}^e} |\hat{h_2}|^2 + N_{21}\right) DT {d_{rd}}^e}{[\eta \frac{P_{s2}}{{d_{sr}}^e} |\hat{h_2}|^2 (1-\rho_d)(D-m_2)T + P_{e2}]}$.

6.3.3 ACPS channel estimation

Similar to the above two schemes, the received signal at the destination is analysed as (5.29). Then, the channel gain between the relay and the destination can be estimated as

$$\hat{g_3} = \frac{\Sigma_{i_{32}=1}^{m_3} \left(\sqrt{\frac{P_{r3}}{{d_{rd}}^e}} g_3 \hat{a}_{3var} + n_{32}[i_{32}]\right)}{m_3 \hat{a}_{3var} \sqrt{\frac{\hat{P_{r3}}}{{d_{rd}}^e}}} = \frac{\sqrt{\frac{P_{r3}}{{d_{rd}}^e}}}{\sqrt{\frac{\hat{P_{r3}}}{{d_{rd}}^e}}} g_3 + \frac{\Sigma_{i_{32}=1}^{m_3} n_{32}[i_{32}]}{m_3 \hat{a}_{3var} \sqrt{\frac{\hat{P_{r3}}}{{d_{rd}}^e}}} = \frac{\sqrt{\frac{P_{r3}}{{d_{rd}}^e}}}{\sqrt{\frac{\hat{P_{r3}}}{{d_{rd}}^e}}} g_3 + \varepsilon_{32} \tag{6.11}$$

where $\varepsilon_{32} = \frac{\Sigma_{i_{32}=1}^{m_{31}} n_{32}[i_{32}]}{m_{31} \hat{a}_{3var}}$ is the estimation error, and the estimated transmission power at relay is $\hat{P_{r3}} = \frac{\eta \frac{P_{s3}}{{d_{sr}}^e} |\hat{h_3}|^2 (1-\rho_c) DT + P_{e3}}{DT}$ from (5.26).

The extended received signal for data transmission is (5.35). Therefore, the end-to-end SNR expression for ACPS can be expressed as

$$\gamma_{3end} = \frac{|\hat{h_3}|^2 |\hat{g_3}|^2 \frac{P_{s3}}{{d_{sr}}^e}}{A_c} \tag{6.12}$$

where $A_c = \frac{P_{s3}}{{d_{sr}}^e} |\hat{g_3}|^2 \varepsilon_{31var} + |\hat{g_3}|^2 N_{31} + \frac{P_{s3}}{{d_{sr}}^e} \varepsilon_{31var} \varepsilon_{32var} + \frac{P_{s3}}{{d_{sr}}^e} \varepsilon_{32var} |\hat{h_3}|^2 + \varepsilon_{32var} N_{31} + \frac{N_{32}}{\frac{\hat{P_{r3}}}{{d_{rd}}^e} \hat{a}_{3var}^2}$.

6.4 End-to-end SNR

In this section, the CDF of end-to-end SNR expressions for three ambient RF added structures are derived first as (6.8),(6.10), and (6.12), respectively. After that, CDFs are continued to derive the mathematical expressions of outage probability, achievable rate, and BER for different schemes, respectively. The particularly methods will be presented in details below.

6.4.1 ACEPS CSI estimation

To obtian the CDF expression, we first have to get the variance value for ε_{11} and variance value for ε_{12}. Since these two values are not related to the P_{r1} in $Var(\varepsilon_{11})$, it has same expression as (5.40). However, from (5.7), ε_{12} will be updated as

$$\varepsilon_{12} = \frac{\Sigma_{i_{12}=1}^{m_1} n_{12}[i_{12}]}{m_1 \hat{a}_{1var} \sqrt{\frac{\hat{P_{r1}}}{{d_{rd}}^e}}} \tag{6.13}$$

where it has a mean of zero. And $|\varepsilon_{12}|^2$ can be calculated as

$$\begin{aligned}
|\varepsilon_{12}|^2 &= \frac{|\Sigma_{i_{12}=1}^{m_1} n_{12}[i_{12}]|^2}{{m_1}^2 \hat{a}_{1var}^2 \frac{\hat{P_{r1}}}{{d_{rd}}^e}} = \frac{|\Sigma_{i_{12}=1}^{m_1} n_{12}[i_{12}]|^2 DT {d_{rd}}^e \left(\frac{P_{s1}}{{d_{sr}}^e} |\hat{h_1}|^2 + N_{11}\right)}{[\eta \frac{P_{s1}}{{d_{sr}}^e} |\hat{h_1}|^2 (1-\rho_p) m_1 T + P_{e1}] {m_1}^2} \\
&= \Sigma_{i_{12}=1}^{m_1} \left(\frac{n_{12}[i_{12}]^2 DT {d_{rd}}^e \left(\frac{P_{s1}}{{d_{sr}}^e} |\hat{h_1}|^2 + N_{11}\right)}{[\eta \frac{P_{s1}}{{d_{sr}}^e} |\hat{h_1}|^2 (1-\rho_p) m_1 T + P_{e1}] {m_1}^2}\right) \\
&+ \Sigma_{k_1=1}^{m_1} \Sigma_{j_{12}=1 k_1 \neq j_{12}}^{m_1} \left(\frac{n_{12}[j_{12}] \times n_{12}[k_1] DT {d_{rd}}^e \left(\frac{P_{s1}}{{d_{sr}}^e} |\hat{h_1}|^2 + N_{11}\right)}{[\eta \frac{P_{s1}}{{d_{sr}}^e} |\hat{h_1}|^2 (1-\rho_p) m_1 T + P_{e1}] {m_1}^2}\right)
\end{aligned} \tag{6.14}$$

and then, the variance of ε_{12} is defined as

$$Var(\varepsilon_{12}) = \frac{N_{12} DT {d_{rd}}^e \left(\frac{P_{s1}}{{d_{sr}}^e} |\hat{h_1}|^2 + N_{11}\right)}{[\eta \frac{P_{s1}}{{d_{sr}}^e} |\hat{h_1}|^2 (1-\rho_p) m_1 T + P_{e1}] m_1}. \tag{6.15}$$

Merging expressions (5.40) and (6.15) in (6.8), the end-to-end SNR expres-

sion for ACEPS can be derived as

$$\gamma_{1end} = \frac{|\hat{g_1}|^2 |\hat{h_1}|^2 \frac{P_{s1}}{{d_{sr}}^e}}{A_d} \tag{6.16}$$

where the $A_d = \frac{N_{11}|\hat{g_1}|^2}{m_1\rho_p} + |\hat{g_1}|^2 N_{11} + \frac{N_{12}N_{11}DTd_{rd}{}^e\left(\frac{P_{s1}}{{d_{sr}}^e}|\hat{h_1}|^2+N_{11}\right)}{[\eta\frac{P_{s1}}{{d_{sr}}^e}|\hat{h_1}|^2(1-\rho_p)m_1T+P_{e1}]{m_1}^2\rho_p} + \frac{\frac{P_{s1}}{{d_{sr}}^e}|\hat{h_1}|^2 N_{12}DTd_{rd}{}^e\left(\frac{P_{s1}}{{d_{sr}}^e}|\hat{h_1}|^2+N_{11}\right)}{[\eta\frac{P_{s1}}{{d_{sr}}^e}|\hat{h_1}|^2(1-\rho_p)m_1T+P_{e1}]m_1} + \frac{N_{12}N_{11}DTd_{rd}{}^e\left(\frac{P_{s1}}{{d_{sr}}^e}|\hat{h_1}|^2+N_{11}\right)}{[\eta\frac{P_{s1}}{{d_{sr}}^e}|\hat{h_1}|^2(1-\rho_p)m_1T+P_{e1}]m_1} + \frac{N_{12}DTd_{rd}{}^e\left(\frac{P_{s1}}{{d_{sr}}^e}|\hat{h_1}|^2+N_{11}\right)}{[\eta\frac{P_{s1}}{{d_{sr}}^e}|\hat{h_1}|^2(1-\rho_p)m_1T+P_{e1}]}.$

Similarly, the instantaneous link signal to noise ratios (SNRs) in the i_{SD} at the destination is (5.44).

In order to get the PDF, the distributions of $\hat{h_1}$ and $\hat{g_1}$ are needed. Same as (5.45), the second-moment expression of $\hat{h_1}$ for ACEPS is identically as CEPS. Therefore, the exponential random variable with scale parameter can be written as (5.46). The similarity probability density function (PDF) and cumulative density function (CDF) are described as (5.47) and (5.48), respectively. Unlike CEPS, the $|\hat{g_1}|^2$ can be written as

$$\begin{aligned} E|\hat{g_1}|^2 &= E|\frac{|\hat{h_1}|}{|\hat{h_1}|}g_1 + \frac{\Sigma_{i_{11}=1}^{m_1} n_{12}[i_{11}]}{m_1\hat{a}_{1var}\sqrt{\frac{\hat{P_{r1}}}{{d_{rd}}^e}}}|^2 \\ &= E(\frac{|\hat{h_1}|^2}{|\hat{h_1}|^2}|g_1|^2) + E(|\frac{\Sigma_{i=1}^{m_1} n_{12}[i_{11}]}{m_1\hat{a}_{1var}\sqrt{\frac{\hat{P_{r1}}}{{d_{rd}}^e}}}|^2) + E(2Re\{\frac{|\hat{h_1}|}{|\hat{h_1}|}g_1 \times \frac{\Sigma_{i_{11}=1}^{m_1} n_{12}[i_{11}]^*}{m_1\hat{a}_{1var}\sqrt{\frac{\hat{P_{r1}}}{{d_{rd}}^e}}}\}) \end{aligned} \tag{6.17}$$

where $|\Sigma_{i_{11}=1}^{m_1} n_{12}[i_{11}]|^2 = 2\Sigma_{k_1=1}^{m_1}\Sigma_{j_{12}=1}^{D} Re\{n_{12}[j_{12}]n_{12}[k_1]^*\} + \Sigma_{i_{11}=1}^{m_1}|n_{12}[i_{11}]|^2$, $E(|g_1|^2) = 2\theta^2$, $E(\Sigma_{i_{11}=1}^{m_1} n_{12}[i_{11}]) = 0$, $n_{12}[j_{12}]n_{12}[k_1] = 0$ and $Re\{\frac{|\hat{h_1}|}{|\hat{h_1}|}|g_1|(\frac{\Sigma_{i_{11}=1}^{m_1} n_{12}[i_{11}]}{m_1\hat{a}_{1var}\sqrt{\hat{P_{r1}}}})\} = 0$, furthermore

$$2\theta^2 E\left\{\frac{|\hat{h_1}|^2}{|\hat{h_1}|^2}\right\} \approx 2\theta^2\frac{2\theta^2}{2\theta^2 + \frac{|N_{11}|}{m_1\rho_p\frac{P_{s1}}{{d_{sr}}^e}}} \approx \frac{4\theta^4}{2\theta^2 + \frac{|N_{11}|}{m_1\rho_p\frac{P_{s1}}{{d_{sr}}^e}}} \tag{6.18}$$

thus, we can get the second-moment expression for $\hat{g_1}$, which can be defined as

$$E\left(|\hat{g_1}|^2\right) \approx \frac{4\theta^4}{2\theta^2 + \frac{|N_{11}|}{m_1 \rho_p \frac{P_{s1}}{{d_{sr}}^e}}} + E\left\{\frac{|N_{12}||DT{d_{rd}}^e||\frac{P_{s1}}{{d_{sr}}^e}|\hat{h_1}|^2 + N_{11}|}{[\eta\frac{P_{s1}}{{d_{sr}}^e}|\hat{h_1}|^2|1-\rho_p|m_1T + P_{e1}]m_1}\right\} = \frac{1}{\lambda_{12}}. \tag{6.19}$$

Assumed $|\hat{h_1}|^2 = x$, the complex expression can be simplified as

$$E\left\{\frac{|N_{12}||DT{d_{rd}}^e||\frac{P_{s1}}{{d_{sr}}^e}|\hat{h_1}|^2 + N_{11}|}{[\eta\frac{P_{s1}}{{d_{sr}}^e}|\hat{h_1}|^2|1-\rho_p|m_1T + P_{e1}]m_1}\right\} = \frac{N_{12}|DT{d_{rd}}^e|\lambda_{11}}{m_1}[\frac{\frac{P_{s1}}{{d_{sr}}^e}}{\eta\frac{P_{s1}}{{d_{sr}}^e}|1-\rho_p|m_1T}\frac{1}{\lambda_{11}}$$
$$+\frac{N_{11}\eta\frac{P_{s1}}{{d_{sr}}^e}|1-\rho_p|m_1T - \frac{P_{s1}}{{d_{sr}}^e}P_{e1}}{(\eta\frac{P_{s1}}{{d_{sr}}^e}|1-\rho_p|m_1T)^2}(-e^{\lambda_{11}\frac{\eta\frac{P_{s1}}{{d_{sr}}^e}|1-\rho_p|m_1TP_{e1}}{(\eta\frac{P_{s1}}{{d_{sr}}^e}|1-\rho_p|m_1T)^2}}Ei(-\lambda_{11}\frac{\eta\frac{P_{s1}}{{d_{sr}}^e}|1-\rho_p|m_1TP_{e1}}{(\eta\frac{P_{s1}}{{d_{sr}}^e}|1-\rho_p|m_1T)^2}))] \tag{6.20}$$

where $E[\frac{N_{11}}{|\hat{h_1}|^2}] = N_{11} \times \int_0^\infty \frac{1}{x}\lambda_{11}e^{-\lambda_{11}x}dx = -\frac{N_{11}}{m_{11}\rho_p P_{s1}}Ei(0)$ has been used. The ${\hat{g_1}}^2$ can be approximated as an exponential random variable, when a small $\hat{g_1}$ has been set up. Therefore, the complex exponential variable with scale parameter can be expressed as

$$\lambda_{12} = \frac{1}{A_e}e^{-\lambda_{sd}x} \tag{6.21}$$

where $A_e = \frac{4\theta^4}{2\theta^2+\frac{|N_{11}|}{m_1\rho_p\frac{P_{s1}}{{d_{sr}}^e}}} + \frac{N_{12}|DT{d_{rd}}^e|\lambda_{11}}{m_1}[\frac{\frac{P_{s1}}{{d_{sr}}^e}}{\eta\frac{P_{s1}}{{d_{sr}}^e}|1-\rho_p|m_1T}\frac{1}{\lambda_{11}} +$
$\frac{N_{11}\eta\frac{P_{s1}}{{d_{sr}}^e}|1-\rho_p|m_1T-\frac{P_{s1}}{{d_{sr}}^e}P_{e1}}{(\eta\frac{P_{s1}}{{d_{sr}}^e}|1-\rho_p|m_1T)^2}(-e^{\lambda_{11}\frac{\eta\frac{P_{s1}}{{d_{sr}}^e}|1-\rho_p|m_1TP_{e1}}{(\eta\frac{P_{s1}}{{d_{sr}}^e}|1-\rho_p|m_1T)^2}}Ei(-\lambda_{11}\frac{\eta\frac{P_{s1}}{{d_{sr}}^e}|1-\rho_p|m_1TP_{e1}}{(\eta\frac{P_{s1}}{{d_{sr}}^e}|1-\rho_p|m_1T)^2}))]$.

Similarly, the PDF and CDF expressions can be performed as $f_{|\hat{g_1}|^2}(x) = \lambda_{12}e^{-\lambda_{12}x}$ and $F_{|\hat{g_1}|^2}(x) = 1 - e^{-\lambda_{12}x}$, respectively.

For the direct link, lets $\lambda_{sd} = \frac{1}{2\theta^2+\frac{N_{sd}}{D\frac{P_{s1}}{{d_{sd}}^e}}}$. The PDF can be calculated as

$$f_{|\hat{h_{sd}}|^2}(x) = \lambda_{sd}e^{-\lambda_{sd}x} \tag{6.22}$$

and its CDF can be calculated as

$$F_{|\hat{h_{sd}}|^2}(x) = 1 - e^{-\lambda_{sd}x}. \tag{6.23}$$

By using these expressions above, the CDF expression of γ_{1end} can be ex-

panded from (6.8) as

$$F_{\gamma_{1end}}(x) = P_{r1}\{\gamma_{1end} < \gamma_{1th}\} = I_{12} + I_{11} \tag{6.24}$$

with the first part as

$$I_{11} = P_{r1}\{P_{s1}|\hat{h_1}|^2 - \frac{\gamma_{1th}N_{11}}{m_1\rho_p} - \gamma_{1th}N_{11} < 0\} \tag{6.25}$$

and the second part as

$$I_{12} = P_{r1}\{|\hat{g_1}|^2 < \frac{A_f}{\left[(\eta\frac{P_{s1}}{{d_{sr}}^e}|\hat{h_1}|^2(1-\rho_p)m_1T + P_{e1})\rho_p{m_1}^2\right]\left(\frac{P_{s1}}{{d_{sr}}^e}|\hat{h_1}|^2 - \frac{\gamma_{1th}N_{11}}{m_1\rho_p} - \gamma_{1th}N_{11}\right)} \\ |\left(\frac{P_{s1}}{{d_{sr}}^e}|\hat{h_1}|^2 - \frac{\gamma_{1th}N_{11}}{m_1\rho_p} - \gamma_{1th}N_{11}\right) > 0\} \tag{6.26}$$

where $A_f = \gamma_{1th}N_{12}N_{11}DT{d_{rd}}^e\left(\frac{P_{s1}}{{d_{sr}}^e}|\hat{h_1}|^2 + N_{11}\right) + m_1\gamma_{1th}\rho_pN_{12}N_{11}DT{d_{rd}}^e\left(\frac{P_{s1}}{{d_{sr}}^e}|\hat{h_1}|^2 + N_{11}\right) + \gamma_{1th}{m_1}^2\rho_pN_{12}DT{d_{rd}}^e\left(\frac{P_{s1}}{{d_{sr}}^e}|\hat{h_1}|^2 + N_{11}\right) + m_1\rho_p\gamma_{1th}\frac{P_{s1}}{{d_{sr}}^e}|\hat{h_1}|^2N_{12}DT{d_{rd}}^e\left(\frac{P_{s1}}{{d_{sr}}^e}|\hat{h_1}|^2 + N_{11}\right)$.

By using the CDF of $|\hat{h_1}|^2$ in (5.48), one has

$$I_{11} = \int_0^{\frac{\gamma_{1th}N_{11}}{m_1\rho_p\frac{P_{s1}}{{d_{sr}}^e}} + \frac{\gamma_{1th}N_{11}}{\frac{P_{s1}}{{d_{sr}}^e}}} f_{|\hat{h_1}|^2}(|\hat{h_1}|^2)dy = F_{|\hat{h_1}|^2}(|\hat{h_1}|^2)dy = 1 - e^{-\frac{\frac{\gamma_{1th}N_{11}}{m_1\rho_p\frac{P_{s1}}{{d_{sr}}^e}} + \frac{\gamma_{1th}N_{11}}{\frac{P_{s1}}{{d_{sr}}^e}}}{2\theta^2 + |\frac{N_{11}}{m_1\rho_p\frac{P_{s1}}{{d_{sr}}^e}}|}} \tag{6.27}$$

Assuming $t = P_{s1}|\hat{h_1}|^2 - \frac{\gamma_{1th}N_{11}}{m_1\rho_p} - \gamma_{1th}N_{11}$ and $P_{s1}|\hat{h_1}|^2 = t + \frac{\gamma_{1th}N_{11}}{m_1\rho_p} + \gamma_{1th}N_{11}$, one has

$$I_{12} = \frac{A_g}{\left[(\eta(1-\rho_p)m_1T\left(t + \frac{\gamma_{1th}N_{11}}{m_1\rho_p} + \gamma_{1th}N_{11}\right) + P_{e1})\rho_p{m_1}^2\right]t} \tag{6.28}$$

where $A_g = [\gamma_{1th}N_{12}N_{11}DT{d_{rd}}^e + m_1\rho_p\gamma_{1th}N_{12}N_{11}DT{d_{rd}}^e + \gamma_{1th}m_1m_1\rho_pN_{12}DT{d_{rd}}^e + m_1\gamma_{1th}N_{12}\rho_pDT{d_{rd}}^e(t + \frac{\gamma_{1th}N_{11}}{m_1\rho_p} + \gamma_{1th}N_{11})](t + \frac{\gamma_{1th}N_{11}}{m_1\rho_P} + \gamma_{1th}N_{11} + N_{11})$.

To simplify by substituting functions which can be written as

$$\frac{[a_1+b_1(t+c_1)](t+c_1)}{d_1t(t+c_1)+g_1t}=\frac{b_1}{d_1}+\frac{(a_1+2b_1c_1)d_1-b_1(d_1c_1+g_1)}{d_1^2t+d_1(d_1c_1+g_1)}+\frac{\frac{ac+b_1c_1^2}{d_1c_1+g_1}}{\frac{d_1}{d_1c_1+g_1}t^2+t} \tag{6.29}$$

where $a_1 = \gamma_{1th}N_{12}N_{11}DT + m_1\rho_p\gamma_{1th}N_{12}N_{11}DT + \gamma_{1th}m_1m_1\rho_pN_{12}DT; b_1 = m_1\gamma_{1th}N_{12}\rho_pDT; c_1 = \frac{\gamma_{1th}N_{11}}{m_1\rho_p} + \gamma_{1th}N_{11}; d_1 = \rho_p{m_1}^2\eta(1-\rho_p)m_1T; g_1 = \rho_p{m_1}^2P_{e1}$.

Following the same measurement procedures, from equation (6.7) with the CDF of $|\hat{g_1}|^2$, the second part can be written as

$$\begin{aligned}
I_{12} &= \int_{P_{s1}|\hat{h_1}|^2-\frac{\gamma_{1th}N_{11}}{m_1\rho_p}-\gamma_{1th}N_{11}}^{\infty} F_{|\hat{g_1}|^2}[\frac{b_1}{d_1}\frac{(a_1+2b_1c_1)d_1-b_1(d_1c_1+g_1)}{d_1^2t+d_1(d_1c_1+g_1)} \\
&+ \frac{\frac{ac+b_1c_1^2}{d_1c_1+g_1}}{\frac{d_1}{d_1c_1+g_1}t^2+t}]f_{|\hat{h_1}|^2}(\frac{t}{P_{s1}}+\frac{\gamma_{1th}N_{11}}{m_1\rho_pP_{s1}}+\frac{\gamma_{1th}N_{11}}{P_{s1}})d_1t \\
&= \int_0^{\infty}(1-e^{-\lambda_{12}[\frac{b_1}{d_1}+\frac{(a_1+2b_1c_1)d_1-b_1(d_1c_1+g_1)}{d_1^2t+d_1(d_1c_1+g_1)}+\frac{\frac{ac+b_1c_1^2}{d_1c_1+g_1}}{\frac{d_1}{d_1c_1+g_1}t^2+t}]}) \\
&\times \frac{1}{\left(2\theta^2+|\frac{N_{11}}{m_1\rho_pP_{s1}}|\right)}e^{-\frac{\frac{t}{P_{s1}}+\frac{\gamma_{1th}N_{11}}{m_1\rho_pP_{s1}}+\frac{\gamma_{1th}N_{11}}{P_{s1}}}{2\theta^2+|\frac{N_{11}}{m_1\rho_pP_{s1}}|}}d_1t\frac{1}{P_{s1}} \\
&\int_0^{\infty}\frac{1}{\left(2\theta^2+|\frac{N_{11}}{m_1\rho_pP_{s1}}|\right)}e^{-\frac{\frac{t}{P_{s1}}+\frac{\gamma_{1th}N_{11}}{m_1\rho_pP_{s1}}+\frac{\gamma_{1th}N_{11}}{P_{s1}}}{2\theta^2+|\frac{N_{11}}{m_1\rho_pP_{s1}}|}}d_1t\frac{1}{P_{s1}} \\
&- \frac{1}{\left(2\theta^2+|\frac{N_{11}}{m_1\rho_pP_{s1}}|\right)}e^{-\frac{\gamma_{1th}N_{11}+\gamma_{1th}N_{11}m_1\rho_p}{2\theta^2m_1\rho_pP_{s1}+N_{11}}} \\
&\int_0^{\infty}e^{-t\frac{m_1\rho_p}{2\theta^2m_1\rho_pP_{s1}+N_{11}}}e^{-\lambda_{12}[\frac{b_1}{d_1}+\frac{(a_1+2b_1c_1)d_1-b_1(d_1c_1+g_1)}{d_1^2t+d_1(d_1c_1+g_1)}+\frac{\frac{ac+b_1c_1^2}{d_1c_1+g_1}}{\frac{d_1}{d_1c_1+g_1}t^2+t}]}d_1t\frac{1}{P_{s1}}.
\end{aligned} \tag{6.30}$$

The unexpected issue was that the integral could not be simplified or changed in form, which leaves us the only resort to use curve fitting to substitute original expression. In the remaining, we have simulated the integral appearance with a fixed value of h, g.

First of all, the function was separated into two exponents

$$e^{-\lambda_{12}[\frac{b_1}{d_1}+\frac{(a_1+2b_1c_1)d_1-b_1(d_1c_1+g_1)}{d_1^2t+d_1(d_1c_1+g_1)}+\frac{\frac{ac+b_1c_1^2}{d_1c_1+g_1}}{\frac{d_1}{d_1c_1+g_1}t^2+t}]}$$
$$= e^{-\frac{\lambda_{12}b}{d_1}} \times \left[e^{-\frac{1}{t+\frac{d_1c_1+g_1}{d_1}}}\right]^{\frac{\lambda_{12}(a_1+2b_1c_1)}{d_1}-\frac{\lambda_{12}b_1(d_1c_1+g_1)}{d_1^2}} \times \left[e^{-\frac{1}{\frac{d_1}{d_1c_1+g_1}t^2+t}}\right]^{\lambda_{12}\frac{ac+b_1c_1^2}{d_1c_1+g_1}}. \tag{6.31}$$

After curve fitting, the results can be derived as

$$e^{-\frac{1}{t+\frac{d_1c_1+g_1}{d_1}}} => [(0.17{m_1}^{-0.83}-0.51)x^{0.15{m_1}^{-0.86}-0.6}e^{(-0.0052{m_1}^{-0.66}-0.04)x}+0.99]$$
$$e^{-\frac{1}{\frac{d_1}{d_1c_1+g_1}t^2+t}} => [(-0.18{m_1}^{-0.72}-0.27)x^{0.33{m_1}^{-0.97}-1.68}e^{(-0.0052{m_1}^{-0.84}+0.03)x}+1]. \tag{6.32}$$

The outage probability can be written as

$$P_{r1} = 1 - \frac{1}{\frac{P_{s1}}{{d_{sr}}^e}\left(2\theta^2+|\frac{N_{11}}{m_1\rho_p\frac{P_{s1}}{{d_{sr}}^e}}|\right)}e^{-\frac{\gamma_{1th}N_{11}+\gamma_{1th}N_{11}m_1\rho_p}{2\theta^2m_1\rho_p\frac{P_{s1}}{{d_{sr}}^e}+N_{11}}}$$
$$\sum_{P_{e1}=0}^{\infty}(0.17{m_1}^{-0.83}-0.51)^{\alpha_1}\times(-0.178{m_1}^{-0.7289}-0.27)^{\alpha_2}e^{-\lambda_{12}\frac{m_1\gamma_{1th}N_{12}\rho_pDT{d_{rd}}^e}{\rho_p{m_1}^2\eta(1-\rho_p)m_1T}}$$
$$\frac{\Gamma([(0.15{m_1}^{-0.86}-0.6)\alpha_1+(0.33{m_1}^{-0.97}-1.68)\alpha_2]+1)}{[(0.00516{m_1}^{-0.66}+0.041)\alpha_1+(0.00518{m_1}^{-0.838}-0.0296)\alpha_2+\frac{m_1\rho_p}{2\theta^2m_1\rho_p\frac{P_{s1}}{{d_{sr}}^e}+N_{11}}]^{\alpha_3}}$$
$$\frac{e^{-\lambda}\lambda^{P_{e1}}}{P_{e1}!} \tag{6.33}$$

where $\alpha_1 = \lambda_{12}(\frac{(\gamma_{1th}N_{12}N_{11}DT+m_1\rho_p\gamma_{1th}N_{12}N_{11}DT+\gamma_{1th}m_1m_1\rho_pN_{12}DT}{\rho_p{m_1}^2\eta(1-\rho_p)m_1T} - \frac{m_1\gamma_{1th}N_{12}\rho_pDT((\rho_p{m_1}^2\eta(1-\rho_p)m_1T)(\frac{\gamma_{1th}N_{11}}{m_1\rho_p}+\gamma_{1th}N_{11})+\rho_p{m_1}^2P_{e1})}{(\rho_p{m_1}^2\eta(1-\rho_p)m_1T)^2} + \frac{2(m_1\gamma_{1th}N_{12}\rho_pDT)(\frac{\gamma_{1th}N_{11}}{m_1\rho_p}+\gamma_{1th}N_{11})}{(\rho_p{m_1}^2\eta(1-\rho_p)m_1T)^2})$,
$\alpha_2 = \lambda_{12}(\frac{(\gamma_{1th}N_{12}N_{11}DT+m_1\rho_p\gamma_{1th}N_{12}N_{11}DT+\gamma_{1th}m_1m_1\rho_pN_{12}DT)(\frac{\gamma_{1th}N_{11}}{m_1\rho_p}+\gamma_{1th}N_{11})}{(\rho_p{m_1}^2\eta(1-\rho_p)m_1T)(\frac{\gamma_{1th}N_{11}}{m_1\rho_p}+\gamma_{1th}N_{11})+\rho_p{m_1}^2P_{e1}} + \frac{(m_1\gamma_{1th}N_{12}\rho_pDT)(\frac{\gamma_{1th}N_{11}}{m_1\rho_p}+\gamma_{1th}N_{11})^2}{(\rho_p{m_1}^2\eta(1-\rho_p)m_1T)(\frac{\gamma_{1th}N_{11}}{m_1\rho_p}+\gamma_{1th}N_{11})+\rho_p{m_1}^2P_{e1}})$ and $\alpha_3 = [(0.15{m_1}^{-0.86}-0.6)\alpha_1 + (0.33{m_1}^{-0.97}-1.68)\alpha_2]+1$.

Then, the achievable rate without direct link can be derived as

$$AR_1 = [1-F_{\gamma_{1end}}(\gamma_{01})]\times\frac{D-m_{11}}{D} \tag{6.34}$$

the achievable rate with a direct link can be derived as

$$AR_{1d} = [1 - F_{\gamma_{sd}}(\gamma_{01})F_{\gamma_{1end}}(\gamma_{01})] \times \frac{D - m_{11}}{D}. \tag{6.35}$$

Moreover, the BER without direct link can be calculated as

$$\begin{aligned} BER_1 &= \int_0^\infty \frac{1}{2} erfc(\sqrt{x}) * dF_{\gamma_{1end}}(x) \\ &= \frac{1}{2}\int_0^\infty \frac{e^{-x}}{\sqrt{x * \pi}} F_{\gamma_{1end}}(x)dx \end{aligned} \tag{6.36}$$

and the BER with direct link can be calculated as

$$\begin{aligned} BER_{1d} &= \int_0^\infty \frac{1}{2} erfc(\sqrt{x}) * d(F_{\gamma_{1end}}(x)F_{\gamma_{sd}}(x)) \\ &= \frac{1}{2}\int_0^\infty \frac{e^{-x}}{\sqrt{x * \pi}} F_{\gamma_{1end}}(x)F_{\gamma_{sd}}(x)dx \end{aligned} \tag{6.37}$$

where $erfc(x)$ is the complementary error function.

6.4.2 ADTPS CSI estimation

Exactly the same as ACEPS, in order to derive the CDF, the $Var(\varepsilon_{21})$ and $Var(\varepsilon_{22})$ must calculated before then. The ε_{21} is (5.63), and the $Var(\varepsilon_{21})$ is (5.64). However, the ε_{22} is different, which can be expressed as

$$\varepsilon_{22} = \frac{\Sigma_{i_{22}=1}^{m_2} n_{22}[i_{22}]}{m_2 \hat{a}_{2var}\sqrt{\frac{\hat{P_{r2}}}{{d_{rd}}^e}}} \tag{6.38}$$

and with

$$\begin{aligned} |\varepsilon_{22}|^2 &= \frac{|\Sigma_{i_{22}=1}^{m_2} n_{22}[i_{22}]|^2}{{m_2}^2 \hat{a}_{2var}^2 \frac{\hat{P_{r2}}}{{d_{rd}}^e}} \\ &= \Sigma_{i_{22}=1}^{m_2}\left(\frac{{n_{22}[i_{22}]}^2 \left(\frac{P_{s2}}{{d_{sr}}^e}|\hat{h_2}|^2 + N_{21}\right) DT{d_{rd}}^e}{[\eta \frac{P_{s2}}{{d_{sr}}^e}|\hat{h_2}|^2 (1-\rho_d)(D-m_2)T + P_{e2}]{m_2}^2}\right) \\ &+ \Sigma_{k_2=1}^{m_2}\Sigma_{j_{22}=1 k_2 \neq j_{22}}^{m_2}\left(\frac{n_{22}[j_{22}] \times n_{22}[k_2]\left(\frac{P_{s2}}{{d_{sr}}^e}|\hat{h_2}|^2 + N_{21}\right) DT{d_{rd}}^e}{[\eta \frac{P_{s2}}{{d_{sr}}^e}|\hat{h_2}|^2 (1-\rho_d)(D-m_2)T + P_{e2}]{m_2}^2}\right). \end{aligned} \tag{6.39}$$

According to the expression above, the variance of ε_{22} is

$$Var(\varepsilon_{22}) = \frac{N_{22}\left(\frac{P_{s2}}{{d_{sr}}^{e}}|\hat{h_2}|^2 + N_{21}\right) DT{d_{rd}}^{e}}{[\eta\frac{P_{s2}}{{d_{sr}}^{e}}|\hat{h_2}|^2(1-\rho_d)(D-m_2)T + P_{e2}]m_2}. \tag{6.40}$$

By using (5.64) and (6.40) in (6.10), the end-to-end SNR function can be defined as

$$\gamma_{2end} = \frac{|\hat{h_2}|^2|g_2|^2\frac{P_{s2}}{{d_{sr}}^{e}}\rho_d}{A_h} \tag{6.41}$$

where $A_h = \frac{\rho_d|g_2|^2N_{21}}{m_2} + |g_2|^2N_{21} + \frac{N_{22}\rho_d\frac{P_{s2}}{{d_{sr}}^{e}}|\hat{h_2}|^2\left(\frac{P_{s2}}{{d_{sr}}^{e}}|\hat{h_2}|^2+N_{21}\right)DT{d_{rd}}^{e}}{[\eta|\hat{h_2}|^2(1-\rho_d)(D-m_2)T+P_{e2}]m_2} + \frac{N_{21}N_{22}\rho_d\left(\frac{P_{s2}}{{d_{sr}}^{e}}|\hat{h_2}|^2+N_{21}\right)DT{d_{rd}}^{e}}{{m_2}^2[\eta\frac{P_{s2}}{{d_{sr}}^{e}}|\hat{h_2}|^2(1-\rho_d)(D-m_2)T+P_{e2}]} + \frac{N_{22}N_{21}\left(\frac{P_{s2}}{{d_{sr}}^{e}}|\hat{h_2}|^2+N_{21}\right)DT{d_{rd}}^{e}}{[\eta\frac{P_{s2}}{{d_{sr}}^{e}}|\hat{h_2}|^2(1-\rho_d)(D-m_2)T+P_{e2}]m_2} + \frac{N_{22}\left(\frac{P_{s2}}{{d_{sr}}^{e}}|\hat{h_2}|^2+N_{21}\right)DT{d_{rd}}^{e}}{[\eta\frac{P_{s2}}{{d_{sr}}^{e}}|\hat{h_2}|^2(1-\rho_d)(D-m_2)T+P_{e2}]}$. Moreover, the distributions of $\hat{h_2}$ and $\hat{g_2}$ are required.

Therefore, the distribution of $\hat{h_2}$ and $\hat{g_3}$ are needed. The second-moment expression of $\hat{h_2}$ can be expressed as

$$\begin{aligned} E(|\hat{h_2}|^2) &= E|h + \frac{\Sigma_{i_{21}=1}^{m_2} n_{21}[i_{21}]}{m_2\sqrt{\frac{P_{s2}}{{d_{sr}}^{e}}}}|^2 \\ &= E\left(|\hat{h_2}|^2 + |\frac{\Sigma_{i_{21}=1}^{m_2} n_{21}[i_{21}]}{m_2\sqrt{\frac{P_{s2}}{{d_{sr}}^{e}}}}|^2 + 2Re\{h_2 \times \frac{\Sigma_{i_{21}=1}^{m_2} n_{21}[i_{21}]^*}{m_2\sqrt{\frac{P_{s2}}{{d_{sr}}^{e}}}}\}\right) \\ &= E(|\hat{h_2}|^2) + |\frac{N_{21}}{m_2\frac{P_{s2}}{{d_{sr}}^{e}}}| \end{aligned} \tag{6.42}$$

where $2Re\{h_2 \times \frac{\Sigma_{i_{21}=1}^{\alpha D} n_{21}[i_{21}]}{\alpha D^2\sqrt{\frac{P_{s2}}{{d_{sr}}^{e}}}}\} = 0$.

Thus, the exponential random variable with scale parameter is

$$\lambda_{21} = \frac{1}{2\theta^2 + |\frac{N_{21}}{m_2\frac{P_{s2}}{{d_{sr}}^{e}}}|}. \tag{6.43}$$

The similarity probability density function (PDF) and cumulative density

function (CDF) are described as $pdf2 = \frac{1}{2\theta^2+|\frac{N_{21}}{m_2\frac{P_{s2}}{d_{sr}{}^e}}|} e^{-\frac{1}{2\theta^2+|\frac{N_{21}}{m_2\frac{P_{s2}}{d_{sr}{}^e}}|}x}$ and $cdf2 = 1 - e^{-\frac{1}{2\theta^2+|\frac{N_{21}}{m_2\frac{P_{s2}}{d_{sr}{}^e}}|}x}$, respectively.

The second-moment expression of $|\hat{g_2}|^2$ can be written as

$$\begin{aligned}
&E(|\hat{g_2}|^2) = Var(|\hat{g_2}|) \\
&= E\left(\frac{|\hat{h_2}|^2}{|\hat{h_2}|^2}|g_2|^2 + |\frac{\Sigma_{i_{22}=1}^{m_2} n_{22}[i_{22}]}{m_2\hat{a}_{2var}\sqrt{\frac{\hat{P_{r2}}}{d_{rd}{}^e}}}|^2 + 2Re\{\frac{|\hat{h_2}|}{|\hat{h_2}|}|g_2| \times |\frac{\Sigma_{i_{22}=1}^{m_2} n_{22}[i_{22}]}{m_2\hat{a}_{2var}\sqrt{\frac{\hat{P_{r2}}}{d_{rd}{}^e}}}|^*\}\right) \\
&= 2\theta^2\frac{|\hat{h_2}|^2}{|\hat{h_2}|^2} + \frac{N_{22}\left(\frac{P_{s2}}{d_{sr}{}^e}|\hat{h_2}|^2 + N_{21}\right)DTd_{rd}{}^e}{[\eta\frac{P_{s2}}{d_{sr}{}^e}|\hat{h_2}|^2(1-\rho_d)(D-m_2)T + P_{e2}]m_2}
\end{aligned} \tag{6.44}$$

where $E(|g_2|^2) = 2\theta^2; E(\Sigma_{i_{22}=1}^{m_2} n_{22}[i_{22}]) = 0; n_{22}[j_{22}]n_{22}[k_2] = 0$ and $Re\{\frac{|\hat{h_2}|}{|\hat{h_2}|}|g_2|(\frac{\Sigma_{i_{22}=1}^{m_2} n_{22}[i_{22}]}{m_2\hat{a}_{2var}\sqrt{\frac{\hat{P_{r2}}}{d_{rd}{}^e}}})\} = 0$, with approximately as

$$2\theta^2 E\left\{\frac{|\hat{h_2}|^2}{|\hat{h_2}|^2}\right\} \approx 2\theta^2\frac{2\theta^2}{2\theta^2 + \frac{|N_{21}|}{m_2\frac{P_{s2}}{d_{sr}{}^e}}} \approx \frac{4\theta^4}{2\theta^2 + \frac{|N_{21}|}{m_2\frac{P_{s2}}{d_{sr}{}^e}}}. \tag{6.45}$$

The second-moment expression for $\hat{g_2}$, which can be defined as

$$E\left(|\hat{g_2}|^2\right) \approx \frac{4\theta^4}{2\theta^2 + \frac{|N_{21}|}{m_2\frac{P_{s2}}{d_{sr}{}^e}}} + E\left\{\frac{N_{22}\left(\frac{P_{s2}}{d_{sr}{}^e}|\hat{h_2}|^2 + N_{21}\right)DTd_{rd}{}^e}{[\eta\frac{P_{s2}}{d_{sr}{}^e}|\hat{h_2}|^2(1-\rho_d)(D-m_2)T + P_{e2}]m_2}\right\} = \frac{1}{\lambda_{22}}. \tag{6.46}$$

Assuming $|\hat{h_2}|^2 = x$, the complex expression can be rewritten as

$$\begin{aligned}
&E\left\{\frac{|N_{22}||DTd_{rd}{}^e||\frac{P_{s2}}{d_{sr}{}^e}|\hat{h_2}|^2 + N_{21}|}{[\eta\frac{P_{s2}}{d_{sr}{}^e}|\hat{h_2}|^2|1-\rho_d|(D-m_2)T + P_{e2}]m_2}\right\} \\
&= \int_0^\infty \frac{|N_{22}||DTd_{rd}{}^e||\frac{P_{s2}}{d_{sr}{}^e}x + N_{21}|}{[\eta\frac{P_{s2}}{d_{sr}{}^e}x|1-\rho_d|(D-m_2)T + P_{e2}]m_2} * f_{|\hat{h_2}|^2}(x)dx \\
&= \frac{N_{22}|DTd_{rd}{}^e|\lambda_{21}}{m_2}[\frac{\frac{P_{s2}}{d_{sr}{}^e}}{\eta\frac{P_{s2}}{d_{sr}{}^e}|1-\rho_d|(D-m_2)T\lambda_{21}} + \frac{N_{21}\eta\frac{P_{s2}}{d_{sr}{}^e}|1-\rho_d|(D-m_2)T - \frac{P_{s2}}{d_{sr}{}^e}P_{e2}}{(\eta\frac{P_{s2}}{d_{sr}{}^e}|1-\rho_d|(D-m_2)T)^2} \\
&(-e^{\lambda_{21}\frac{\eta\frac{P_{s2}}{d_{sr}{}^e}|1-\rho_d|(D-m_2)TP_{e2}}{(\eta\frac{P_{s2}}{d_{sr}{}^e}|1-\rho_d|(D-m_2)T)^2}}Ei(-\lambda_{21}\frac{\eta\frac{P_{s2}}{d_{sr}{}^e}|1-\rho_d|(D-m_2)TP_{e2}}{(\eta\frac{P_{s2}}{d_{sr}{}^e}|1-\rho_d|(D-m_2)T)^2}))]
\end{aligned} \tag{6.47}$$

where $E[\frac{N_{21}}{|\hat{h_2}|^2}] = N_{21} \times \int_0^\infty \frac{1}{x}\lambda_{21}e^{-\lambda_{21}x}dx = -\frac{N_{21}}{m_{21}\rho_p P_{s1}}Ei(0)$ has been used, where $\hat{g_2}^2$ can be approximated as an exponential random variable, when a small $\hat{g_1}$ has been set up.

Therefore, a complex exponential variable with scale parameter is

$$\lambda_{22} = \frac{1}{A_j} \tag{6.48}$$

where $A_j = \frac{4\theta^4}{2\theta^2+\frac{|N_{21}|}{m_2\frac{P_{s2}}{d_{sr}{}^e}}} + \frac{N_{22}|DTd_{rd}{}^e|\lambda_{21}}{m_2}[\frac{\frac{P_{s2}}{d_{sr}{}^e}}{\eta\frac{P_{s2}}{d_{sr}{}^e}|1-\rho_d|(D-m_2)T\lambda_{21}} + \frac{N_{21}\eta\frac{P_{s2}}{d_{sr}{}^e}|1-\rho_d|(D-m_2)T-\frac{P_{s2}}{d_{sr}{}^e}P_{e2}}{(\eta\frac{P_{s2}}{d_{sr}{}^e}|1-\rho_d|(D-m_2)T)^2}(-e^{\lambda_{21}\frac{\eta\frac{P_{s2}}{d_{sr}{}^e}|1-\rho_d|(D-m_2)TP_{e2}}{(\eta\frac{P_{s2}}{d_{sr}{}^e}|1-\rho_d|(D-m_2)T)^2}}Ei(-\lambda_{21}\frac{\eta\frac{P_{s2}}{d_{sr}{}^e}|1-\rho_d|(D-m_2)TP_{e2}}{(\eta\frac{P_{s2}}{d_{sr}{}^e}|1-\rho_d|(D-m_2)T)^2}))]$, with the CDF of γ_{2end} can be derived as (5.71).

It can be separated into two parts as

$$I_{21} = P_{r2}\{\left(\rho_d\frac{P_{s2}}{d_{sr}{}^e}|\hat{h_2}|^2 - \frac{\gamma_{2th}\rho_d N_{21}}{m_2} - \gamma_{2th}N_{21}\right) < 0\} \tag{6.49}$$

and

$$I_{22} = P_{r2}\{|g_2|^2 < \frac{A_k}{\left[(\eta\frac{P_{s2}}{d_{sr}{}^e}|\hat{h_2}|^2(1-\rho_d)(D-m_2)T + P_{e2})m_2{}^2\right]\left(\rho_d\frac{P_{s2}}{d_{sr}{}^e}|\hat{h_2}|^2 - \frac{\gamma_{2th}\rho_d N_{21}}{m_2} - \gamma_{2th}N_{21}\right)} | \left(\rho_d\frac{P_{s2}}{d_{sr}{}^e}|\hat{h_2}|^2 - \frac{\gamma_{2th}\rho_d N_{21}}{m_2} - \gamma_{2th}N_{21}\right) > 0\} \tag{6.50}$$

where $A_k = \gamma_{2th}N_{22}m_2\frac{P_{s2}}{d_{sr}{}^e}|\hat{h_2}|^2\rho_d\left(\frac{P_{s2}}{d_{sr}{}^e}|\hat{h_2}|^2 + N_{21}\right)DTd_{rd}{}^e + \gamma_{2th}N_{21}N_{22}\rho_d\left(\frac{P_{s2}}{d_{sr}{}^e}|\hat{h_2}|^2 + N_{21}\right)DTd_{rd}{}^e + \gamma_{2th}m_2N_{22}N_{21}\left(\frac{P_{s2}}{d_{sr}{}^e}|\hat{h_2}|^2 + N_{21}\right)DTd_{rd}{}^e + \gamma_{2th}N_{22}m_2{}^2\left(\frac{P_{s2}}{d_{sr}{}^e}|\hat{h_2}|^2 + N_{21}\right)DTd_{rd}{}^e$.

By using the CDF of $|\hat{h_2}|^2$ in 5.68, one has

$$I_{21} = P_{r2}\{\rho_d\frac{P_{s2}}{d_{sr}{}^e}|\hat{h_2}|^2 - \frac{\gamma_{2th}\rho_d N_{21}}{m_2} - \gamma_{2th}N_{21} < 0\} = P_{r2}\{|\hat{h_2}|^2 < \frac{\gamma_{2th}N_{21}}{m_2\frac{P_{s2}}{d_{sr}{}^e}} + \frac{\gamma_{2th}N_{21}}{\rho_d\frac{P_{s2}}{d_{sr}{}^e}}\}$$
$$= \int_0^{\frac{\gamma_{2th}N_{21}}{m_2\frac{P_{s2}}{d_{sr}{}^e}}+\frac{\gamma_{2th}N_{21}}{\rho_d\frac{P_{s2}}{d_{sr}{}^e}}} f_{|\hat{h_2}|^2}(y)dy = F_{|\hat{h_2}|^2}(y)dy = 1 - e^{-\frac{\frac{\gamma_{2th}N_{21}}{m_2\frac{P_{s2}}{d_{sr}{}^e}}+\frac{\gamma_{2th}N_{21}}{\rho_d\frac{P_{s2}}{d_{sr}{}^e}}}{2\theta^2+|\frac{N_{21}}{m_2\frac{P_{s2}}{d_{sr}{}^e}}|}}. \tag{6.51}$$

Assuming $\rho_d \frac{P_{s2}}{{d_{sr}}^e} y - \frac{\gamma_{2th}\rho_d N_{21}}{m_2} - \gamma_{2th} N_{21} = t$ and $\rho_d \frac{P_{s2}}{{d_{sr}}^e} y = t + \frac{\gamma_{2th}\rho_d N_{21}}{m_2} + \gamma_{2th} N_{21}$, the expression is substituted as $\frac{[a_2+b_2(t+c_2\rho_d)](\frac{t}{\rho_d}+c_2)}{d_2 t(\frac{t}{\rho_d}+c_2)+g_2 t}$, where $a_2 = \gamma_{2th}N_{21}N_{22}\rho_d DT{d_{rd}}^e + \gamma_{2th}{m_2}^2 N_{22}N_{21}DT{d_{rd}}^e + \gamma_{2th}N_{22}{m_2}^2 DT{d_{rd}}^e; b_2 = \gamma_{2th}N_{22}m_2 DT{d_{rd}}^e; c_2 = \frac{\gamma_{2th}N_{21}}{m_2} + \frac{\gamma_{2th}N_{21}}{\rho_d} + N_{21}; d_2 = {m_2}^2\eta(1-\rho_d)(D-m_2)T; g_2 = P_{e2}{m_2}^2$.

Thus, one has

$$
\begin{aligned}
I_{22} =& \int_{\frac{\gamma_{2th}N_{21}}{m_2\rho_d\frac{P_{s2}}{{d_{sr}}^e}}+\frac{\gamma_{2th}N_{21}}{\frac{P_{s2}}{{d_{sr}}^e}\rho_d}}^{\infty} F_{|\hat{g_2}|^2}[\frac{b_2}{d_2} + \frac{(\frac{a_2}{\rho_d}+2b_2c_2)\frac{d_2}{\rho_d} - \frac{b_2}{\rho_d}(d_2c_2+g_2)}{\frac{{d_2}^2}{{\rho_d}^2}t + \frac{d_2}{\rho_d}(d_2c_2+g_2)} + \frac{\frac{a_2c_2+b_2c_2^2\rho_d}{d_2c_2+g_2}}{\frac{d_2}{(d_2c_2+g_2)\rho_d}t^2+t}] \\
& f_{|\hat{h_2}|^2}(\frac{t}{\frac{P_{s2}}{{d_{sr}}^e}} + \frac{\gamma_{2th}N_{21}}{m_2\rho_d\frac{P_{s2}}{{d_{sr}}^e}} + \frac{\gamma_{2th}N_{21}}{\frac{P_{s2}}{{d_{sr}}^e}\rho_d})d_2t \\
=& \int_0^{\infty}(1 - e^{-\lambda_{22}[\frac{b_2}{d_2}+\frac{(\frac{a_2}{\rho_d}+2b_2c_2)\frac{d_2}{\rho_d}-\frac{b_2}{\rho_d}(d_2c_2+g_2)}{\frac{{d_2}^2}{{\rho_d}^2}t+\frac{d_2}{\rho_d}(d_2c_2+g_2)}+\frac{\frac{a_2c_2+b_2c_2^2\rho_d}{d_2c_2+g_2}}{\frac{d}{(d_2c_2+g_2)\rho_d}t^2+t}]}) \\
& \times \frac{1}{\left(2\theta^2 + |\frac{N_{21}}{m_2\frac{P_{s2}}{{d_{sr}}^e}}|\right)} e^{-\frac{\frac{t}{\frac{P_{s2}}{{d_{sr}}^e}\rho_d}+\frac{\gamma_{2th}N_{21}}{m_2\frac{P_{s2}}{{d_{sr}}^e}}+\frac{\gamma_{2th}N_{21}}{\frac{P_{s2}}{{d_{sr}}^e}\rho_d}}{2\theta^2+|\frac{N_{21}}{m_2\frac{P_{s2}}{{d_{sr}}^e}}|}} d_2t\frac{1}{\frac{P_{s2}}{{d_{sr}}^e}} \\
& \int_0^{\infty} \frac{1}{\left(2\theta^2 + |\frac{N_{21}}{m_2\frac{P_{s2}}{{d_{sr}}^e}}|\right)} e^{-\frac{\frac{t}{\frac{P_{s2}}{{d_{sr}}^e}\rho_d}+\frac{\gamma_{2th}N_{21}}{m_2\frac{P_{s2}}{{d_{sr}}^e}}+\frac{\gamma_{2th}N_{21}}{\rho_d\frac{P_{s2}}{{d_{sr}}^e}}}{2\theta^2+|\frac{N_{21}}{m_2\frac{P_{s2}}{{d_{sr}}^e}}|}} d_2t\frac{1}{\frac{P_{s2}}{{d_{sr}}^e}} \\
& - \frac{1}{\left(2\theta^2 + |\frac{N_{21}}{m_2\frac{P_{s2}}{{d_{sr}}^e}}|\right)} e^{-\frac{\gamma_{2th}N_{21}\rho_d+\gamma_{2th}N_{21}m_2}{2\theta^2 m_2\rho_d\frac{P_{s2}}{{d_{sr}}^e}+\rho_d N_{21}}} \\
& \int_0^{\infty} e^{-\lambda_{22}[\frac{b_2}{d_2}+\frac{(\frac{a_2}{\rho_d}+2b_2c_2)\frac{d_2}{\rho_d}-\frac{b_2}{\rho_d}(d_2c_2+g_2)}{\frac{{d_2}^2}{{\rho_d}^2}t+\frac{d_2}{\rho_d}(d_2c_2+g_2)}+\frac{\frac{a_2c_2+b_2c_2^2\rho_d}{d_2c_2+g_2}}{\frac{d}{(d_2c_2+g_2)\rho_d}t^2+t}-\frac{tm_2}{2\theta^2 m_2\rho_d\frac{P_{s2}}{{d_{sr}}^e}+\rho_d N_{21}}]} d_2t\frac{1}{\frac{P_{s2}}{{d_{sr}}^e}}.
\end{aligned}
\tag{6.52}
$$

Through curve fitting, we can get the approximate expression as

$$
\begin{aligned}
& e^{-\frac{1}{t+\frac{\rho_d(d_2c_2+g_2)}{d}}} => [(0.053{m_2}^{-0.95} - 0.5)x^{0.45{m_2}^{-0.96}-0.6}e^{(\frac{-0.041m_2-0.0097}{m_2+0.18})x} + 1] \\
& e^{-\frac{1}{\frac{d_2}{(d_2c_2+g_2)\rho_{d_2}}t^2+t}} => [(-0.079{m_2}^{-0.91} - 0.31)x^{0.15{m_2}^{-0.89}-1.47}e^{(-0.02{m_2}^{-0.81}+0.089)x} + 1].
\end{aligned}
\tag{6.53}
$$

Finally, the outage probability function can be written as

$$P_{r2} = 1 + (\rho_d - 1) * e^{-\frac{\gamma_{2th}N_{21}\rho_d + \gamma_{2th}N_{21}m_2}{2\theta^2 m_2 \rho_d \frac{P_{s2}}{{d_{sr}}^e} + \rho_d N_{21}}} - \frac{1}{\frac{P_{s2}}{{d_{sr}}^e}\left(2\theta^2 + |\frac{N_{21}}{m_2 \frac{P_{s2}}{{d_{sr}}^e}}|\right)} e^{-\frac{\gamma_{2th}N_{21}\rho_d + \gamma_{2th}N_{21}m_2}{2\theta^2 m_2 \rho_d \frac{P_{s2}}{{d_{sr}}^e} + \rho_d N_{21}}}$$

$$\sum_{P_{e2}=0}^{\infty} (0.05254{m_2}^{-0.952} - 0.5023)^{\alpha_3} \times (-0.07916{m_2}^{-0.9075} - 0.3097)^{\alpha_4} e^{-\lambda_{12}\frac{\gamma_{2th}N_{22}m_2 DT{d_{rd}}^e}{{m_2}^2\eta(1-\rho_d)(D-m_2)T}}$$

$$\frac{\Gamma((0.4533{m_2}^{-0.9616} - 0.6022)\alpha_3 + (0.1469{m_2}^{-0.8948} - 1.472)\alpha_4 + 1)}{A_l} \frac{e^{\lambda}\lambda^{P_{e2}}}{P_{e2}!} \tag{6.54}$$

where $\alpha_3 = \lambda_{22}(\frac{\gamma_{2th}N_{21}N_{22}\rho_d DT{d_{rd}}^e + \gamma_{2th}m_2 N_{22}N_{21}DT{d_{rd}}^e + \gamma_{2th}N_{22}{m_2}^2 DT{d_{rd}}^e}{{m_2}^2\eta(1-\rho_d)(D-m_2)T} + \frac{2\rho_d\gamma_{2th}N_{22}m_2 DT{d_{rd}}^e(\frac{\gamma_{2th}N_{21}}{m_2} + \frac{\gamma_{2th}N_{21}}{\rho_d} + N_{21})}{{m_2}^2\eta(1-\rho_d)(D-m_2)T} - \rho_d\gamma_{2th}N_{22}m_2 DT{d_{rd}}^e \frac{{m_2}^2\eta(1-\rho_d)(D-m_2)T(\frac{\gamma_{2th}N_{21}}{m_2} + \frac{\gamma_{2th}N_{21}}{\rho_d} + N_{21}) + P_{e2}{m_2}^2}{({m_2}^2\eta(1-\rho_d)(D-m_2)T)^2})$, $\alpha_4 = \lambda_{22}\frac{(\gamma_{2th}N_{21}N_{22}\rho_d DT{d_{rd}}^e + \gamma_{2th}m_2N_{22}N_{21}DT{d_{rd}}^e + \gamma_{2th}N_{22}{m_2}^2 DT{d_{rd}}^e)(\frac{\gamma_{2th}N_{21}}{m_2} + \frac{\gamma_{2th}N_{21}}{\rho_d} + N_{21})}{{m_2}^2\eta(1-\rho_d)(D-m_2)T(\frac{\gamma_{2th}N_{21}}{m_2} + \frac{\gamma_{2th}N_{21}}{\rho_d} + N_{21}) + P_{e2}{m_2}^2} + \lambda_{22}\frac{\rho_d\gamma_{2th}N_{22}m_2 DT{d_{rd}}^e(\frac{\gamma_{2th}N_{21}}{m_2} + \frac{\gamma_{2th}N_{21}}{\rho_d} + N_{21})^2}{{m_2}^2\eta(1-\rho_d)(D-m_2)T(\frac{\gamma_{2th}N_{21}}{m_2} + \frac{\gamma_{2th}N_{21}}{\rho_d} + N_{21}) + P_{e2}{m_2}^2}$ and $A_l = [(\frac{0.041m_2 + 0.0097}{m_2 + 0.18})\alpha_3 + (0.02{m_2}^{-0.82} - 0.089)\alpha_4 + \frac{m_2}{2\theta^2 m_2\rho_d\frac{P_{s2}}{{d_{sr}}^e} + \rho_d N_{21}}]^{\alpha_{41}}$ and $\alpha_{41} = (0.45{m_2}^{-0.96} - 0.6)\alpha_3 + (0.15{m_2}^{-0.9} - 1.472)\alpha_4 + 1$. Thus, the achievable rate without direct link can be derived as

$$AR_2 = [1 - F_{\gamma_{2end}}(\gamma_{02})] \times (\frac{D - m_{21}}{D}) \tag{6.55}$$

and the achievable rate with a direct link can be derived as

$$AR_{2d} = [1 - F_{\gamma_{2end}}(\gamma_{02})F_{\gamma_{sd}}(\gamma_{02})] \times (\frac{D - m_{21}}{D}). \tag{6.56}$$

The BER without direct link can be calculated as

$$BER_2 = \frac{1}{2}\int_0^{\infty} \frac{e^{-x}}{\sqrt{x * \pi}} F_{\gamma_{2end}}(x)dx \tag{6.57}$$

and the BER with direct link can be calculated as

$$BER_2 = \frac{1}{2}\int_0^{\infty} \frac{e^{-x}}{\sqrt{x * \pi}} F_{\gamma_{2end}}(x)F_{\gamma_{sd}}(x)dx. \tag{6.58}$$

6.4.3 ACPS CSI estimation

Similarly, the $Var(\varepsilon_{31})$ and $Var(\varepsilon_{32})$ need to achieve first, with the same methods, the variances of ε_{31} can be calculated as (5.77).

Unlike ε_{31}, with the additional ambient RF energy, the variances of ε_{32} can be written as

$$Var(\varepsilon_{32}) = \frac{N_{32}DTd_{rd}{}^{e}\left(\frac{P_{s3}}{d_{sr}{}^{e}}\left|\hat{h_3}\right|^2 + N_{31}\right)}{[\eta\frac{P_{s3}}{d_{sr}{}^{e}}\left|\hat{h_3}\right|^2(1-\rho_c)DTd_{rd}{}^{e} + P_{e3}]m_3}. \tag{6.59}$$

By using (5.77) and (6.59) into (6.12), the end-to-end SNR expression can be derived as

$$\gamma_{3end} = \frac{|\hat{g_3}|^2\left|\hat{h_3}\right|^2\frac{P_{s3}}{d_{sr}{}^{e}}}{A_m} \tag{6.60}$$

, where $A_m = \frac{N_{31}|\hat{g_3}|^2}{m_3\rho_c} + |\hat{g_3}|^2N_{31} + \frac{N_{32}N_{31}DTd_{rd}{}^{e}\left(\frac{P_{s3}}{d_{sr}{}^{e}}\left|\hat{h_3}\right|^2+N_{31}\right)}{[\eta\frac{P_{s3}}{d_{sr}{}^{e}}\left|\hat{h_3}\right|^2(1-\rho_c)DTd_{rd}{}^{e}+P_{e3}]m_3{}^2\rho_c}$
$+ \frac{\frac{P_{s3}}{d_{sr}{}^{e}}\left|\hat{h_3}\right|^2N_{32}DTd_{rd}{}^{e}\left(\frac{P_{s3}}{d_{sr}{}^{e}}\left|\hat{h_3}\right|^2+N_{31}\right)}{[\eta\frac{P_{s3}}{d_{sr}{}^{e}}\left|\hat{h_3}\right|^2(1-\rho_c)DTd_{rd}{}^{e}+P_{e3}]m_3} + \frac{N_{32}N_{31}DTd_{rd}{}^{e}\left(\frac{P_{s3}}{d_{sr}{}^{e}}\left|\hat{h_3}\right|^2+N_{31}\right)}{[\eta\frac{P_{s3}}{d_{sr}{}^{e}}\left|\hat{h_3}\right|^2(1-\rho_c)DTd_{rd}{}^{e}+P_{e3}]m_3} +$
$\frac{N_{32}DTd_{rd}{}^{e}\left(\frac{P_{s3}}{d_{sr}{}^{e}}\left|\hat{h_3}\right|^2+N_{31}\right)}{[\eta\frac{P_{s3}}{d_{sr}{}^{e}}\left|\hat{h_3}\right|^2(1-\rho_c)DTd_{rd}{}^{e}+P_{e3}]}.$

To improve future derivation, the variance value of $\left|\hat{h_3}\right|^2$ and $|\hat{g_3}|^2$ are needed. The PDF of $\left|\hat{h_3}\right|^2$ is (5.80), and the CDF is (5.81), where $\lambda_{31} = \frac{1}{2\theta^2+|\frac{N_{31}}{m_3\rho_c\frac{P_{s3}}{d_{sr}{}^{e}}}|}$.

However, the PDF and CDF of $|\hat{g_3}|^2$ are given as $f_{|\hat{g_3}|^2}(x) = \lambda_{32}e^{-\lambda_{32}x}$ and $F_{|\hat{g_3}|^2}(x) = 1 - e^{-\lambda_{32}x}$, respectively, and the parameter scale can be derived as

$$\lambda_{32} = \frac{1}{A_n} \tag{6.61}$$

where $A_n = \frac{4\theta^4}{2\theta^2+\frac{|N_{31}|}{m_3\rho_c\frac{P_{s3}}{d_{sr}{}^{e}}}} + \frac{N_{32}|m_3T|\lambda_{31}}{m_3}[\frac{\frac{P_{s3}}{d_{sr}{}^{e}}}{\eta\frac{P_{s3}}{d_{sr}{}^{e}}|1-\rho_c|m_3T}\frac{1}{\lambda_{31}} +$
$\frac{N_{31}\eta\frac{P_{s3}}{d_{sr}{}^{e}}|1-\rho_c|m_3T-\frac{P_{s3}}{d_{sr}{}^{e}}P_{e3}}{(\eta\frac{P_{s3}}{d_{sr}{}^{e}}|1-\rho_c|m_3T)^2}(-e^{\lambda_{31}\frac{\eta\frac{P_{s3}}{d_{sr}{}^{e}}|1-\rho_c|m_3TP_{e3}}{(\eta\frac{P_{s3}}{d_{sr}{}^{e}}|1-\rho_c|m_3T)^2}}Ei(-\lambda_{31}\frac{\eta\frac{P_{s3}}{d_{sr}{}^{e}}|1-\rho_c|m_3TP_{e3}}{(\eta\frac{P_{s3}}{d_{sr}{}^{e}}|1-\rho_c|m_3T)^2}))]$.

According to the expressions above, the CDF of γ_{3end} can be derived from

(6.60), one has

$$F_{\gamma_{3end}}(x) = P_{1r}\{\gamma_{3end} < x\} = I_{31} + I_{32}. \tag{6.62}$$

These two different parts can be separated as

$$I_{31} = P_{r3}\{\left(\rho_c \frac{P_{s3}}{{d_{sr}}^e}|\hat{h_3}|^2 - \frac{\gamma_{3th}N_{31}}{\rho_c m_3} - \gamma_{3th}N_{31}\right) < 0\} \tag{6.63}$$

and

$$I_{32} = P_{r3}\{|\hat{g_3}|^2 < \frac{A_o}{\left[\left[\eta\frac{P_{s3}}{{d_{sr}}^e}|\hat{h_3}|^2(1-\rho_c)DT{d_{rd}}^e + P_{e3}\right]{m_3}^2\rho_c\right]\left(\rho_c\frac{P_{s3}}{{d_{sr}}^e}|\hat{h_3}|^2 - \frac{\gamma_{3th}N_{31}}{\rho_c m_3} - \gamma_{3th}N_{31}\right)} | \left(\rho_c \frac{P_{s3}}{{d_{sr}}^e}|\hat{h_3}|^2 - \frac{\gamma_{3th}N_{31}}{\rho_c m_3} - \gamma_{3th}N_{31}\right) > 0\} \tag{6.64}$$

where $A_o = \gamma_{3th}\rho_c N_{32} m_3 \frac{P_{s3}}{{d_{sr}}^e}|\hat{h_3}|^2\left(\frac{P_{s3}}{{d_{sr}}^e}|\hat{h_3}|^2 + N_{31}\right)DT{d_{rd}}^e + \gamma_{3th}N_{31}N_{32}\left(\frac{P_{s3}}{{d_{sr}}^e}|\hat{h_3}|^2 + N_{31}\right)DT{d_{rd}}^e + \gamma_{3th}m_3\rho_c N_{32}N_{31}\left(\frac{P_{s3}}{{d_{sr}}^e}|\hat{h_3}|^2 + N_{31}\right)DT{d_{rd}}^e + \gamma_{3th}N_{32}\rho_c{m_3}^2\left(\frac{P_{s3}}{{d_{sr}}^e}|\hat{h_3}|^2 + N_{31}\right)DT{d_{rd}}^e$, respectively.

By using the CDF of $|\hat{h_3}|^2$ in 5.81, one has

$$I_{31} = P_{r3}\{\left(\rho_c\frac{P_{s3}}{{d_{sr}}^e}|\hat{h_3}|^2 - \frac{\gamma_{3th}N_{31}}{\rho_c m_3} - \gamma_{3th}N_{31}\right) < 0\} = P_{r3}\{|\hat{h_3}|^2 < \frac{\gamma_{3th}N_{31}}{\rho_c m_3\frac{P_{s3}}{{d_{sr}}^e}} + \frac{\gamma_{3th}N_{31}}{\frac{P_{s3}}{{d_{sr}}^e}\rho_c}\}$$
$$= \int_0^{\frac{\gamma_{3th}N_{31}}{\rho_c m_3\frac{P_{s3}}{{d_{sr}}^e}} + \frac{\gamma_{3th}N_{31}}{\frac{P_{s3}}{{d_{sr}}^e}\rho_c}} f_{|\hat{h_3}|^2}(y)dy = F_{|\hat{h_3}|^2}(y)dy = 1 - e^{-\frac{\frac{\gamma_{3th}N_{31}}{\rho_c m_3\frac{P_{s3}}{{d_{sr}}^e}} + \frac{\gamma_{3th}N_{31}}{\frac{P_{s3}}{{d_{sr}}^e}\rho_c}}{2\theta^2 + |\frac{N_{31}}{m_3\rho_c\frac{P_{s3}}{{d_{sr}}^e}}|}} \tag{6.65}$$

where $\rho_c\frac{P_{s3}}{{d_{sr}}^e}|\hat{h_3}|^2 - \frac{\gamma_{3th}N_{31}}{\rho_c m_3} - \gamma_{3th}N_{31} = t$ and $\rho_c\frac{P_{s3}}{{d_{sr}}^e}|\hat{h_3}|^2 = t + \frac{\gamma_{3th}N_{31}}{\rho_c m_3} + \gamma_{3th}N_{31}$; $\frac{P_{s3}}{{d_{sr}}^e}|\hat{h_3}|^2 = \frac{t}{\rho_c} + \frac{\gamma_{3th}N_{31}}{{\rho_c}^2 m_3} + \frac{\gamma_{3th}N_{31}}{\rho_c}$ is assumed.

The second part I_{32} can be interpreted as

$$
\begin{aligned}
I_{22} &= \int_{\frac{\gamma_{3th}N_{31}}{m_3\rho_c^2\frac{P_{s3}}{{d_{sr}}^e}}+\frac{\gamma_{3th}N_{31}}{\frac{P_{s3}}{{d_{sr}}^e}\rho_c}}^{\infty} F_{|\hat{g_3}|^2}[\frac{b_3}{d_3}+\frac{(\frac{a_3}{\rho_c}+2b_3c_3)\frac{d_3}{\rho_c}-\frac{b_3}{\rho_c}(d_3c_3+g_3)}{\frac{d_3^2}{{\rho_c}^2}t+\frac{d_3}{\rho_c}(d_3c_3+g_3)}+\frac{\frac{a_3c_3+b_3c_3^2\rho_c}{d_3c_3+g_3}}{\frac{d_3}{(d_3c_3+g_3)\rho_c}t^2+t}] \\
&f_{|\hat{h_3}|^2}(\frac{t}{\rho_c\frac{P_{s3}}{{d_{sr}}^e}}+\frac{\gamma_{3th}N_{31}}{m_3\rho_c^2\frac{P_{s3}}{{d_{sr}}^e}}+\frac{\gamma_{3th}N_{31}}{\frac{P_{s3}}{{d_{sr}}^e}\rho_c})d_3t \\
&= \int_0^{\infty}(1-e^{-\lambda_{32}[\frac{b_3}{d_3}+\frac{(\frac{a_3}{\rho_c}+2b_3c_3)\frac{d_3}{\rho_c}-\frac{b_3}{\rho_c}(d_3c_3+g_3)}{\frac{d_3^2}{{\rho_c}^2}t+\frac{d_3}{\rho_c}(d_3c_3+g_3)}+\frac{\frac{a_3c_3+b_3c_3^2\rho_c}{d_3c_3+g_3}}{\frac{d_3}{(d_3c_3+g_3)\rho_c}t^2+t}]}) \\
&\times\frac{1}{\left(2\theta^2+|\frac{N_{31}}{m_3\rho_c\frac{P_{s3}}{{d_{sr}}^e}}|\right)}e^{-\frac{\frac{t}{\rho_c\frac{P_{s3}}{{d_{sr}}^e}}+\frac{\gamma_{3th}N_{31}}{m_3\rho_c^2\frac{P_{s3}}{{d_{sr}}^e}}+\frac{\gamma_{3th}N_{31}}{\frac{P_{s3}}{{d_{sr}}^e}\rho_c}}{2\theta^2+|\frac{N_{31}}{m_3\rho_c\frac{P_{s3}}{{d_{sr}}^e}}|}}d_3t\frac{1}{\frac{P_{s3}}{{d_{sr}}^e}} \\
&\int_0^{\infty}\frac{1}{\left(2\theta^2+|\frac{N_{31}}{m_3\rho_c\frac{P_{s3}}{{d_{sr}}^e}}|\right)}e^{-\frac{\frac{t}{\frac{P_{s3}}{{d_{sr}}^e}\rho_c}+\frac{\gamma_{3th}N_{31}}{m_3\rho_c^2\frac{P_{s3}}{{d_{sr}}^e}}+\frac{\gamma_{3th}N_{31}}{\frac{P_{s3}}{{d_{sr}}^e}\rho_c}}{2\theta^2+|\frac{N_{31}}{m_3\rho_c\frac{P_{s3}}{{d_{sr}}^e}}|}}d_3t\frac{1}{\frac{P_{s3}}{{d_{sr}}^e}} \\
&-\frac{1}{\left(2\theta^2+|\frac{N_{31}}{m_3\rho_c\frac{P_{s3}}{{d_{sr}}^e}}|\right)}e^{-\frac{\gamma_{3th}N_{31}+\gamma_{3th}N_{31}m_3\rho_c}{2\theta^2m_3\rho_c\frac{P_{s3}}{{d_{sr}}^e}+N_{31}}} \\
&\int_0^{\infty}e^{-\lambda_{32}[\frac{b_3}{d_3}+\frac{(\frac{a_3}{\rho_c}+2b_3c_3)\frac{d_3}{\rho_c}-\frac{b_3}{\rho_c}(d_3c_3+g_3)}{\frac{d_3^2}{{\rho_c}^2}t+\frac{d_3}{\rho_c}(d_3c_3+g_3)}+\frac{\frac{a_3c_3+b_3c_3^2\rho_c}{d_3c_3+g_3}}{\frac{d}{(d_3c_3+g_3)\rho_c}t^2+t}]-\frac{tm_3}{2\theta^2m_3\rho_c\frac{P_{s3}}{{d_{sr}}^e}+N_{31}}}d_3t\frac{1}{\frac{P_{s3}}{{d_{sr}}^e}}.
\end{aligned}
\tag{6.66}
$$

By means of curve fitting, the approximate numeric expressions can be transformed as

$$
\begin{aligned}
&e^{-\frac{1}{t+\frac{\rho_d(d_3c_3+g_3)}{d}}} => \\
&[(0.1154{m_3}^{-0.8571}-0.4076)x^{0.1109{m_1}^{-0.8867}-0.5188}e^{(\frac{-0.04452m_3-0.03081}{m_3+0.6072})x}+0.9883] \\
&e^{-\frac{1}{\frac{d_3}{(d_3c_3+g_3)\rho_{d_3}}t^2+t}} => \\
&[(-0.1138{m_3}^{-0.7688}-0.4424)x^{0.2295{m_3}^{-0.7929}-1.222}e^{(-0.1211{m_1}^{-0.2713}+1.951)x}+0.9995] \\
&=(0.1154{m_3}^{-0.8571}-0.4076)^{\alpha_5}(-0.1138{m_3}^{-0.7688}-0.4424)^{\alpha_6}e^{\frac{-\lambda_{32}\gamma_{3th}N_{32}m_3DT{d_{rd}}^e}{{m_3}^2\rho_c\eta(1-\rho_c)DT{d_{rd}}^e}}.
\end{aligned}
\tag{6.67}
$$

Finally, the outage probability function can be given as

$$P_{r3} = 1-(\rho_c-1)e^{-\frac{\frac{\gamma_{3th}N_{31}}{\rho_c}+\gamma_{3th}N_{31}m_3\rho_c}{2\theta^2 m_3\rho_c\frac{P_{s3}}{d_{sr}{}^e}+|N_{31}|}} - \frac{1}{\frac{P_{s3}}{d_{sr}{}^e}\left(2\theta^2+|\frac{N_{31}}{m_3\rho_c\frac{P_{s3}}{d_{sr}{}^e}}|\right)}e^{-\frac{\frac{\gamma_{3th}N_{31}}{\rho_c}+\gamma_{3th}N_{31}m_3\rho_c}{2\theta^2 m_3\rho_c\frac{P_{s3}}{d_{sr}{}^e}+|N_{31}|}}$$

$$\sum_{P_{e3}=0}^{\infty}(0.1154{m_3}^{-0.8571}-0.4076)^{\alpha_5}(-0.1138{m_3}^{-0.7688}-0.4424)^{\alpha_6}e^{\frac{-\lambda_{32}\gamma_{3th}N_{32}m_3DTd_{rd}{}^e}{{m_3}^2\rho_c\eta(1-\rho_c)DTd_{rd}{}^e}}$$

$$\frac{\Gamma((0.1109{m_1}^{-0.8867}-0.5188)\alpha_5+(0.2295{m_3}^{-0.7929}-1.222)\alpha_6+1)}{[(\frac{-0.04452m_3-0.03081}{m_3+0.6072})\alpha_5+(-0.1211{m_1}^{-0.2713}+1.951)\alpha_6-\frac{m_3}{2\theta^2 m_3\rho_c\frac{P_{s3}}{d_{sr}{}^e}+N_{31}}]^{A_p}}\frac{e^{\lambda}\lambda^{P_{e3}}}{P_{e3}!}. \tag{6.68}$$

where $\alpha_5 = \frac{\rho_c\lambda_{32}(\frac{\gamma_{3th}N_{31}N_{32}DTd_{rd}{}^e+\gamma_{3th}m_3\rho_cN_{32}N_{31}DTd_{rd}{}^e+\gamma_{3th}N_{32}\rho_c{m_3}^2DTd_{rd}{}^e}{\rho_c}+)}{{m_3}^2\rho_c\eta(1-\rho_c)DTd_{rd}{}^e} + \frac{\rho_c\lambda_{32}(2(\gamma_{3th}N_{32}m_3DTd_{rd}{}^e)(\frac{\gamma_{3th}N_{31}}{\rho_c^2m_3}+\frac{\gamma_{3th}N_{31}}{\rho_c}))}{{m_3}^2\rho_c\eta(1-\rho_c)DTd_{rd}{}^e} - \frac{\lambda_{32}b_3\rho_c((m_3{}^2\rho_c\eta(1-\rho_c)DTd_{rd}{}^e)(\frac{\gamma_{3th}N_{31}}{\rho_c^2m_3}+\frac{\gamma_{3th}N_{31}}{\rho_c})+{m_3}^2\rho_cP_{e3})}{({m_3}^2\rho_c\eta(1-\rho_c)DTd_{rd}{}^e)^2}$

and $\alpha_6 = \lambda_{32}(\frac{(\gamma_{3th}N_{31}N_{32}DTd_{rd}{}^e+\gamma_{3th}m_3\rho_cN_{32}N_{31}DTd_{rd}{}^e+\gamma_{3th}N_{32}\rho_c{m_3}^2DTd_{rd}{}^e)(\frac{\gamma_{3th}N_{31}}{\rho_c^2m_3}+\frac{\gamma_{3th}N_{31}}{\rho_c})}{({m_3}^2\rho_c\eta(1-\rho_c)DTd_{rd}{}^e)(\frac{\gamma_{3th}N_{31}}{\rho_c^2m_3}+\frac{\gamma_{3th}N_{31}}{\rho_c})+{m_3}^2\rho_cP_{e3}}$

$+\frac{(\gamma_{3th}N_{32}m_3DTd_{rd}{}^e)(\frac{\gamma_{3th}N_{31}}{\rho_c^2m_3}+\frac{\gamma_{3th}N_{31}}{\rho_c})^2\rho_c}{({m_3}^2\rho_c\eta(1-\rho_c)DTd_{rd}{}^e)(\frac{\gamma_{3th}N_{31}}{\rho_c^2m_3}+\frac{\gamma_{3th}N_{31}}{\rho_c})+{m_3}^2\rho_cP_{e3}})$ and $A_p = (0.1109{m_1}^{-0.8867}-0.5188)\alpha_5+(0.2295{m_3}^{-0.7929}-1.222)\alpha_6+1$.

Thus, the achievable rate without direct link can be derived as

$$AR_3 = (1-F_{\gamma_{3end}}(\gamma_{03}))\times(\frac{D-m_{31}}{D}) \tag{6.69}$$

and the achievable rate with a direct link can be derived as

$$AR_{3d} = (1-F_{\gamma_{3end}}(\gamma_{03})F_{\gamma_{sd}}(\gamma_{03}))\times(\frac{D-m_{31}}{D}). \tag{6.70}$$

The BER without direct link can be calculated as

$$BER_3 = \frac{1}{2}\int_0^{\infty}\frac{e^{-x}}{\sqrt{x*\pi}}F_{\gamma_{3end}}(x)dx \tag{6.71}$$

and the BER with direct link can be calculated as

$$BER_{3d} = \frac{1}{2}\int_0^{\infty}\frac{e^{-x}}{\sqrt{x*\pi}}F_{\gamma_{3end}}(x)F_{\gamma_{sd}}(x)dx. \tag{6.72}$$

The expressions can be used to calculate the OP, AR and BER for the three structures.

6.5 Numerical results and discussion

In this section, the outage probability, the achievable rate will be discussed with regards to simulation results.

First of all, we have fixed $P_{s1} = P_{s2} = P_{s3} = 1$, $\eta = 0.5, D = 100, N_{11} = N_{12} = N_{21} = N_{22} = N_{31} = N_{32} = 1$. To define $\gamma_1 = \frac{|h|^2}{2\sigma^2}$ as the instantaneous SNR of the SR link, and $\gamma_2 = \frac{|g|^2}{2\sigma^2}$ as the instantaneous SNR of the RD link, where $g_1 = g_2 = g_3 = g$, $h_1 = h_2 = h_3 = h$. The values of g and h are changed with γ_1 and γ_2.

6.5.1 Outage probability evaluation

The outage probability for three structures is analysed in this subsection.

Fig. 6.1 illustrates the relationship between outage probability of the ACEPS structure versus the power splitting ratio ρ_p, when γ_1 and γ_2 both are fixed at 10 dB, respectively. Thus, it can be observed that the optimal values are $m_{11} = 95$ and $\rho_p = 0.1$, and the biggest OP is around 0.98.

Fig. 6.2 is similar to Fig. 6.1 for outage probability of the ACEPS structure versus the power splitting ratio ρ_p, except the γ_1 and γ_2 were fixed at 10 dB and 20 dB, respectively. Therefore, we can get the optimal $m_{11} = 30$ and $\rho_p = 0.1$, and the biggest OP is around 0.718.

Fig. 6.3 presents the relationship between outage probability of the ADTPS structure versus the power splitting ratio ρ_d, when γ_1 and γ_2 are fixed both at 10 dB, respectively. The optimal values are $m_{21} = 80$ and $\rho_d = 0.15$, which can be found in the graph, and the biggest OP is around 0.644.

Fig. 6.4 has same condition as Fig. 6.3 for outage probability of the ADTPS structure versus the power splitting ratio ρ_d, apart from the γ_1 and γ_2 are fixed at 10 dB and 20 dB, respectively. Thus, the optimal values are $m_{21} = 90$ and $\rho_d = 0.15$, and the OP is around 0.364.

Fig. 6.5 illustrates the relationship between outage probability of the ACPS structure versus the power splitting ratio ρ_c, when γ_1 and γ_2 were fixed both at 10 dB, respectively. The optimal values are $m_{31} = 80$ and $\rho_c = 0.2$ can be found in the

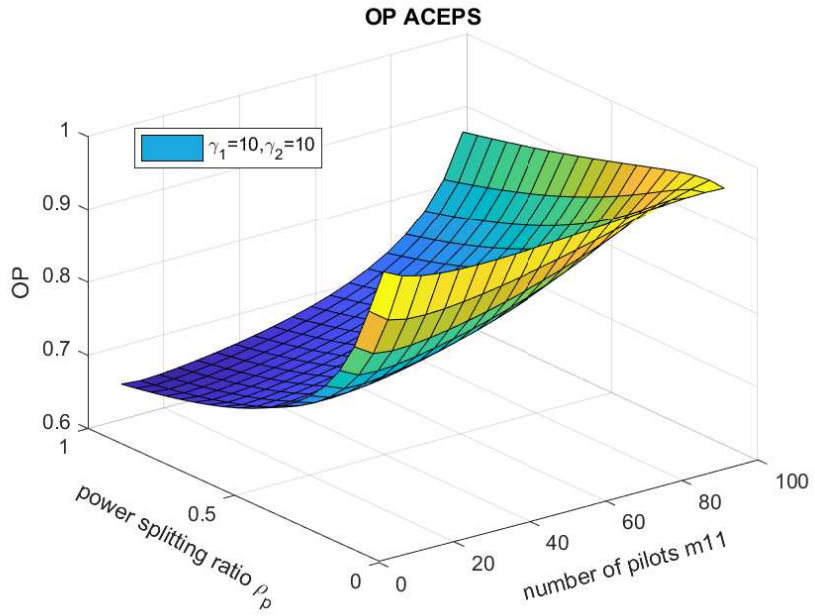

Figure 6.1: Outage probability of CEPS with direct link versus the power splitting ratio ρ_p, when γ_1 and γ_2 are fixed at 10dB and 10dB.

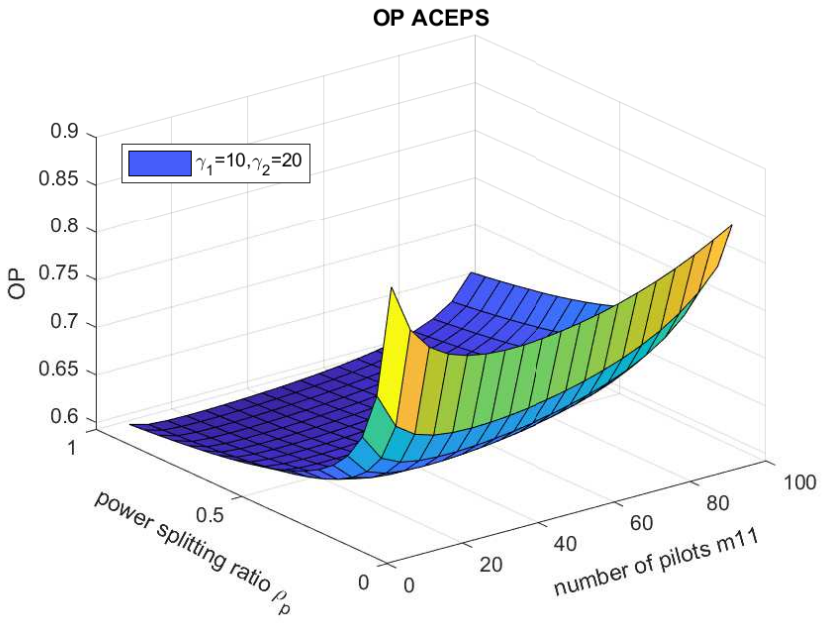

Figure 6.2: Outage probability of CEPS with direct link versus the power splitting ratio ρ_p, when γ_1 and γ_2 are fixed at 10dB and 20dB.

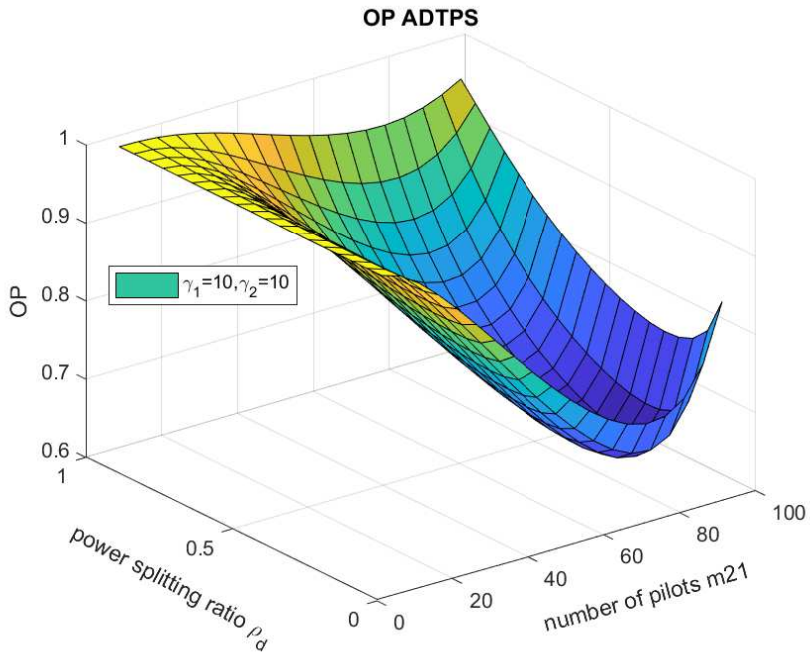

Figure 6.3: Outage probability of ADTPS with direct link versus the power splitting ratio ρ_d, when γ_1 and γ_2 are fixed at 10dB and 10dB.

graph, and the biggest OP is around 0.6.

Fig. 6.6 was same as Fig. 6.5 for outage probability of the ACPS structure versus the power splitting ratio ρ_c, apart from the γ_1 and γ_2 are fixed at 10 dB and 20 dB, respectively. Thus, the optimal values are $m_{31} = 90$ and $\rho_c = 0.15$, and the OP is around 0.337.

From the about results, we can see when γ_2 increases, the outage probability is drop-down.

6.5.2 Achievable rate evaluation

In this subsection, the achievable rate is studied with regard to the calculated results. Fig. 6.7 shows the relationship between the achievable rate of the ACEPS structure versus the power splitting ratio ρ_p, when γ_1 and γ_2 are fixed both at 10 dB, respectively. Therefore, we can see that the AR increases first and then falls when m_{11} or ρ_p increases. In such a case, it can be observed that the optimal values

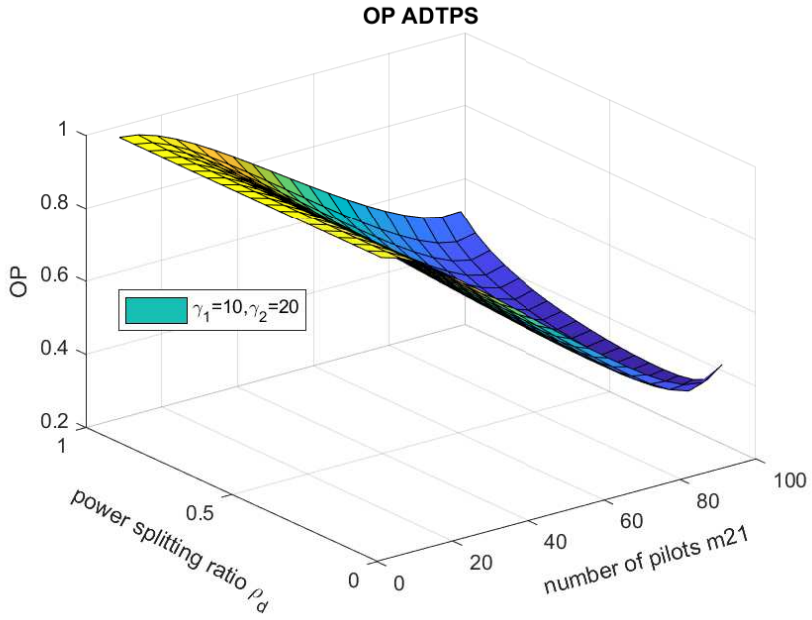

Figure 6.4: Outage probability of ADTPS with direct link versus the power splitting ratio ρ_d, when γ_1 and γ_2 are fixed at 10dB and 20dB.

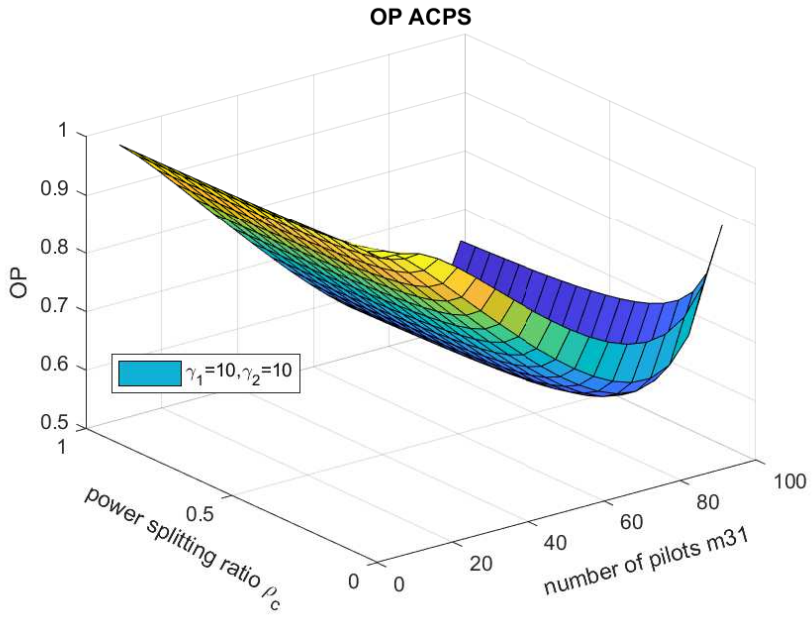

Figure 6.5: Outage probability of ACPS with direct link versus the power splitting ratio ρ_c,when γ_1 and γ_2 are fixed at 10dB and 20dB.

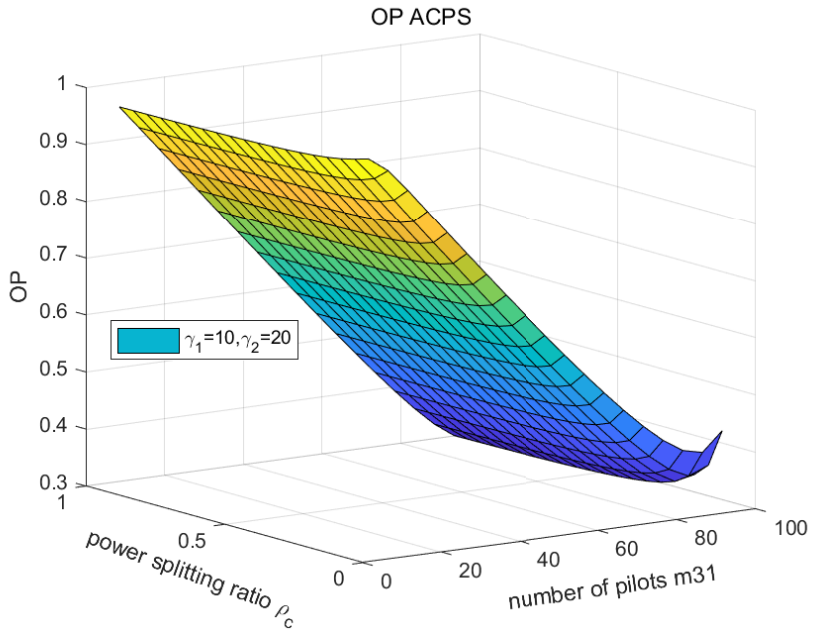

Figure 6.6: Outage probability of ACPS with direct link versus the power splitting ratio ρ_c,when γ_1 and γ_2 are fixed at 10dB and 20dB.

are $m_{11} = 15$ and $\rho_p = 0.25$, and the maximum AR is around 0.1657. Fig. 6.8 is similar to Fig. 6.7, except that γ_1 , γ_2 are fixed at 10 dB and 20 dB, respectively. In this case, the rate has the same fluctuation as 6.7. The optimal values are $m_{11} = 25$ and $\rho_p = 0.2$, and the maximum rate is around 0.288. Thus, the performance of the ACEPS structure can be improved by increasing γ_2, but the optimal values will change too.

Fig. 6.9 shows the relationship between the achievable rate of the ADTPS structure versus the power splitting ratio ρ_d, when γ_1 and γ_2 are both fixed at 10 dB, respectively. Thus, we can see that the AR increases first and then falls when m_{21} or ρ_d increases. In this case, it can be observed that the optimal values are $m_{21} = 80$ and $\rho_d = 0.2$, and the maximum AR is around 0.2866. Fig. 6.10 is the same as Fig. 6.9, apart from γ_1 , γ_2 are fixed at 10 dB and 20 dB, respectively. In this case, the rate has the same fluctuation as 6.9. The optimal values are $m_{21} = 90$ and $\rho_d = 0.1$, and the maximum rate is around 0.563. Thus, the performance of the ADTPS structure can be improved by increasing γ_2, and the optimal values will change too.

Fig. 6.11 illustrates the relationship between the achievable rate of the ACPS

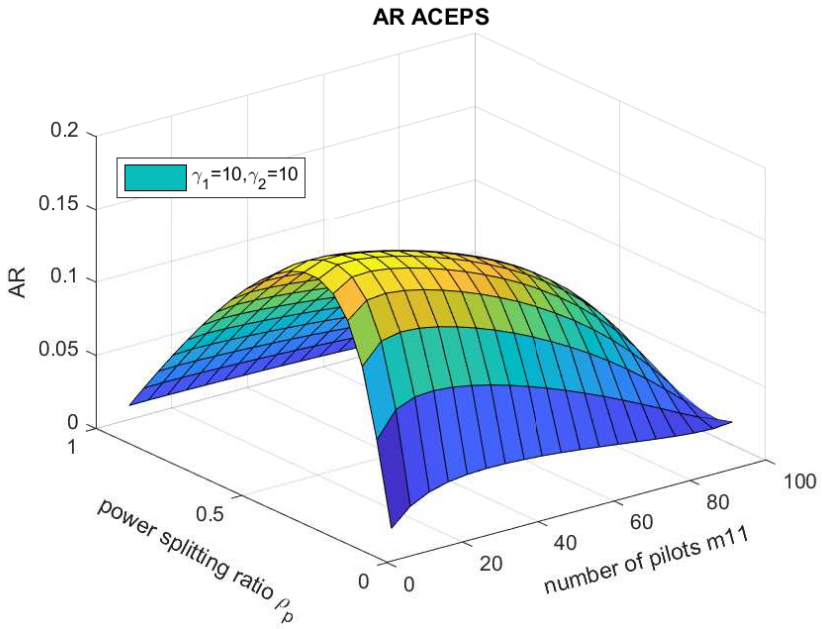

Figure 6.7: Achievable rate of CEPS with direct link versus the power splitting ratio ρ_p, when γ_1 and γ_2 are fixed at 10dB and 10dB.

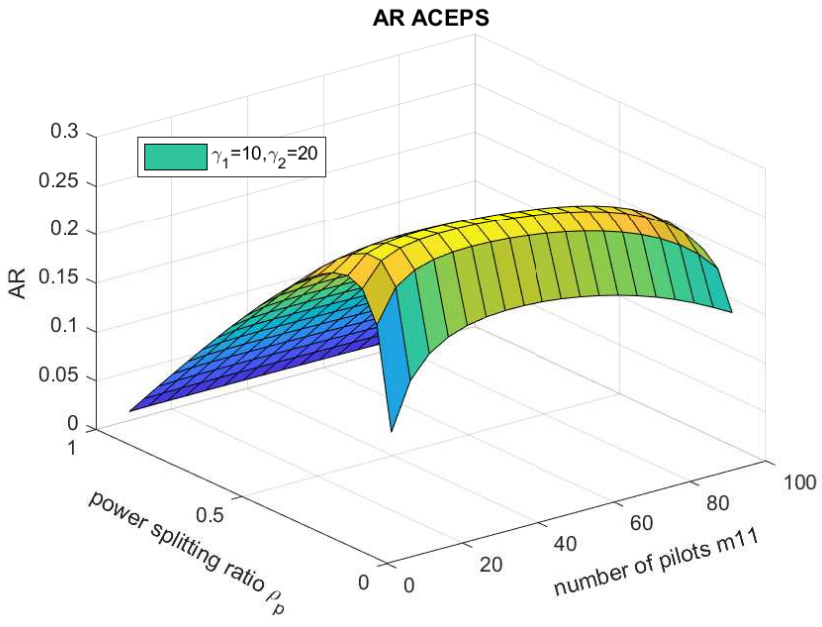

Figure 6.8: Achievable rate of CEPS with direct link versus the power splitting ratio ρ_p, when γ_1 and γ_2 are fixed at 10dB and 20dB.

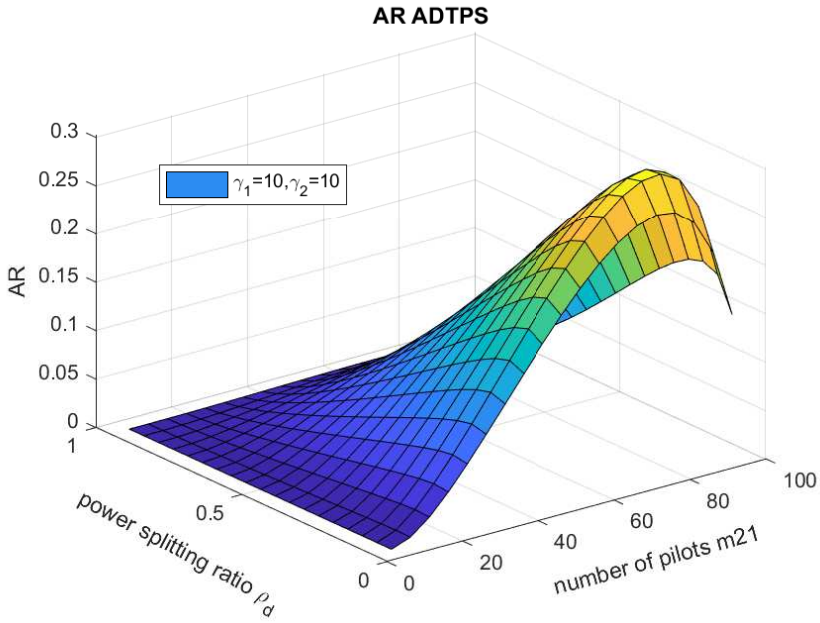

Figure 6.9: Achievable rate of ADTPS with direct link versus the power splitting ratio ρ_d, when γ_1 and γ_2 are fixed at 10dB and 10dB.

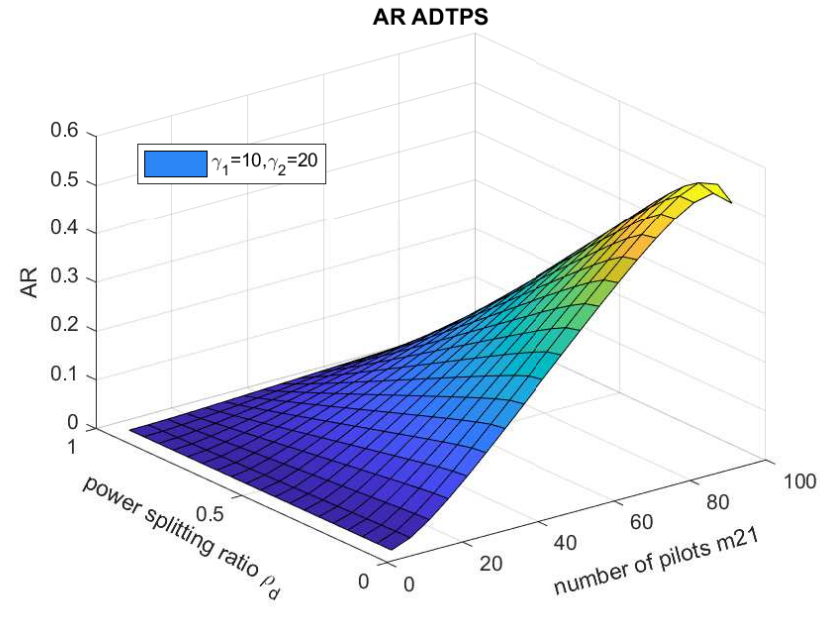

Figure 6.10: Achievable rate of ADTPS with direct link versus the power splitting ratio ρ_d, when γ_1 and γ_2 are fixed at 10dB and 20dB.

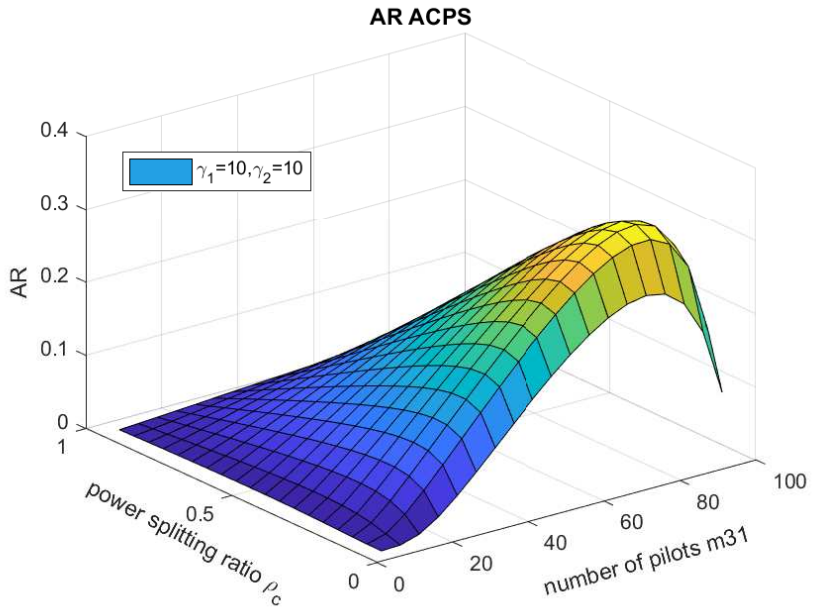

Figure 6.11: Achievable rate of ACPS with direct link versus the power splitting ratio ρ_c,when γ_1 and γ_2 are fixed at 10dB and 20dB.

structure versus the power splitting ratio ρ_c, when γ_1 and γ_2 are both fixed at 10 dB, respectively. Thus, we can see that the AR increases first and then falls when m_{31} or ρ_c increases. In this case, it can be observed that the optimal values are $m_{31} = 80$ and $\rho_c = 0.2$, and the maximum AR is around 0.318. Fig. 6.12 is the same as Fig. 6.1, apart from γ_1 , γ_2 are fixed at 10 dB and 20 dB, respectively. In this case, the rate has the same fluctuation as 6.9. The optimal values are $m_{31} = 90$ and $\rho_c = 0.1$, and the maximum rate is around 0.581. Thus, the performance of the ACPS structure can be improved by increasing γ_2, and the optimal values will change too.

From the earlier results, first of all, we can recognise that with the increasing of γ_2, the maximum AR was increased at the same time, which indicates larger γ_2 can bring better performance. Secondly, we can discern that the ACPS structure has the biggest achievable rate than the other two. Therefore ACPS has the best performance between three structures. Compared Fig. 5.6 with Fig. 6.7, Fig. 5.8 with Fig. 6.9, and Fig. 5.10 with Fig. 6.11, respectively. The ambient energy added structures have a significant improvement compare to the structures in Chapter 5, which appeared with larger achievable rate value under the same conditions.

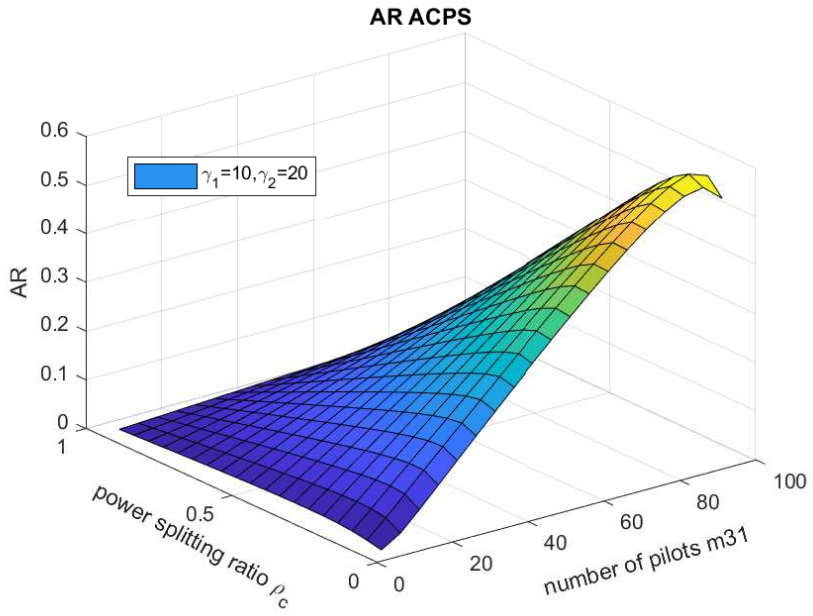

Figure 6.12: Achievable rate of ACPS with direct link versus the power splitting ratio ρ_c,when γ_1 and γ_2 are fixed at 10dB and 20dB.

6.6 Conclusions

In this chapter, three improved ambient added EH structures were investigated. Different from the schemes presented in Chapter 5, in this work, we considered the energy from the source and the energy from the ambient at the same time. Both the distance and the direct link were considered during the investigation. The outage probability, achievable rate and bit-error-rate expressions were examined, to reach the maximum achievable rate and the minimum bit-error-rate for optimisation objective. Numerical results verified that the optimal values for different structures. We also noticed that the ambient added schemes have better achievement than using the energy from the source individually, when the data packet size was fixed. Analysing three structures, we observe that ACPS has better capability than the other two structures.

Chapter 7

Conclusions and further work

RF energy harvesting (RFEH) in relaying is one of the most advanced communication models, which applies EH to raise the signal transmission efficiency in relaying.

This thesis focuses on the investigation of RFEH in relaying, where the information is transmitted from the SR and then from relay to destination. Meanwhile, the relay harvests energy from the source or ambient RF simultaneously. All energy harvested at the relay node will be used to broadcast information from the relay to the destination. The information data packet from the SR includes channel estimation, information decoding and EH. The information data packet for RD link includes information decoding and channel estimation. The system was designed based on AF relaying. As the main objective of this thesis, the relation between uplink and downlink performance was analysed first, and the performance under the wireless powered communication was then investigated. Under the TS EH protocol, the performance of the optimal EH in AF relaying was analysed in regard to the achievable rate and BER. Furthermore, an in depth investigation for novel optimal EH schemes by AF relaying was also conducted. Different combinations of PS and TS models for novel EH schemes were designed, and the ambient added EH structures with more efficient models were also presented in this thesis.

The research aims to offer an optimised EH structure, which provides a physical foundation for further research. The detailed simulation and theoretical results are beneficial for future practical implementations, such as applying EH under numerous types of communication systems.

In Section 7.1, the achievements of the main chapters will be summarised. Moreover, a summary is given in Section 7.2 and further work presented in Section 7.3.

7.1 Conclusions for main chapters

Chapter 3: In this chapter, we considered the link correlation of the uplink and downlink in the design of a wireless powered communication (WPC) system. Both the semi-closed expressions for the achievable rate and the series expressions for the BER of the WPC system were presented with the uplink and downlink correlations. Followed with these expressions, the performance of link correlation for a more realistic and accurate system design was analysed. In the numerical examples of the simulation part, either average fading power in the uplink or average fading power in the downlink was fixed. The simulation used the model in [178] to generate 10^6 random values of $|g_i|$ and $|h_i|$, and averaged them over the instantaneous rate and the BER. The numerical results quantified the performance degradation due to the link correlation. In these results, the rate of degradation was significant when $\tau_0 < 0.6$ or less than 60% of the transmission time was used for EH. They also shown that the transmission power has the largest impact, followed by the Nakagami m parameter and the Doppler shift, on the achievable rate in the correlated case. This led to a considerably different choice of the optimum harvesting time, as compared with the independent case. On the other hand, the BER change was noticeable but not as significant as the rate change. The transmission power and the Nakagami m parameter still has the largest impact. For the sum rate of two users, a global maximum exists at certain values of τ_0 and τ_1.

Chapter 4: In this chapter, an AF relaying system with pilot-based channel estimation and time-switching (TS) EH was studied. Both half-duplex model and BPSK were used in this chapter, and the optimisation was based on AF relaying communications system. The closed-form expressions for channel capacity, achievable rate and BER were derived for the proposed EH scheme. The variable parameters, such as the channel estimation ratio for the first hop α_1, the channel estimation ratio for the second hop α_2, the data transmission ratio β, the total pilots value D, the energy from SR P_s, the energy from relay to the destination P_r, the noise power for the first hop N_1, the noise power from relay to the destination N_2, and the conversion efficiency η, were all discussed. The numerical results of

the outage probability and the BER versus the ratio of channel estimation indicates that the channel estimation ratio in the first and second hop has a significant effect on the system. With the increase of channel estimation ratio, the outage probability reduced first and then increased. Similarly, for the outage probability and the BER versus the ratio of data transmission, they also have a specific effect on the system capacity. With the increase of data transmission, the outage probability and BER also dropped down first and then raised up. The system performance shows that with a fixed alternate coefficient, and an increase of the variables α_1,α_2 and β, the outage probability and BER have the likeness change curve, which decreased first and then increased. Therefore, the optimal allocation between the three parts of the data packet in the first hop, and the two parts of the data packet in the second hop, were achieved. The results illustrate the optimal ratio for channel estimation and data transmission. In the simulation graphs, the abrupt changing point shows the optimum value.

Chapter 5: In this chapter, three novel structures using simultaneous wireless information and power transfer in EH AF relaying were investigated. Moreover, two EH protocols: TS and PS were considered at the same time in this chapter. The closed-form expressions for achievable rate and BER were derived for three proposed novel structures. The parameters used in this part of the study, with channel estimation ratio, information decoding ratio, and power splitting ratio, were comprehensively discussed. The numerical results of the achievable rate versus channel estimation pilots number and power splitting ratio, BER versus channel estimation pilots number and power splitting ratio, outage probability versus channel estimation pilots, were indicated. During the performance analysis, the distance and direct link were also considered. The outcomes show the achievable rates of the three different structures, and one can see that the CEPS has a lower maximum achievable rate than DTPS and CPS. Additionally, DTPS and CPS have similar optimal achievable rates from the calculations, and CPS has a slightly bigger maximum achievable rate than the DTPS's.

Therefore, CPS has the best performance among these three structures, and CEPS has the worst. The results show the optimal values for channel estimation pilots and power splitting ratio series. The research described in Chapter 5 is based on AF relaying duel-hop communications system.

Chapter 6: In this chapter, based on the three structures designed in Chapter 5, the additional RF ambient energy was considered. The direct link and the

distance are also examined concurrently. The upgraded structures were named as ACEPS, ADTPS and ACPS. The closed-form expressions of the outage probability, achievable rate and BER were derived. The variable arguments include the pilots for channel estimation and the power splitting ratio, were investigated. The numerical results of the outage probability versus channel estimation pilots number and power splitting ratio, achievable rate versus channel estimation pilots number and power splitting ratio, were demonstrated, in order to obtain the best proportion from different schemes.

Therefore, the results provide the optimal values for channel estimation pilots and power splitting ratio series for these ambient RF added structures. The outcomes show that ambient RF added schemes have more high-grade performance than harvest energy from the source independently. By comparing these three structures, one can observe that ACPS has a better capability than the other two. The research described in Chapter 6 is based on AF relaying duel-hop communications system.

7.2 Summary of the discussion

This thesis contributes in the following two ways: analysing the performance of the relation between uplink and downlink in the WPC system, and applying the TS and PS EH protocols toward the AF relaying system, to invent the most desirable harvest energy structure.

For the first goal, the relation between uplink and downlink in a wireless powered communication system was designed and studied. In this thesis, we considered the link correlation in the design of WPC systems. However, it is well known that the practical channels can be described by the Jakes' model that induces time correlation. Furthermore, this work derives the semi-closed expressions for the achievable rate and series expressions for the BER of the WPC systems in the presence of link correlation. The effect of link correlation can be quantified for more accurate and realistic system designs using these expressions. This work also studies Nakagami m fading as well. Thus, our results include previous works as a particular case even when the link correlation is not considered. The Nakagami m model can be used to describe the specific propagation scenarios for land radio and indoor radio.

For the second goal, in the AF relaying system, we first studied the EH in-

dependently use time-switching EH protocol in Chapter 4. Furthermore, we have hatched up three EH structures with both TS and PS into the EH models. For different entities in EH scenarios, this work considered data packets with channel estimation, EH and information decoding. The CDF of the end-to-end SNR for the three novel EH structures were derived. These functions support the derivation of the achievable rate and BER as well as the optimal power allocation. The performance of the EH structures with regard to the achievable rate and BER were investigated. Throughout the analysis of the achievable rate and BER, the existence of the optimal number of pilots for channel estimation and the optimal value of power splitting ratio were obtained. In Chapter 6, we involved additional ambient RF energy into those structures proposed in Chapter 5. Using the same process, the numerical results show the necessity of ambient RF energy to promote the efficiency of signal transmission in real life.

7.3 Further work

The work conducted in this thesis shows that the EH is a promising discipline with great potentials in real life applications, which can be beneficial for various manufacturing industries. Further research can expand based on the current work.

In this thesis, we only considered a duel-hop system during the AF transmission, and the future work can spread to decode-and-forward and multi-hop systems with better spectral efficiency. This thesis investigated the half-duplex transmission, which the signal can only transmit in a single direction. In the future, full-duplex can be implemented with comprehensive capability and better performance where data can be transmitted in both directions on a signal carrier at the same time. Meanwhile, the system model can be more complicated as the two-way signal transmission need to be examined further. The thesis only analysed the single relay system with channel state information. Therefore, the future work can examine the multi-relays and multi-hops transmission channel information, with channel estimation estimated in each relay. In such case, it can promote practical applications to analysis the realistic of EH and extend the application fields. Besides, we haven't investigated the interference in the relaying system. For future work, the influence of interference for spectral transmission can be considered.

In this work, the power was harvested from the source and ambient environ-

ment, in addition, the dedicated RF source can be used for the third power source selection. An increase in the total amount of energy the relay can harvest and improve the efficiency of EH.

In this thesis, three parts of data packets: channel estimation, data transmission and EH were analysed. Other factors, like edge computing, spectrum sensing and backscatter communication can be added, based on the application requirements. Fundamental relaying signal transmission model was studied. In the future, under the different communication systems like cellular communications, sensor communications, and optical communication, we can apply the optimal EH structure into these communication networks to investigate their EH efficiencies.

On top of that, the relevant EH experiments can be studied, in order to verify the proposed EH structures with optimal ratio discovered from numerical results in this thesis. Besides that, the large intelligence surface is popular in recent years, as an alternative of relaying, so that the rate and energy efficiency of wireless channels can be improved by deploying software-controlled metasurfaces to reflect signals from the source to destination, especially when the direct path is weak.

Bibliography

[1] Z. Yang, A. Erturk, and J. Zu, "On the efficiency of piezoelectric energy harvesters," *Extreme Mechanics Letters*, vol. 15, pp. 26–37, 2017.

[2] M. Cansiz, D. Altinel, and G. K. Kurt, "Efficiency in rf energy harvesting systems: A comprehensive review," *Energy*, 2019.

[3] https://ourworldindata.org/grapher/renewable-energy-consumption.

[4] https://www.greengalaxies.net/knowledge-bank/energy/types.

[5] https://eu.poughkeepsiejournal.com/story/tech/science/environment/2018/05/02/solar-energy-renewables/438026002/.

[6] https://www.ryansearch.net/blog/march_2015/kinetic-vs-potential-leadership.

[7] https://sites.google.com/site/jhbahk/simulation-tools.

[8] https://electromagnetic-energy.com/.

[9] Z. Hou, H. Chen, Y. Li, and B. Vucetic, "Incentive mechanism design for wireless energy harvesting-based internet of things," *IEEE Internet of Things Journal*, vol. 5, pp. 2620–2632, 2017.

[10] https://www.analog.com/en/technical-articles/energy-harvesting-with-low-power-solar-panels.html.

[11] https://en.wikipedia.org/wiki/Thermoelectric_generator.

[12] D. Zhu, S. Roberts, T. Mouille, M. J. Tudor, and S. P. Beeby, "General model with experimental validation of electrical resonant frequency tuning of electromagnetic vibration energy harvesters," *Smart Materials and Structures*, vol. 21, no. 10, p. 105039, 2012.

[13] A. Anika Shahabuddin, P. Dewanjee Shalu, and N. Akter, "Optimized process design of rf energy harvesting circuit for low power devices," *International Journal of Applied Engineering Research*, vol. 13, pp. 849–854, 11 2017.

[14] P. K. Jha, S. S. Shree, and D. S. Kumar, "Achievable rate analysis of cooperative relay assisted opportunistic-noma under rician fading channels with channel state information," *arXiv preprint arXiv:1709.08224*, 2017.

[15] X. Fang, S. Misra, G. Xue, and D. Yang, "Smart Grid the new and improved power grid: A survey," *IEEE communications surveys & tutorials*, vol. 14, no. 4, pp. 944–980, 2011.

[16] A. Hande, T. Polk, W. Walker, and D. Bhatia, "Indoor solar energy harvesting for sensor network router nodes," *Microprocessors and Microsystems*, vol. 31, no. 6, pp. 420–432, 2007.

[17] A. Weddell, N. Harris, and N. White, "An efficient indoor photovoltaic power harvesting system for energy-aware wireless sensor nodes," 2008.

[18] V. Raghunathan, A. Kansal, J. Hsu, J. Friedman, and M. Srivastava, "Design considerations for solar energy harvesting wireless embedded systems," in *Proceedings of the 4th international symposium on Information processing in sensor networks*. IEEE Press, 2005, p. 64.

[19] M. H. Shubbak, "The technological system of production and innovation: The case of photovoltaic technology in china," *Research Policy*, vol. 48, no. 4, pp. 993–1015, 2019.

[20] M. Bazilian, I. Onyeji, M. Liebreich, I. MacGill, J. Chase, J. Shah, D. Gielen, D. Arent, D. Landfear, and S. Zhengrong, "Re-considering the economics of photovoltaic power," *Renewable Energy*, vol. 53, pp. 329–338, 2013.

[21] R. M. Swanson, "Photovoltaics power up," *Science*, vol. 324, no. 5929, pp. 891–892, 2009. [Online]. Available: https://science.sciencemag.org/content/324/5929/891

[22] Y. Chen, *Energy Harvesting Communications: Principles and Theories*. Wiley-IEEE Press, 2019.

[23] S. L. Piano and K. Mayumi, "Toward an integrated assessment of the performance of photovoltaic power stations for electricity generation," *Applied energy*, vol. 186, pp. 167–174, 2017.

[24] S. Roundy, P. K. Wright, and J. Rabaey, "A study of low level vibrations as a power source for wireless sensor nodes," *Computer communications*, vol. 26, no. 11, pp. 1131–1144, 2003.

[25] T. Starner and J. A. Paradiso, "Human generated power for mobile electronics," *Low-power electronics design*, vol. 45, pp. 1–35, 2004.

[26] T. v. Büren, P. Lukowicz, and G. Tröster, "Kinetic energy powered computingan experimental feasibility study," in *Proceedings of the 7th IEEE International Symposium on Wearable Computers*. IEEE Computer Society, 2003, p. 22.

[27] H. S. Han, Y. H. Kim, S. Y. Kim, S. Um, and J. M. Hyun, "Performance measurement and analysis of a thermoelectric power generator," in *2010 12th IEEE Intersociety Conference on Thermal and Thermomechanical Phenomena in Electronic Systems*. IEEE, 2010, pp. 1–7.

[28] V. Leonov, "Thermoelectric energy harvesting of human body heat for wearable sensors," *IEEE Sensors Journal*, vol. 13, no. 6, pp. 2284–2291, 2013.

[29] L. Da Xu, W. He, and S. Li, "Internet of things in industries: A survey," *IEEE Transactions on industrial informatics*, vol. 10, no. 4, pp. 2233–2243, 2014.

[30] X. Lu, P. Wang, D. Niyato, D. I. Kim, and Z. Han, "Wireless networks with rf energy harvesting: A contemporary survey," *IEEE Communications Surveys & Tutorials*, vol. 17, no. 2, pp. 757–789, 2014.

[31] P. Saffari, A. Basaligheh, V. J. Sieben, and K. Moez, "An rf-powered wireless temperature sensor for harsh environment monitoring with non-intermittent operation," *IEEE Transactions on Circuits and Systems I: Regular Papers*, vol. 65, no. 5, pp. 1529–1542, 2017.

[32] F. Azmat, Y. Chen, and N. Stocks, "Predictive modelling of rf energy for wireless powered communications," *IEEE Communications Letters*, vol. 20, no. 1, pp. 173–176, 2015.

[33] Y. Chen and H.-S. Oh, "A survey of measurement-based spectrum occupancy modeling for cognitive radios," *IEEE Communications Surveys & Tutorials*, vol. 18, no. 1, pp. 848–859, 2014.

[34] M. Piñuela, P. D. Mitcheson, and S. Lucyszyn, "Ambient rf energy harvesting in urban and semi-urban environments," *IEEE Transactions on microwave theory and techniques*, vol. 61, no. 7, pp. 2715–2726, 2013.

[35] M. H. Ouda, P. Mitcheson, and B. Clerckx, "Optimal operation of multitone waveforms in low rf-power receivers," in *2018 IEEE Wireless Power Transfer Conference (WPTC)*. IEEE, 2018, pp. 1–4.

[36] Solarcellsperformanceanduse".solarbotics.net.

[37] S. Essig, C. Allebé, T. Remo, J. F. Geisz, M. A. Steiner, K. Horowitz, L. Barraud, J. S. Ward, M. Schnabel, A. Descoeudres *et al.*, "Raising the one-sun conversion efficiency of iii–v/si solar cells to 32.8% for two junctions and 35.9% for three junctions," *Nature Energy*, vol. 2, no. 9, p. 17144, 2017.

[38] S. Beeby and N. M. White, *Energy harvesting for autonomous systems*. Artech House, 2010.

[39] J. Kymissis, C. Kendall, J. Paradiso, and N. Gershenfeld, "Parasitic power harvesting in shoes," in *Digest of Papers. Second International Symposium on Wearable Computers (Cat. No. 98EX215)*. IEEE, 1998, pp. 132–139.

[40] N. White, P. Glynne-Jones, and S. Beeby, "A novel thick-film piezoelectric micro-generator," *Smart Materials and Structures*, vol. 10, no. 4, p. 850, 2001.

[41] R. Guigon, J.-J. Chaillout, T. Jager, and G. Despesse, "Harvesting raindrop energy: experimental study," *Smart Materials and Structures*, vol. 17, no. 1, 2008.

[42] V.-K. Wong, J.-H. Ho, and E. H. Yap, "Dynamics of a piezoelectric beam subjected to water droplet impact with water layer formed on the surface," *Journal of Intelligent Material Systems and Structures*, vol. 26, no. 16, pp. 2170–2180, 2015.

[43] V. K. Wong, J. H. Ho, and E. H. Yap, "Experimental study of a piezoelectric rain energy harvester," in *Advanced Materials Research*, vol. 1043. Trans Tech Publ, 2014, pp. 263–267.

[44] M. Al Ahmad, "Piezoelectric water drop energy harvesting," *Journal of electronic materials*, vol. 43, no. 2, pp. 452–458, 2014.

[45] S. Gart, J. E. Mates, C. M. Megaridis, and S. Jung, "Droplet impacting a cantilever: A leaf-raindrop system," *Physical Review Applied*, vol. 3, no. 4, p. 044019, 2015.

[46] M. A. Ilyas and J. Swingler, "Piezoelectric energy harvesting from raindrop impacts," *Energy*, vol. 90, pp. 796–806, 2015.

[47] N. Adroja, S. B. Mehta, and P. Shah, "Review of thermoelectricity to improve energy quality," *Int. J. Emerg. Technol. Innov. Res*, vol. 2, pp. 847–850, 2015.

[48] E. Menke, Q. Li, and R. Penner, "Bismuth telluride (bi2te3) nanowires synthesized by cyclic electrodeposition/stripping coupled with step edge decoration," *Nano Letters*, vol. 4, no. 10, pp. 2009–2014, 2004.

[49] K. Biswas, J. He, I. D. Blum, C.-I. Wu, T. P. Hogan, D. N. Seidman, V. P. Dravid, and M. G. Kanatzidis, "High-performance bulk thermoelectrics with all-scale hierarchical architectures," *Nature*, vol. 489, no. 7416, p. 414, 2012.

[50] G. B. Ansell, M. A. Modrick, J. Longo, K. Poeppeimeler, and H. Horowitz, "Structure of calcium manganese oxide ca2mn3o8," *Acta Crystallographica Section B: Structural Crystallography and Crystal Chemistry*, vol. 38, no. 6, pp. 1795–1797, 1982.

[51] D. Van Wageningen and T. Staring, "The qi wireless power standard," in *Proceedings of 14th International Power Electronics and Motion Control Conference EPE-PEMC 2010*. IEEE, 2010, pp. S15–25.

[52] S. Keyrouz, H. Visser, and A. Tijhuis, "Multi-band simultaneous radio frequency energy harvesting," in *2013 7th European Conference on Antennas and Propagation (EuCAP)*. IEEE, 2013, pp. 3058–3061.

[53] M. Ali, L. Albasha, and N. Qaddoumi, "Rf energy harvesting for autonomous wireless sensor networks," in *2013 8th International Conference on Design & Technology of Integrated Systems in Nanoscale Era (DTIS)*. IEEE, 2013, pp. 78–81.

[54] A. M. AbdelTawab and A. Khattab, "Efficient multi-band energy harvesting circuit for wireless sensor nodes," in *2016 Fourth International Japan-Egypt Conference on Electronics, Communications and Computers (JEC-ECC)*. IEEE, 2016, pp. 75–78.

[55] V. Kuhn, C. Lahuec, F. Seguin, and C. Person, "A multi-band stacked rf energy harvester with rf-to-dc efficiency up to 84%," *IEEE transactions on microwave theory and techniques*, vol. 63, no. 5, pp. 1768–1778, 2015.

[56] M. A. Rosli, S. A. Z. Murad, and R. Ismail, "A 900-2400 mhz ac-dc rectifier circuit for radio frequency energy harvesting," in *MATEC Web of Conferences*, vol. 78. EDP Sciences, 2016, p. 01096.

[57] A. Nimo, T. Beckedahl, T. Ostertag, and L. Reindl, "Analysis of passive rf-dc power rectification and harvesting wireless rf energy for micro-watt sensors," *AIMS Energy*, vol. 3, no. 2, pp. 184–200, 2015.

[58] H. Sun, Y.-x. Guo, M. He, and Z. Zhong, "Design of a high-efficiency 2.45-ghz rectenna for low-input-power energy harvesting," *IEEE Antennas and Wireless Propagation Letters*, vol. 11, pp. 929–932, 2012.

[59] H. Sun and W. Geyi, "A new rectenna with all-polarization-receiving capability for wireless power transmission," *IEEE Antennas and Wireless Propagation Letters*, vol. 15, pp. 814–817, 2015.

[60] H. Sun, "An enhanced rectenna using differentially-fed rectifier for wireless power transmission," *IEEE Antennas and Wireless Propagation Letters*, vol. 15, pp. 32–35, 2015.

[61] U. Olgun, C.-C. Chen, and J. L. Volakis, "Wireless power harvesting with planar rectennas for 2.45 ghz rfids," in *2010 URSI International Symposium on Electromagnetic Theory*. IEEE, 2010, pp. 329–331.

[62] D. Wang and R. Negra, "Design of a dual-band rectifier for wireless power transmission," in *2013 IEEE Wireless Power Transfer (WPT)*. IEEE, 2013, pp. 127–130.

[63] K. Niotaki, A. Georgiadis, A. Collado, and J. S. Vardakas, "Dual-band resistance compression networks for improved rectifier performance," *IEEE Transactions on Microwave Theory and Techniques*, vol. 62, no. 12, pp. 3512–3521, 2014.

[64] A. Collado and A. Georgiadis, "Conformal hybrid solar and electromagnetic (em) energy harvesting rectenna," *IEEE Transactions on Circuits and Systems I: Regular Papers*, vol. 60, no. 8, pp. 2225–2234, 2013.

[65] T. Oka, T. Ogata, K. Saito, and S. Tanaka, "Triple-band single-diode microwave rectifier using crlh transmission line," in *2014 Asia-Pacific Microwave Conference*. IEEE, 2014, pp. 1013–1015.

[66] S. Abbasian and T. Johnson, "High efficiency gan hemt synchronous rectifier with an octave bandwidth for wireless power applications," in *2016 IEEE MTT-S International Microwave Symposium (IMS)*. IEEE, 2016, pp. 1–4.

[67] C. Song, Y. Huang, J. Zhou, P. Carter, S. Yuan, Q. Xu, and Z. Fei, "Matching network elimination in broadband rectennas for high-efficiency wireless power transfer and energy harvesting," *IEEE Transactions on Industrial Electronics*, vol. 64, no. 5, pp. 3950–3961, 2016.

[68] V. Marian, B. Allard, C. Vollaire, and J. Verdier, "Strategy for microwave energy harvesting from ambient field or a feeding source," *IEEE Transactions on Power Electronics*, vol. 27, no. 11, pp. 4481–4491, 2012.

[69] F. Bolos, D. Belo, and A. Georgiadis, "A uhf rectifier with one octave bandwidth based on a non-uniform transmission line," in *2016 IEEE MTT-S International Microwave Symposium (IMS)*. IEEE, 2016, pp. 1–3.

[70] C. Song, Y. Huang, J. Zhou, J. Zhang, S. Yuan, and P. Carter, "A high-efficiency broadband rectenna for ambient wireless energy harvesting," *IEEE Transactions on Antennas and Propagation*, vol. 63, no. 8, pp. 3486–3495, 2015.

[71] S. Sudevalayam and P. Kulkarni, "Energy harvesting sensor nodes: Survey and implications," *IEEE communications Surveys & tutorials*, vol. 13, no. 3, pp. 443–461, 2010.

[72] A. Seyedi and B. Sikdar, "Energy efficient transmission strategies for body sensor networks with energy harvesting," *IEEE Transactions on Communications*, vol. 58, no. 7, pp. 2116–2126, 2010.

[73] K. Huang and V. K. Lau, "Enabling wireless power transfer in cellular networks: Architecture, modeling and deployment," *IEEE Transactions on Wireless Communications*, vol. 13, no. 2, pp. 902–912, 2014.

[74] Y. Liu, Y. Zhang, R. Yu, and S. Xie, "Integrated energy and spectrum harvesting for 5G wireless communications," *IEEE Network*, vol. 29, no. 3, pp. 75–81, 2015.

[75] E. Hossain and M. Hasan, "5G cellular: key enabling technologies and research challenges," *arXiv preprint arXiv:1503.00674*, 2015.

[76] P. Liu, S. Gazor, I.-M. Kim, and D. I. Kim, "Noncoherent relaying in energy harvesting communication systems," *IEEE Transactions on Wireless Communications*, vol. 14, no. 12, pp. 6940–6954, 2015.

[77] S. Buzzi, I. Chih-Lin, T. E. Klein, H. V. Poor, C. Yang, and A. Zappone, "A survey of energy-efficient techniques for 5g networks and challenges ahead," *IEEE Journal on Selected Areas in Communications*, vol. 34, no. 4, pp. 697–709, 2016.

[78] Z. Ding, Y. Liu, J. Choi, Q. Sun, M. Elkashlan, H. V. Poor *et al.*, "Application of non-orthogonal multiple access in lte and 5g networks," *arXiv preprint arXiv:1511.08610*, 2015.

[79] T. A. Khan, A. Alkhateeb, and R. W. Heath, "Millimeter wave energy harvesting," *IEEE Transactions on Wireless Communications*, vol. 15, no. 9, pp. 6048–6062, 2016.

[80] A. A. Nasir, X. Zhou, S. Durrani, and R. A. Kennedy, "Relaying protocols for wireless energy harvesting and information processing," *IEEE Transactions on Wireless Communications*, vol. 12, no. 7, pp. 3622–3636, 2013.

[81] N. Abramson, "The aloha system: another alternative for computer communications," in *Proceedings of the November 17-19, 1970, fall joint computer conference*. ACM, 1970, pp. 281–285.

[82] E. C. Van Der Meulen, "Three-terminal communication channels," *Advances in applied Probability*, vol. 3, no. 1, pp. 120–154, 1971.

[83] E. C. Van der Meulen, "Transmission of information in a t-terminal discrete memoryless channel." 1969.

[84] E. Van der Meulen, "A survey of multi-way channels in information theory: 1961-1976," *IEEE Transactions on Information Theory*, vol. 23, no. 1, pp. 1–37, 1977.

[85] T. Cover and A. E. Gamal, "Capacity theorems for the relay channel," *IEEE Transactions on information theory*, vol. 25, no. 5, pp. 572–584, 1979.

[86] J. N. Laneman and G. W. Wornell, "Energy-efficient antenna sharing and relaying for wireless networks." in *WCNC*, 2000, pp. 7–12.

[87] A. A. Huurdeman, *The worldwide history of telecommunications*. Wiley Online Library, 2003.

[88] G. Miao, J. Zander, K. W. Sung, and S. B. Slimane, *Fundamentals of mobile data networks*. Cambridge University Press, 2016.

[89] Q. Li, R. Q. Hu, Y. Qian, and G. Wu, "Cooperative communications for wireless networks: techniques and applications in lte-advanced systems," *IEEE Wireless Communications*, vol. 19, no. 2, pp. 22–29, 2012.

[90] C. Hoymann, W. Chen, J. Montojo, A. Golitschek, C. Koutsimanis, and X. Shen, "Relaying operation in 3gpp lte: challenges and solutions," *IEEE Communications Magazine*, vol. 50, no. 2, pp. 156–162, 2012.

[91] K.-S. Hwang, Y.-C. Ko, and M.-S. Alouini, "Performance analysis of two-way amplify and forward relaying with adaptive modulation over multiple relay network," *IEEE Transactions on Communications*, vol. 59, no. 2, pp. 402–406, 2011.

[92] L. Song, "Relay selection for two-way relaying with amplify-and-forward protocols," *IEEE Transactions on Vehicular Technology*, vol. 60, no. 4, pp. 1954–1959, 2011.

[93] X. Zhang, A. Ghrayeb, and M. Hasna, "On hierarchical network coding versus opportunistic user selection for two-way relay channels with asymmetric data rates," *IEEE Transactions on Communications*, vol. 61, no. 7, pp. 2900–2910, 2013.

[94] S. N. Islam, P. Sadeghi, and S. Durrani, "Error performance analysis of decode-and-forward and amplify-and-forward multi-way relay networks with binary phase shift keying modulation," *IET Communications*, vol. 7, no. 15, pp. 1605–1616, 2013.

[95] Y. Kong, Y. Kwon, and G. Park, "Robust localization over obstructed interferences for inbuilding wireless applications," *IEEE Transactions on Consumer Electronics*, vol. 55, no. 1, pp. 105–111, 2009.

[96] E. R. Pelet, J. E. Salt, and G. Wells, "Effect of wind on foliage obstructed line-of-sight channel at 2.5 ghz," *IEEE transactions on broadcasting*, vol. 50, no. 3, pp. 224–232, 2004.

[97] C.-K. Toh, "Maximum battery life routing to support ubiquitous mobile computing in wireless ad hoc networks," *IEEE communications Magazine*, vol. 39, no. 6, pp. 138–147, 2001.

[98] S. T. Hung, D. C. Hopkins, and C. R. Mosling, "Extension of battery life via charge equalization control," *IEEE Transactions on Industrial Electronics*, vol. 40, no. 1, pp. 96–104, 1993.

[99] F. Qu, D. Duan, L. Yang, and A. Swami, "Signaling with imperfect channel state information: A battery power efficiency comparison," *IEEE Transactions on Signal Processing*, vol. 56, no. 9, pp. 4486–4495, 2008.

[100] J. Park and B. Clerckx, "Joint wireless information and energy transfer in a two-user mimo interference channel," *IEEE Transactions on Wireless Communications*, vol. 12, no. 8, pp. 4210–4221, 2013.

[101] R. Atallah, M. Khabbaz, and C. Assi, "Energy harvesting in vehicular networks: A contemporary survey," *IEEE Wireless Communications*, vol. 23, no. 2, pp. 70–77, 2016.

[102] M. Mao, N. Cao, Y. Chen, and Y. Zhou, "Multi-hop relaying using energy harvesting," *IEEE Wireless Communications Letters*, vol. 4, no. 5, pp. 565–568, 2015.

[103] J.-M. Kang, I.-M. Kim, and D. I. Kim, "Wireless information and power transfer: Rate-energy tradeoff for nonlinear energy harvesting," *IEEE Transactions on Wireless Communications*, vol. 17, no. 3, pp. 1966–1981, 2017.

[104] Y. Chen, W. Feng, R. Shi, and N. Ge, "Pilot-based channel estimation for af relaying using energy harvesting," *IEEE Transactions on Vehicular Technology*, vol. 66, no. 8, pp. 6877–6886, 2017.

[105] K. Lee and J.-P. Hong, "Energy-efficient resource allocation for simultaneous information and energy transfer with imperfect channel estimation," *IEEE Transactions on Vehicular Technology*, vol. 65, no. 4, pp. 2775–2780, 2015.

[106] S. Timotheou and I. Krikidis, "Joint information and energy transfer in the spatial domain with channel estimation error," in *2013 IEEE online conference on green communications (OnlineGreenComm)*. IEEE, 2013, pp. 115–120.

[107] I. Ahmed, A. Ikhlef, D. W. K. Ng, and R. Schober, "Power allocation for a hybrid energy harvesting relay system with imperfect channel and energy state information," in *2014 IEEE Wireless Communications and Networking Conference (WCNC)*. IEEE, 2014, pp. 990–995.

[108] Y. Zhou and Y. Chen, "Novel energy-harvesting af relaying schemes with channel estimation errors," *IEEE Systems Journal*, 2019.

[109] B. Rankov and A. Wittneben, "Spectral efficient protocols for half-duplex fading relay channels," *IEEE Journal on selected Areas in Communications*, vol. 25, no. 2, pp. 379–389, 2007.

[110] J. N. Laneman, D. N. Tse, and G. W. Wornell, "Cooperative diversity in wireless networks: Efficient protocols and outage behavior," *IEEE Transactions on Information theory*, vol. 50, no. 12, pp. 3062–3080, 2004.

[111] G. Amarasuriya, C. Tellambura, and M. Ardakani, "Asymptotically-exact performance bounds of af multi-hop relaying over nakagami fading," *IEEE Transactions on Communications*, vol. 59, no. 4, pp. 962–967, 2011.

[112] S. Savazzi and U. Spagnolini, "On the pilot spacing constraints for continuous time-varying fading channels," *IEEE Transactions on Communications*, vol. 57, no. 11, pp. 3209–3213, 2009.

[113] D. R. Pauluzzi and N. C. Beaulieu, "A comparison of snr estimation techniques for the awgn channel," *IEEE Transactions on communications*, vol. 48, no. 10, pp. 1681–1691, 2000.

[114] X. Zhou, R. Zhang, and C. K. Ho, "Wireless information and power transfer: Architecture design and rate-energy tradeoff," *IEEE Transactions on communications*, vol. 61, no. 11, pp. 4754–4767, 2013.

[115] D. Gesbert, H. Bolcskei, D. A. Gore, and A. J. Paulraj, "Outdoor mimo wireless channels: Models and performance prediction," *IEEE Transactions on Communications*, vol. 50, no. 12, pp. 1926–1934, 2002.

[116] F. Gao, R. Zhang, and Y.-C. Liang, "Optimal channel estimation and training design for two-way relay networks," *IEEE Transactions on Communications*, vol. 57, no. 10, pp. 3024–3033, 2009.

[117] O. Amin, B. Gedik, and M. Uysal, "Channel estimation for amplify-and-forward relaying: Cascaded against disintegrated estimators," *IET communications*, vol. 4, no. 10, pp. 1207–1216, 2010.

[118] C. S. Patel and G. L. Stuber, "Channel estimation for amplify and forward relay based cooperation diversity systems," *IEEE Transactions on Wireless Communications*, vol. 6, no. 6, pp. 2348–2356, 2007.

[119] F. Gao, T. Cui, and A. Nallanathan, "On channel estimation and optimal training design for amplify and forward relay networks," *IEEE Transactions on Wireless Communications*, vol. 7, no. 5, pp. 1907–1916, 2008.

[120] A. S. Behbahani and A. Eltawil, "On channel estimation and capacity for amplify and forward relay networks," *Global Telecommunications Conference, 2008. IEEE GLOBECOM 2008. IEEE*, pp. 1–5, 2008.

[121] F. A. Khan, Y. Chen, and M.-S. Alouini, "Novel receivers for af relaying with distributed stbc using cascaded and disintegrated channel estimation," *IEEE Transactions on Wireless Communications*, vol. 11, no. 4, pp. 1370–1379, 2012.

[122] H. Yomo and E. D. Carvalho, "A csi estimation method for wireless relay network," *IEEE Communications letters*, vol. 11, no. 6, pp. 480–482, 2007.

[123] E. L. Veretelnikova and I. L. Elantseva, "Selection of factor for root mean square minimum error criterion," in *2016 13th International Scientific-Technical Conference on Actual Problems of Electronics Instrument Engineering (APEIE)*, vol. 2. IEEE, 2016, pp. 221–223.

[124] V. A. Aalo, C. Mukasa, and G. P. Efthymoglou, "Effect of mobility on the outage and ber performances of digital transmissions over nakagami-m fading channels," *IEEE Transactions on Vehicular Technology*, vol. 65, no. 4, pp. 2715–2721, 2015.

[125] K. Wang, Y. Chen, M.-S. Alouini, and F. Xu, "Ber and optimal power allocation for amplify-and-forward relaying using pilot-aided maximum likelihood estimation," *IEEE Transactions on Communications*, vol. 62, no. 10, pp. 3462–3475, 2014.

[126] H. Mheidat and M. Uysal, "Non-coherent and mismatched-coherent receivers for distributed stbcs with amplify-and-forward relaying," *IEEE Transactions on Wireless Communications*, vol. 6, no. 11, pp. 4060–4070, 2007.

[127] J.-M. Kang, I.-M. Kim, and D. I. Kim, "Wireless information and power transfer: Rate-energy tradeoff for nonlinear energy harvesting," *IEEE Transactions on Wireless Communications*, vol. 17, no. 3, pp. 1966–1981, 2018.

[128] J. G. Proakis and M. Salehi, *Digital communications*. McGraw-hill New York, 2001, vol. 4.

[129] Y. Chen, K. Wang, and J. Chen, "Hard-decision fusion with arbitrary numbers of bits for different samples," *IEEE Transactions on Vehicular Technology*, vol. 62, no. 2, pp. 879–884, 2012.

[130] M. K. Simon and M.-S. Alouini, *Digital communication over fading channels*. John Wiley & Sons, 2005, vol. 95.

[131] B. Sklar, "Rayleigh fading channels in mobile digital communication systems. i. characterization," *IEEE Communications magazine*, vol. 35, no. 7, pp. 90–100, 1997.

[132] A. Chockalingam, M. Zorzi, L. B. Milstein, and P. Venkataram, "Performance of a wireless access protocol on correlated rayleigh-fading channels with capture," *IEEE Transactions on Communications*, vol. 46, no. 5, pp. 644–655, 1998.

[133] https://www.mathworks.com/help/comm/ref/comm.bpskmodulator.constellation.html.

[134] J. K. Cavers, "An analysis of pilot symbol assisted modulation for rayleigh fading channels (mobile radio)," *IEEE transactions on vehicular technology*, vol. 40, no. 4, pp. 686–693, 1991.

[135] B. Shah and S. Hinedi, "The split symbol moments snr estimator in narrow-band channels," *IEEE transactions on aerospace and electronic systems*, vol. 26, no. 5, pp. 737–747, 1990.

[136] R. B. Kerr, "On signal and noise level estimation in a coherent pcm channel," *IEEE Transactions on Aerospace and Electronic Systems*, no. 4, pp. 450–454, 1966.

[137] C. Gilchriest, "Signal-to-noise monitoring," *JPL Space Programs Summary*, vol. 4, no. 37-27, pp. 169–184, 1966.

[138] R. Matzner, "An snr estimation algorithm for complex baseband signals using higher order statistics," *Facta Universitatis (Nis)*, vol. 6, no. 1, pp. 41–52, 1993.

[139] A. Brandao, L. B. Lopes, and D. C. McLemon, "In-service monitoring of multipath delay and cochannel interference for indoor mobile communication systems," in *Proceedings of ICC/SUPERCOMM'94-1994 International Conference on Communications*. IEEE, 1994, pp. 1458–1462.

[140] A. Wiesel, J. Goldberg, and H. Messer-Yaron, "Snr estimation in time-varying fading channels," *IEEE Transactions on Communications*, vol. 54, no. 5, pp. 841–848, 2006.

[141] M. O. Hasna and M.-S. Alouini, "Harmonic mean and end-to-end performance of transmission systems with relays," *IEEE Transactions on communications*, vol. 52, no. 1, pp. 130–135, 2004.

[142] https://en.wikipedia.org/wiki/Bit_error_rate.

[143] S. A. Hassan and M. A. Ingram, "Snr estimation for a non-coherent binary frequency shift keying receiver," in *GLOBECOM 2009-2009 IEEE Global Telecommunications Conference*. IEEE, 2009, pp. 1–5.

[144] N. C. Sagias and R. K. Mallik, "On the statistics of the error propagation effect of binary differential phase-shift keying," *IEEE Wireless Communications Letters*, vol. 6, no. 6, pp. 718–721, 2017.

[145] H. Ju and R. Zhang, "Throughput maximization in wireless powered communication networks," *IEEE Transactions on Wireless Communications*, vol. 13, no. 1, pp. 418–428, 2014.

[146] I. Krikidis, S. Timotheou, S. Nikolaou, G. Zheng, D. W. K. Ng, and R. Schober, "Simultaneous wireless information and power transfer in modern communication systems," *IEEE Communications Magazine*, vol. 52, no. 11, pp. 104–110, 2014.

[147] R. Zhang and C. K. Ho, "Mimo broadcasting for simultaneous wireless information and power transfer," *IEEE Transactions on Wireless Communications*, vol. 12, no. 5, pp. 1989–2001, 2013.

[148] D. W. K. Ng, E. S. Lo, and R. Schober, "Wireless information and power transfer: Energy efficiency optimization in ofdma systems," *IEEE Transactions on Wireless Communications*, vol. 12, no. 12, pp. 6352–6370, 2013.

[149] X. Chen, X. Wang, and X. Chen, "Energy-efficient optimization for wireless information and power transfer in large-scale mimo systems employing energy beamforming," *IEEE Wireless Communications Letters*, vol. 2, no. 6, pp. 667–670, 2013.

[150] C. R. Valenta and G. D. Durgin, "Harvesting wireless power: Survey of energy-harvester conversion efficiency in far-field, wireless power transfer systems," *IEEE Microwave Magazine*, vol. 15, no. 4, pp. 108–120, 2014.

[151] T. Le, K. Mayaram, and T. Fiez, "Efficient far-field radio frequency energy harvesting for passively powered sensor networks," *IEEE Journal of solid-state circuits*, vol. 43, no. 5, pp. 1287–1302, 2008.

[152] J. Guo and X. Zhu, "An improved analytical model for rf-dc conversion efficiency in microwave rectifiers," in *2012 IEEE/MTT-S International Microwave Symposium Digest*. IEEE, 2012, pp. 1–3.

[153] E. Boshkovska, D. W. K. Ng, N. Zlatanov, and R. Schober, "Practical non-linear energy harvesting model and resource allocation for swipt systems," *IEEE Communications Letters*, vol. 19, no. 12, pp. 2082–2085, 2015.

[154] L. R. Varshney, "Transporting information and energy simultaneously," in *2008 IEEE International Symposium on Information Theory*. IEEE, 2008, pp. 1612–1616.

[155] A. A. Nasir, X. Zhou, S. Durrani, and R. A. Kennedy, "Wireless-powered relays in cooperative communications: Time-switching relaying protocols and throughput analysis," *IEEE Transactions on Communications*, vol. 63, no. 5, pp. 1607–1622, 2015.

[156] W. Huang, H. Chen, Y. Li, and B. Vucetic, "On the performance of multi-antenna wireless-powered communications with energy beamforming," *IEEE Transactions on Vehicular Technology*, vol. 65, no. 3, pp. 1801–1808, 2016.

[157] G. Yang, C. K. Ho, R. Zhang, and Y. L. Guan, "Throughput optimization for massive mimo systems powered by wireless energy transfer," *IEEE Journal on Selected Areas in Communications*, vol. 33, no. 8, pp. 1640–1650, 2015.

[158] L. Liu, R. Zhang, and K.-C. Chua, "Multi-antenna wireless powered communication with energy beamforming," *IEEE Transactions on Communications*, vol. 62, no. 12, pp. 4349–4361, 2014.

[159] X. Kang, C. K. Ho, and S. Sun, "Full-duplex wireless-powered communication network with energy causality," *IEEE Transactions on Wireless Communications*, vol. 14, no. 10, pp. 5539–5551, 2015.

[160] Y. Chen, K. T. Sabnis, and R. A. Abd-Alhameed, "New formula for conversion efficiency of rf eh and its wireless applications," *IEEE Transactions on Vehicular Technology*, vol. 65, no. 11, pp. 9410–9414, 2016.

[161] I. S. Gradshteyn and I. M. Ryzhik, *Table of integrals, series, and products*. Academic press, 2014.

[162] Z. Ding, S. M. Perlaza, I. Esnaola, and H. V. Poor, "Power allocation strategies in energy harvesting wireless cooperative networks," *IEEE Transactions on Wireless Communications*, vol. 13, no. 2, pp. 846–860, 2014.

[163] Y. Chen, "Energy-harvesting af relaying in the presence of interference and nakagami-m fading," *IEEE Transactions on Wireless Communications*, vol. 15, no. 2, pp. 1008–1017, 2016.

[164] I. Krikidis, G. Zheng, and B. Ottersten, "Harvest-use cooperative networks with half/full-duplex relaying," *Wireless Communications and Networking Conference (WCNC), 2013 IEEE*, pp. 4256–4260, 2013.

[165] A. Minasian, S. ShahbazPanahi, and R. S. Adve, "Energy harvesting cooperative communication systems," *IEEE Transactions on Wireless Communications*, vol. 13, no. 11, pp. 6118–6131, 2014.

[166] N. Zhao, F. R. Yu, and V. C. Leung, "Opportunistic communications in interference alignment networks with wireless power transfer," *IEEE Wireless Communications*, vol. 22, no. 1, pp. 88–95, 2015.

[167] ——, "Wireless energy harvesting in interference alignment networks," *IEEE Communications Magazine*, vol. 53, no. 6, pp. 72–78, 2015.

[168] J. Guo, N. Zhao, F. R. Yu, X. Liu, and V. C. Leung, "Exploiting adversarial jamming signals for energy harvesting in interference networks," *IEEE Transactions on Wireless Communications*, vol. 16, no. 2, pp. 1267–1280, 2017.

[169] T. Riihonen, S. Werner, and R. Wichman, "Hybrid full-duplex/half-duplex relaying with transmit power adaptation," *IEEE Transactions on Wireless Communications*, vol. 10, no. 9, pp. 3074–3085, 2011.

[170] R. U. Nabar, H. Bolcskei, and F. W. Kneubuhler, "Fading relay channels: Performance limits and space-time signal design," *IEEE Journal on Selected Areas in communications*, vol. 22, no. 6, pp. 1099–1109, 2004.

[171] Y. Chen, R. Shi, W. Feng, and N. Ge, "Af relaying with energy harvesting source and relay," *IEEE Transactions on Vehicular Technology*, vol. 66, no. 1, pp. 874–879, 2016.

[172] A. Zafar, R. M. Radaydeh, Y. Chen, and M.-S. Alouini, "Enhancing the efficiency of constrained dual-hop variable-gain af relaying under nakagami-m fading," *IEEE Transactions on Signal Processing*, vol. 62, no. 14, pp. 3616–3630, 2014.

[173] A. Hussain, K. Lee, S.-H. Kim, S.-H. Chang, and D. I. Kim, "Performance analysis of dual-hop variable-gain relaying with beamforming over κ–μ fading channels," *IET Communications*, vol. 11, no. 10, pp. 1587–1593, 2017.

[174] S. Kim, R. Vyas, J. Bito, K. Niotaki, A. Collado, A. Georgiadis, and M. M. Tentzeris, "Ambient RF energy-harvesting technologies for self-sustainable

standalone wireless sensor platforms," *Proceedings of the IEEE*, vol. 102, no. 11, pp. 1649–1666, 2014.

[175] T. Soyata, L. Copeland, and W. Heinzelman, "Rf energy harvesting for embedded systems: A survey of tradeoffs and methodology," *IEEE Circuits and Systems Magazine*, vol. 16, no. 1, pp. 22–57, 2016.

[176] M. Mi, M. H. Mickle, C. Capelli, and H. Swift, "Rf energy harvesting with multiple antennas in the same space," *IEEE Antennas and Propagation Magazine*, vol. 47, no. 5, pp. 100–106, 2005.

[177] F. Yildiz, "Potential ambient energy-harvesting sources and techniques." *Journal of technology Studies*, vol. 35, no. 1, pp. 40–48, 2009.

[178] N. C. Beaulieu and C. Cheng, "Efficient nakagami-m fading channel simulation," *IEEE Transactions on Vehicular Technology*, vol. 54, no. 2, pp. 413–424, 2005.